GENERATION OF ULTRA-SHORT PULSE LASERS USING GRAPHENE AND TOPOLOGICAL INSULATOR BASED 2D NANOMATERIALS

HAZLIHAN BIN HARIS

FACULTY OF ENGINEERING
UNIVERSITY OF MALAYA
KUALA LUMPUR

2018

GENERATION OF ULTRA-SHORT PULSE LASERS USING GRAPHENE AND TOPOLOGICAL INSULATOR BASED 2D NANOMATERIALS

HAZLIHAN BIN HARIS

THESIS SUBMITTED IN FULFILMENT OF THE REQUIREMENTS FOR THE DEGREE OF DOCTOR OF PHILOSOPHY

FACULTY OF ENGINEERING
UNIVERSITY OF MALAYA
KUALA LUMPUR

2018

UNIVERSITY OF MALAYA
ORIGINAL LITERARY WORK DECLARATION

Name of Candidate: HAZLIHAN BIN HARIS

Matric No: KHA140102

Name of Degree: DOCTOR OF PHILOSHOPY

Title of Project Paper/Research Report/Dissertation/Thesis ("this Work"):

GENERATION OF ULTRA-SHORT PULSE LASERS USING GRAPHENE AND TOPOLOGICAL INSULATOR

Field of Study: PHOTONIC

I do solemnly and sincerely declare that:

(1) I am the sole author/writer of this Work;
(2) This Work is original;
(3) Any use of any work in which copyright exists was done by way of fair dealing and for permitted purposes and any excerpt or extract from, or reference to or reproduction of any copyright work has been disclosed expressly and sufficiently and the title of the Work and its authorship have been acknowledged in this Work;
(4) I do not have any actual knowledge nor do I ought reasonably to know that the making of this work constitutes an infringement of any copyright work;
(5) I hereby assign all and every rights in the copyright to this Work to the University of Malaya ("UM"), who henceforth shall be owner of the copyright in this Work and that any reproduction or use in any form or by any means whatsoever is prohibited without the written consent of UM having been first had and obtained;
(6) I am fully aware that if in the course of making this Work I have infringed any copyright whether intentionally or otherwise, I may be subject to legal action or any other action as may be determined by UM.

Candidate's Signature   Date:

Subscribed and solemnly declared before,

Witness's Signature   Date:

Name:

Designation:

GENERATION OF ULTRA-SHORT PULSE LASERS USING GRAPHENE AND TOPOLOGICAL INSULATOR

ABSTRACT

In this work, fabrication of passive Saturable absorbers (SA) using 2D nanomaterials such as Graphene and Topological insulator (TIs) based was demonstrated. The fabricated passive SA was integrated in an Ytterbium-Doped Fiber Laser (YDFL) and Erbium-Doped Fiber Laser (EDFL) system for a ultra-short pulsed laser generation via mode-locking. UV-Vis-NIR spectrophotometer, Raman spectroscopy and Field Emission Scanning Electron Microscopy (FESEM) were used to verify the existence and investigate the optical properties of the fabricated SA. The SA was also characterized for nonlinear optical properties to study the SA parameters such as saturation intensity, modulation depth and non-saturable loss. The fabricated SA was applied to the end facet of a fiber ferrule, which was then mated to another clean ferrule connector to act as a passive SA, which was integrated into a ring YDFL and EDFL for pulsed laser generation.

In addition, by using the Graphene SA into the YDFL cavity, a stable pulse laser was generated at 1052.89 nm wavelength with repetition rate of 4.5 MHz and pulse energy of 1.52 nJ. Next, mode locked YDFL with graphene oxide SA was generated at 1053 nm wavelength with repetition rate of 6 MHz and pulse energy of 1.65 nJ. An operating wavelength of approximately 1051 nm was generated when TI based SA (Bi2Se3) was used as a Mode-locker in a passively Mode-locked YDFL. Repetition rates is 8.3 MHz while a pulse energy of 1.5 nJ was recorded by using TI Bi2Se3 as SA. A stable Mode-locking operation was successfully obtained at the central operating wavelength of YDFL dropped from the initial 1050.28 nm with the addition of TI Bi2Te3 SA. The repetition rate of 9.5 MHz and pulse energy was 2.14 nJ.

Ultra-short pulses beyond 1.5 μm region wavelength with durations below 200 fs were generated through a Mode-locked in EDFL seeded by used fabricated SA. A stable passive Mode-locked EDFL operating at 1565 nm wavelength demonstrated using graphene SA as Mode-locker. In anomalous regime with estimated group delay dispersion, GDD of -0.22 ps^2, the soliton mode locked EDFL pulse was generated with repetition rate of 20.7 MHz, pulse width of 0.88 ps and pulse energy of 1.5 nJ. A stable bound soliton appeared at wavelength 1564 nm with inserting about 13.2 m single mode fiber, SMF into EDFL cavity. In the particular case there were 7 solitons in bunch with repetition rate of 11.9 MHz and anomalous regime GDD of -0.37 ps^2. The pulse width of 1.04 ps and pulse energy of 1.97 nJ by using passively graphene SA as SA. Other fabricated SA (graphene oxide, TI bismuth selenide and TI bismuth telluride) were used to reliably Mode-locked erbium soliton fiber lasers producing picosecond pulses at 1.56 μm. Various modes of pulse operation were studied using the above mentioned SA. Soliton mode-mocking was realized using graphene and TIs based SA

Keywords: Ultra-short pulse laser, Fiber lasers, Saturable absorber, Mode-locked laser, Nanomaterials

PENGHASILAN PENDENYUTAN ULTRA PENDEK LASER DENGAN MENGGUNAKAN GRAPHENE DAN PENEBAT TOPOLOGI YANG BERASASKAN BAHAN NANO 2D

ABSTRAK

Pembuatan penyerap boleh tepu (SA) pasif menggunakan graphene dan penebat topologi (SA) ditunjukkan. TIs yang dihasilkan diintegrasikan di dalam sistem gentian laser berdopan-Ytterbium (YDFL) dan gentian laser berdopan-Erbium (EDFL) untuk menghasilkan laser berdenyutan melalui penguncian mod. Spektrofotometer UV-Vis-NIR, kespektroskopan Raman dan Kemikroskopan Elektron Imbasan Pancaran Medan (FESEM) digunakan untuk mengesahkan kehadiran dan menguji pemilikan optikal TIs yang telah dihasilkan. TIs juga dicirikan untuk pemilikan optikal tidak linear bagi mengkaji parameter TIs seperti keamatan penepuan, kedalaman modulasi dan kehilangan tidak tepu. TIs diletakkan pada permukaan penghubung gentian, kemudian disambungkan kepada penghubung gentian lain melalui penyambung gentian untuk bertindak sebagai TIs pasif, yang mana diintegrasikan ke dalam kaviti cincin YDFL dan EDFL untuk mengahsilkan laser berdenyutan .

Tambahan pula dengan menggunakan TIs graphene ke dalam rongga YDFL, laser pendenyutan telah dihasilkan dengan stabil di panjang gelombang 1052.89 nm dengan kadar pengulangan 4.5 MHz dan tenaga pendenyutan sebanyak 1.52 nJ. Seterusnya mod terkunci telah dihasilkan dengan menggunakan graphene oksida sebagai TIs, di panjang gelombang 1053 nm dengan kadar pengulangan 6 MHz dan pendenyutan tenaga sebanyak 1.65 nJ. Seterusnya, dengan beroperasi di panjang gelombang yang menghampiri 1051 nm, telah dihasilkan pengunci mod pasif dengan menggunakan Bi2Se3 sebagai TIs dalam mod terkunci pasif YDFL dengan merekodkan nilai kadar pengulangan 8.3 MHz dan tenaga pendenyutan sebanyak 1.5 nJ. Selain itu, pengunci mod beroperasi stabil berjaya dihasilkan di panjang gelombang tengah 1050.28 nm dengan menggunakan SA Bi2Te3 sebagai TIs dengan mempunyai nilai kadar pengulangan 9.5 MHz dan tenaga pendenyutan sebanyak 2.14 nJ.

Pendenyutan ultra pendek di rantau 1.5 μm panjang gelombang dengan berdurasikan dibawah 200 fs telah dihasilkan melalui mod terkunci di dalam EDFL dengan menggunakan TIs yang telah difabrikasi pada sebelum ini. Mod terkunci pasif EDFL beroprasi stabil di panjang gelombang 1565 nm dengan menggunakan TIs graphene sebagai pengunci mod. Dalam rejim penyebaran ganjil dengan anggaran kumpulan kelewatan penyebaran, GDD ialah -0.22 ps^2, soliton mod terkunci pendenyutan EDFL telah dihasilkan dengan kadar pengulangan 20.7 MHz, lebar denyut ialah 0.88 ps dan tenaga pendenyutan sebanyak 1.5 nJ. Soliton terikat muncul di panjang gelombang 1564 nm dengan memasukan 13.2 m gentian mod tunggal, SMF ke dalam rongga EDFL. Dalam kes tertentu terhasil 7 soliton dalam sekumpulan dengan kadar pengulangan 11.9 MHz dan rejim penyebaran ganjil untuk GDD ialah -0.37 ps^2. Mempunyai lebar denyut 1.04 ps dan tenaga pendenyutan sebanyak 1.97 nJ dengan menggunakan TIs graphene pasif. Selain itu, kesemua TIs yang telah difabrikasi (graphene oksida, SA bismuth

selenide dan SA bismuth telluride) telah digunakan untuk penghasilan soliton mod terkunci erbium gentian laser dalam nilai pendenyutan ps di 1.56 µm. Pelbagai mod operasi denyutan dikaji dengan menggunakan TIs tersebut. Penguncian mod soliton dicapai dengan menggunakan TIs berasakan graphene dan SA.

Keywords (kata kunci): Pendenyutan ultra pendek laser, Gentian laser, Laser mod terkunci, Penyerap boleh tepu, Bahan nano

ACKNOWLEDGEMENTS

Foremost, I would like to express my deepest gratitude to my supervisors, Prof. Ir. Dr. Sulaiman Wadi Harun and Prof. Ir. Dr. Hamzah Arof. Their guidance and continuous support were essential for the development of this thesis project. I could not have imagined a better mentor than both of them. Their insightful experience has always been immensely helpful.

From the bottom of my heart, I wish to thank my parents, Haris Puteh and Norjinah Amat, my siblings (Sadan, Kiah, Putri, Dinui and Cham) and all my family members for their endless love, encouragement and pray. I am grateful for their fully support in every trials that comes my way.

I'm ever thankful to my supportive lab seniors especially Abang Fauzan, Kak Ina, Zhi-zhi Tan, Kak Husna and Kak Arni. Then the sleepless nights friends, who were working together before the deadlines Ajib and Illa not to forget to Carol, Kak Aminah, Kak Nurul, Ummi, Taufiq, Fauzi, Akhi Faizal, Ashadi, Haziezol, Hafiz, Haziq and Farid for all the fun we have had in the period education. Thanks for being there for me during all the struggling time.

Finally, I would like to thank everybody who was important to the successful realization of the thesis, as well as expressing my apology that I could not mention personally one by one.

TABLE OF CONTENTS

CHAPTER 3: FABRICATION AND CHARACTERIZATION OF GRAPHENE AND TOPOLOGICAL INSULATOR AS SATURABLE ABSORBER 67

LIST OF FIGURES

LIST OF TABLES

LIST OF SYMBOLS AND ABBREVIATIONS

α_s	:	Modulation depth
β_2	:	Group velocity dispersion parameter
I	:	Light intensity
I_{sat}	:	Saturation intensity
α_{ns}	:	Non-saturable absorption
f_{rep}	:	Pulse repetition rate
λ	:	Wavelength
$\Delta\lambda$	:	Spectral bandwidth (at FWHM)
n	:	Refractive index
c	:	Speed of light
υ	:	Frequency of optical wave
$\Delta\upsilon$	:	Optical spectral bandwidth (in hertz)
dB	:	Decibel
μs	:	Microsecond
ps	:	Picosecond
fs	:	Femtosecond
nm	:	Nanometer
τ_p	:	Pulse duration
$sech^2$	:	Secant hyperbolic
BP	:	Black Phosphorus
CNTs	:	Carbon Nanotubes
CW	:	Continues Wave
EDF	:	Erbium-Doped Fiber

EDFA	:	Erbium-Doped Fiber Amplifier
EDFL	:	Erbium-Doped Fiber Laser
Bi_2Se_3	:	Bismuth Selenide
Bi_2Te_3	:	Bismuth Telluride
TI	:	Topological Insulator
YDF	:	Ytterbium-Doped Fiber
YDFA	:	Ytterbium-Doped Fiber Amplifier
YDFL	:	Ytterbium-Doped Fiber Laser
FWHM	:	Full-Width at Half Maximum
GVD	:	Group Velocity Dispersion
LASER	:	Light Amplification by Stimulated Emission of Radiation
NOLM	:	Nonlinear Optical Loop Mirror
NPR	:	Nonlinear Polarization Rotation
OTDM	:	Optical Time Division Multiplexing
SA	:	Saturable Absorber
SESAMs	:	Semiconductor Saturable Absorption Mirrors
SPM	:	Self-Phase Modulation
SWCNT	:	Single-Walled Carbon Nanotubes
GO	:	Graphene Oxide
Gr	:	Graphene
TMD	:	Transition Metal Dichalcogenide
WDM	:	Wavelength Division Multiplexing
ISO	:	Isolator
PC	:	Polarization Controller
2D	:	Two Dimensional
Er	:	Erbium

Yb   :   Ytterbium

Tm   :   Thulium

Bi   :   Bismuth

CHAPTER 1: INTRODUCTION

1.1 Background

During the last decade world-wide laser markets have grown tremendously. Continuous-wave and pulsed laser sources have started to be employed in a broad range of completely new application fields. The requirements of industrial applications have routed the development towards compact, maintenance-free, efficient systems with clean Gaussian-shaped beam quality and moderate cost. The fiber laser is a good candidate to meet the above-mentioned criteria. Owing to the nature of the fiber laser cavity, which in the ideal case is constituted only of fiber components and does not have any free-space optics or other bulk elements, the fiber laser offers unprecedented reliability and turn-key operation. Additionally, the output light with nearly ideal beam quality is delivered initially in an optical fiber and is thus easily routed towards specific targets.

The engine of the fiber laser cavity is the active medium; doped fiber. Doped fibers employed in lasers are typically able to provide broad gain spectra with relatively high gain. This allows building of efficient lasers with great potential for wide wavelength tuning and ultrashort pulse generation. The wavelength regions covered by doped fibers and fiber lasers. Ytterbium- (Yb) and erbium (Er)-doped fibers and lasers have been intensively researched during the last two decades and the results have already been successfully commercialized. However, the gain bandwidth of Er-doped fiber is covered to the wavelength range from 1.53 µm to ~1.62 µm, whereas Yb-doped fiber lasers typically operate close to 1 µm.

Pulsed fiber lasers have various industrial and scientific applications in the fields of material processing, bio-medicine, optical communications, spectroscopy, imaging, and ranging. In particular, ultrafast mode-locked and energetic Q-switched fiber lasers delivering pulses with durations from several tens of femtoseconds to a few hundred nanoseconds are gaining more and more interest in micromachining (Brabec et al., 1992; M. Fermann et al., 1993; Set et al., 2003), eye and dental surgeries (Goh et al., 2005; Yim et al., 2008), tissue welding (Y. C. Chen et al., 2002), optical coherence tomography (Kataura et al., 2000; Solodyankin et al., 2008), and LIDAR (Sze Y Set et al., 2004; F Wang et al., 2008; S Yamashita et al., 2004). Table 1.1 summarizes several applications of pulsed fiber lasers at different wavelength regimes.

Table 1.1 : Applications of mode-locked and Q-switched fiber lasers.

Gain Fiber	Wavelength range (μm)	Application
Ytterbium (Yb)	0.98-1.11	High-precision cutting and drilling, micro patterning, cold ablation, surgeries and frequency doubling
Erbium (Er)	1.53-1.65	Optical communication, Eye-safe LIDAR and Bio-medicine
Thulium (Tm)	1.8-2.1	Eye-safe LIDAR, directed infrared countermeasures (DIRCM), minimally invasive surgery and CO_2 – spectroscopy.

The generation of pulsed laser can be either via active or passive pulsing methods, depending on the applications involved. Active technique synchronizes to the cavity repetition rate via an external modulator while passive technique synchronizes a within the laser resonator via an all optical nonlinear process. Due to the need for an external modulator, active pulse laser construction is rather bulky and complex in comparison to the simpler and compact construction of passive pulse laser, where its mechanism depends only on the generation of saturable absorption action. Saturable absorbers (SAs) used in passive pulse laser can be either real SAs (e.g. carbon nanotubes (CNTs), graphene) or artificial SAs (nonlinear polarization rotation (NPR)). Overall, passive technique is more cost efficient and robust compare to the active technique (Conroy et al., 1998; J. Sotor et al., 2012).

A passive Q-switching and mode-locking pulses trains, such as nonlinear optical loop mirror (NOLM) (Zhong et al., 2010), nonlinear polarization rotation (NPR) (A. Luo et al., 2011), semiconductor saturable absorption mirrors (SESAMs) (Gomes et al., 2004; Z.-C. Luo et al., 2011), single wall carbon nanotubes (SWCNTs) (Fauzan Ahmad et al., 2016; Anyi, Ali, et al., 2013), and graphene SAs (Saleh et al., 2014). In the NOLM approach, a long fiber must be used to produce sufficient nonlinear phase shifts. The NPR technique utilizes dispersion and nonlinearity management to generate laser. However, it is often sensitive to ambient factors such as vibration and temperature, which limits its practical applications. SESAM is the dominated passive mode locking. However, SESAMs require complex design to improve their damage threshold and work only in a narrow wavelength range. A simpler and cost-effective alternative relies on SWCNTs. However, SWCNTs have a low damage threshold and their operating wavelength depends on the diameters of the nanotube (Choi et al., 2009). Therefore, a strong aspiration to seek new high-performance of SAs with broadband operation for fiber laser systems. Since the first demonstration of two dimensional (2D) nanomaterial like

graphene based SA (Bao et al., 2011), graphene has been studied and developed for passive Q-switching and mode locking applications (X. Liu et al., 2013; Xie et al., 2012). Compared to the previous SAs, graphene has the advantages of ultrafast recovery time and broadband saturable absorption. But the absence of band gap and the low absorption co-efficiency (2.3%/layer) of graphene have also restraint its applications. These limitations lead to the intensive research on other 2D nanomaterials which can complement the graphene. Therefore, this study aimed to explore the use of various graphene and topological insulator based SAs were developed as potential SAs. Which presents in various mode-locked ytterbium-doped fiber lasers (YDFLs) and erbium-doped fiber lasers (EDFLs).

1.2 History of mode-locked lasers

The history of mode-locked lasers began not long after the first demonstration of a laser in 1960 by Maiman. The first laser, ruby laser was first demonstrated at Hughes Research Laboratory in California. Meanwhile, the first mode-locked laser was demonstrated at Bell Laboratories in New Jersey (Hargrove et al., 1964). He used an extremely clever acousto-optic technique to provide a loss modulation in a Helium-Neon laser cavity, which led to the laser being actively mode-locked. While the pulses were still relatively long by today's standards (several nanoseconds), this demonstration opened the door for many more researchers to push the boundaries of ultrashort optical pulses. The passive mode-locked laser was first demonstrated in 1965 by Mocker and Collins. This laser was based on transient locking of the modes of a multimode Q-switched laser and required no active modulator (Delgado-Pinar et al., 2006). Since only a few modes were involved in this process, the pulse widths were on the order of 10s of ns. The component that locked the modes in their laser was a saturable Q-switching dye (cryptocyanine in methanol).

The drawback to this dye was that it required the laser to be Q-switched in order to saturate and thus the laser emitted mode locked pulses only at the Q-switched intervals. The transient nature of the mode locked pulses proved to be problematic in practical applications in ultrafast spectroscopy and nonlinear optics. This problem was solved in 1972 when Ippen *et al.* introduced a laser based on the saturable dye (Rhodamine 6G) that could mode lock continuously (Shank et al., 1974). The pulses from this laser were found to have pulse widths of only 1.5 picoseconds. After this demonstration, researchers pushed the gain bandwidth further with other types of saturable dyes, and developed external cavity pulse compression techniques of a 6 fs pulse (based on adding new spectral content through nonlinearity, then recompressing through chromatic dispersion) (R. L. Fork et al., 1987).

This discussion of the development of mode locked lasers would not be complete without a look at fast saturable absorber systems. The saturable absorber effect can be simulated by optical phenomenon (Mollenauer et al., 1986). This approach has several advantages including the fact that the recovery time of an optically based saturable absorber can be extremely fast (¼ a few optical cycles) since it does not depend on an atomic/molecular resonance. These types of absorbers have led to the shorter pulses width.

1.3 Motivation of the study

Mode-locked based fiber lasers have been applied in various areas, e.g. remote sensing, laser materials processing, medicine, and telecommunications (Y.-S. Chen et al., 2015). Passively Mode-locked fiber lasers are cost efficient, simple, flexible, and compact in design in contrast to actively Mode-locked fiber lasers (Bonaccorso et al., 2014; Jaroslaw Sotor et al., 2014). Over the years, different types of SAs (e.g. transition metal-doped metals (Mirov et al., 2013), graphene (Z. Tiu et al., 2014), semiconductor saturable

absorber mirrors (SESAM) (J. Y. Huang et al., 2009), and gold nanocrystals (T. Jiang et al., 2012) have been used to construct passively Mode-locked ytterbium-doped fiber lasers (YDFLs) and erbium-doped fiber lasers (EDFLs).

It has been recently discovered that 2D nanomaterials have various advantages (short recovery period, vast operation wavelength, and easy manufacturing process) that precedes their predecessors as a viable cost-effective option for passive mode locker (A. H. Castro Neto et al., 2011). Yet, there is still lack of research works on passive Mode-locking using 2D nanomaterials as SAs. In this dissertation, we developed a new SA based on both graphene and topological insulator based 2D nanomaterials for generate ultra-short pulse.

1.4   Thesis Objectives

This thesis aims to design and develop mode-locked fiber lasers based on doped fibers covering from 1μm to 1.55- μm region. To achieve this, several objectives have been outlined to guide the research direction:

1. To fabricate and characterize graphene based (graphene and graphene oxide) and topological insulators based (Bismuth Selenide and Bismuth Telluride) thin films for application as a passive saturable absorber (SA).

2. To demonstrate the generation of ultra-short pulses train operating at 1-micron region by using the fabricated SAs in conjunction with YDF as a gain medium.

3. To demonstrate the generation of ultra-short pulses train operating at 1.5-micron region by using the fabricated SAs in conjunction with EDF as a gain medium.

4. To demonstrate the generation of various soliton pulses by manipulating of cavity dispersion and length.

1.5 Pulsed laser as source proposed in industrial application.

Pulsed operation of lasers refers to any laser not classified as continuous wave, so that the optical power appears in pulses of some duration at some repetition rate. This encompasses a wide range of technologies addressing a number of different motivations. Some lasers are pulsed simply because they cannot be run in continuous mode.

The application requires the production of pulses having as large an energy as possible. Since the pulse energy is equal to the average power divided by the repetition rate, this goal can sometimes be satisfied by lowering the rate of pulses so that more energy can be built up in between pulses. In laser ablation for example, a small volume of material at the surface of a work piece can be evaporated if it is heated in a very short time, whereas supplying the energy gradually would allow for the heat to be absorbed into the bulk of the piece, never attaining a sufficiently high temperature at a particular point.

Other applications rely on the peak pulse power (rather than the energy in the pulse), especially in order to obtain nonlinear optical effects. For a given pulse energy, this requires creating pulses of the shortest possible duration utilizing techniques such as Mode-Locked. Mode-Locked pulse range duration is less than 200 ns. In this work, picosecond was obtained and it is suitable for industrial applications like machining cutting, medical (ink tattoo removal) and LiDAR (Light Detection Range).
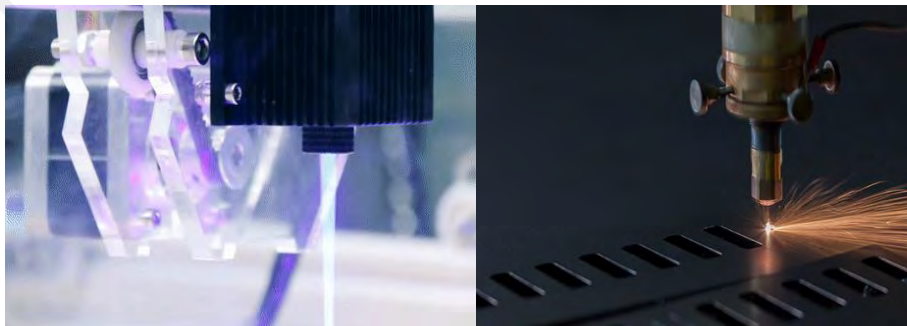
(a)

(b)

(c)

Figure 1.1: Applications of mode-locked fiber lasers: (a) Machining cutting source, (b) Medical (tattoo removal) source and (c) LiDAR source (remote weapon station).

1.6 Thesis Overview

This thesis aimed to develop various soliton mode-locked fiber lasers using the newly developed passive SA based on 2D nanomaterials. Graphene and topological insulators-based SA film were proposed for generation of narrow optical pulses with ultra-high repetition rate and high peak power. This first chapter described the background to the research project, laying the foundations of this thesis work. The motivations behind this research work were highlighted, then mode-locking concept and laser applications were briefly recalled. The literature reviews behind this research work will be described in Chapter 2. This chapter will provide an overview of some important

concepts of fiber lasers, Erbium-doped fiber laser, Ytterbium-doped fiber laser, mode-locking, saturable absorption, 2D nanomaterials etc.

Chapter 3 will describe the technique developed to fabricate graphene and TI based SAs, then these SAs were analyzed using Raman spectroscopy and Field Emission Scanning Electron Microscopy (FESEM) and characterized in terms of absorption and modulation depth. Four types of 2D nanomaterial based SAs were successfully fabricated and characterized; graphene, graphene oxide, Bi2Se3 and Bi2Te3. The graphene film SA was fabricated using a chemically exfoliated graphene flakes, which were embedded into a PEO polymer. Multi-layer GO fabricated based on a modified Hummers method was also embedded into PEO film to construct the GO based SA. Bi2Se3 and Bi2Te3 based SAs were obtained by optical deposition method. The developed SAs will be used to generate mode-locked fiber lasers, which the results are presented in Chapters 4 and 5.

Chapter 4 will describe the technique developed to generate ultra-short pulsed lasers using those SAs as a mode-locker and YDF as a gain medium. The fabricated SAs were integrated in the YDFL cavity by sandwiching the SA thin film between two fiber connectors. The performance of these lasers compared and discussed in this chapter. Chapter 5 will demonstrate various mode-locked soliton fiber lasers, which were obtained by using the previously developed graphene and topological insulator based SAs in an EDFL cavity. Finally, Chapter 6 concludes the thesis, summarizing the attained results, re-stating the novelty aspects of this work and suggesting future research developments.

CHAPTER 2: LITERATURE REVIEW

2.1 Introduction

This chapter concentrates on the rare-earth-ion doped fibers that are used as gain media in high power and ultra-short pulse fiber lasers. The main emphasis is on the relatively unexplored and novel gain fiber materials important for this work is ytterbium and erbium fibers. The emission band of Yb-doped fibers is centered around 1μm and the emission band of the Er-doped fibers around 1.55 μm.

2.2 Ytterbium (Yb)-doped fibers

Yb is an element that belongs to the group of rare earth metals. It provides optical amplification and gain around 1 μm wavelength (R. Paschotta et al., 1997; Photonics). As an optically active element, it is already well known and has been rather intensively studied during the last two decades. Initially, Yb-activated glass was proposed for laser material as early as 1962 (Etzel et al., 1962; Gandy et al., 1965; Snitzer, 1966). However, the first Yb-based silica gain fiber was demonstrated 25 years later, in 1988 (i Ponsoda et al., 2013; Jaff, 2012; Koponen et al., 2006). Since then, Yb-doped fibers have been extensively employed to create efficient, high power and pulsed fiber lasers. These lasers operating at 1μm find various applications in the fields of laser welding (Chong, 2008; Kelleher et al., 2010; Osellame et al., 2012; J. Wang et al., 2012), material processing (Bachmann, 2003; Minoshima et al., 2001; Steen et al., 2010), eye surgery (F Ahmad et al., 2013; Chang et al., 2012; Linke et al., 2016) and other biomedical applications (Keiser, 2008; Mary et al., 2014; Vij et al., 2013).

Figure 2.1 shows a sub-level in energy diagram of Yb ions and the sub-level splitting is depended on the position and concentration of Yb glass (Zervas, 2014; Zervas

et al., 2014). Typically, ytterbium ions absorb the pump radiation and transfer the excitation energy to erbium ions. Even though the erbium ions could directly absorb radiation e.g. at 980 nm (Figure 2.1), ytterbium co-doping can be useful because of the higher ytterbium absorption cross sections and the higher possible ytterbium doping density in typical laser glasses, so that a much shorter pump absorption length and a higher gain can be achieved. Ytterbium co-doping is also sometimes used for praseodymium-doped up conversion fiber lasers. In other words, Yb has a very simple electronic level structure, with only one excited state manifold (2F9/2) within the reach from the ground-state manifold (2F7/2). The simple electronic structure excludes excited-state absorption and also a variety of detrimental quenching processes. The upper state lifetimes are typically in the order of 10 to fs, which is beneficial for Q-switching and mode-locking pulses. The Yb ion possesses a number of emission transitions within the 950 – 1100 nm wavelength range. Furthermore, the homogeneous and inhomogeneous broadening of these transitions within a glass host, leads to a wide and continuous emission spectrum in the 1 micron band. The lifetimes of emission and absorption spectrum depend on the host materials (M. Weber et al., 1983)
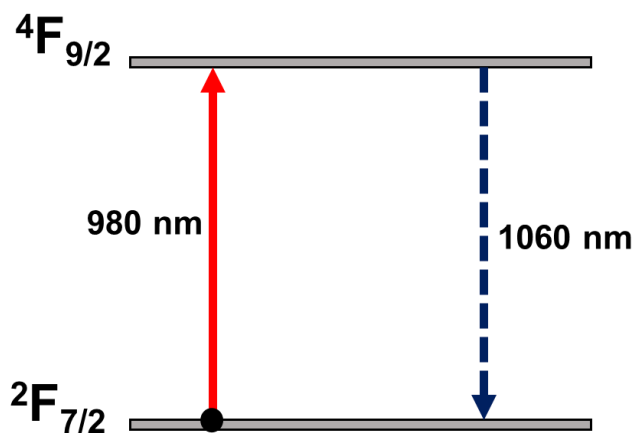
Figure 2.1 : Schematic energy-level diagram of the Yb ion in silica.

2.3   Erbium (Er)-doped fibers

Another commonly used rare earth metal element is erbium. Er ions provide gain in a broad wavelength range around 1.55 μm, in the low-loss transmission window of optical fibers (Ahmed et al., 2014; Payne et al., 1993). This wavelength range is particularly interesting and important for optical communications. Therefore, Er-fibers were intensively studied during the end of the 20th century. The first Er-fibers were manufactured and reported in 1985 followed by demonstrations of Er-doped fiber amplifiers and lasers during 1987 (Q. Bao et al., 2009b; Martin E Fermann et al., 1999; Z. Luo et al., 2010). The main absorption bands of Er ions from the aspect of optical pumping appear at ~980 nm and at 1480 nm (in-band pumping). These wavelengths are well-suited for commercial semiconductor laser diodes. The absorption and emission cross-sections of erbium are shown in Fig. 2.2. In lasers, the Er behaves as a quasi-three-level system as confirmed by experimental relaxation oscillation measurements (Fan et al., 1987; Kuleshov et al., 1997; K. Wang et al., 2013). Er-fibers are often co-doped with Yb-ions (sensitizer ions). Co-doping improves the pumping efficiency at 1480 nm. In addition to telecommunication applications, Er-fibers are typically beneficial for ultrafast mode-locked fiber lasers because the fiber gain spectrum is broad and the fiber dispersion at 1.55 μm is anomalous (Brida et al., 2014; X. Liu et al., 2013). Anomalous dispersion supports the soliton pulse regime of mode-locked fiber lasers (Khazaeinezhad et al., 2015; D. Li et al., 2016; Usechak et al., 2005). In the soliton pulse regime, the anomalous dispersion and nonlinearity of the fiber are balanced, leading to very stable, self-adjusting soliton pulses that are resistant to noise and losses. High-quality soliton pulses are particularly beneficial in long-distance high-speed optical fiber communications (Arumugam, 2001; Nakazawa et al., 2000).
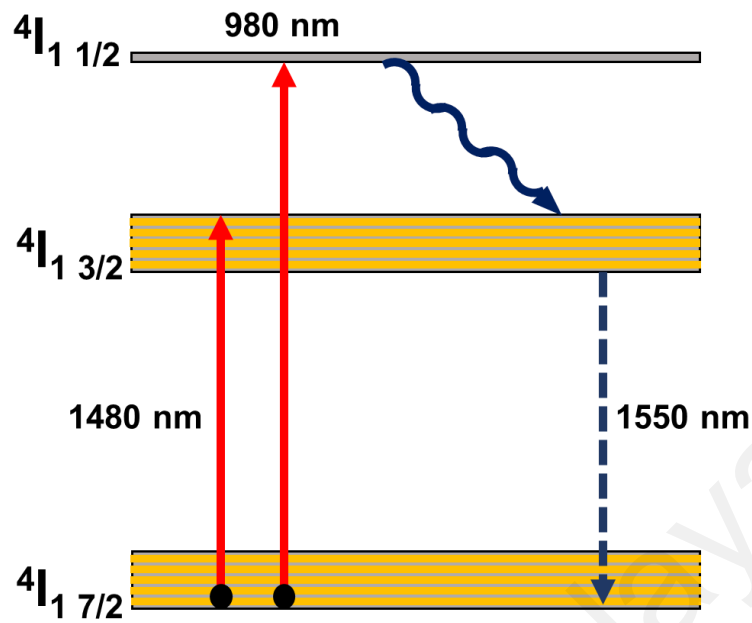
Figure 2.2 : Energy level diagram for Er+3 ion. The 4I13/2 state is the metastable state (lifetime ≈ 10 ms).

The trivalent erbium ion, when pumped with 980 nm light, is excited to the ^{4}I$_{11/2}$ state, which decays to ^{4}I$_{13/2}$ as shown in (Figure 2.2). The decay between ^{4}I$_{11/2}$ and ^{4}I$_{13/2}$ is non-radiative (multiple phonon decay) and occurs within a few µs, while the metastable state (4 I13/2) has a lifetime of ≈ 10 ms. Since the ^{4}I$_{11/2}$ state has such a short lifetime, we can make the approximation that this highest excited state has zero steady-state population (i.e. no population accumulates). This approximation reduces the number of participating energy levels to two; the upper ($N2$) and lower ($N1$) energy levels. These levels describe the number of erbium ions, where the rate equations can be written as;

$$\frac{dN_1}{dt} = A_{21}N_2 + (N_2\sigma_e^s - N_1\sigma_e^s)\frac{I_s}{h\nu_s} + \left(N_2\sigma_e^p - N_1\sigma_a^p\right)\frac{I_p}{h\nu_p} \qquad (2.1)$$

$$\frac{dN_2}{dt} = -A_{21}N_2 + \left(N_1\sigma_a^s - N_2\sigma_e^s\right)\frac{I_s}{h\nu_s} + \left(N_1\sigma_a^p - N_2\sigma_e^p\right)\frac{I_p}{h\nu_p} \qquad (2.2)$$

where A_{21} represents the spontaneous emission while $\sigma_{e(a)}^{s(p)}$ represents the cross section for stimulated emission (absorption) at signal (pump) wavelength. $I_{s(p)}$ is the signal (pump) intensity and $h\nu_{s(p)}$ is the energy of each individual signal (pump) photon. The total number of photons passing through a given area or photon flux can be obtained by dividing the beam intensity by the photon energy of the beam.

Population inversion must be obtained to achieve lasing and thus $N_2 > N_1$. The threshold of the laser operation occurs when the ion density in N_2 just equals N_1. By setting the equations (2.1) and (2.2) equal and solving for the pump intensity, the threshold intensity for the population inversion is obtained as;

$$I_{pth} = \frac{h\nu_p}{\tau(\sigma_a^p - \sigma_e^p)} \qquad (2.3)$$

For 980 nm pumping, this intensity is calculated to be around 6 kW/cm^2. Since the mode field area of a single mode Erbium-doped fiber (EDF) is around 20 μm^2, the pump threshold is estimated to be in the order of a few mW for a lossless cavity. However, due to the losses in the coupling of the pump diode to the fiber, the output coupler and splicing points, the actual pump power threshold is on the order of 10s of mW.

The evolution of signal beam as it propagates through the active fiber is governed by the following simple differential equation;

$$\frac{dI_s(z)}{dz} = (N_2\sigma_e^s - N_1\sigma_a^s)I_s(z) \Rightarrow I_s(z) = I_0 e^{gl} \qquad (2.4)$$

where I_0 is the signal intensity entering the gain medium, g is the gain (g = $N_2\sigma_e^s - N_1\sigma_a^s$) and l is the total length of the active fiber. Assuming the absorption of the signal

beam is zero, thus $g = N_2\sigma_e^s$. The gain is then dependent only on the population of the excited state (N_2) and the emission cross section of the excited Erbium atoms at the signal wavelength (σ_e^s). The emission cross section is a constant, thus to determine the gain, only N_2 should be found. Using Equation 2.4, the evolution of N_2 can be simplified as;

$$\frac{dN_2}{dt} = -A_{21}N_2 + (-N_2\sigma_e^s)\frac{I_s}{hv_s} + (N_1\sigma_a^p)\frac{I_p}{hv_p} \tag{2.5}$$

In the small signal regime, the pump intensity is much larger than the signal intensity ($I_p \gg I_s$). Using this approximation along with the fact that we are analyzing a steady-state scenario (d=dt → 0) we can ignore the I_s term and set the left-hand side of Equation 2.5 equal to zero. Solving for N_2 yields:

$$N_2(I_s \ll I_p) = \tau N_1\sigma_a^p\frac{I_p}{hv_p} = \tau R \tag{2.6}$$

where τR is the rate at which ground state atoms are excited to the metastable state. This equation shows that the density of excited atoms in the small-signal regime is simply given by the lifetime of the exited state (τ) multiplied by excitation rate R. Using the fact that $g = N_2\sigma_e^s$, the small signal gain is $g_o = \tau N_2\sigma_e^s R$.

As the signal beam is increased to higher intensity, however, we must take into account the term in Equation (2.6) that involves I_s. Solving for N_2 yields:

$$N_2 = \frac{N_2(I_s \ll I_p)}{1 + I_s/I_{sat}} \tag{2.7}$$

And the large input signal gain is thus;

$$g = \frac{g_o}{1 + I_s/I_{sat}} \tag{2.8}$$

where $I_{sat} = 1/\sigma_e^s \tau$ is the saturation intensity. Then, the differential change in signal intensity per length of gain in the strong pump regime is given as;

$$\frac{dI_s}{dz} = \frac{I_s g_o}{1 + I_s/I_{sat}} \qquad (2.9)$$

The picture of the signal evolution is now complete. At low input signal regime, there is an exponential increase in the number of signal photons in the gain medium. However, as the signal level is increased further the gain begins to saturate and asymptotically approaches a value of $\sim I_{sat} g_o = R$. Thus, at high input signal regime, the signal intensity increases linearly with the pump intensity.

The fundamental characteristics of lasing, small-signal gain, and gain saturation have now been explained for Erbium-doped fiber laser (EDFL). The laser is used extensively throughout this thesis.

2.4   Operating regimes of a laser

Generally, the operating regimes of the laser are classified based on their temporal characteristics of output emission into few main modes – continuous wave (CW), Q-switching, mode-locking, and Q-switched mode-locking (Itoh et al., 2011; U. Keller, Weingarten, Kartner, Kopf, Braun, Jung, Fluck, Honninger, Matuschek, & derAu, 1996). The output power of CW mode is stationary while the other modes exhibit non-linear or pulsation output over time (Figure 2.3). This study focused on the generation of pulsed laser in Q-switching and mode-locking region using self-fabricated passive saturable absorbers (SAs).

(a)

(b)

(c)

(d)
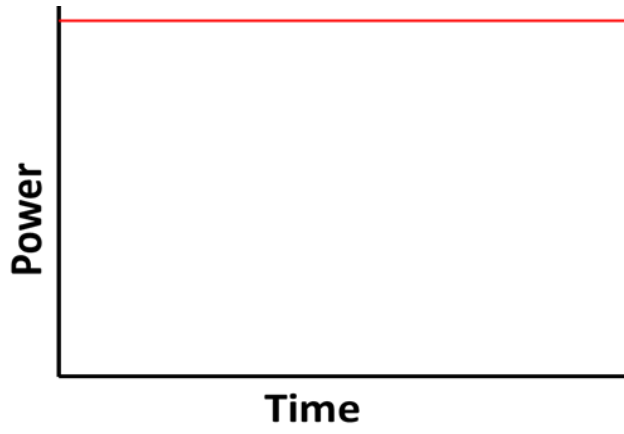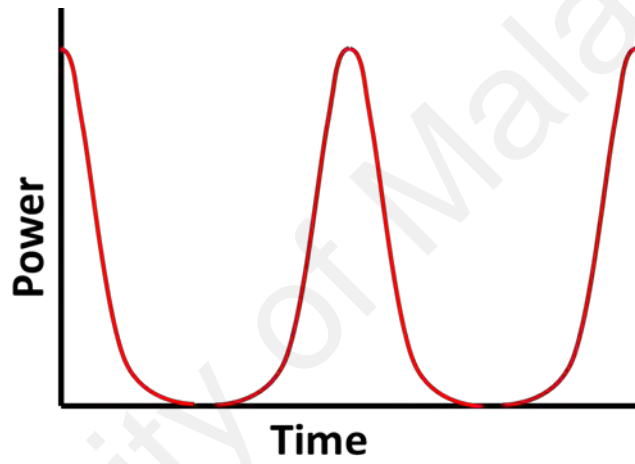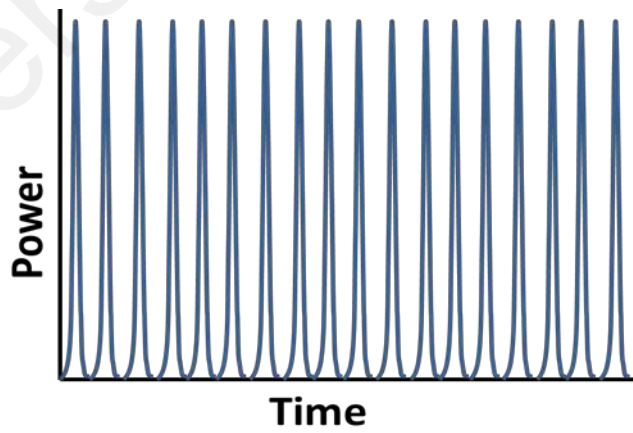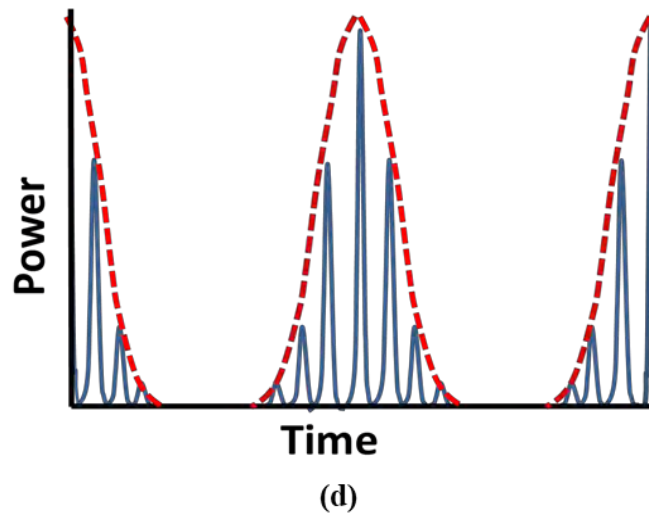
Figure 2.3 : Different types of laser operating regime. (a) Continuous wave (CW) (b) Q-switching. (c) CW mode locking. (d) Q-switched mode locking (Adapted from Keller et al., 1996).

2.5   Q-switched fiber lasers

This chapter describes the basic principles of Q-switching. The most common Q-switching methods are reviewed with a focus on passively Q-switched fiber lasers.

2.5.1   Basic principles of Q-switching

In general, Q-switching laser is a pulsed laser with the ability to store maximum potential energy and generate huge energetic pulses within a short time domain (typically in the range of nanoseconds) by modulating its intra-cavity losses mechanism. The Q value (also known as the quality factor) can be calculated by the equation (Xinju, 2010) :

$$Q = 2\pi v_o \left(\frac{energy\ stored\ in\ cavity}{energy\ lost\ per\ second} \right) \qquad (2.10)$$

Where

v_o represents the laser's central frequency.

To further simplify the equation, the assumption made is as follow:

- *W* represents energy stored within the cavity.

- δ denotes the rate of energy loss for single-path light propagation within the laser cavity.

Suppose:

L represents the resonator length,

n represents the medium's refractive index, and

c represents light velocity.

Then duration of single-path light propagation is given as:

$$= \frac{c}{nL}$$

Energy stored: $\qquad = W$

Energy lost per second:

$$= \frac{\delta W c}{nL}$$

And equation 2.1 becomes

$$Q = 2\pi v_o \frac{W}{\delta W c / nL}$$

$$= \frac{2\pi n L}{\delta \lambda_o} \qquad (2.11)$$

λ_o is the central wave length of laser in the vacuum.

Q value is inversely proportional to the resonator loss (δ) with the condition values of λ_o and L are definite (equation 2.11) and their relationships with the light oscillation occurring within the laser's cavity are as summarized below:

a) When Q value is low due to high loss (δ), the oscillation initiation threshold is increased, making initiation harder.

b) When Q value is high due to minimal loss (δ), oscillation is easily started due to the resulting low initiation threshold.

Based on equation 2.11, laser's threshold can be easily modified by applying a sudden change to the loss (δ) or the Q value of the resonator (Xinju, 2010). Changes in δ of a resonator will modify the Q value accordingly, resulting in a Q-switched operation. The modulation of δ within the laser's cavity can be performed either actively or passively, using modulators or SAs respectively. The mechanism underlying the Q-switch operation involves the building up of a large inversion by the pumping of laser while the resonator losses are sustained at high levels, resulting in a large gain of stored potential energy in the laser medium. When the resonator δ is reduced abruptly, the stored energy is then released in the form of an intense pulse (M. C. Gupta et al., 2006). Usually, spontaneous emission denotes the start of pulse growth. The high initial inversion will drop and peaks again, producing pulses. Generally, Q-switched lasers are applied in fields that need short pulses but with high pulse energies and peak powers (Siegman, 1986).

2.5.2 Active Q-Switching

Active Q switching involves the use of external means to modulate the loss inside the laser cavity, such as the use of an acousto-optic modulator (AOM) – diffract and change light frequency using sound waves (Riesbeck et al., 2009) or electro-optic modulator (EOM) – modify phase, frequency, amplitude or polarization of light beam using an optical device with electro-optic effect (Foster et al., 2006; Y. Zhao et al., 2000), thereby controlling the output characteristics of the generated pulse.

2.5.3 Passive Q-switching

In contrast to its active counterpart, a passively Q-switched laser does not require an external modulator as the cavity loss is controlled by SA. This makes passive Q-switching low cost, easier to implement and simpler to operate (Popa et al., 2011; Popa et al., 2010).

There are several types of SAs with different parameters, for different applications, including metal doped crystals (Laroche et al., 2002; Philippov et al., 2004), Semiconductor saturable absorber mirrors (SESAMs) (U. Keller, 2003; Spuhler et al., 2005), SWCNTs (F. Ahmad et al., 2014; Ismail et al., 2012; Rozhin et al., 2004), graphene (A. C. Ferrari et al., 2006; H Haris et al., 2015; H. Yang et al., 2014), graphene oxide (GO) (Adnan et al., 2016; Markom et al., 2018; Saleh et al., 2014) and reduced graphene oxide (rGO) (Guo et al., 2012; S. Liu et al., 2012; Z. Yin et al., 2012). There are also devices that exhibit decreasing optical losses for higher densities artificially by polarization effect, such as the nonlinear polarization rotation (NPR) (Anyi, Haris, et al., 2013; Matniyaz, 2018; W. Wang et al., 2012). The transmission of SA is dependent on the incoming light intensity, i.e., absorption will occur to light with low intensity while light with high intensity will be released, based on the recovery period.

2.6   Mode-locked fiber lasers

The term mode-locking refers to the requirement of phase locking many different frequency modes of a laser cavity. This locking has the result of inducing a laser to produce a continuous train of extremely short pulses rather than a CW of light. In principle, though, a continuous train of pulses can be generated by a Q-switching technique as described in the previous sub-section. The difference between these two pulsing mechanisms lies in the optical phase of the pulses. The mode locked pulses are phase coherent with each other, while the Q switched pulses are not. This simple fact has massive implications in regards to the application of these two types of lasers.

To understand the mode locking process, we will begin by looking at a CW laser with a Fabry-Perot cavity in the frequency domain. Fig. 2.4 (a) shows a single longitudinal mode CW laser where only one resonant mode of the laser cavity ($v=c/2nL$) overlaps in frequency with the gain medium. Thus, the laser emits a CW beam with a narrow range of frequencies ($E(t) = E_1 e^{i(\omega_1 t + \phi_1)}$). In general, however, the gain medium could overlap with several modes and the output of such a laser can be described in the time domain as:

$$E(t) = \sum_n^N E_n e^{i(\omega_n t + \phi_n)} \tag{2.12}$$

where the sum is over all of the lasing cavity modes, E_n is the amplitude of the nth mode, ω_n is the angular frequency of the nth mode, and ϕ_n is the phase of the nth mode. For the single-mode laser, this sum just has one term as given above. As we will see, the phase term plays the key role in the difference between incoherent multimode lasing and mode locking.

As the gain bandwidth of the laser is increased to overlap with more of the cavity modes as shown in (Figure 2.4 (b)), multimode lasing will be generated. In this configuration, there are 3 terms in Equation (2.13). The output of such a laser depends critically on the phase relationship between the 3 modes. If each mode has a randomly varying phase with respect to the other modes, then a time domain detector on the output would show us that the laser is emitting a CW beam with a large amount of intensity noise as shown in (Figure 2.5 (a)), while a frequency domain detector would show us that the energy was contained in narrow spikes (with lots of intensity noise) spaced evenly by the free spectral range (FSR) of the cavity. However, if we can fix the relative phases to a set value, then the situation changes dramatically (Figure 2.5(b) and (c)). With fixed phase relationships, the three modes can combine to interfere in such a way as to constructively interfere at multiples of the roundtrip time of the cavity, while they destructively interfere elsewhere. This process creates shorter pulses as the number of phase locked modes increases.

(a)

(b)
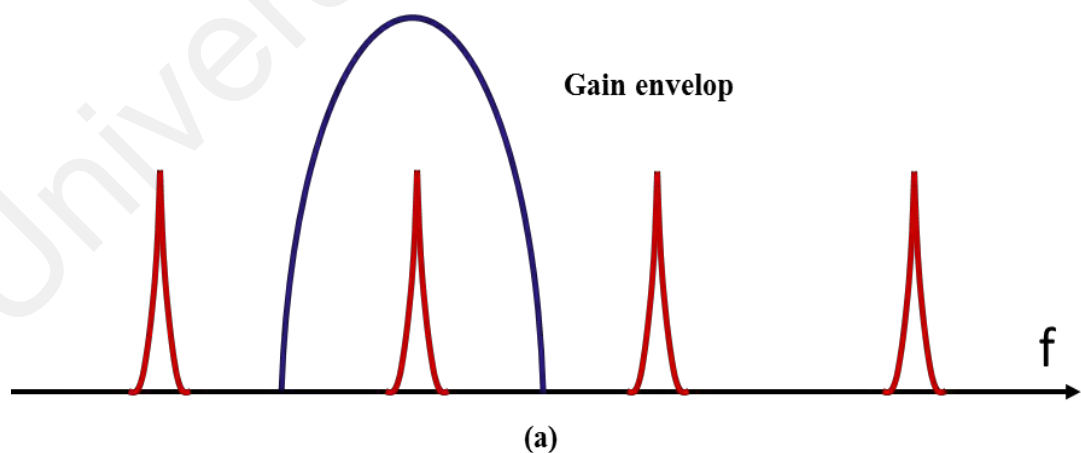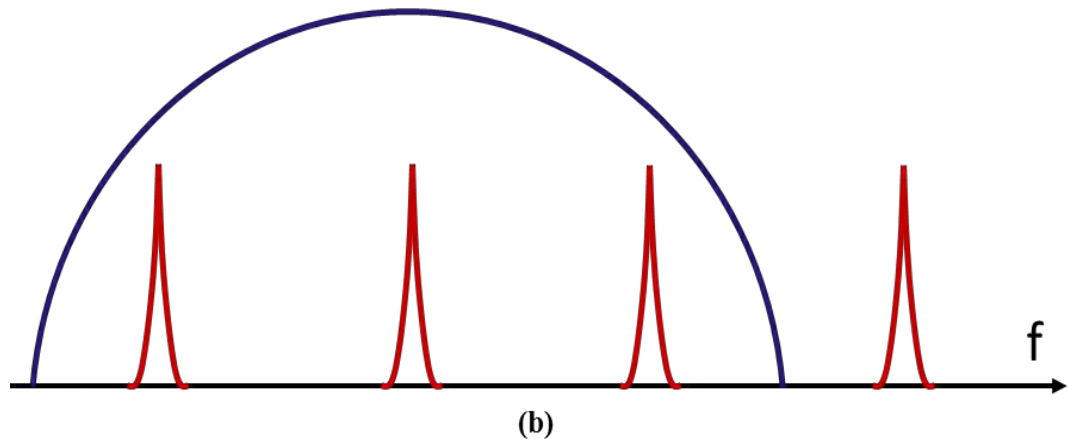
Figure 2.4 : Resonant cavity modes and the gain spectrum of a laser for (a) single mode lasing (b) multimode lasing
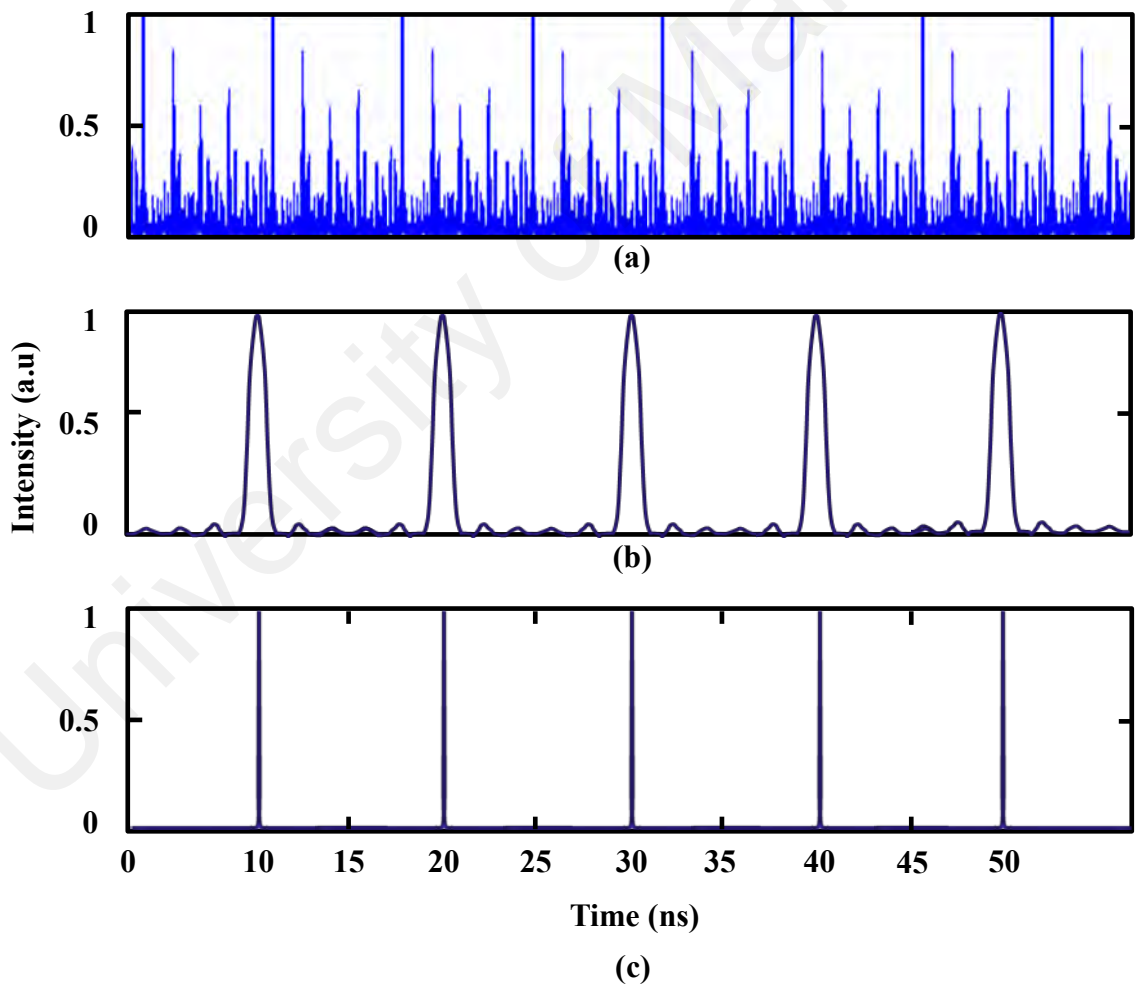
Figure 2.5 : The output pulse train in time domain when (a) No phase coherence between the multiple longitudinal modes (b) 10% of the modes are phase coherence (c) all the modes are phase coherence.

Mode-locking is a technique to generate an ultrashort pulse laser. It can be realized using a passive technique based on SA. An ultrashort pulse can emerge when a SA modulates the loss once per cavity round-trip and all longitudinal modes have a fixed phase relationship (Faubert et al., 1982; Meiser, 2013; Trebino, 2012). Thus, the mode-locking of the oscillating laser produces an ultrashort pulses train (ranging from ns to fs duration) at defined repetition rate in MHz corresponding to the free spectra range of laser cavity or the number of obtained pulses per second (M. Fermann et al., 1997; Haus, 2000; Riidiger Paschotta et al., 2003). The estimation of pulse repetition rate, f in passive mode-locking technique is given by;

$$Repetition\ rate, f\ (ring\ cavity) = \frac{c}{nL} \tag{2.13}$$

where c, n, and L denote the speed of light $(3 \times 10^8 ms^{-1})$ refractive index of the medium (1.46 for silica fiber), and total cavity length, respectively. It is shown from the equation that the repetition rate is determined by the total cavity length for a passive mode-locking, and therefore, the higher pulse repetition rate is obtained for a shorter cavity length.

The pulse width of the laser indicates the full width at half maximum (FWHM) of the power versus time and a very short pulse width can be realized by a mode-locked laser. The higher numbers of longitudinal modes that have a fixed phase relationship can translate to a shorter pulse width. The short pulse duration of the mode-locking mode is useful for many applications including fast optical data transmission, and time-resolving process. The relationship between pulse width and bandwidth of the optical fiber pulses is referred to a time bandwidth product (TBP). As described by the principle of Heisenberg, the TBP of the pulse is impossible to drop below a limit of TBL,

$$T_{BL} \leq \Delta t \times \Delta v \qquad (2.14)$$

where Δt and Δv denotes the temporal width (in seconds) and the spectral width (in hertz) of the pulse, which measured at FWHM. The limit of TBP or T_{BL} is depended on the pulse shape. The bandwidth of the pulse is depended on the spectral bandwidth and operating wavelength of the output spectrum of the laser. It is given as;

$$The\ bandwdith\ (BW)\ = \Delta\lambda \times \frac{c}{\lambda^2} \qquad (2.15)$$

where Δλ is th spectral bandwidth at FWHM, and λ is the center of the wavelength of output spectrum. The pulse width is given as;

$$Pulse\ width\ (PW) = \frac{T_{BL}}{BW} \qquad (2.16)$$

From both equations (2.15) and (2.16), it is obtained that the pulse width can also be estimated from a given optical bandwidth. Generally, the pulse width of mode-locking pulses is usually measured by using an auto-correlator, which its function according to the estimated pulse shape. The pulse shape consists of Gaussian, and Secant hyperbolic, depending on the output spectrum, characteristic of the mode-locking operation, and total cavity dispersion. The Gaussian pulse shape is obtained when the cavity dispersion is closed to zero or equal to zero as in a stretched pulse laser. Mode locking methods can be divided into two classes: active and passive. In active mode locking, some external source is used to drive the mode locking element, while in passive mode locking a saturable absorber is commonly used.

Mode locked pulses in time and frequency domains are shown in (Figure 2.6). In the time domain, the mode locked laser produces an equidistant pulse train, with a period defined by the round-trip time of a pulse inside the laser cavity TR and a pulse duration τp (U. Keller, 2003). In the frequency domain, this results in a phase locked frequency

comb with a constant mode spacing that is equal to the pulse repetition rate vR = 1/TR. The spectral width of the envelope of this frequency comb is inversely proportional to the pulse duration. The fundamental repetition rate of a mode lock laser is determined by its cavity length, as shown in the equations below.

$$\text{Repetition rate (for linear cavity)} = \frac{c}{2nL} \tag{2.17}$$

$$T_R = \frac{2nL \text{ (for linear cavity) or nL (for ring cavity)}}{c} \tag{2.18}$$

Equations (2.17) and (2.18) can be used to calculate the fundamental repetition rate for linear and ring cavity respectively. Here, c, n and L represents the speed of light, refractive index and length of the cavity respectively. As the round-trip time, TR, is the inverse of repetition rate, therefore, TR is depending on the cavity type. Sometimes the repetition rate can be some integer multiple of the fundamental repetition rate. In this case, it is called harmonic mode locking (Becker et al., 1972).
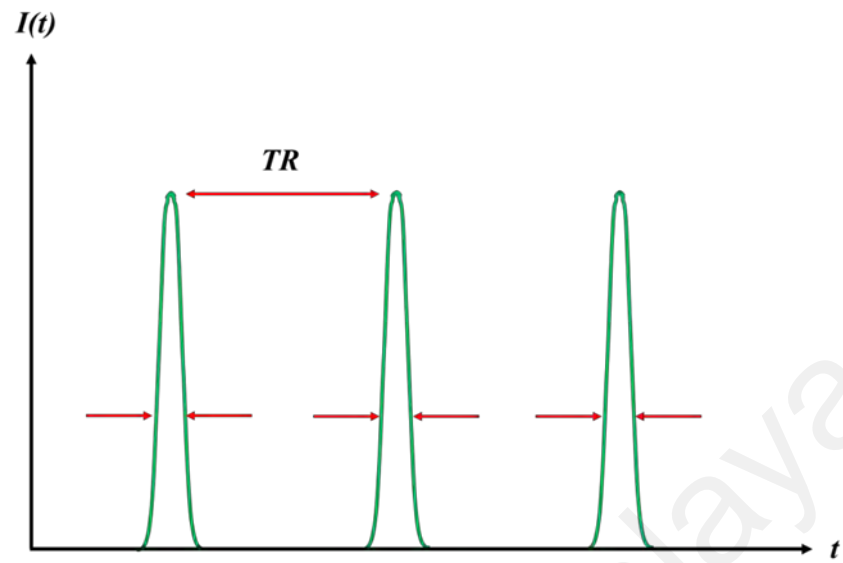
Time domain

(a)
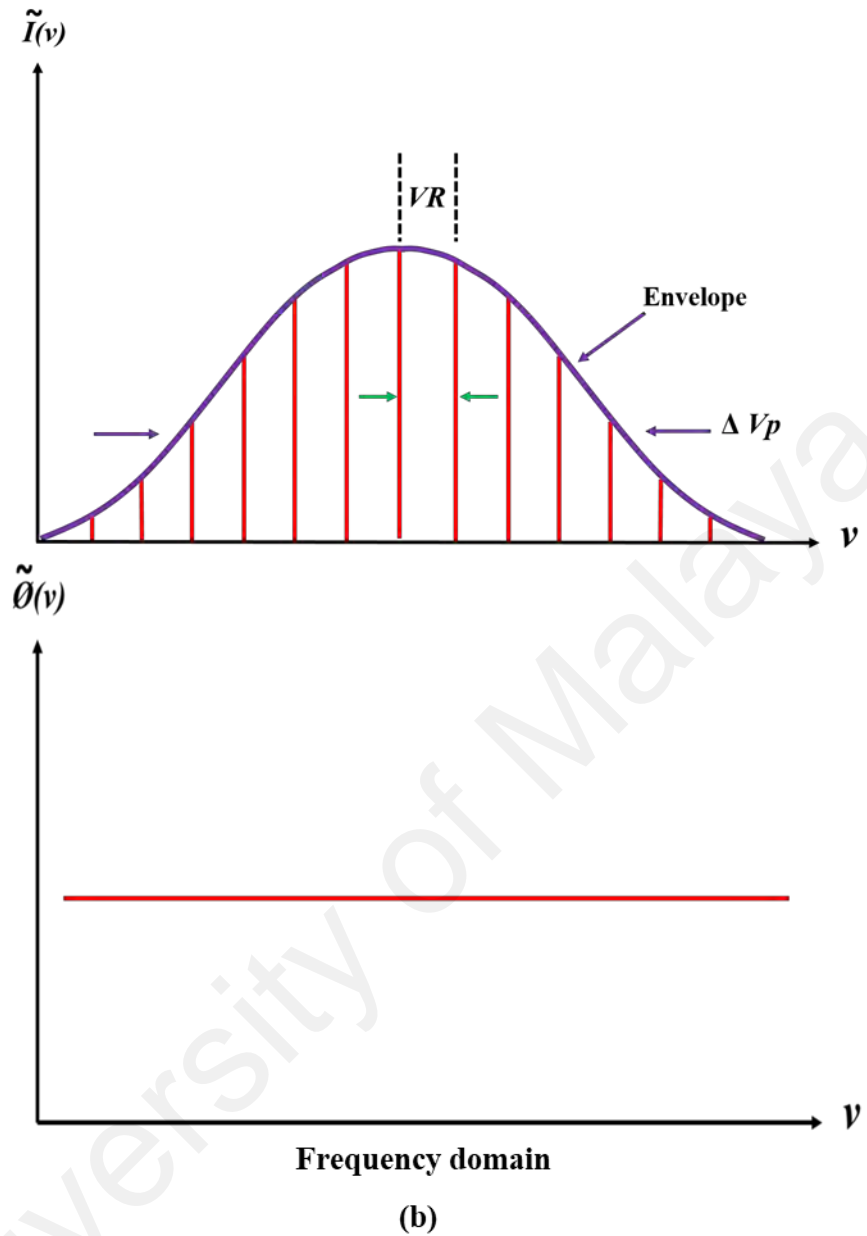
Figure 2.6 : Mode-locked pulses in (a) the time and (b) frequency domain (Keller, 2003)

Active mode-locking requires an active element driven by an external electronic signal to modulate the loss inside the fiber cavity. There are two type types of modulator which is amplitude modulation (AM) and frequency modulation (FM) (Bowers et al., 1989; A. Siegman et al., 1974). The used of modulator is to provide a high-speed pulse train that an order higher of the fundamental repetition rate. In AM mode locking, the loss cavity is periodically modulated and the pulse is built up at the position, having a minimum loss in the fiber cavity. The repetition rate reported by applying AM for mode locking as high as 3.77 GHz (K. K. Gupta et al., 2002). FM mode locking is carried out by repeated up or down frequency chirping. After many round trips is built up and shortened because the chirped light is swept out of the gain bandwidth of the laser. By applying FM for mode locking, the repetition rate of about 40 GHz was reported with a shorter pulse width compared to AM mode-locking (Nakazawa et al., 2000).

2.6.1 Historical Perspective of Mode Locking

Mode-locking was first proposed theoretically in the mid-1960s (Lamb Jr, 1964), shortly followed by the first demonstration of active mode-locking using a HeNe laser (Hargrove et al., 1964). Passively mode-locked lasers were also demonstrated soon after based on a ruby laser (Mocker et al., 1965), and an Nd:glass laser cavities (DeMaria et al., 1966). However, the development of passively mode-locked laser was plagued by the problem of self-Q-switching instabilities in solid-state lasers. This continued to be a problem for most of the passively mode-locked solid-state lasers until the first intra-cavity saturable absorber was designed correctly in 1992 to prevent self Q-switching instabilities (U Keller et al., 1992). For some time, in the 1970s and 1980s, the good progress in passively mode-locking using dye lasers had diverted research interest away from solid-state lasers. Q-switching instabilities are not a problem for dye lasers. The first passive mode-locked dye laser with subpicosecond was demonstrated in 1974 (Shank et al., 1974), followed by sub-100 fs in 1981 (R. Fork et al., 1981). Kerr lens mode locking of

Ti:sapphire laser was discovered in 1991 to produce the shortest laser pulses (Spence et al., 1991; Telle et al., 1999). In 1992, self-starting and stable passive mode locking was demonstrated for the first time using semiconductor saturable absorber mirrors (SESAMs) as a saturable absorber (U. Keller et al., 1992). Recently, carbon nanotubes and graphene have been used in passively mode-locked lasers as saturable absorbers (Q. Bao et al., 2009a; S. Y. Set et al., 2004; Han Zhang, Tang, Zhao, Bao, et al., 2009). They have the benefits of faster response times than SESAM and can be directly deposited on the fiber end. Further discussion of passive mode locking based on new nanomaterials as saturable absorbers will be presented in the next section.

2.6.2   Active mode-locking

Active mode-locking requires an active element driven by an external electronic signal to modulate the loss inside the fiber cavity. There are two type types of modulator which is amplitude modulation (AM) and frequency modulation (FM) (Bowers et al., 1989; A. Siegman et al., 1974). The used of modulator is to provide a high-speed pulse train that an order higher of the fundamental repetition rate. In AM mode locking, the loss cavity is periodically modulated and the pulse is built up at the position, having a minimum loss in the fiber cavity. The repetition rate reported by applying AM for mode locking as high as 3.77 GHz (K. K. Gupta et al., 2002). FM mode locking is carried out by repeated up or down frequency chirping. After many round trips is built up and shortened because the chirped light is swept out of the gain bandwidth of the laser. By applying FM for mode locking, the repetition rate of about 40 GHz was reported with a shorter pulse width compared to AM mode-locking (Nakazawa et al., 2000).

2.6.3   Passive mode locking

Passive mode locking is a method that not requires any external trigger where the nonlinear element is part of the laser cavity. The characteristic of the output pulse is governed by the material used as saturable absorber (Martin E Fermann et al., 1995; U. Keller, 2003). They are two types of saturable absorber either artificial effect or a real saturable absorber. In this work, the major interest is to fabricate saturable absorber for passively mode-locked fiber laser. Thus, this section will review more on passively mode-locked fiber laser by employing a nonlinear polarization rotation (NPR) method; SESAMs, graphene and topological insulator based saturable absorber.

2.6.4   Soliton Pulse Lasers

The term 'soliton' was introduced by Zabusky and Kruskal in 1965, which was originally used to refer to localized solutions of integrable nonlinear systems (Zabusky et al., 1965). Such solutions are extraordinary because solitons maintain their shape and velocity after interfering with each other and remain in order when interacting with radiation waves. In optics, integrable conventional solitons result from the interplay between the dispersion and nonlinear effects (Grelu et al., 2012). Also, the word soliton refers to special kinds of wave packets that can propagate undistorted over long distances (Q. Lin et al., 2007) . Soliton pulses are largely shaped by the GVD and SPM. The saturable absorber does not need to be fast, only to initiate and stabilize the pulses against the broad continuum pulses (Y.-Y. Liu et al., 2016). Soliton mode-locking operates in an anomalous dispersion regime with a hyperbolic secant (sech2) intensity profile (Haus, 2000; Xueming Liu, 2011).

2.6.5   Bound soliton mode locking

Bound states of solitons known as high-order soliton solutions of the nonlinear Schro̎dinger equation (NLSE) have been extensively studied (Blow et al., 1988; Merle et al., 2005; Serkin et al., 2002). A bound state of solitons of the NLSE is formed because two or more fundamental solitons coexist, and they have the same velocity and locate at the same position. Recently, another form of bound solitons has also been theoretically predicted (Z. Wang et al., 2015; R. I. Woodward et al., 2015) to exist in nonlinear dynamical systems such as the Ginzburg-Landau equation (Akhmediev et al., 2005; Deissler, 1985; Doering et al., 1988), and the coupled nonlinear Schro̎dinger equations (Bandrauk et al., 1994; Radhakrishnan et al., 1995; Zakharov et al., 1982). In contrast, the formation of these bound solitons is due to a direct interaction between the solitons, and the propagation of them is characterized by the fact that the solitons have discrete, fixed separations. It is well known that the dynamics of passively mode-locked fiber soliton lasers can be well modelled by the complex Ginzburg-Landau equation (Akhmediev et al., 2005; Deissler, 1985). The same equation also describes the soliton propagation in the long-distance optical transmission lines (Evangelides et al., 1992; Mollenauer et al., 1986). It would be expected that the predicted bound states of solitons could be observed in these systems. However, to the best of our knowledge, so far no bound states of solitons of this form have been experimentally confirmed in the systems. Two effects in optical fibers are detrimental to the formation of the predicted bound states of solitons. One is the Raman effect. Theoretical studies have shown that a strong Raman effect destroys the bound solitons (Q. Bao et al., 2009b; Bednyakova et al., 2013; Su et al., 1980). Another one is the random-phase variations of the solitons, which causes random soliton interactions. Although in fiber soliton lasers, the influence of the Raman effect can be significantly reduced by the effect of laser gain dispersion (Bonaccorso et al., 2014; Chernikov et al., 1993), no efficient way has been found to suppress the random

relative phase variations between solitons. In this paper, we report on an experimental observation of bound states of solitons in a passively mode-locked fiber soliton laser. We confirm experimentally the existence of stable bound states of solitons with discrete, fixed soliton separations.

2.6.6   Vector soliton mode locking

Vector soliton solutions in PT-symmetric coupled waveguides and their relevant properties are considered by analytically and numerically solving the coupled nonlinear Schrödinger equations with linear-coupling and gain-loss effects (B. Liu et al., 2015; Suchkov et al., 2016). The results show that vector one- and two-soliton solutions, and even multi-soliton solutions are stable in certain regions against both initial random perturbation for amplitude and longitudinal random fluctuation along propagation direction for gain-loss. The Newton's cradle dynamics is also investigated (Driben et al., 2013). Based on vector soliton solutions on a finite background, nonlinear Talbot recurrence effects excited by linearly modulated continuous waves are discussed, and the results show that the recurrence patterns of the nonlinear Talbot effects can be drawn by suitably choosing a frequency modulation factor (Ambrosio; Garanovich et al., 2012). Finally, the evolution of the vector Peregrine solution is also studied by initially exciting a small localized perturbation on a continuous-wave background. Actually, solitons propagating in single mode fiber (SMF) can exhibit complicated polarization dynamics as the result of the SMF supporting the two orthogonal polarization modes (Collings et al., 2000; Ning et al., 2014). Except that the polarization-maintaining fibers are utilized in the fiber laser, the laser cavity always displays small amounts of random birefringence. Consequently, it is also significative to consider the vector nature of solitons generated in the fiber laser. Based on the laser cavities without the polarization discrimination devices, different vector soliton dynamics were observed in passively mode-locked fiber lasers, such as polarization-locked vector solitons (PLVSs) (H. Li et al., 2015; H Zhang et al.,

2008; L. Zhao et al., 2008), polarization-rotating vector solitons (PRVSs) (Mou et al., 2012; Jaroslaw Sotor et al., 2015; L. Zhao, Tang, Wu, et al., 2009), and group velocity locked vector solitons (GVLVSs) (Jin et al., 2016; Jin et al., 2015; Y. Luo et al., 2017). As mentioned above, the generation of multi-soliton patterns is an important physical phenomenon in fiber lasers. Thus, investigating vector nature of multi-soliton patterns is beneficial for further revealing the intrinsically physical features of multi-soliton dynamic patterns. For example, as a type of the multi-soliton patterns, soliton flow in fiber laser is a dynamic process. From the viewpoint of fundamental physics, it would be interesting to know whether the polarization-locked and the polarization-rotating vector soliton flow could be observed during its dynamic flowing or not. Thus, for further comprehending the fundamental physics of multi-soliton operations, there would be a strong motivation to investigate the vector nature of multi-soliton patterns.

2.7   Pulsed laser generation using SA

A saturable absorber (SA) is an optical component that exhibit reduced optical loss at high optical densities. Fundamentally, light is absorbed when the photon energy is enough to excite carriers to the conduction band from the valence band. However, strong excitation by high light intensies will saturate the absorption as the transition of carriers is hindered by the absence of more possible final states, thus resulting in lower absorption (Figure 2.7(a)). Pulses are formed when light intensity increase passes through the SA as only low intensity light will be suppressed (Figure 2.7(b)). This phenomenon is found to be occurring in different types of media as well, e.g. graphene, glasses, crystals doped with ions and semiconductors (Siegman, 1986; Zhipei Sun et al., 2010).
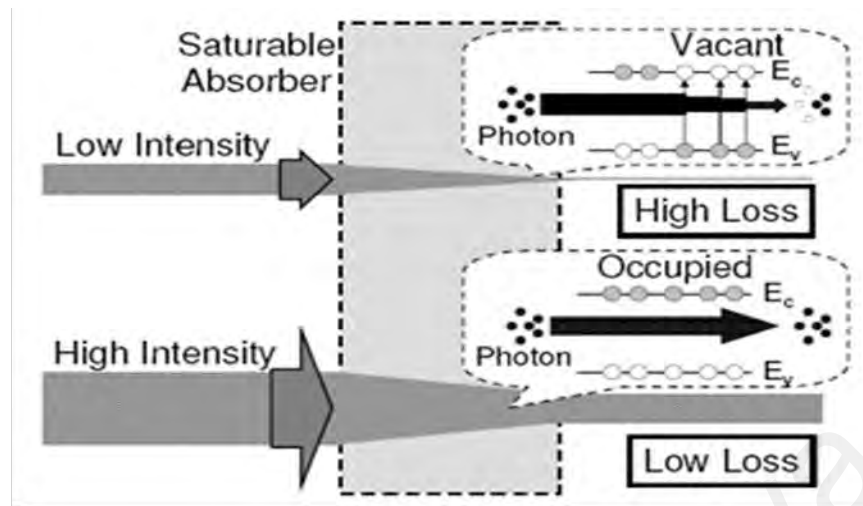
(a)
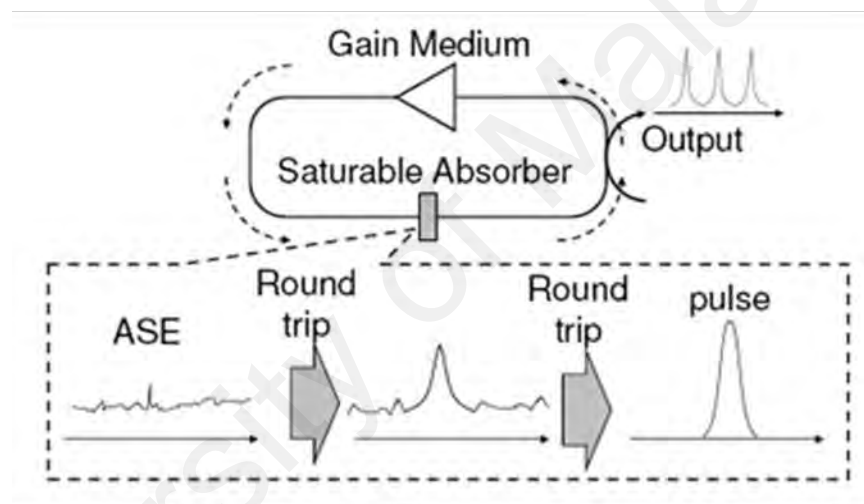
(b)

Figure 2.7 : Simplified illustration of saturable absorption. (a) Light incident at low intensities and high intensities – excitement of carriers to the conduction band from the valence band; (b) Pulse formation. (Adapted from Kashiwagi & Yamashita, 2009).

Incorporation of SAs in the generation of pulse laser optimizes several important parameters, including absorption (e.g. linear absorption, non-saturable losses ratio, and absorption saturation intensity and fluence), modulation depth, operation bandwidth, and damage threshold (U. Keller, Weingarten, Kartner, Kopf, Braun, Jung, Fluck, Honninger, Matuschek, & Au, 1996; Frank Wang et al., 2008).

2.8   Modulation depth and non-saturable loss

The SA fabricated has to be able to provide optical absorption (saturable and non-saturable losses) at the laser's operating wavelength. Since high light intensity reduces saturable loss, the loss can be minimized to zero ("bleaching") by the introduction or pulse with very high energy.

All mode-locking theories state that the pulse duration (τ) is inversely proportional to the modulation depth ($\Delta R \approx 2q_0$) of the SA (Antonelli et al., 2007; Boehm et al., 1962; I. Jung et al., 1997):

$$\tau \, \alpha \, \frac{1}{q_0^{\eta}} \tag{2.11}$$

q_0 denotes modulation depth; η represents a mode-locking theory-dependent factor.

On the other hand, non-saturable losses are usually caused by the malfunction of materials and can occasionally decrease a device's damage threshold. Generally, shorter pulses are generated by high modulation length. The total absorption should be sufficiently low such that the CW and mode-locking thresholds are still reachable, yet adequately high for the introduction of adequate saturable loss to discriminate different light intensities. The ratio of saturable to non-saturable loss should be maximized as any additional non-saturable loss would cause the laser to operate beyond its threshold, rendering it unstable.

2.9   Absorption saturation intensity and fluence

The absorption saturation intensity and fluence are among the important parameters in the generation of pulse lasers. When pulses were formed from the fluctuation of noises, SA acts as a fast SA (having a recovery time well below the width of the noise fluctuations). Thus, the CW intensity on the SA reflects the absorption saturation. The absorption coefficient for a two-level system can be represents by (Siegman, 1986):

$$\alpha = \frac{\alpha_0}{1 + \frac{I}{I_{sat}}} \tag{2.12}$$

α_0 , I and I_{sat} denotes the small signal absorption coefficient, CW intensity, and saturation intensity, respectively, as I_{sat} can be calculated by:

$$I_{sat} = \frac{hv}{\sigma_A T_A} \tag{2.13}$$

hv represents energy of photon, σ_A denotes transition's absorption cross section, and T_A represents the recovery period of the absorption saturation.

Absorption is said to be saturated when the intensity increases and the absorption coefficient approaches zero. Usually, high saturation intensity is required or else pulse cannot be formed due to insufficient modulation in absorption as the absorption is saturated by the intensity of CW.

2.10   Absorption saturation recovery time

The SA recovery time affects pulse formation, such as self-starting feature and the duration of minimum attainable pulse. It should be faster than the cavity round trip time in order to sufficiently distinguish between pulsed and CW operation (Geim et al., 2007; M. C. Gupta et al., 2006).

The SAs used in this study have a bitemporal response time (D. Sun et al., 2012). The relaxation time in time-resolved experiments is often classified into two typical time scales: fast and slow. A fast relaxation time (~100 fs) is often associated with the collision of carrier-carrier intraband and the emission of phonon; a slow relaxation time (on a picosecond scale) on the other hand is linked to the relaxation of electron interband and the cooling of hot phonons (Breusing et al., 2009; Kampfrath et al., 2005). This bitemporal response is beneficial in SA applications as slow time constant aids in self-starting while fast time constant enables short laser pulses to be generated.

Finally, an ideal SA needs only minor adjustment and friendly towards the laser design. On top of that, the SA should be easy to fabricate, cheap and can be multi-configured for integration into laser's cavity.

2.11   Wavelength dependence

Ideally, the absorption saturation would not be affected by the changing wavelength to avoid limit in generation of laser pulse by unnecessary introduction of a gain filter. Graphene and TIs based 2D nanomaterials SA exhibits a broad wavelength range which is wavelength independent due to the large absorption of incident light per layer and the ultrafast dynamics of charge carriers (Nair et al., 2008; G. Sobon, 2015; Shinji Yamashita, 2012).

Finally, an ideal SA needs only minor adjustment and friendly towards the laser design. On top of that, the SA should be easy to fabricate, cheap and can be multi-configured for integration into laser's cavity.

2.12   Two Dimensional (2D) Nanomaterials

The term nanomaterial was introduced in the 1970s to describe the low-dimensional nanomaterials structures with size-dependent properties. There are many layered nanomaterials with strong in plan chemical bonds and weak coupling between the layers. The structure of these layers provides the opportunity to be cleaved into individual freestanding atomic layers. These layers with one dimension precisely restricted to a single layer are called 2D nanomaterial (Butler et al., 2013; Nair et al., 2008). Recently, the fabrication of 2D nanomaterials have become an important field in current materials research due to their physicochemical properties, which are different from the bulk counterpart. Mainly, 2D nanomaterials with certain geometry show unique shape-dependent features and successful applications in nanoelectronics devices (Antonio H. Castro Neto, 2007; Xuesong Li et al., 2009). Also, 2D nanomaterials are developing innovative applications in electronics and optoelectronics (Q. H. Wang et al., 2012; Wilson et al., 1969). To this day, 'new' nanomaterials are emerging by exfoliating few-layer forms of existing materials and nanomaterial-enabled optical systems are beginning to transition from laboratories to commercial products. In this section the fundamental optical properties, production methods and optical characterization methods of three types of 2D nanomaterials will be discussed.

2.12.1 Graphene based saturable absorber

Graphene based saturable absorber is prospective candidate to generate ultrashort pulsed laser in broad wavelength. Graphene exhibit in layer form, thus not affected by diameter, which is one of the drawbacks of SWCNTs to be used in different wavelength region. Graphene exhibit with gapless band structure and this give advantages of the optical properties that independent of the wavelength. Graphene feature with strong optical nonlinearity and sub picosecond relaxation times that suitable for laser mode-locking in a wide spectral range (Z Sun et al., 2012; Zhipei Sun et al., 2010). The generation of ultra-short pulses achieved with graphene saturable absorber was first demonstrated by Zhang et al., 2009. Graphene synthesis for mode-locked fiber laser had been demonstrated using liquid phase exfoliation (LPE), chemical vapor decomposition CVD, carbon segregation, graphene oxide (GO), reduced (rGO) and micro-mechanical cleavage (Bonaccorso et al., 2010; Ganatra et al., 2014). The most common approach to integrate of graphene based saturable absorber is by sandwiching between fiber connector, apart from that, other reported method including free-space coupling, evanescent field interaction and placement inside PCF (D. Sun et al., 2012; K. Wang et al., 2013).
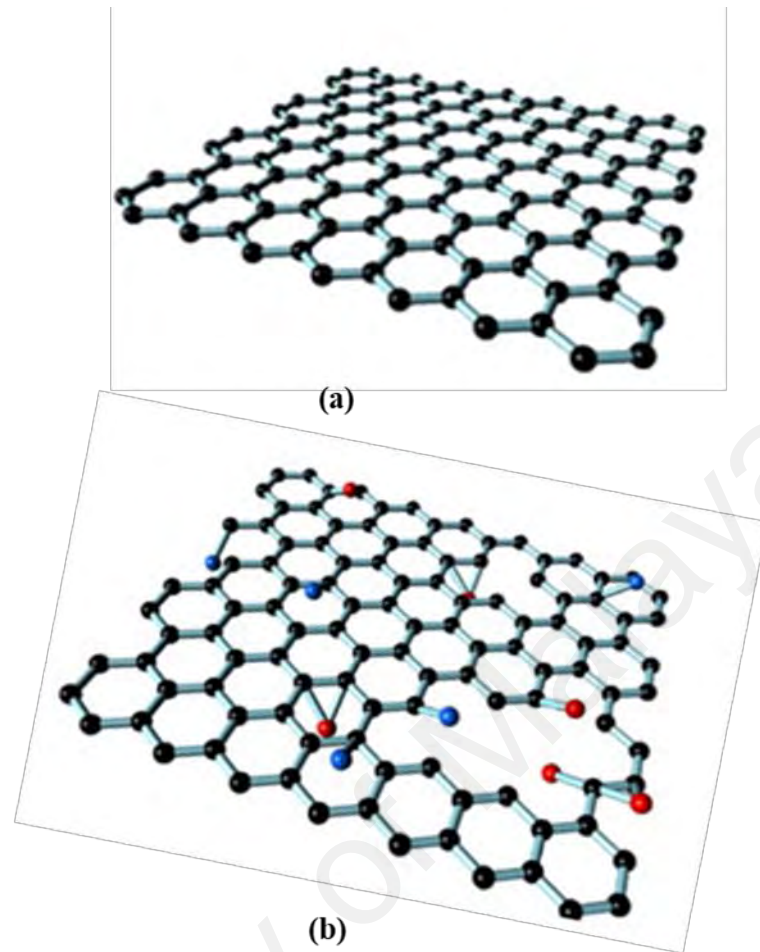
Figure 2.8 : The illustration of atomic arrangements in 2D nanomaterials, (a) graphene and (b) graphene oxide (Frindt et al., 1963; Geim et al., 2010).

2.12.2 Topological Insulator

Topological insulators (TI) are an exciting, new topic in condensed matter physics. The discovery of TIs was unusual for the field of condensed matter, in that they were predicted theoretically before they were observed in the lab. Several papers were published in 2005 and 2006 that predicted the existence of a type of material that would permit the movement of electrons only on its surface (Joensen et al., 1986; Mak et al., 2010), and TIs were observed later in 2007 (Splendiani et al., 2010). We in the field are interested in Topological Insulators because of their unique conductive properties. The

bulk of a TI acts as an insulator, while the surface allows the flow of electrons (Bertolazzi et al., 2011; Mak et al., 2012). Apart of TI as a piece of rubber or plastic with a thin layer of metal, only it achieves this conductive behavior by itself. You can achieve a similar effect through the Quantum Hall Effect. The (non-quantum) Hall Effect states that when you subject an electron current to a magnetic field, the carriers will tend toward one side of the conductor, creating a potential difference laterally within the material. In high quality samples at low temperatures, you can start to measure quantum effects on the carriers. The Quantum Hall Effect states that, due to quantum effects, the carriers that have collected along the edge will move along the surface. This is similar to the behavior in TIs, but they are able to do this without the use of an external magnetic field. TIs also have a unique effect on electron spin. The carriers that move along the surface of a TI are spin-locked (Frindt, 1965; Q. H. Wang et al., 2012). This means that the spin of each electron is perpendicular to its momentum. Figure 1a shows this as compared to a conventional insulator, and Figure 1b shows the band structure of a topological insulator.

Three main compounds of TI materials are Bismuth (III) Selenide (Bi_2Se_3), Bismuth (III) Telluride (Bi_2Te_3), and Antimony telluride (Sb_2Te_3). The Bi_2Se_3 and Bi_2Te_3 are binary chalcogenides of bismuth Bi_2X_3 with complex layer structures, as shown in (Figure 2.7) the crystal structure of Bi_2Se_3 and Bi_2Te_3, and directly react with the elements at 500-900ºC. Bi_2Se_3 and Bi_2Te_3 have small band gaps about 1.35 and 1.21 eV, respectively, so they exhibit semiconductor properties. They can be used in television cameras, optoelectronic and switching devices, and thermoelectric refrigerator due to their properties as thermoelectric and semiconducting materials. These materials can be synthesized by physical or chemical methods (Zhan et al., 2012). Chemical methods are widely used to prepare thin film of TI materials due to easy fabrication and large surface deposition (S. Wang et al., 2014).
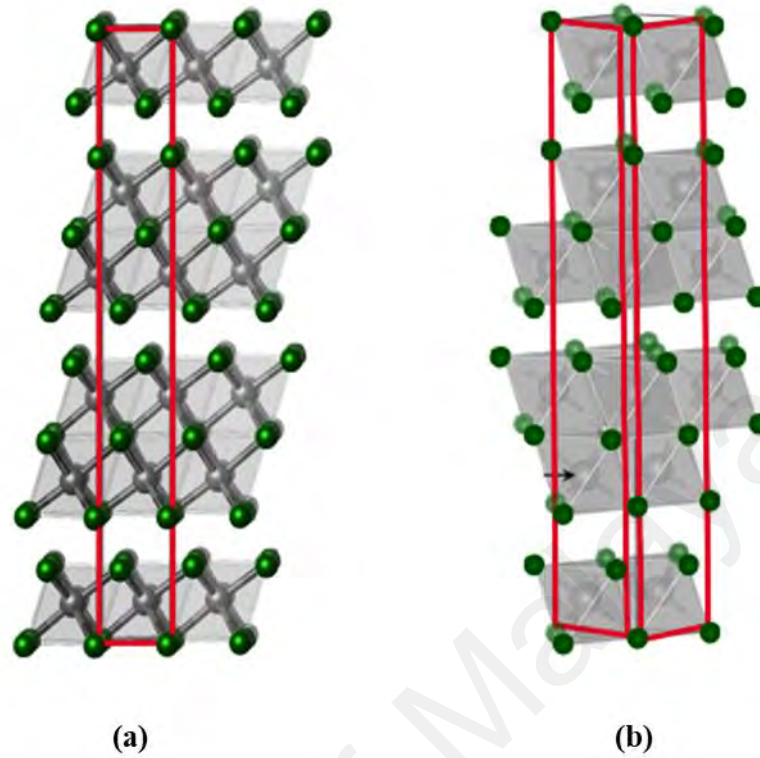
Figure 2.9 : The crystal structure of (a) Bi₂Se₃, and (b) Bi₂Te₃ (Coleman et al., 2011; R. Woodward, 2015).

TIs also have a unique effect on electron spin. The carriers that move along the surface of an electron spin (Kasap et al., 2006). This means that the spin of each electron is perpendicular to its momentum. (Figure 2.8 (a)) shows this as compared to a conventional insulator, and (Figure 2.8 (b)) shows the band structure of a topological insulator.
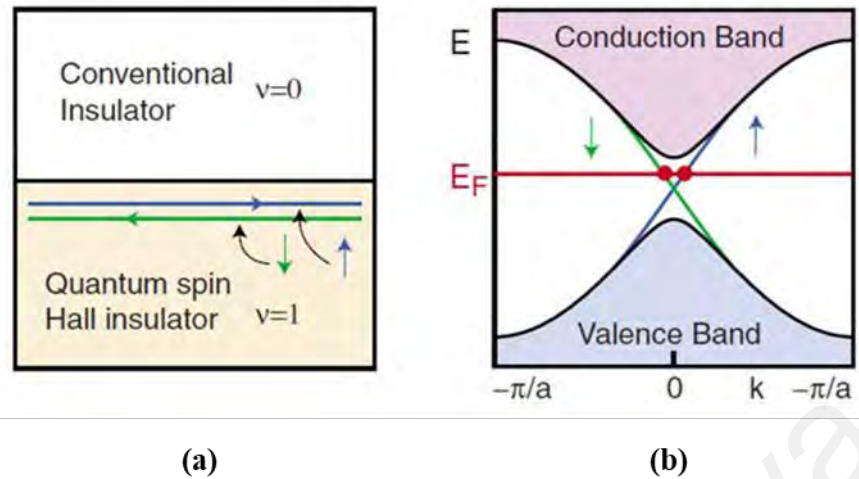
Figure 2.10 : (a) A visual representation of the quantum hall effect and (b) the band structure of a topological insulator (Druffel, 1997; R. Woodward, 2015).

As the electrons move to the right at the top of the material, their spins must be directed upwards. Those that move left have their spins reversed. These velocity-spin relationships would be switched for electrons at the bottom surface of the material. One effect of being spin-locked is that the electrons have a very high mobility, because scattering the carriers would require flipping their spin. This is impossible to do because that state is simply not available. These unique properties of TIs make them promising materials for research; there is great interest as saturable absorber to get mode-locked pulse.

2.13   Summary

This chapter has summarized the major historical developments leading to the success of fiber lasers today and introduced the main fundamental and technological concepts that use in this thesis. At first, the pulse generation techniques and the nonlinear effects in optical fiber have been briefly described. Also, the historical evolution of the saturable absorbers technologies has been highlighted and reviewed the fundamental optical properties, production methods and optical characterization methods of 2D nanomaterials, like graphene and Tis based. The following chapters intend to demonstrate, 2D nanomaterials as saturable absorbers for ultra-short pulse generation in ytterbium and erbium-doped fiber lasers.

CHAPTER 3: FABRICATION AND CHARACTERIZATION OF GRAPHENE AND TOPOLOGICAL INSULATOR AS SATURABLE ABSORBER

3.1 Introduction

Recently, two dimensional (2D) material, graphenes have obtained more interest for SA applications since they can in a wider spectral range without any chirality and diameter control (Z. Sun et al., 2010). Graphene is a flat monolayer of carbon atom tightly packed into two dimensional (2D) honeycomb lattice. It can be stacked to form 3D graphite, rolled to form 1D nanotube and wrapped to form 0D fullerenes (Allen et al., 2009). In 2008, Nair et al has demonstrated that despite being only one atom thick, graphene absorbs a significant ($\pi\alpha$=2.3%) fraction of incident white light due to its unique electronic structure. The optical absorption is also found to be frequency independent and proportional to the number of layers (Kuzmenko et al., 2008; Shinji Yamashita, 2012). Graphene oxide (GO) has also been seen as a good saturable absorber as an alternative form of graphene which exhibits ultra-fast relaxation and strong nonlinear saturable absorption (Bonaccorso et al., 2010; Sobon et al., 2016). Apart from that, fabrication of GO based SA is also easier due to the good solubility of the material in water (X. Huang et al., 2011).

In the past few years, investigation of new class of 2D nanomaterials, regarded as topological insulators (TIs) have also been carried out for various applications including mode-locked pulsed laser generation (Chi et al., 2014). They are s new kind of electronic state of matter, which have conducting states on the surface and then the electrons can only move along the surface of the materials and are an insulator in its interior that can support the conductive surface states (Sung et al., 2014). TI possess graphene-like energy bandgap structure with Dirac cones characteristics and exhibits a very broad and

relatively flat light absorption compared to graphene (J.-H. Yang et al., 2017). Additionally, TI also demonstrates high third order nonlinear refractive index, at the level of 10^{-14} m^2/W (S. B. Lu et al., 2013). Several TIs are identified such as Bi_2Te_3 and Bi_2Se_3 have found much attention (Sung et al., 2014).

In this chapter, the fabrication and characterization of graphene and TI based saturable absorbers are demonstrated.

3.2 Fabrication and characterization of graphene based SA

There are several approaches to synthesize graphene for SA applications such as liquid phase exfoliation (LPE) (Ciesielski et al., 2014), chemical vapour deposition (CVD) (Xuesong Li et al., 2010), reduced graphene oxide (rGO) (Sreeprasad et al., 2011) and micro-mechanical cleavage (Z. Sun et al., 2012). One of the drawbacks to the synthesis graphene by LPE method is the incorporation of organic solvents (J. T.-W. Wang et al., 2013; H. Yang et al., 2014). CVD approach in producing graphene flakes requires high temperature and difficult to transfer to devices, while chemical oxidation of graphite in rGO approach could disrupt the electronic structure of the produced graphene (Georgakilas et al., 2012). Graphene prepared by micro-mechanical cleavage using highly ordered pyrolytic graphite (HOPG) as starting material enabled a graphene samples with a good optoelectronics property (Bonaccorso et al., 2010; Trudeau, 2015), but the process is very tedious and time consuming as demonstrated by Chang et al., (2010).

Recently, electrochemically exfoliated graphene has been applied as conductive electrodes (Parvez et al., 2013). This cost effective and simple process in producing graphene flakes is attractive and should be explored for possible application in optoelectronics applications especially in ultrafast laser generation. Electrochemical exfoliation of graphite to produce graphene flakes require simple apparatus (DC power supply, graphite electrode and electrolyte), work at room temperature and the process

only took several hours to complete. Liu et al. (2008) demonstrated an electrochemical exfoliation graphene using two graphite rods in ionic liquids with a constant potential of 10–20V. Dimethylformamide (DMF) is used to disperse the graphene flakes and they characterize the graphene flakes with a length of 700nm, width of 500nm and thickness about 1.1 nm respectively.

In this section, a fabrication of graphene flakes is demonstrated using an electrochemical exfoliation process wherein a specific voltage is applied between the two graphite rods in ionic liquid and the exfoliation of the anode occurs after several hours (H. Haris et al., 2016; Wei et al., 2012). To prepare a SA film, the graphene flakes are mixed with polyethylene oxide (PEO) as the host polymer to form a precursor solution. A suitable amount of precursor was spread thinly on the petri dish and let dry in the room temperature to form the film based SA.

In constructing a graphene SA, the first step is to produce graphene flakes using the electrochemical exfoliation process. A constant voltage difference of 20 V was applied to two electrodes (graphite rods) placed 1 cm apart in an electrolysis cell filled with electrolyte (1% sodium dodecyl sulphate (SDS) in deionized water) as shown in (Figure 3.1). During the electrochemical exfoliation process, hydroxyl and oxygen radicals were produced due to electrolysis of the water at the electrode. The chemical reactions involved are;

$$H_2O \rightarrow OH^- + H^+ \tag{3.1}$$

$$CH_3(CH_2)\,11OSO_3Na \rightarrow CH_3\,(CH_2)11OSO^{3-} + Na^+ \tag{3.2}$$
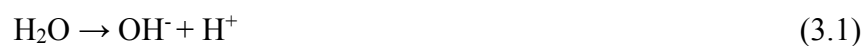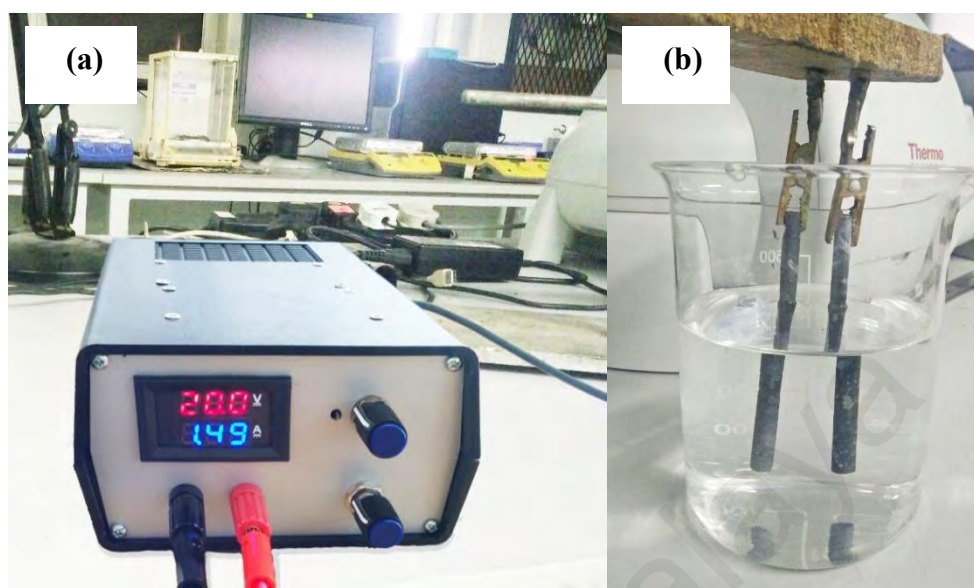
Figure 3.1: A real image of the experimental setup for electrochemical exfoliation of graphene (a) DC power supply (b) graphite rods as cathode and anode immerse in electrolyte.

When an electrical potential was applied between the electrodes, the negative ions moved towards the anode while the positive ions to the cathode. The dedocyl sulphate ions accumulated at the anode and interacted and attached itself to the surface of the graphite rod. This resulted in the loosening of the graphene layers from the graphite rod (Gao et al., 2011; J. Lu et al., 2009). Several minutes after voltage was applied, bubbles were observed at the cathode due to the formation of hydrogen gas as shown in (Figure 3.2 (a)). At the anode, the interaction of the dodecyl sulphate ions with the graphite surface occurred and after two hours the solution turned darker due to exfoliated graphene flakes, as shown in (Figure 3.2 (b)). The exfoliation process was continued for 2 hours to obtain a stable graphene suspension in the SDS solution. (Figure 3.3) the graphene suspension after the electrochemical process.
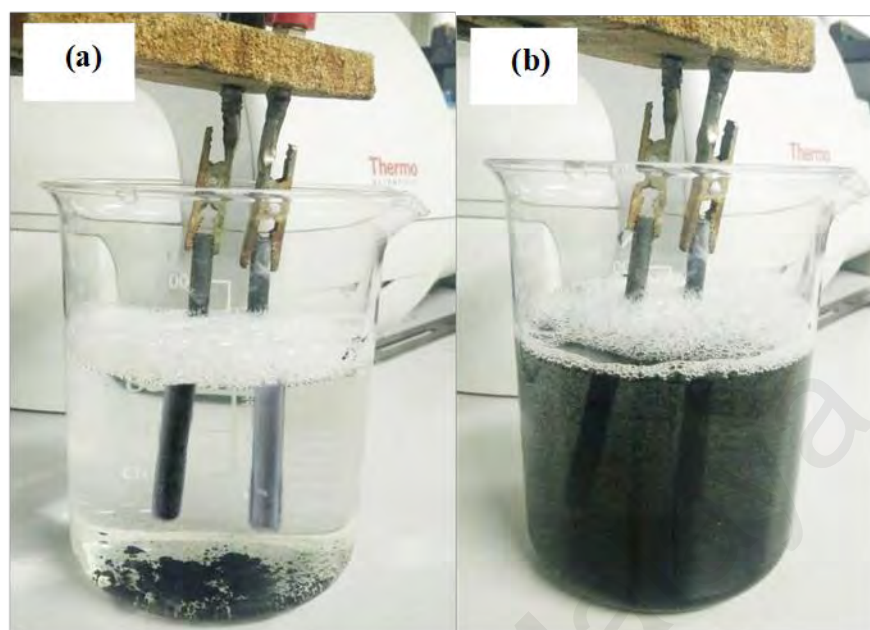
Figure 3.2: The image of electrolyte (a) After several minutes where bubbles were observed at the cathode due to the formation of hydrogen gas (b) after two hours of exfoliation process

Figure 3.3: The graphene suspension after the electrochemical process.

The stable graphene suspension was centrifuged at 3000 rpm for 30 min to remove large agglomerates. Afterward, the supernatant portion of the suspension was decanted. The concentration of the centrifuged graphene was estimated from the weight of the suspension used. To fabricate the composite, 1 g of polyethylene oxide (PEO) (Mw = 1 000 000 gmol^{-1}) was dissolved in 120 ml of deionized water. The graphene solution obtained from the electrochemical exfoliation was then mixed with PEO solution at ratios of 1:4 of graphene:PEO in ml respectively. The solution was dried in petri dishes at 56°C to obtain free standing films with 50 µm thickness. (Figure 3.4 (a) and (b)) shows the real and Field Emission Scanning Electron Microscopy (FESEM) image of the film, respectively. (Figure 3.4 (b)) indicates that the graphene in randomly distributed in the polymer composites. (Figure 3.5) shows the EDX spectrum of film, which indicates the existence of significant amount of carbon and oxygen elements in the film.
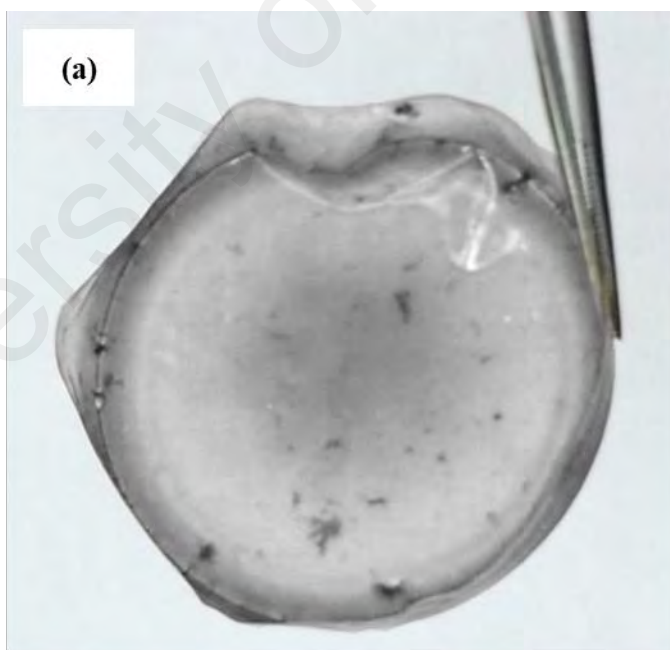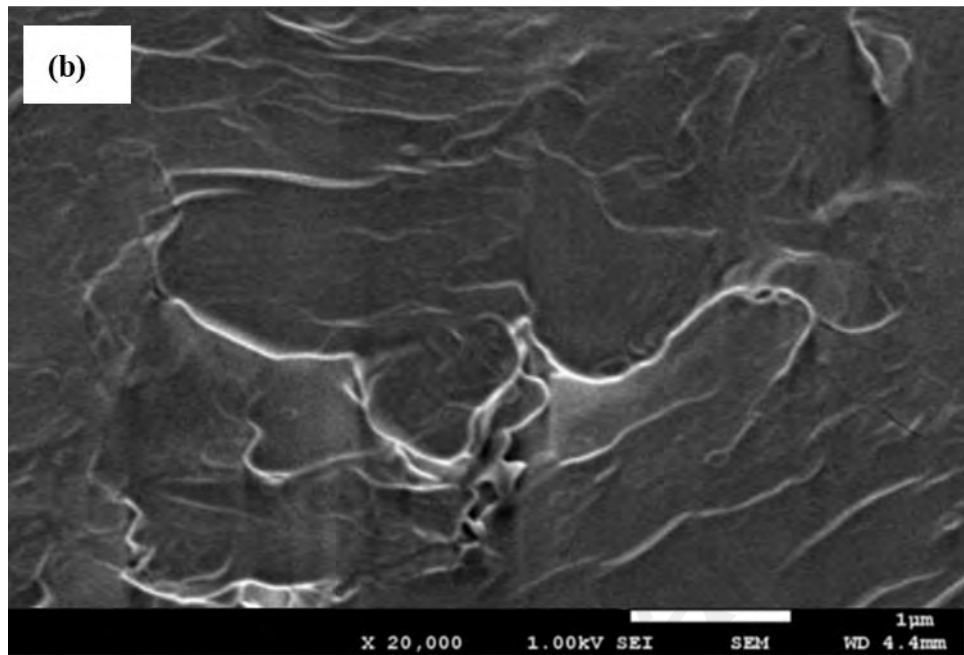
Figure 3.4: (a) Real and (b) FESEM images of the graphene PEO composite film
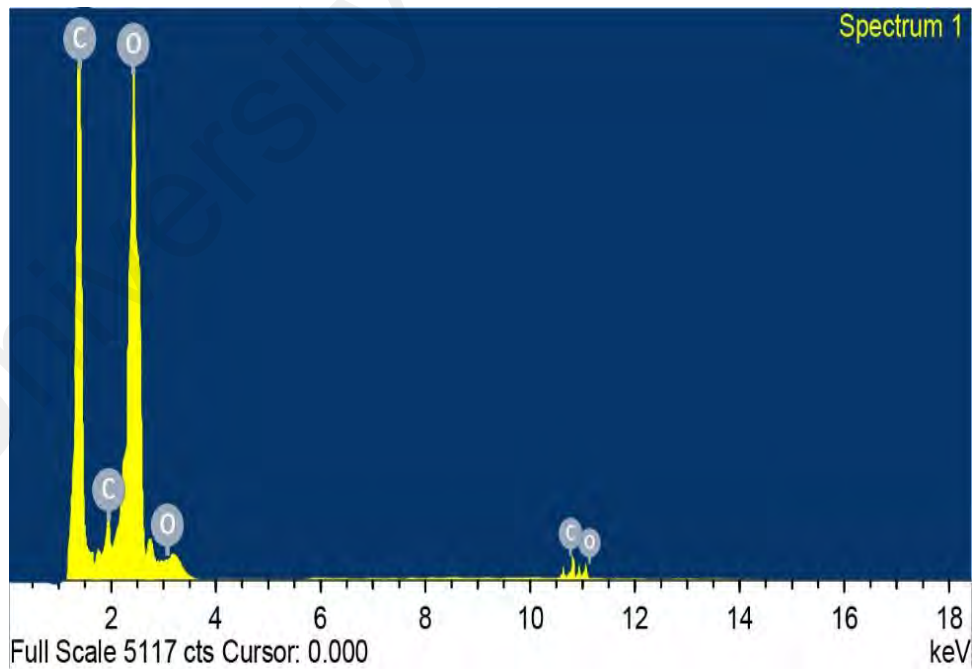
Figure 3.5: EDX spectrum for the graphene PEO composite film

Raman spectroscopy is widely used to characterize crystal structure, disorder and defects in graphene-based materials (Zhu et al., 2010). Raman spectrum of the fabricated film was obtained using a probe beam of 532 nm as shown in (Figure 3.6). As observed in the figure, the D peak indicates the existence of defects in the sample at 1351 cm^{-1}. The G peak observed at 1617 cm^{-1} corresponds to the Raman active E_{2g} phonon at Brillioun zone centre of graphite (Wei et al., 2012). The intensity ratio of the D to G band of the graphene sheets is about 1.2, as expected due to small size of the graphene sample. The existence of multi-layered graphene can be confirmed by considering the ratio of G to 2D peak which is higher than 0.5 (J. Lu et al., 2009). To further characterize the film, the linear transmission of the graphene film was also recorded by using a broadband white light source. The linear transmission spectrum is shown in (Figure 3.7), which indicates the absorption of about 20% at 1550 nm region. (Figure 3.8) shows nonlinear curve of the film, which is obtained by using a mode-locked fiber laser with 2.38 MHz repetition rate and 330 fs pulse width as the input pump. As shown in the figure, the modulation depth is measured to be around 16.2 % with non-saturable absorption of 22 % and saturation intensity of 87MW/cm^2.
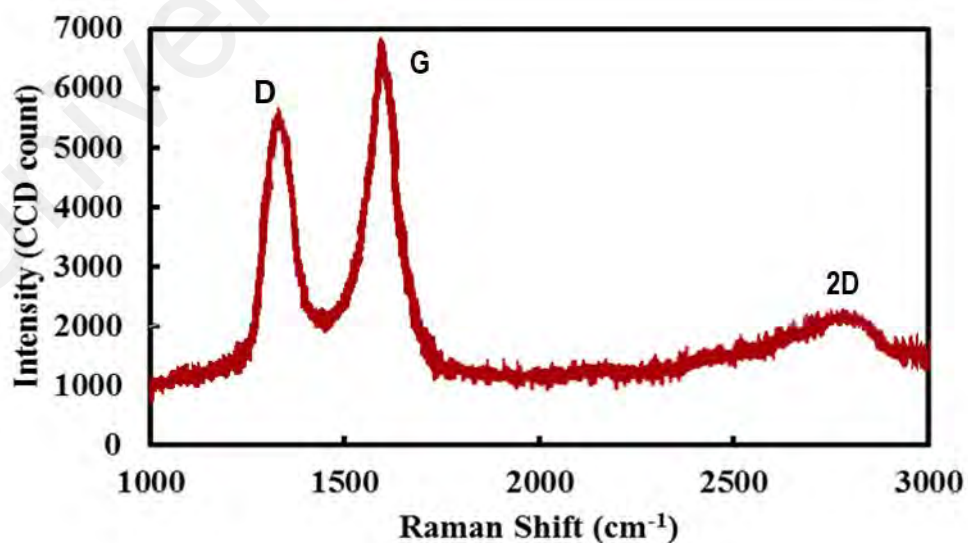
Figure 3.6 : Raman spectrum from the graphene film.
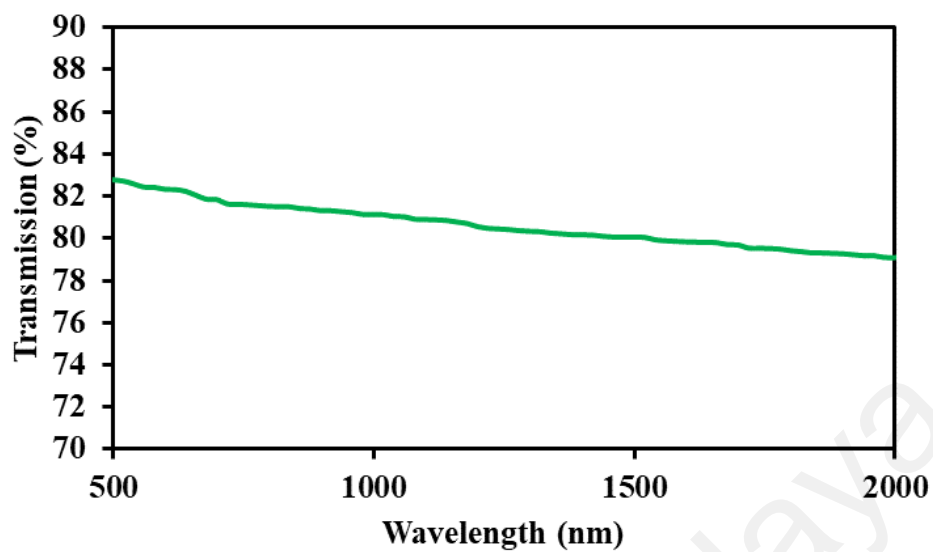
Figure 3.7 : Linear transmission spectrum of the graphene film
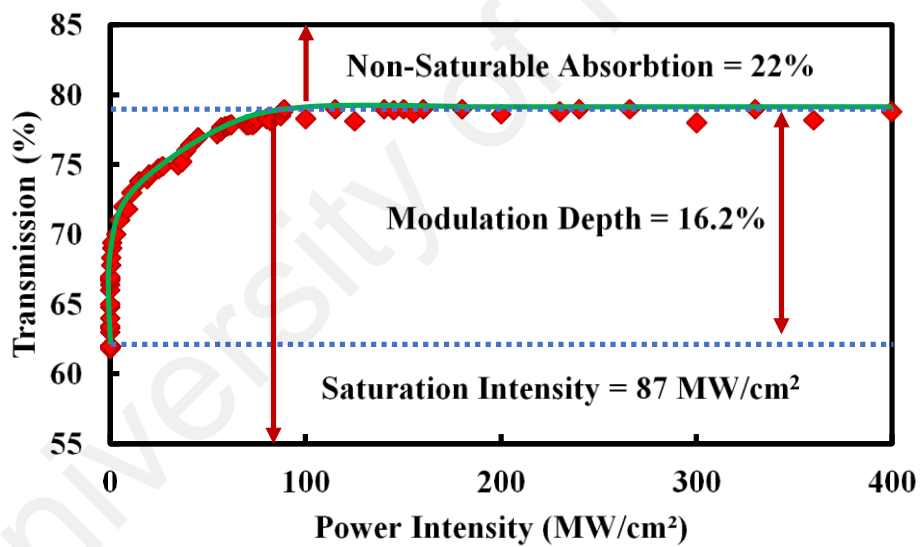
Figure 3.8 : Nonlinear transmission curve of the graphene film at 1550 nm, which indicates a modulation depth of 16.2%

3.3   Preparation and characterization of graphene oxide based saturable absorber

In this section, graphene oxide (GO) was prepared through a modified Hummers method from expanded acid washed graphite flakes. The synthesis involves the following steps. First, 18g of graphite flakes were mixed with 320 mL of sulfuric acid (H_2SO_4), 80 mL of phosphoric acid (H_3PO_4) and 18 g of potassium permanganate ($KMnO_4$) by using a magnetic stirrer. After adding all the materials slowly, the one-pot mixture was left for stirring for 3 days to allow the oxidation of graphite. The colour of the mixture changes from dark purplish green to dark brown. Later, H_2O_2 solution was added to stop the oxidation process, and the colour of the mixture changes to bright yellow, indicating a high oxidation level of graphite. The graphite oxide formed was rinsed three times with 1 M of HCl aqueous solution (to remove the sulfate ions) and repeatedly with deionized water (to remove chloride ions) until a pH of 4–5 was achieved. The washing process was carried out using simple decantation of supernatant via a centrifugation technique with a centrifugation force of 10,000 g. During the washing process with deionized (DI) water, the graphite oxide experienced exfoliation, which resulted in the thickening of the graphene solution, forming a GO gel. The GO gel was then mixed with DI water to obtain a GO solution. The preparation process is illustrated in (Figure 3.9).
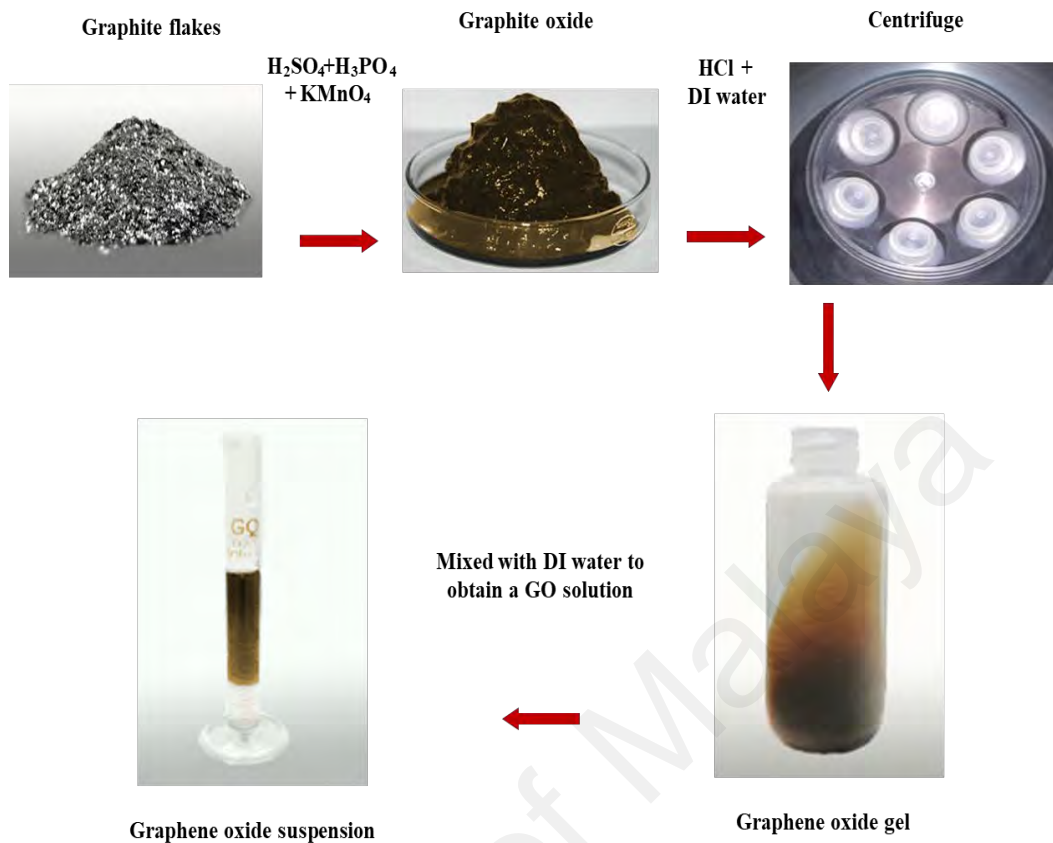
Figure 3.9 : Preparation of GO solution

To prepare the polymer, 1 g PEO (average molecular weight of 1×10^6 g/mol) is dissolved in 120 ml DI water using hot plate stirrer with the aid of magnetic stirrer. From the experiment, it will take around three hours to fully dissolve the PEO in DI water. GO-PEO composite was fabricated by adding a different quantity of dispersed GO suspension containing GO into a solution of 1 g PEO in deionized water and thoroughly mixed them using an ultra-sonification process as shown in (Figure 3.10 (a)). In this experiment, the mixer is put into ultra-sonic bath (Branson 2510, 40 kHz) for about one hour to produce a stable GO-PEO composite solution (Fig. 3.10(b)). In this part, only small amount of the PEO solution (0.6 ml – 2 ml) are used to minimize the use of GO. This mixture of PEO and GO is then left dry at room temperature to obtain GO-PEO film. (Figs. 3.11 (a) and (b)) show the actual image and the Field Emission Scanning Electron Microscope

(FESEM – JSM 7600 F) image of the GO PEO film. A close-up examination of the GO layer formed, shows orderly layered GO, verifying further the formation of GO paper (Dikin et al., 2007). (Figure 3.12) shows EDX spectra of the GO, which showing an oxygen content of 43% wt and carbon content is 57% wt.

Figure 3.10 : Preparation of the GO composite solution (a) Mixing of GO solution with the PEO host polymer using an ultrasonic bath (b) the mixed suspension GO polymer solution
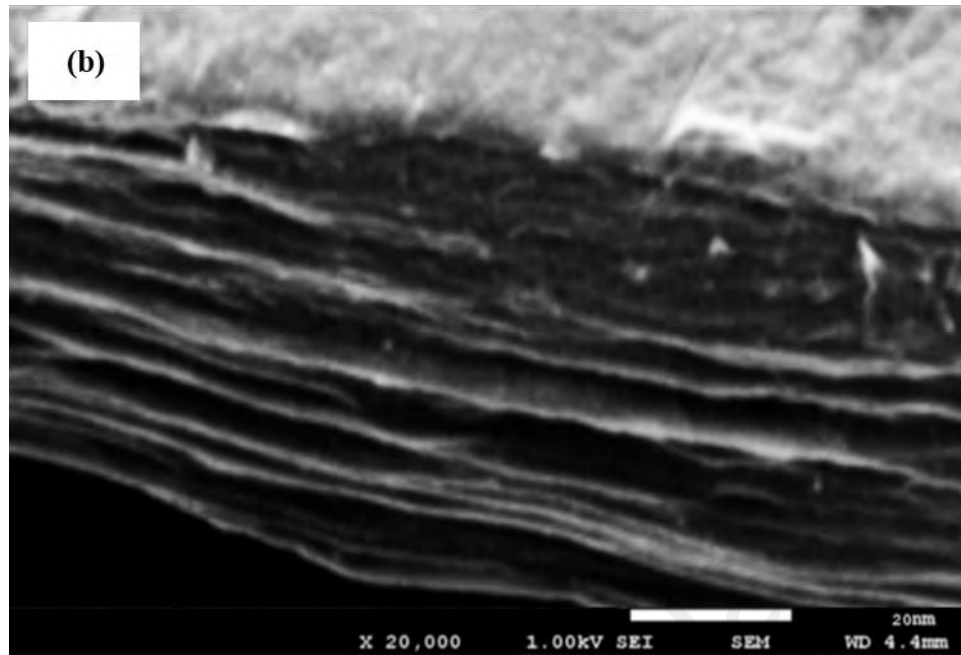
Figure 3.11 : The image of GO PEO film after let dry at room temperature (a) actual (b) FESEM image
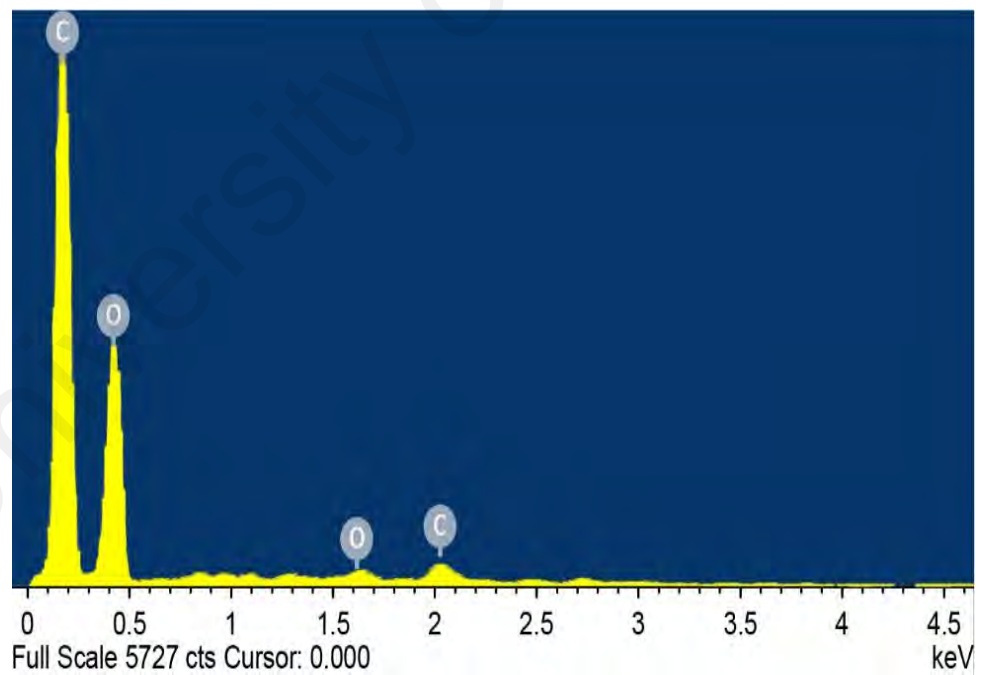
Figure 3.12 : EDX spectrum for the GO PEO composite film

(Figure 3.13) shows the Raman spectrum of the fabricated GO, which clearly discerning that the position of D and G peak at 1359 cm^{-1} and 1600 cm^{-1}, respectively. The D band is due to defect-induced breathing mode of sp^2 rings and the G band is due to the first order scattering of the E$_{2g}$ phonon of sp^2 carbon atoms (Andrea C Ferrari et al., 2013). As observed in the figure, the G band of the GO is located at a higher frequency (of 1600 cm^{-1}) compare to graphite (1580 cm^{-1}) and the result is agreed very well with the finding reported by Kudin et al.,(2008). The (I$_D$/I$_G$) intensity ratio for GO is obtained at around 0.85. The ratio corresponds to the measure of disorder degree and is inversely proportional to the average size of the sp^2 clusters (Sobon et al., 2012). (Figure 3.14) shows the linear transmission spectrum for the GO film. It shows an absorption of about 15% at 1550 nm region. The measured nonlinear curve of the GO-PEO film is shown in (Figure 3.15). It indicates that the film has nonlinear saturable absorption or modulation depth of 24.1%, saturable intensity of 72 MW/cm^2 and non-saturable absorption of 35.1%.
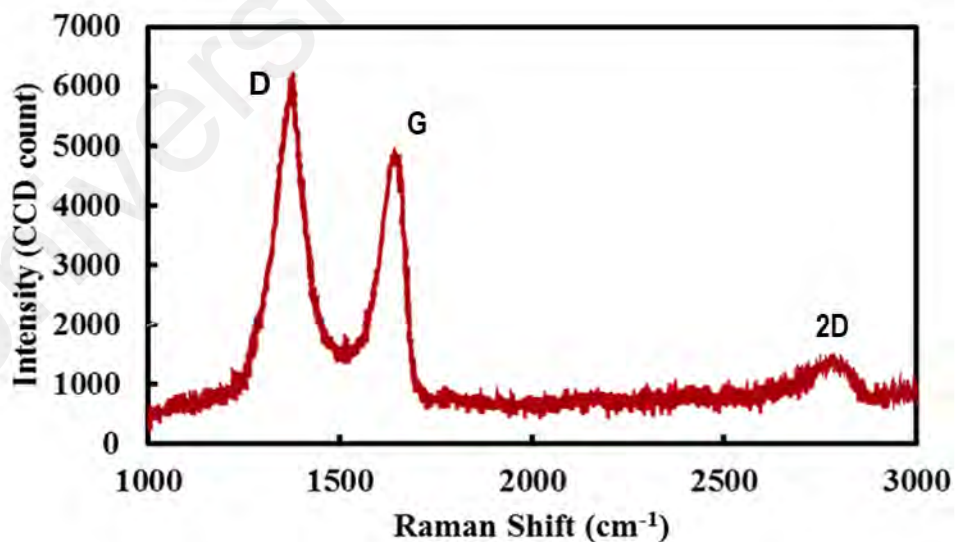
Figure 3.13 : Raman spectrum from the GO film.
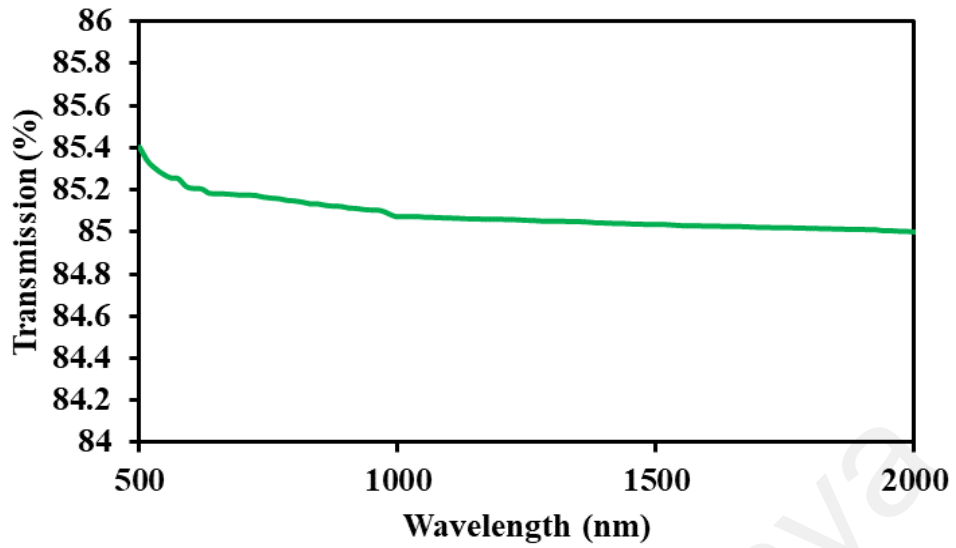
Figure 3.14 : Linear transmission spectrum of the GO film.
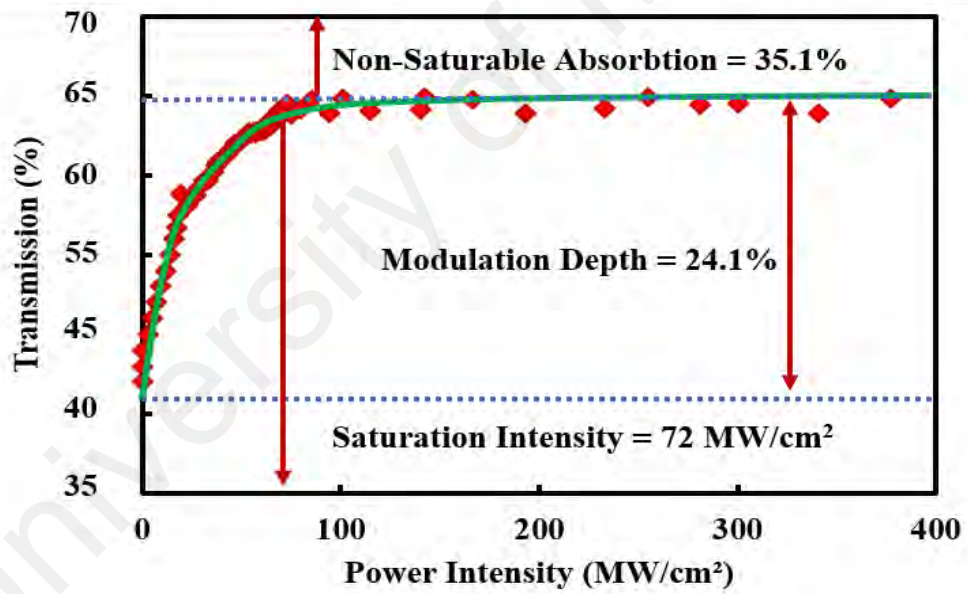
Figure 3.15 : Nonlinear transmission characteristic of the GO film

3.4 Preparation and characterization of topological insulator-based SA

This thesis also aims to explore the capability of passive SAs made of topological insulators (TIs) for generating mode-locked lasers. TIs have a large modulation depth with an efficient saturable absorption property and thus they are expected to be suitable for use as SA material. In this section, two different TI SAs; Bi_2Se_3 and Bi_2Te_3 are prepared and characterized. The preparation of both TI SAs is explained in detail in this section.

Firstly, 5 mg of Bi_2Se_3 nano-sheets were dissolved in 50 ml of isopropyl alcohol by using a hot plate stirrer. This mixture is stirred with the aid of a magnetic stirrer for 24 hours. After the mixture has dispersed well with the isopropyl alcohol, it was ultra-sonificated for another 6 hours to produce Bi_2Se_3 composite as shown in (Figure 3.16 (a)). Secondly, this Bi_2Se_3 composite is put into an ultra-sonic bath (Branson 2510, 40 kHz) for about an hour in order to produce a stable Bi_2Se_3 composite solution (TI suspension) as shown in (Figure 3.16 (b)). Then, optical deposition process was carried out to place the Bi_2Se_3 nanosheets onto the end surface of the ferrule so that a SA device can be constructed. A light beam from 1480 nm laser diode was launched into a single-mode fiber (SMF) pigtail with incident power of 50 mW. The output fiber ferrule of the SMF is then dipped into the prepared Bi_2Se_3 suspension solution for about 20 minutes as illustrated in (Figure 3.16 (c)). After that, we took the fibre ferrule out of the TI suspension to allow evaporation for another 15 minutes. This procedure is repeated for three times in order to enhance Bi_2Se_3 adhesion onto the fibre core. Finally, the TI Bi_2Se_3 SA was successfully fabricated as we obtained deposited TI nano-sheets on the fibre core. This procedure was repeated for Bi_2Te_3 sample to obtain a Bi_2Te_3 based SA.
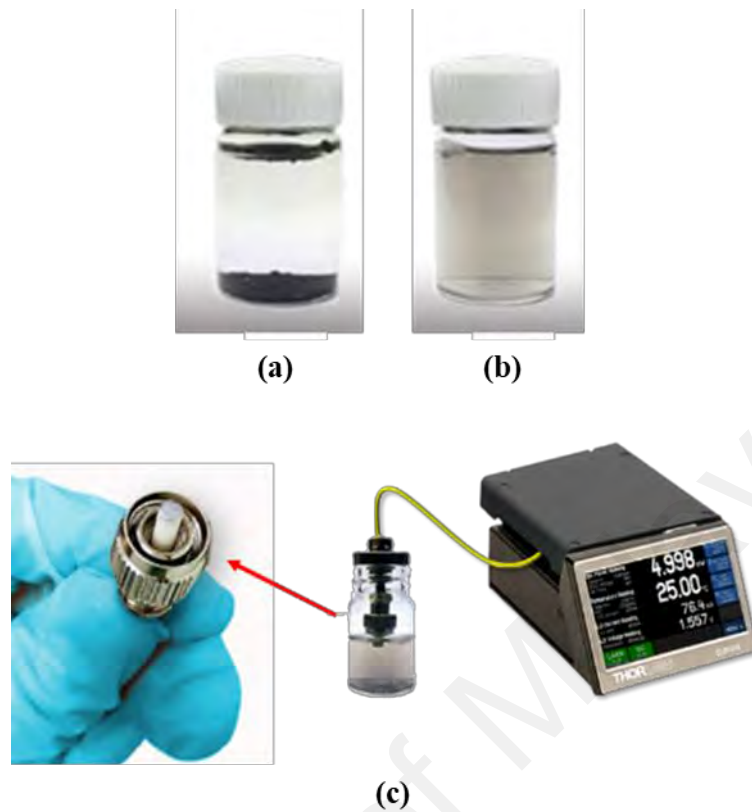
Figure 3.16 : Preparation of TI Bi₂Se₃ SA (a) Bi₂Se₃ composite solution before ultrasonic bath and (b) stable Bi₂Se₃ composite solution (c) Fibre ferrule in the TI suspension during optical deposition process.

In order to conveniently characterize the exfoliated Bi_2Se_3 and Bi_2Te_3, we dropped the Bi_2Se_3 and Bi_2Te_3 composite onto a cuprum plate by the spin-coating method as showed in (Figure 3.17), and then evaporating to dryness in an oven. Then, the field emission scanning electron microscopy (FESEM) measurement, Raman spectroscopy, and EDX analysis were performed on the sample and the results are presented. As shown in (Figures 3.18 (a) and (b)), the FESEM image of exfoliated Bi_2Se_3 and Bi_2Te_3 synthesized from Bi_2Se_3 and Bi_2Te_3 nano-sheet which produce layers-like complex flakes. The thickness of the few-layer Bi_2Se_3 and Bi_2Te_3 was measured to be around 3-4 nm. (Figure 3.19 (a) and (b)) shows the Raman spectrum from the Bi_2Se_3 and Bi_2Te_3, respectively. (Figure 3.19 (a)) clearly indicates three peaks assigned with different vibrational modes based on Raman selection rules. A_{1g}^1 mode at 72 cm⁻¹, E_g^2 mode at 133

cm^{-1}, and A_{1g}^2 mode at 173.6 cm^{-1}. All these three peaks recorded within the scanned frequency range and agreed well with the previously reported experimental and calculated phonon vibration modes of Bi$_2$Se$_3$ (Shahil et al., 2012). As for (Figure 3.19 (b)), five peaks were assigned with different vibrational modes based on Raman selection rules. E_g^1 mode at 40.1 cm^{-1}, A_{1g}^1 at 59.4 cm^{-1}, E_g^2 at 101.1 cm^{-1}, A_{1u}^2 at 116.1 cm^{-1}, and A_{1g}^2 at 139.2 cm^{-1}.

Figure 3.17 : Bi$_2$Se$_3$ composite onto a cuprum plate by the spin-coating method

(a)
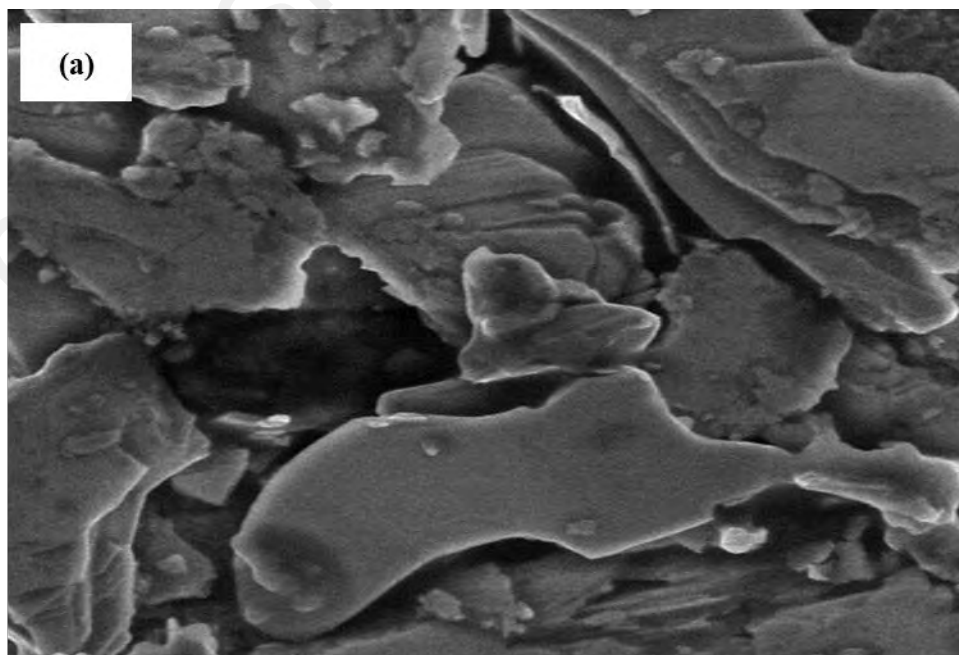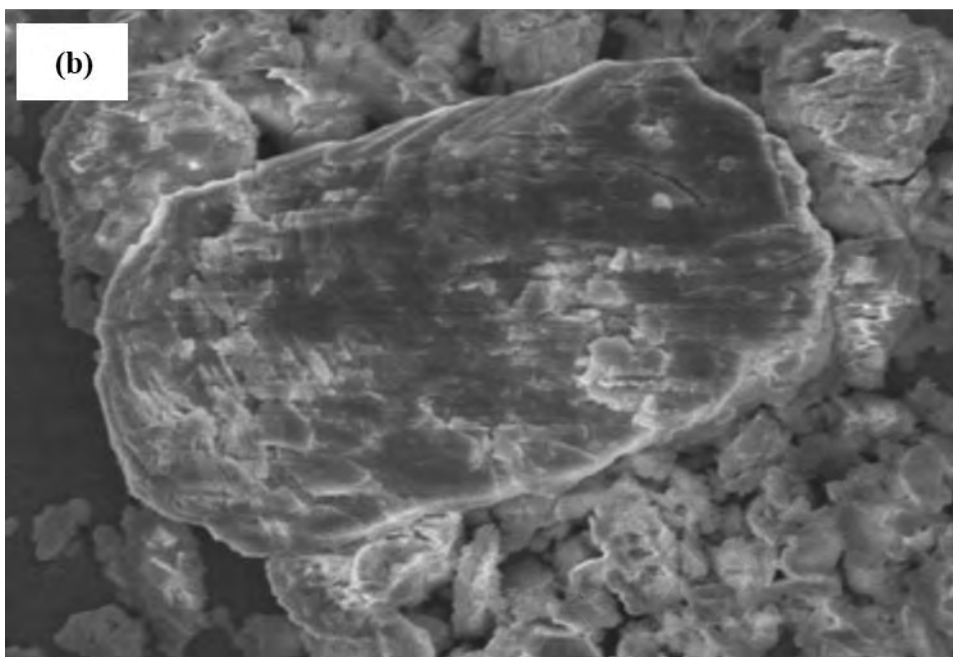
Figure 3.18 : FESEM image of layered (a) Bi$_2$Se$_3$ and (b) Bi$_2$Te$_3$
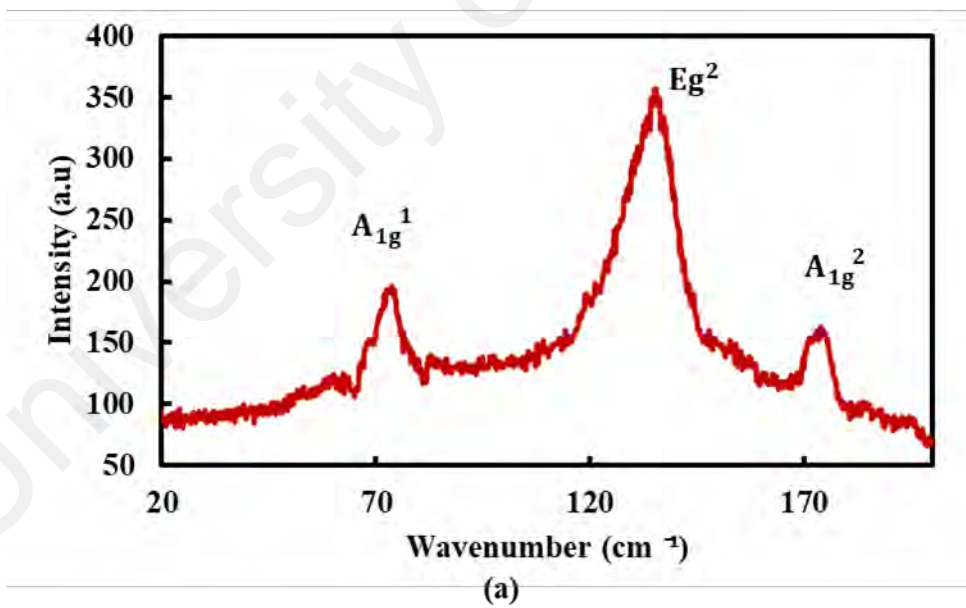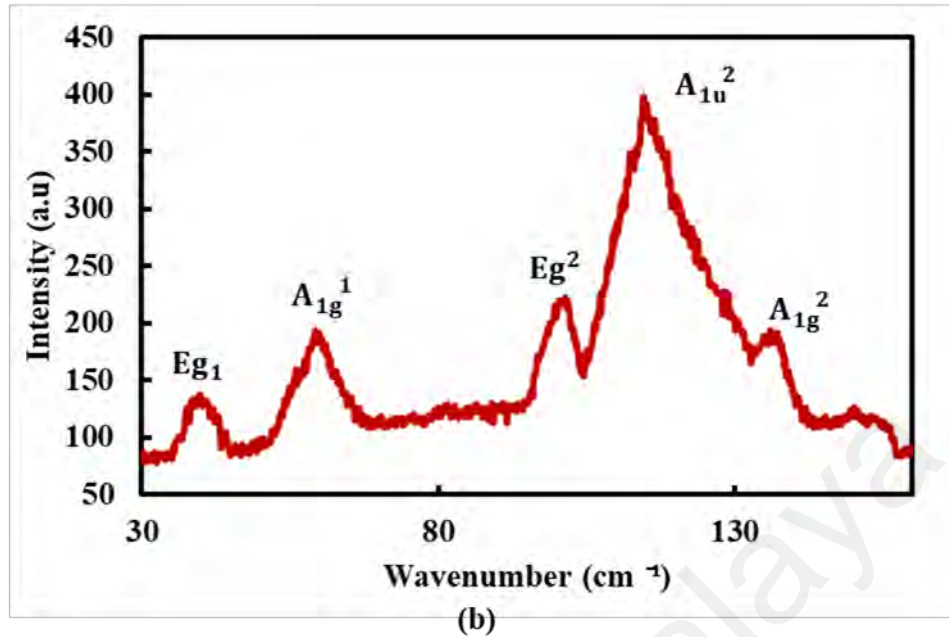
Figure 3.19 : Raman spectrum of layered (a) Bi₂Se₃ and (b) Bi₂Te₃

The compositions of Bi_2Se_3 and Bi_2Te_3 in the composite solution were analyzed with EDX as shown in (Figures 3.20 (a) and (b)), respectively. The Bi_2Se_3 material has 52.92 weight % Bi and 47.08 weight % Se element while Bi_2Te_3 material consists of 52.76 weight % Bi and 47.24 weight % Te element. A linear transmission measurement was also carried out on the prepared Bi_2Se_3 and Bi_2Te_3 samples. The transmission spectrum was measured using a white light source and an optical spectrometer and the result is shown in (Figures 3.21 (a) and (b)) for Bi_2Se_3 and Bi_2Te_3 SAs, respectively. The nearly flat linear absorption in wavelength region from 600 nm to 2000 nm in both figures clearly show that both Bi_2Se_3 and Bi_2Te_3 SAs have a broadband optical response and can operate in both 1 micron and 1.5 micron regions. It is measured that the Bi_2Se_3 and Bi_2Te_3 SAs have a linear absorption of 17% and 18% respectively at 1.5 micron region.
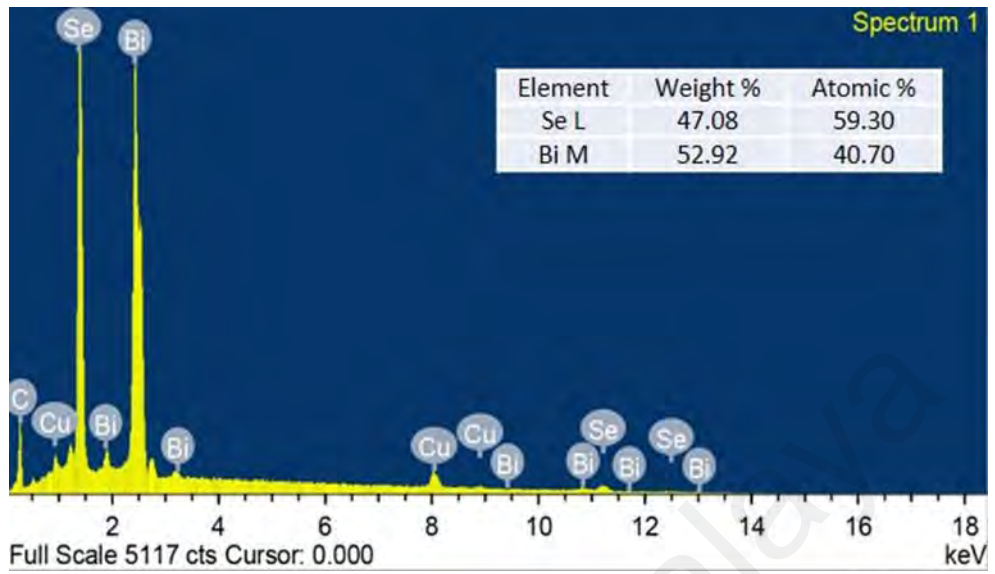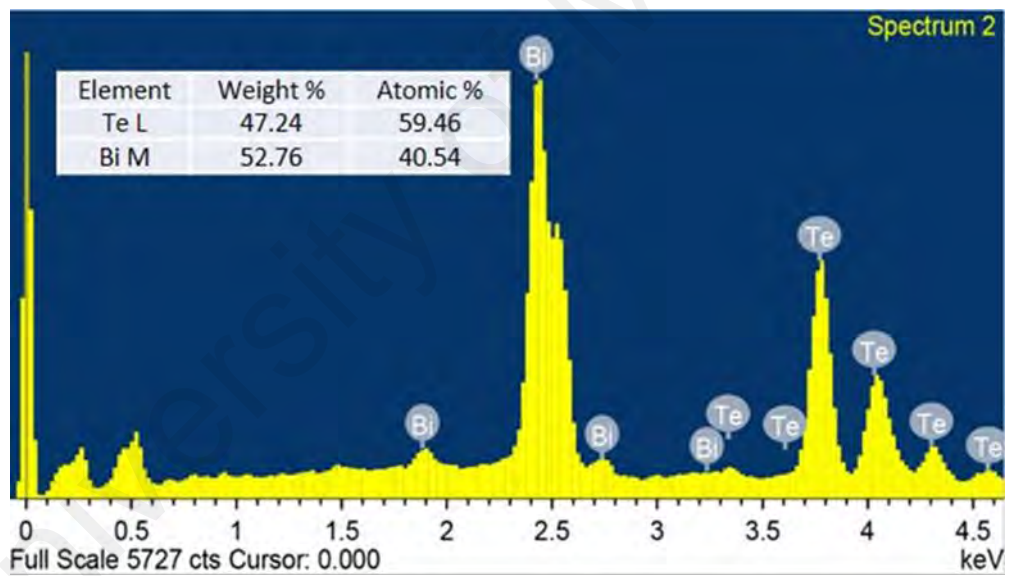
Figure 3.20 : EDX spectrum for the deposited SA devices (a) Bi$_2$Se$_3$ and (b) Bi$_2$Te$_3$
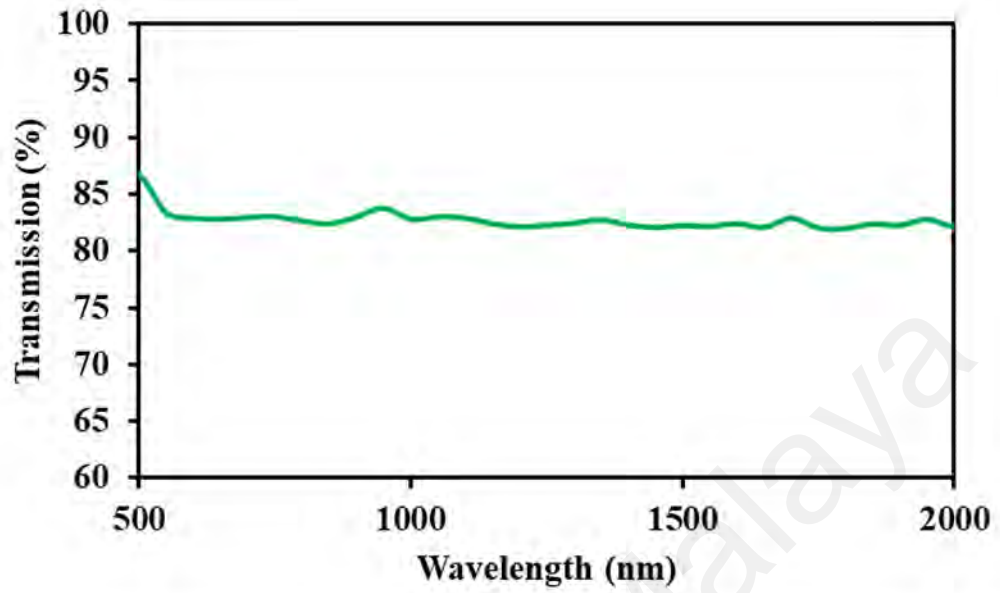
(a)
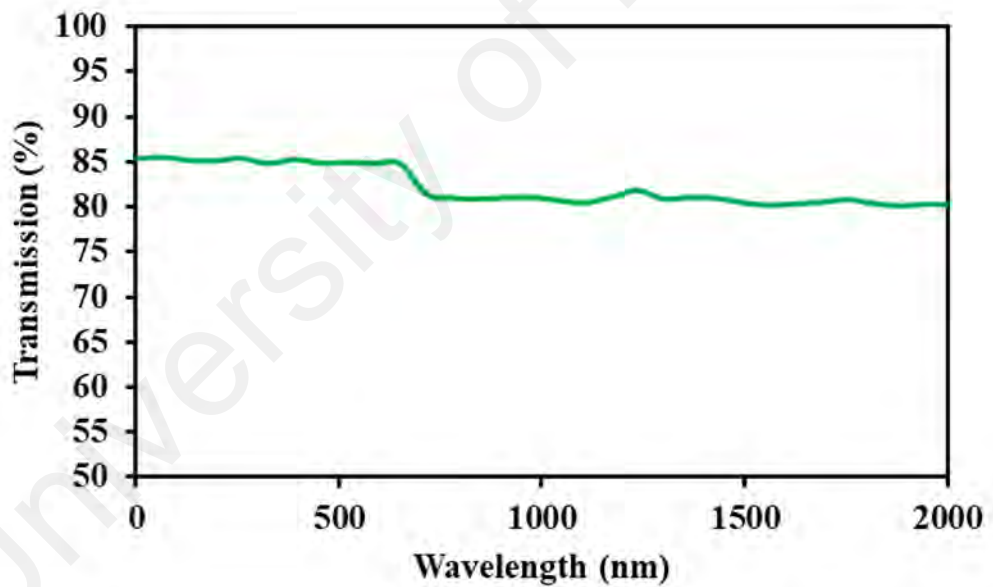
(b)

**Figure 3.21 : Linear transmission spectrum for the deposited SA devices (a)
Bi_2Se_3 and (b) Bi_2Te_3**

The nonlinear optical response property for the Bi_2Se_3 and Bi_2Te_3 was finally

investigated to confirm its saturable absorption by applying dual optical power meter

technique. A self-constructed mode-locked fiber laser (1558.2 nm wavelength, 1.25 ps pulse width, 21.8 MHz repetition rate) is used as the input pulse source. (Figure 3.22) shows the nonlinear transmission curve. The curve was fitted with the following equation 3.3 :

$$T(I) = 1 - \left(\frac{\alpha_s}{2} \left(1 + \frac{I}{I_{sat}} \right) + \alpha_{ns} \right) \tag{3.3}$$

where $T(I)$ is the transmission, α_s is the modulation depths, I is the input intensity, I_{sat} is the saturation intensity, and α_{ns} is the non-saturable absorption. Upon fitting the measured experimental data by the above equation, we can conclude that the saturation intensity I_{sat} for Bi_2Se_3 and Bi_2Te_3 are about 90.8 MW/cm^2 and 102 MW/cm^2 respectively. The modulation depths are about 39.8 % and 41.4% for Bi_2Se_3 and Bi_2Te_3. Non-saturable absorption is measured to be about 9.8 % and 10% as depicted in (Figure 3.22 (a)) and (Figure 3.22 (b)).

(a)
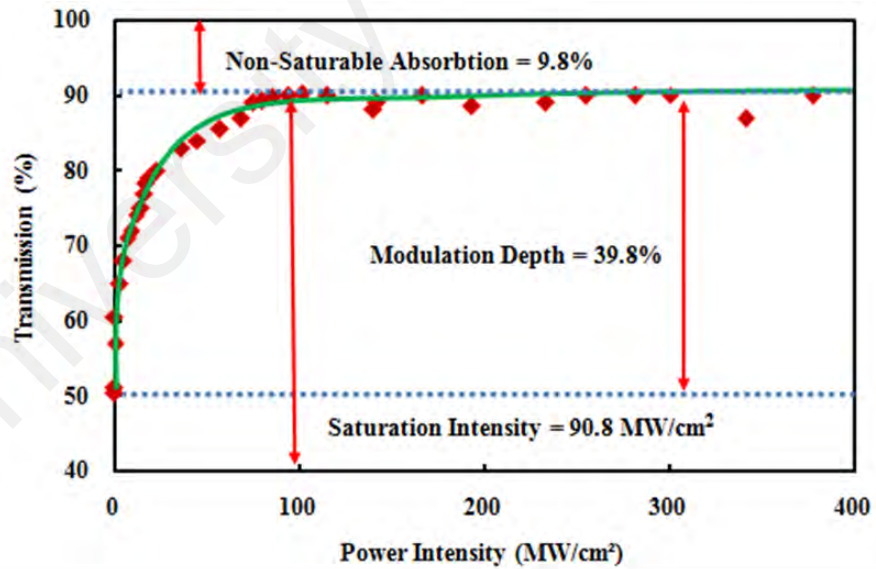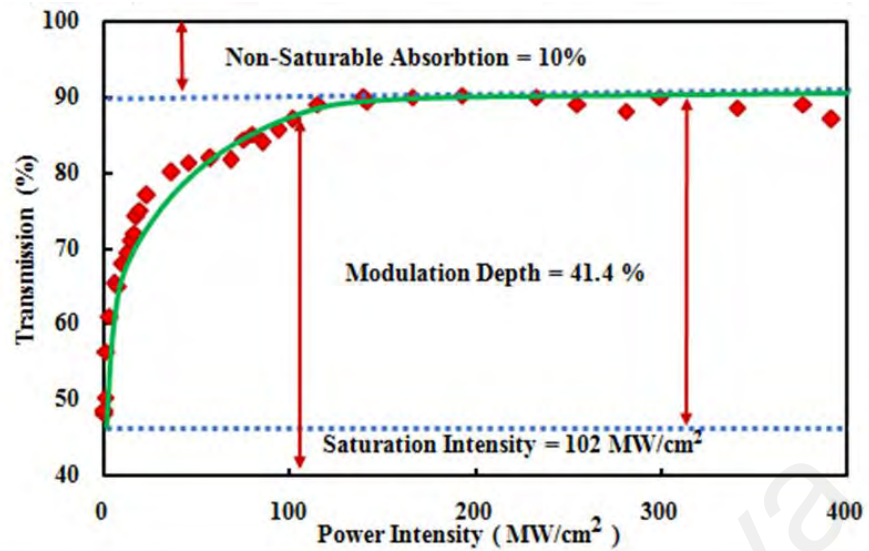
Figure 3.22 : Nonlinear curves for (a) Bi₂Se₃ and (b) Bi₂Te₃ SA devices.

3.5   Summary

Four types of 2D nanomaterial based SAs were successfully fabricated and characterized; graphene based and TI based. The graphene film SA was fabricated using a chemically exfoliated graphene flakes, which were embedded into a PEO polymer. The fabricated graphene PEO film SA exhibits modulation depth, non-saturable absorption and saturating intensity at 16.2 %, 22% and 87 MW/cm^2, respectively. Multi-layer GO fabricated based on a modified Hummers method was also embedded into PEO film to construct the GO based SA. The GO film has nonlinear saturable absorption or modulation depth of 24.1%, saturable intensity of 72 MW/cm^2 and non-saturable absorption of 35.1%. Bi₂Se₃ and Bi₂Te₃ based SAs were obtained by optical deposition method. Both Bi₂Se₃ and Bi₂Te₃ SAs have a broadband optical absorption covering both 1 micron and 1.5 micron regions. The modulation depths are about 39.8 % for Bi₂Se₃ and 41.4% for Bi₂Te₃ based SA at 1550 nm region.

CHAPTER 4: PASSIVELY MODE-LOCKED YTTERBIUM-DOPED FIBER LASERS WITH GRAPHENE AND TOPOLOGICAL INSULATOR AS SATURABLE ABSORBER

4.1 Introduction

Ytterbium-doped fiber lasers operating at 1 μm region have attracted much interest in the last few years for many applications especially in industrial material processing, spectroscopy, and medical surgery (Martin E. Fermann et al., 2013; Shi et al., 2014). This is attributed to the large gain bandwidth and exceptional efficiency of ytterbium-doped fibers (YDFs), as well as the convenience of pumping with 980nm laser diodes. The association of these characteristics with the compact size, high stability and efficient heat dissipation of fiber technology make the YDFLs practical alternatives to bulk laser systems. With the recent development of various passive saturable absorbers (SAs), these devices can now be designed to achieve ultra-short pulse operation via mode-locking approach (Richardson et al., 2010; Grzegorz Sobon, 2015; Chujun Zhao et al., 2012). Generally, pulsed laser system is most desired when involves solid or tissue cutting due to its cleaner, accurate and precise penetration compared to traditional continuous wave (CW) laser system (Ghany et al., 2005; Hoy et al., 2014; Steen et al., 2010). Some of the applications require ultrashort pulse which is in term of picoseconds or femtoseconds pulse width that would provide higher transmission capacity in telecommunications, more sampling rate in surface scanning and deeper surface penetration in material processing (Meijer et al., 2002; Wolfe et al., 2003).

Passively mode-locked fiber lasers have attracted a wide interest in recent years due to their many advantages including natural being compact, cost-effective and easy to setup (U. Keller, 2003; Konstantin S Novoselov et al., 2012; Sibbett et al., 2012). The

buildup of ultrashort pulses from noise and subsequent stabilization require the use of a fast SA such as nonlinear polarization rotation (NPR) (Matniyaz, 2018; J. Peng et al., 2018; X. Yang et al., 2009), a nonlinear optical loop mirror (NOLM, or similarly a nonlinear amplifying loop mirror NALM) (Aguergaray et al., 2012), semiconductor SA mirrors (SESAMs) (I. D. Jung et al., 1997; Kornaszewski et al., 2012; J. Li et al., 2014) and a high-modulation depth SA material (Q. L. Bao et al., 2009; Chi et al., 2014; Jaroslaw Sotor et al., 2014). NPR, NOLM and NALM techniques manipulate a nonlinear optical element inside the laser cavity to turn the laser continuous wave output into a train of ultrashort optical pulses. However, it is difficult to produce a highly stable mode-locked laser by these approaches. (SESAMs) currently dominate passive mode-locking, however, they have a narrow tuning range (tens of nanometers) and require complex fabrication and packaging. A simpler and cost-effective alternative relies on single-walled carbon nanotubes (SWCNTs), where the working wavelength is defined by choosing the SWCNT diameter (i.e., band gap) (Villeneuve et al., 2011). Tunability is possible by using a wide diameter distribution. However, when operating at a particular wavelength, the SWCNTs not in resonance are not used and give insertion losses, compromising device performance. Novel nonlinear materials with broadband absorption are therefore required for wideband, tunable operation (Tawfique Hasan et al., 2014).

In the previous chapter, various graphene and topological insulator based SAs were developed as potential SAs. This chapter presents various mode-locked YDFLs, which were obtained by using those SAs as a mode-locker. The SAs are in the form of composite film, which were integrated in the YDFL cavity by sandwiching the SA thin film between two fiber connectors.

4.2   Mode-locked YDFL with a graphene film

Graphene is an allotrope of carbon in two-dimensional crystal form that has extraordinary electrical and optical properties (Bhattarai; Ezawa, 2008; Sahoo et al., 2009). The atomic-thin nano-scale material also exhibits linear optical absorption and saturable absorption properties, which important parameters in order to generate pulse laser (Geim et al., 2010; Kostya S Novoselov et al., 2004). The linear dispersion of the Dirac electrons in graphene enable a wideband of operating wavelength where for any excitation, there will always be an electron hole pair in resonance (Bonaccorso et al., 2014; Bonaccorso et al., 2010; Zhipei Sun et al., 2010). Moreover, the relaxation of carriers in a single layer graphene is around 200 fs (Carbone et al., 2011; Kadi et al., 2015; Malic et al., 2013) and other papers have included other factors that enable graphene to become an excellent SA (Malic et al., 2017; D. Sun et al., 2012; Yu et al., 2011).The application of graphene based SA for pulsed laser generation lasers has been demonstrated in many literatures (D. Sun et al., 2012) due to their unique properties including a high repetition rate, short pulse duration, high peak power and broad spectrum (X. Li et al., 2015; Muhammad, 2014; Yao et al., 2015). Here, an ultrafast fiber laser mode-locked at 1 μm was demonstrated using a newly developed graphene thin film as SA. The graphene film SA exhibits modulation depth of 16.2 % and it was fabricated using a chemically exfoliated graphene flakes, which were embedded into a PEO polymer as described in the previous chapter.

(Figure 4.1) shows the laser cavity configuration, which employs a 1m long with Ytterbium-doped fiber (YDF) as a gain medium and the fabricated graphene composite film as a mode-locker. The YDF (Yb1200-4/125) used has a core and cladding diameters of 4 μm and 125 μm respectively, with a numerical aperture of 0.20, as well as the cut-off wavelength of 1010 nm, Ytterbium ion absorption of 280 dB/m at 920 nm and group velocity dispersion (GVD) of 24.22 ps^2/km. It was pumped by a 980 nm laser diode (LD)

via a 980/1064 nm wavelength division multiplexer (WDM). The mode-locker wasassembled by sandwiching the graphene PEO between two fiber connectors with a fiber adapter, as schematized in (Figure 4.1). An index matching gel was applied to the ferrule to reduce the insertion loss and help in fixing the film onto the core region of the fiber end. The insertion loss of the SA device was measured to be around 4 dB at 1050 nm region.

An isolator was placed after the output coupler to maintain unidirectional operation while a polarization controller (PC) was used to optimize the mode-locking. A laser light was coupled out of the cavity via a 90/10 coupler by allowing 90% of the light to oscillate in the cavity. A 3dB coupler (50:50 coupler) was then used outside the laser cavity to further split the output equally into two ports for spectral and time domain measurements. The optical spectrum analyzer (OSA, Yokogawa AQ6370B) was used for the spectral analysis of the mode-locked YDFL with a spectral resolution of 0.02 nm, whereas the oscilloscope (LeCroy,352A) and 7.8 GHz radio-frequency (RF, Anritsu MS2683A) spectrum analyzer are used to observe the output pulse train of the mode-locked operation in the form of electrical signal via a 1.2 GHz InGaAs photodetector (Thorlabs DET01CFC).The mode-locked YDFL has a total cavity length of 28 m with a total net dispersion in the normal regime of 35.025 ps/km.nm, where the rest of the ring cavity is a single-mode fiber (HI 1060) with a GVD of -21.9 ps^2/km.

Figure 4.1 : Configuration of the mode-locked YDFL with graphene PEO film as SA.

Figure 4.2: Schematic diagram of the mode-locked YDFL with graphene PEO

film as SA.

The threshold pump power for continuous wave lasing is 81.9 mW. When the pump power was increased to 120.9 mW, stable mode-locking can be initiated by introducing a disturbance to the intracavity fiber. Once stable output was achieved, no further polarization controller adjustment was needed. It is always possible to decrease the pump power to 120.9 mW while maintaining mode-locking. When mode-locked, the laser produces a pulse train at a rate of 4.5 MHz. The mode-locking operation was maintained as the pump power was increased up to the maximum pump power of 203.5 mW.

(Figure 4.3) shows a typical output spectrum of the YDFL with and without the SA the maximum pump power of 203.5 mW. Without the integration of any SA into the cavity, the YDFL generates CW lasing operating at 1063.9 nm. The laser operates at a shorter wavelength of 1052.9 nm with the incorporation of SA. This was attributed to the cavity loss which increases with the insertion of SA. Thus the operating wavelength shifts to a shorter wavelength region which provides a higher gain to compensate for the loss. The full width at half-maximum (FWHM) bandwidth is 8.1 nm, which confirms the of the mode-locked laser operates in anomalous regime. Two pairs of Kelly sidebands were clearly observed on the optical spectrum, indicating that the mode-locked operation was in soliton regime. The side bands formation results from intracavity periodical perturbations.
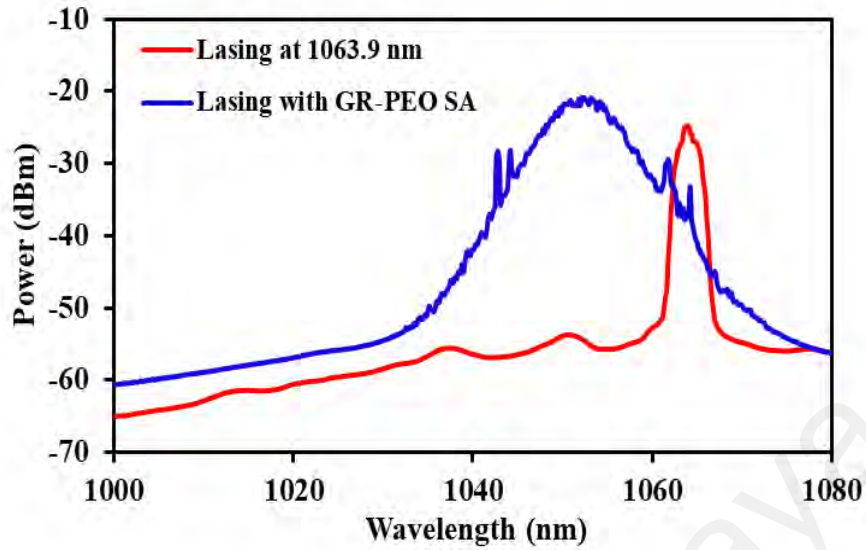
Figure 4.3: Output spectra of the YDFL with and without the composite SA device at maximum pump power of 203.5 mW.

(Figure 4.4 (a)) shows the typical oscilloscope trace within a period of 20 µs. It shows a stable mode-locking operation at the repetition rate of 4.5 MHz, which well corresponds to the cavity length of 28 m. The pulse period (peak to peak spacing) is approximately 222 ns. The envelope of a single pulse is shown in (Figure 4.4 (b)), which indicates the pulse width size of about 78 ns. However, due to the limitation resolution of the oscilloscope, the actual pulse width is much broader. As an alternative, the pulse width can also be determined by using the time-bandwidth product (TBP) equation. Since our cavity in anomalous dispersion, the pulse width size was fitted to sech pulse profile of 0.315 (R. Woodward, 2015). A minimum possible pulse width was calculated to be around 0.14 ps.
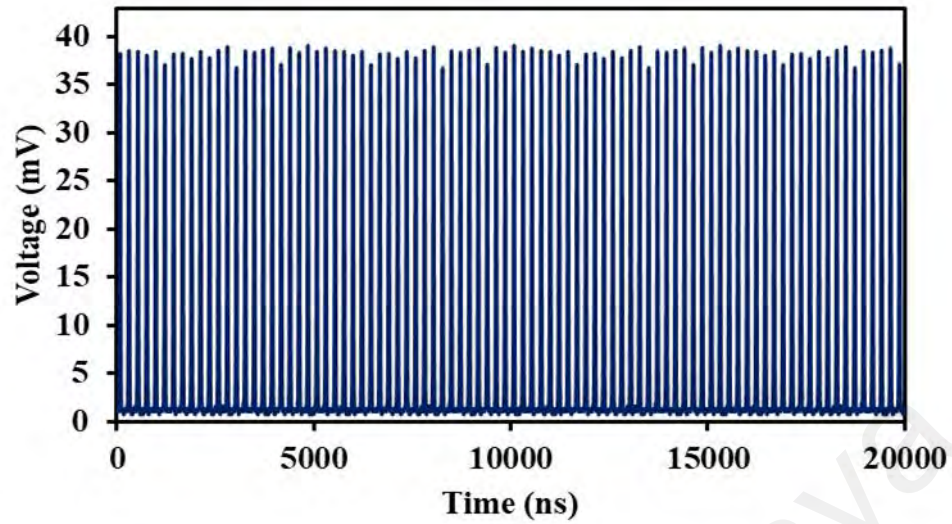
(a)
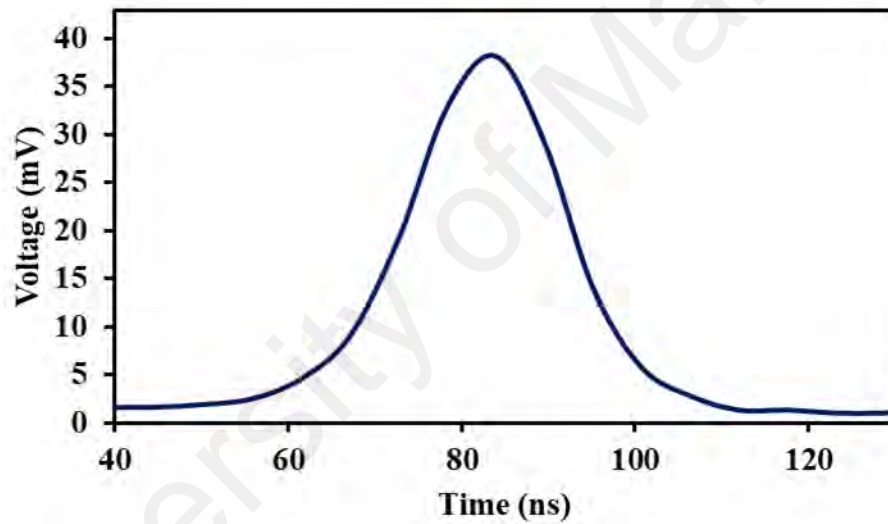
(b)

Figure 4.4: (a) Typical pulse train and (b) a single pulse envelope for the mode-locked YDFL at pump power of 203.5 mW.

The RF spectrum of the mode-locked laser was depicted in (Figure 4.5). The fundamental cavity frequency was 4.5 MHz (corresponding to the cavity round-trip time 222 ns). The electrical signal to noise ratio (SNR) was about 44 dB demonstrating the mode-locking state was quite stable. To check the operation stability, the pump power has been changed below to the threshold pump power and it is found that the mode-

locking state could start each time when the pump was retuned back above the pump power of 120.9 mW. Furthermore, a 2-day continuously measurement on the mode-locking state was also carried out at the pump power of 203.5 mW, and the results revealed that the central peak locations and 3 dB bandwidths remained relatively stable. It should be pointed out that the rotation of PC still greatly impacted the mode-locking state. To verify whether the graphene SA contributed to the passive mode-locking, the SA device was replaced by the same type of ferrule without the fabricated film. In this case, even carefully adjusted PC orientation and changed pump power in the range from 120.9 mW to 203.5 mW, the mode-locking state could not be observed again. This result demonstrated that the mode-locking behavior was caused not by the nonlinear polarization rotation (NPR) effect under the same condition, which testified that the graphene SA was indeed contributing to the mode-locking operation.
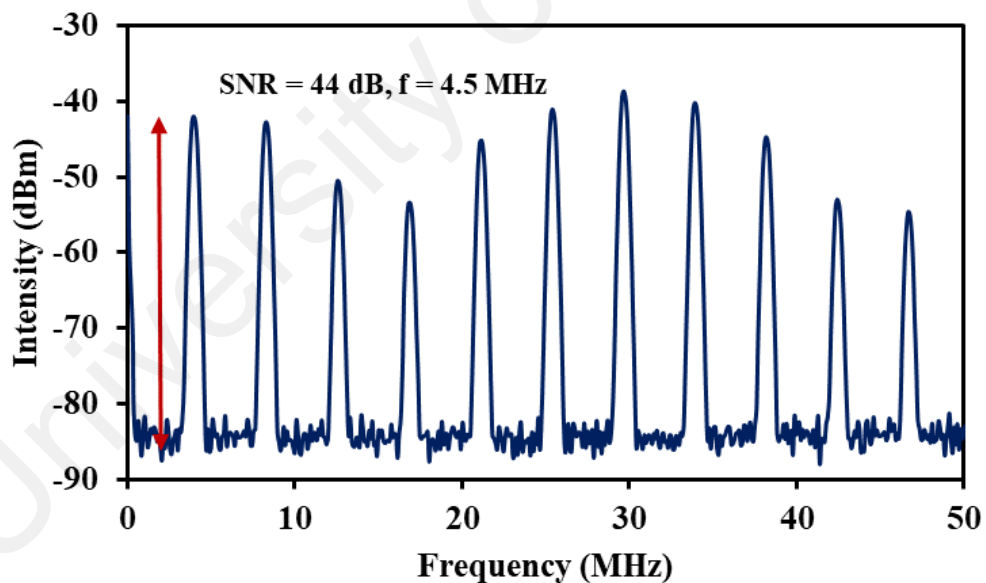
Figure 4.5 : RF spectrum taken at pump power of 203.5 mW..

(Figure 4.6) shows the average power and pulse energy of the mode-locked YDFL against pump power. Both average power and pulse energy increased with the increment of pump power. The first lasing was a continuous wave, which its average power is

approximately 2.91 mW at a pump power of 120 mW, however the output power of the mode-locked YDFL is linearly increased from 2.91 to 6.8 mW when the pump power was also increased from 120.9 to 203.5 mW as shown in (Figure 4.6). The maximum pulse energy was approximated 1.5 nJ at 203.5 mW pump power as illustrated in Figure 4.6. From the data, the calculated maximum peak power was 6.6 kW.
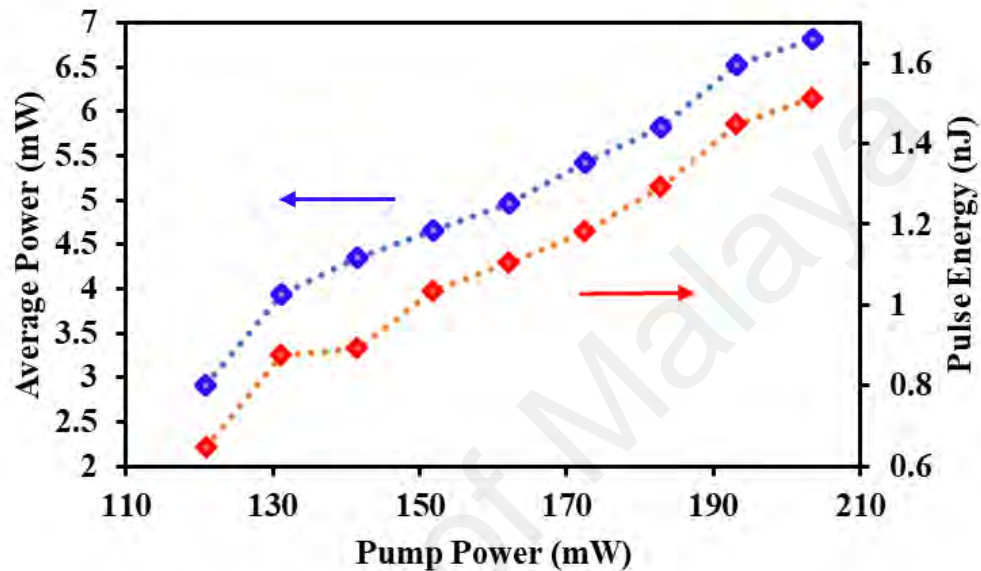
Figure 4.6 : Average power and pulse energy as a function of 980 nm pump power for the proposed mode-locked YDFL with graphene PEO SA.

4.3   Mode-locking pulse generation with graphene oxide (GO) SA

Due to its semi-metallicity, strong electro-absorption, nonlinear saturable absorption, and broadband conductance, graphene was investigated intensively in the fields of nano-electronics and photonics. The application of graphene has been successfully demonstrated as transparent flexible conductors, a broadband optical modulator, passive mode-lockers and a polarizer (J Lee et al., 2013). Amongst the remarkable features of graphene, its nonlinear saturable absorption is very attractive, since its gapless linear dispersion provides an ultra-broad operating bandwidth. In the previous section, graphene has been used as saturable absorber for passive mode-locked lasers. These pulsed lasers are essential devices for a variety of applications, such as high speed optical communications, biomedical imaging, and material processing medicine (Kobtsev et al.,

2008; Q. Lin et al., 2007; Y. Xu et al., 2009). Graphene oxide (GO) has forseen as good saturable absorber as an alternative form of graphene which exhibits ultra-fast relaxation and strong nonlinear saturable absorption (Bao et al., 2017; Gu et al., 2016; Sobon et al., 2016). Apart from that, fabrication of SA by using GO provide an easy handling due to good solubility in water (Matyba et al., 2010; S. Yin et al., 2011).

In this section a mode-locked operating at 1053 nm was demonstrated using a simple and inexpensive graphene-oxide (GO) based SA. The GO was synthesized via chemical oxidation of graphite flakes at room temperature. The GO-PEO composite solution is left to dry at room temperature for a day to form a free-standing carbon-based membrane material, which is known as GO-PEO film SA. The GO-PEO thin film was integrated in the YDFL system, which adopted similar setup as in (Figure 4.1) except for the use of GO-PEO film as a mode-locker to achieve a stable pulse train with a repetition rate of 6 MHz. The total cavity length of the ring setup was measured to be around 24 m, which is shorter than the previous YDFL. Therefore, the repetition rate of this laser is higher than the previous laser. The proposed GO based mode-locked YDFL cavity operates anomalous dispersion regime with GDD of -0.489 ps^2 and total net dispersion of -20.397 ps^2/km.

Stable and self-starting mode-locked operation was obtained just by adjusting the pump power over a threshold of 81.9 mW. (Figure 4.7) shows the spectrum when the 980 nm at the maximum pump power of 203.5 mW. As observed in the figure, the laser operates at 1053 nm region with the FWHM value of 14.26 nm and the spectral broadens with the increase of pump power due to self-phase modulation (SPM) effect in the cavity. A few Kelly sidebands are also clearly observed on the optical spectrum, indicating that the mode-locked operation is in soliton regime. The pulse width of the YDFL can be determined by using the time-bandwidth product (TBP) equation. Based on the dispersion

characteristic of the cavity, the pulse width size was fitted to sech² pulse profile of 0.315 (Antoncini, 2006). A minimum possible pulse width was estimated to be approximately 0.08 ps based on the FWHM value of 14.26 nm.

The mode-locked pulse generation was limited to the maximum pump power of 203.5 mW. No pulse was observed beyond this pump power. (Figures. 4.8(a) and (b)) show the oscilloscope trace of the mode-locked pulse train at 20 µs and 1.5 µs time span, respectively. It was observed in (Figure 4.8 (a)) that the mode-locking operation is very stable with any Q-switching instabilities. The period of pulses train was measured to be around 165 ns as shown in (Figure 4.8(b)), which equivalents to repetition rate of 6 MHz. The RF spectrum of the mode-locking pulses was depicted in (Figure 4.9) as measured by connecting a high sensitivity photo detector to a RF spectrum analyzer. As shown in (Figure 4.9), the major peak was the cavity repetition rate of 6 MHz with a signal to noise ratio (SNR) of 66 dB. The fundamental cavity frequency corresponds well to the cavity length of 24m. The power stability performance was also monitored for 2 days within 2% variation.
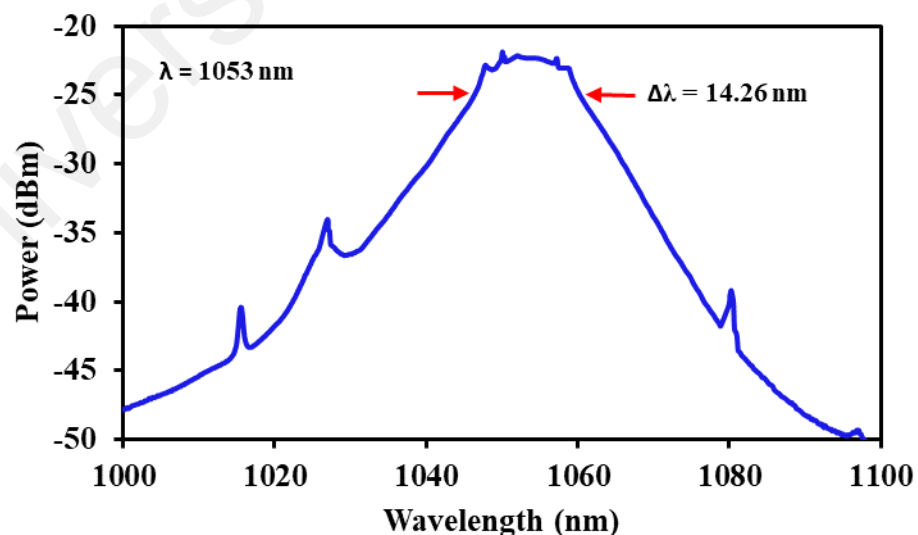
Figure 4.7 : Output spectrum of the mode-locked YDFL at pump power of 203.5 mW, which indicates the FWHM bandwidth of 14.6 nm.
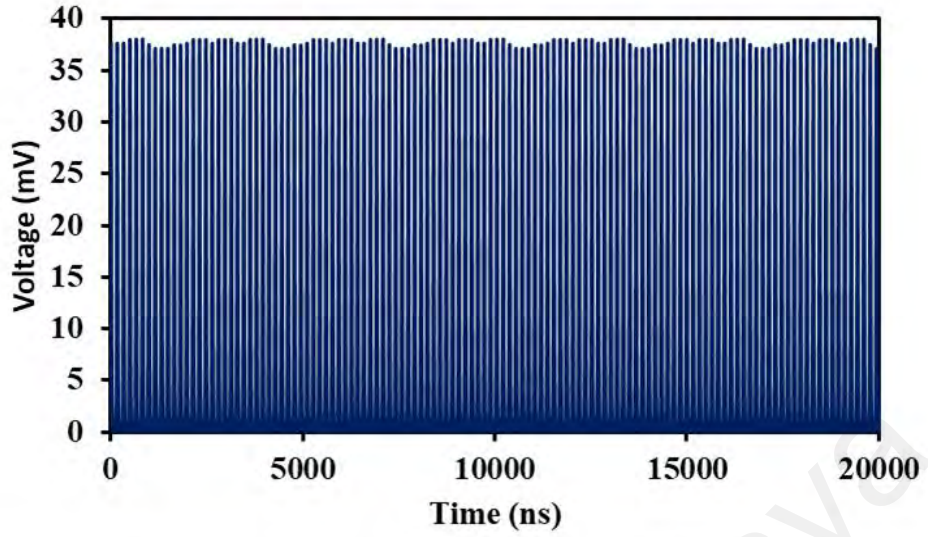
(a)
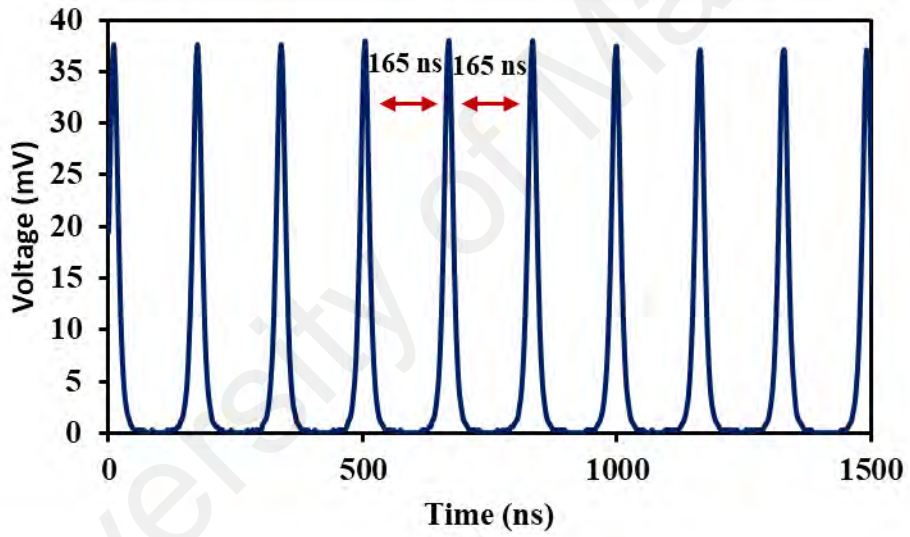
(b)

Figure 4.8 : Typical pulses train of the mode-locked YDFL at pump power of 203.5 mW at time spans of (a) 20 µs (b) 1.5 µs.
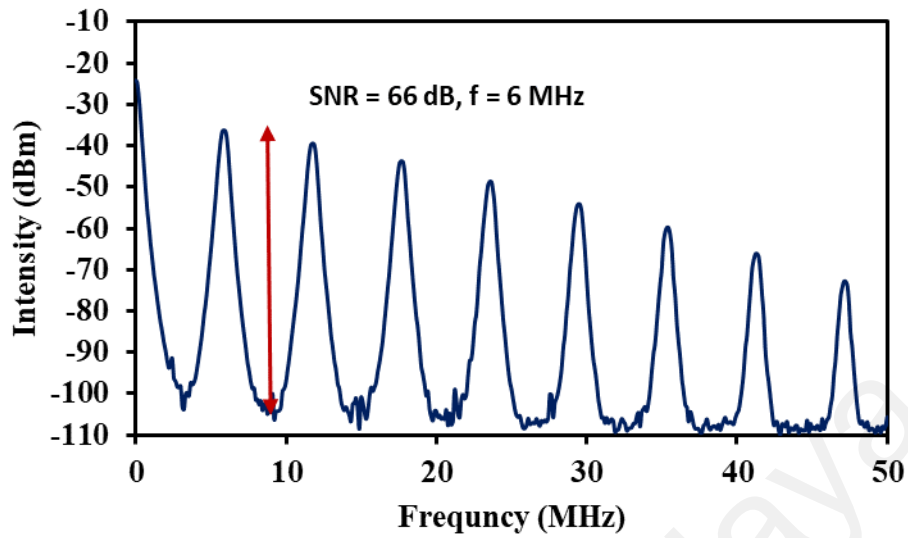
Figure 4.9 : RF spectrum of the mode-locked YDFL at pump power of 203.5 mW.

The relation between the output power and pump power was shown in (Figure 4.10). Under the mode-locking regime, the obtained output power increases from 3.2 mW to 9.9 mW as the pump power was increased from 100.2 to 203.5 mW. This gives a slope efficiency (SE) of 6.8%. The relation between the pulse energy and pump power was also investigated and shown in the same figure. It was observed that the pulse energy increases linearly with the pump, with the maximum pulse energy of 1.65 nJ. Based on the average pump power, the maximum peak power was calculated to be around 1.3 kW.
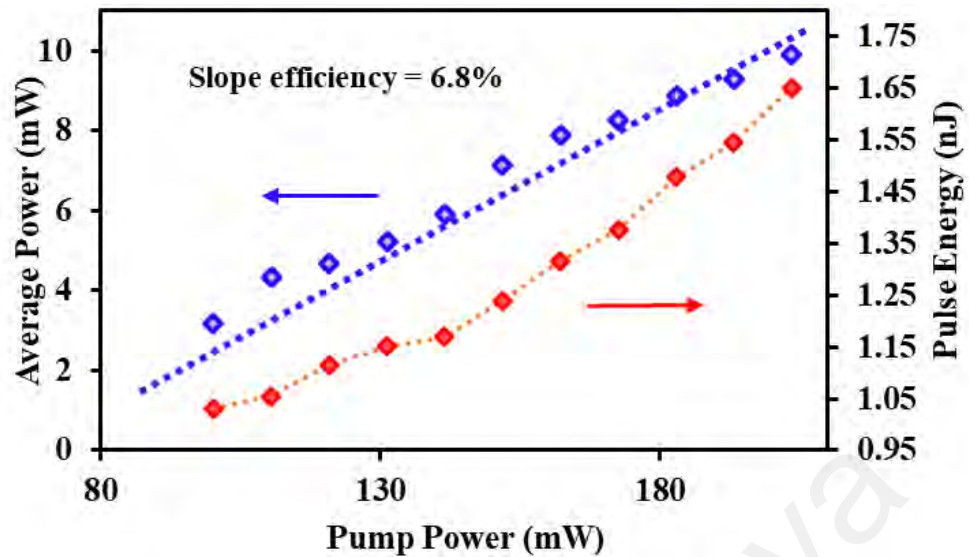
Figure 4.10 : Average output power and pulse energy as a function of 980 nm pump power for the mode- locked YDFL with GO-PEO SA.

4.4 Mode-locked YDFL with topological insulator bismuth selenide.

Topological insulators (TIs) have gained much attention in basic and applied physics research due to the existence of "topologically protected" gapless surface states (Ando, 2013). Such quantum states are immune to non-magnetic impurities as the electron momentum remains locked to its spin (Sengupta, 2014). The discovery of the protected states with a strong spin-orbit coupling at room temperature in real materials (such as Bi_2Se_3, Bi_2Te_3, and SbTe) without the application of an external magnetic field is also interesting for device applications in spintronics and fault-tolerant quantum computing (H. Peng et al., 2012; Sapkota et al., 2017). Bismuth selenide (Bi_2Se_3) was theoretically predicted and experimentally observed to be a two-dimensional (2D) topological insulator with a single Dirac cone (H. Peng et al., 2012). It was classified as a strong topological insulator, where the surface states retain zero-gap despite the presence of atomic-level non-magnetic impurities. Bi_2Se_3 has attracted great attention in physics and chemistry because of its remarkable thermoelectric, optical and photoelectric properties (Anku et al., 2018; B. A. Hasan, 2014).

In this section, passively mode-locked Ytterbium-doped fiber laser (YDFL) are demonstrated using a few-layers Bi_2Se_3 in a fully fiber-integrated laser cavity. The setup of the passively mode-locked YDFL system was similar with (Figure 4.1), except that the SA was substituted with TI Bi_2Se_3 SA. The mode-locked YDFL has a total cavity length of around 20 m with a group delay dispersion (GDD) in anomalous regime of -0.4022 ps^2 and total net dispersion of -20.11 ps^2/km.

The self-started mode-locked operation was achieved at threshold pump power of 110.5 mW. The mode-locking operation was maintained with further increase of pump power up to 211.1 mW. (Figure 4.11) shows the optical spectrum of mode-locking state of the fiber laser at the maximum pump power of 211.1 mW. The YDFL operates at center wavelength of 1051.8 nm with 3 dB bandwidth of 1.05 nm. There are no obvious Kelly spectral sidebands in the spectrum. (Figure 4.12) shows the typical mode-locked pulse train at the maximum pump power of 211.1 mW. It indicates the pulses period (peak to peak spacing) of 120.5 ns, which can be translated to the pulse repetition rate of 8.3 MHz. This has confirmed that the operation of laser is in the mode-locking state and the operation was remaining stable until 211.1 mW pump power. As seen in the same figure, the pulse width is about 6.2 ns under the oscilloscope resolution and that is much broader than the real pulse width. As an alternative, the mathematical calculation based on time-bandwidth product (TBP) can be used for estimating the pulse width. As the TBP was assumed to be 0.315 for $Sech^2$ pulse profile, the minimum possible pulse width was estimated to be approximately 1.107 ps.
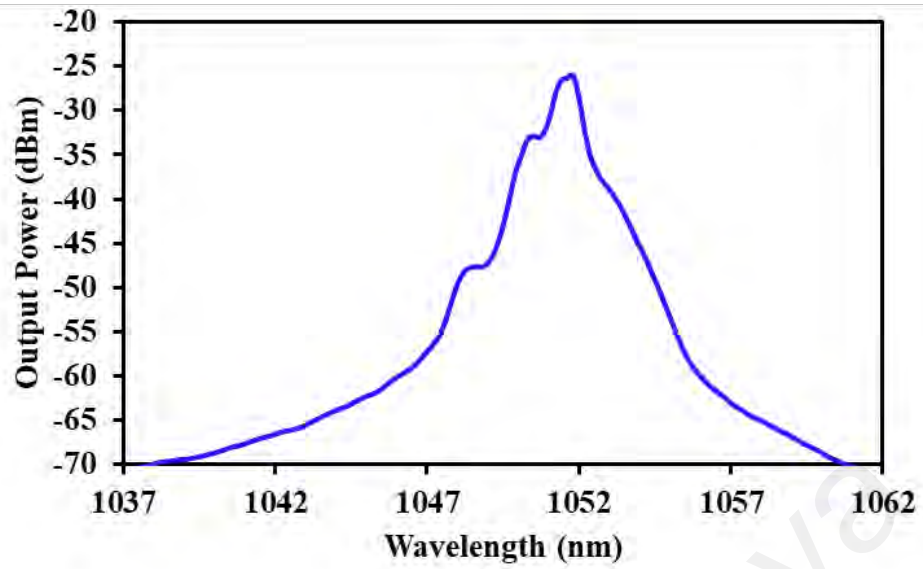
Figure 4.11 : Optical spectrum of the Bi$_2$Se$_3$ based mode-locked YDFL at the maximum pump power of 211.1 mW.
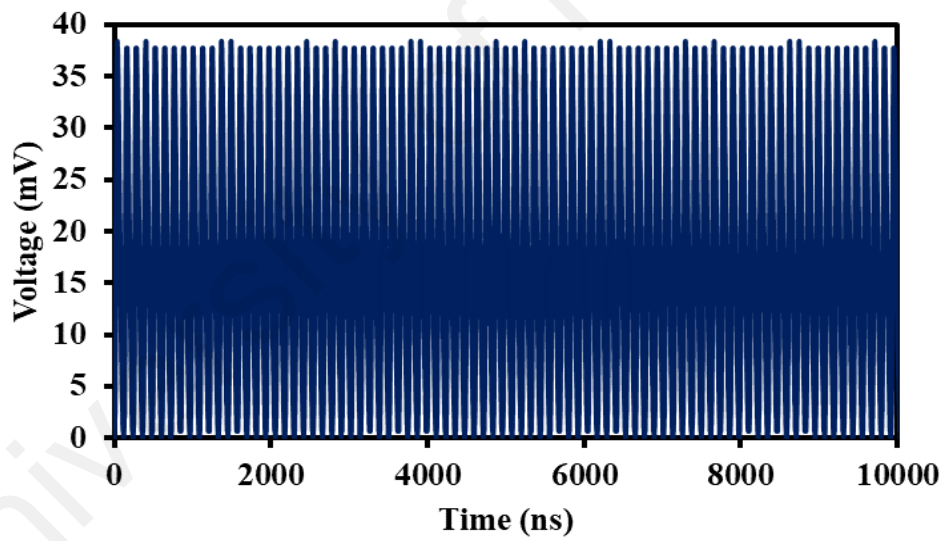
Figure 4.12 : Typical pulse train of the Bi$_2$Se$_3$ based mode-locked YDFL at the maximum pump power of 211.1 mW.

(Figure 4.13 (a)) shows the RF spectrum of the YDFL with a fundamental frequency at 8.3 MHz. The frequency shows a SNR of about 41 dB (Fig. 4.13 (b)), which indicates a stability of the laser. However, the SNR is so much lower than the previous graphene oxide based mode-locked YDFLs. This is most probably due to the operation of this laser, which is not fully in soliton regime due to the absence of obvious and symmetry Kelly sidebands in the spectrum. It is worthy to note that no presence of mode-locking pulse train was observed when the SA was removed.
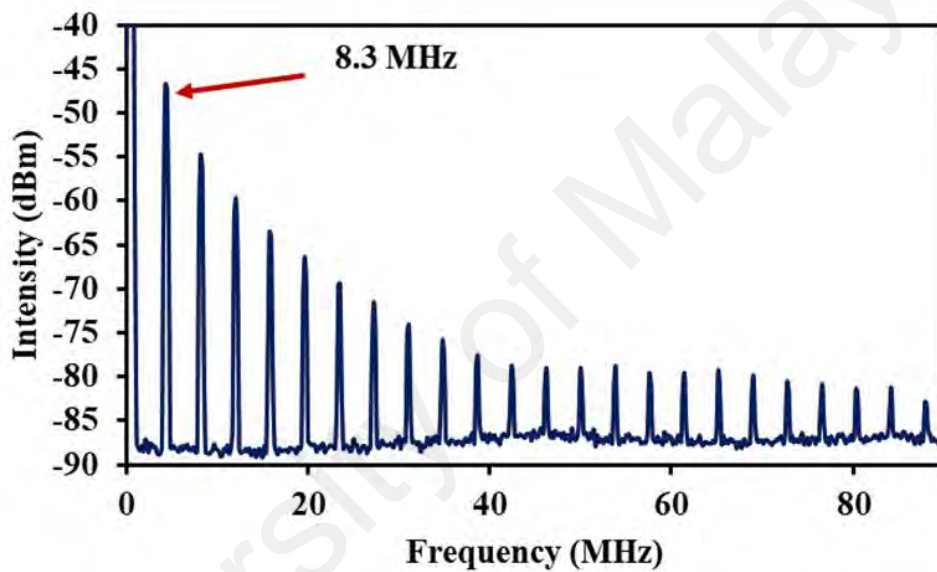
(a)
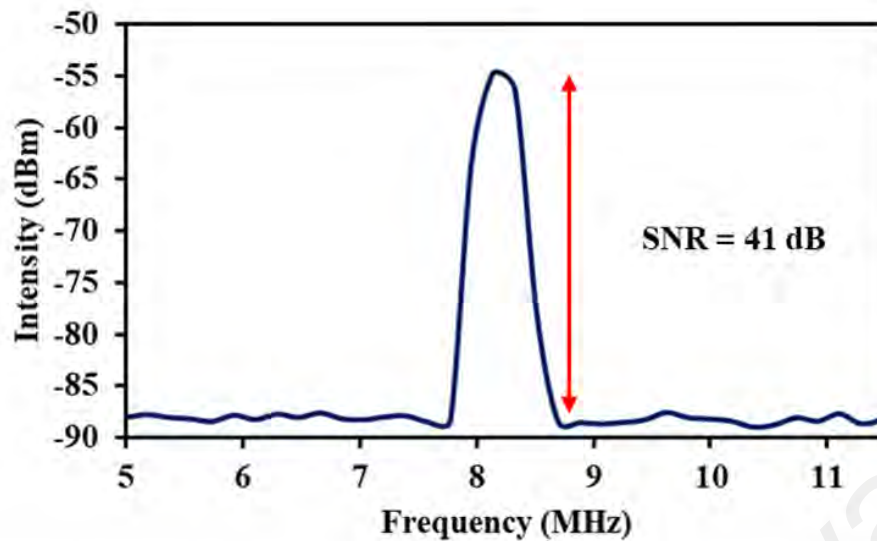
(b)

Figure 4.13 : RF spectrum of (a) the Bi$_2$Se$_3$ based mode-locked YDFL at the maximum pump power of 211.1 mW (b) the enlarged figure at the fundamental frequency region.

(Figure 4.14) shows the average output power and pulse energy at various pump powers. Both output power and pulse energy are linearly increased with increasing in pump power. At 110.5 mW pump power, the maximum output power and pulse energy was obtained to be around 211.1 mW and 1.5 nJ, respectively. The mode-locked pulse disappears when the pump power was increased above 211.1 mW.
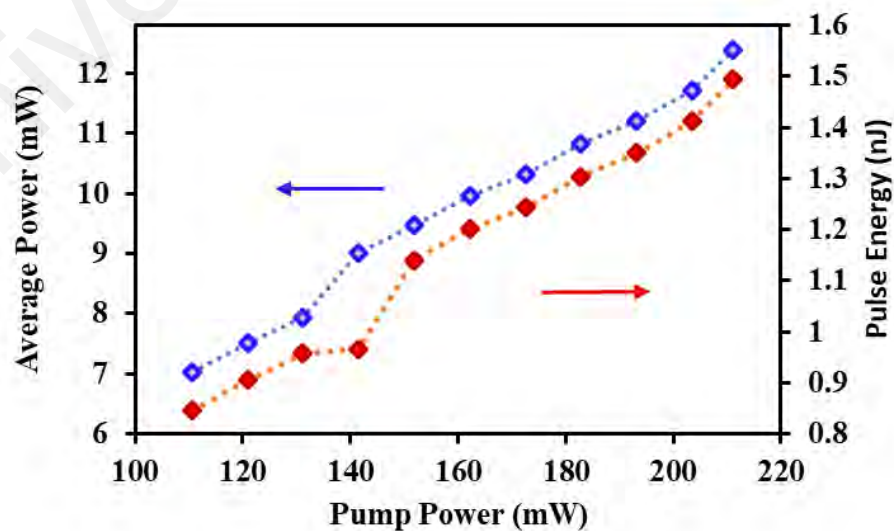
Figure 4.14 : Average output power and pulse energy as a function of 980 nm pump power for the mode- locked YDFL with TI Bi$_2$Se$_3$ SA.

4.5   Mode-locked ytterbium-doped fiber laser with topological insulator bismuth telluride

Passively mode-locking techniques based on various passive SAs have been used to obtain low cost and compact ultrafast lasers as described in previous sections. SA whose light absorbance decreasing with the increasing of light intensity was considered to be an effective method to achieve the mode-locking operation in fiber lasers (M. Liu et al., 2018; C. Zhao et al., 2012). As previously described, SESAMs (I. D. Jung et al., 1997), carbon nanotubes (A. Martinez et al., 2008), zero-gap material graphene (Q. L. Bao et al., 2009), graphene oxide (M. A. Ismail et al., 2014) and topological insulators (TIs) have achieved great success in SA applications for the advantages of wavelength-independent saturable absorbing characteristics, low saturable absorbing threshold (Z.-C. Luo, Liu, et al., 2013), and large modulation depth (Junsu Lee et al., 2014) as well as cheap cost and easy fabrication method (Junsu Lee et al., 2014). In particular, a class of stoichiometric materials, Bi_2Te_3, Bi_2Se_3, and Sb_2Te_3, which have been theoretically predicted to be the simplest topological insulators whose surface states consist of a single Dirac cone at the Γ point, have been experimentally studied and are considered to be a kind of promising SAs (Hajlaoui et al., 2012; Hossain et al., 2011; H. Tang et al., 2011).

The usefulness of Dirac material as SAs was firstly discovered by Bernald et al (2012). Since then, intensive investigations have been conducted by different groups to determine the ultimate potential of TIs as a base material for SA. The demonstrations included mode-locking of lasers at various wavelength regions (Harith Ahmad et al., 2017; Jhon et al., 2018). Recently, great efforts have been done to promote the development of TIs-based SAs in Q-switching and mode-locking (Junsu Lee et al., 2014; Parvizi et al., 2011; Sun et al., 2018). In the previous section, a mode-locked YDFL was demonstrated using a Bi_2Se_3 based SA device as a mode-locker. Here, Bi_2Te_3 material was proposed and demonstrated as a SA device to realize a mode-locking pulses train in

YDFL cavity. The schematic diagram of the proposed Bi_2Te_3 based YDFL is similar to (Figure 4.1). It uses the same components except for the SA device, which was substituted with TI Bi_2Te_3 SA. The total cavity length of the ring setup was measured to be around 18 m. The laser operates in anomalous dispersion regime with total net dispersion of -19.9 ps^2/km and Group Delay Dispersion of -0.35802 ps^2.

In the experiments, the fiber laser starts the mode-locking operation above pump power of 220 mW and the operation was stable with a variation of pump power up to 203.5 mW. As shown in (Figure 4.15), the optical spectrum of mode-locking pulses at 162.2 mW pump power was centered at 1050.23 nm and the 3 dB bandwidth is 2.3 nm. There are no Kelly sidebands observed on the optical spectrum, indicating that the generated pulses have a heavy chirp due to long cavity.
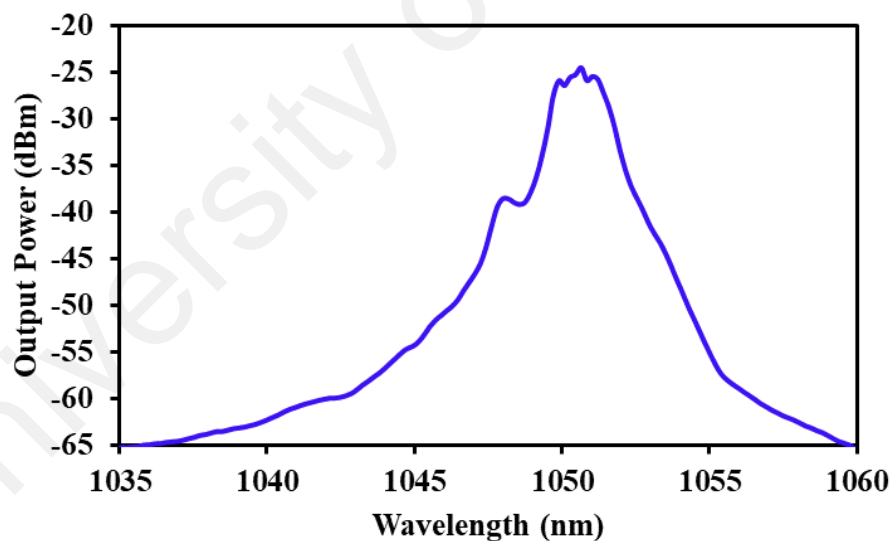
Figure 4.15 : Optical spectrum of the mode-locked YDFL at maximum pump power of 162.2 mW.

(Figure 4.16 (a)) shows the typical oscilloscope trace for the mode-locked pulses train, which indicates the fiber laser operates in a very stable mode-locking state. It has a pulse period of about 105.26 ns (Fig. 4.16 (b)), which corresponds to pulse repetition rate

of 9.5 MHz. As the pulse width size was fitted to sech pulse profile of 0.315 (Antoncini, 2006; R. Woodward, 2015), a minimum possible pulse width should be higher than 0.5 ps. However, the actual pulse width was estimated to be slightly longer, which was primarily attributed to the generated stretched pulses. (Figure 4.17 (a)) shows the radio-frequency spectrum measurement of the output pulses. A strong signal peak with a fundamental repetition rate of 9.5 MHz was clear observed and the measured signal-to-noise ratio is about 44 dB (Fig. 4.17 (b)). This demonstrates that the mode-locking state was quite stable. In order to verify whether the mode-locking operation was purely caused by the saturable absorption of the Bi_2Te_3 SA, the SA device was removed out of the ring laser cavity. In this case, the mode-locking operation could not be obtained no matter how to rotate the PC and adjust the pump power.
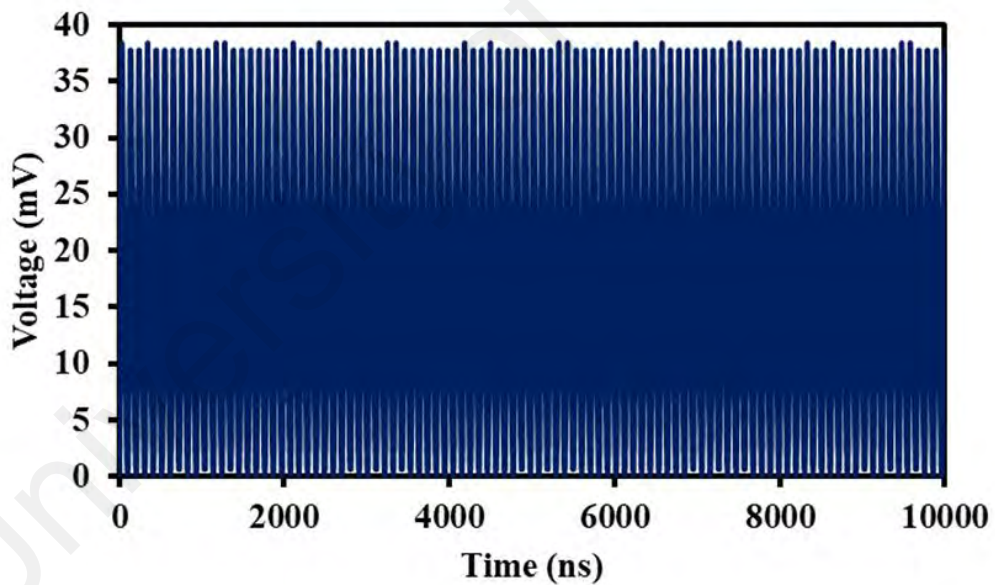
(a)
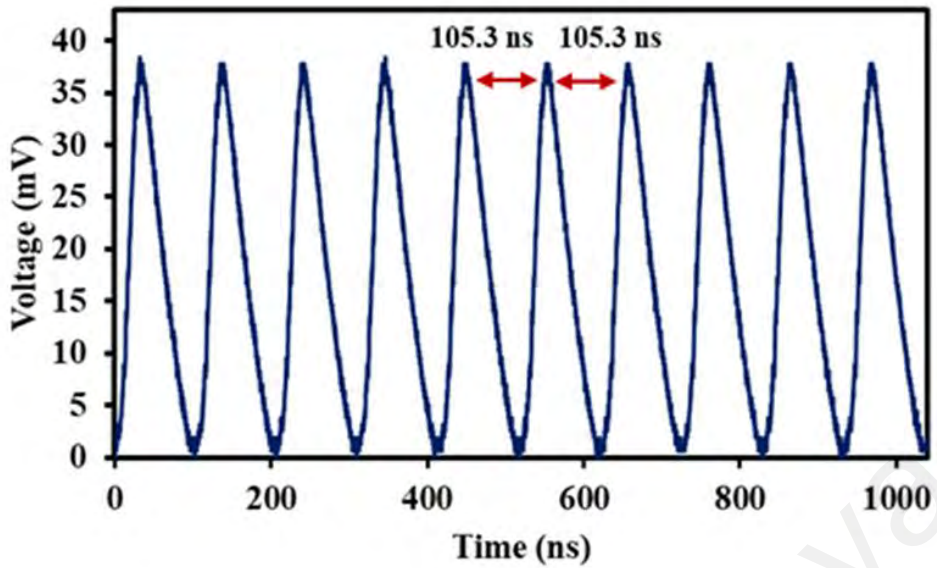
(b)

Figure 4.16 : (a) Typical oscilloscope trace of the mode-locked YDFL at pump power of 203.5 mW and (b) the enlarged spectrum indicating that a time interval of 105.3 ns between the pulses.
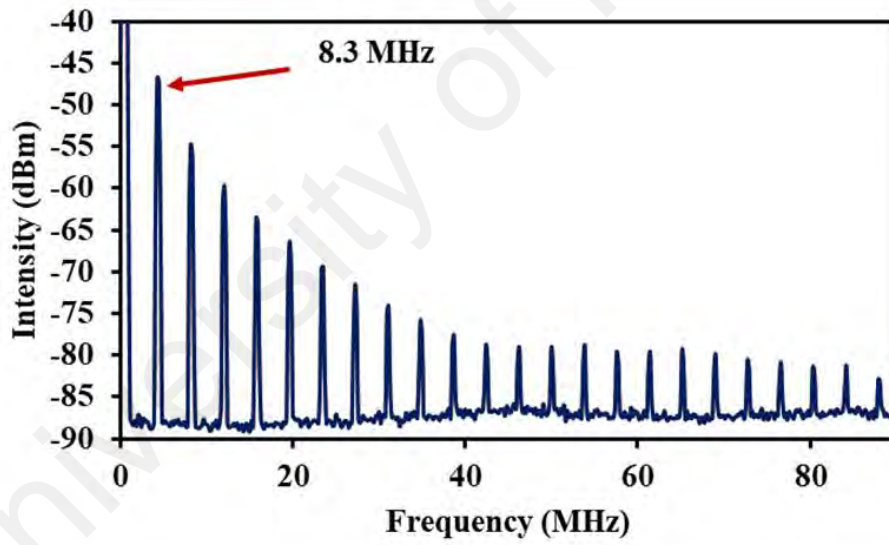
(a)
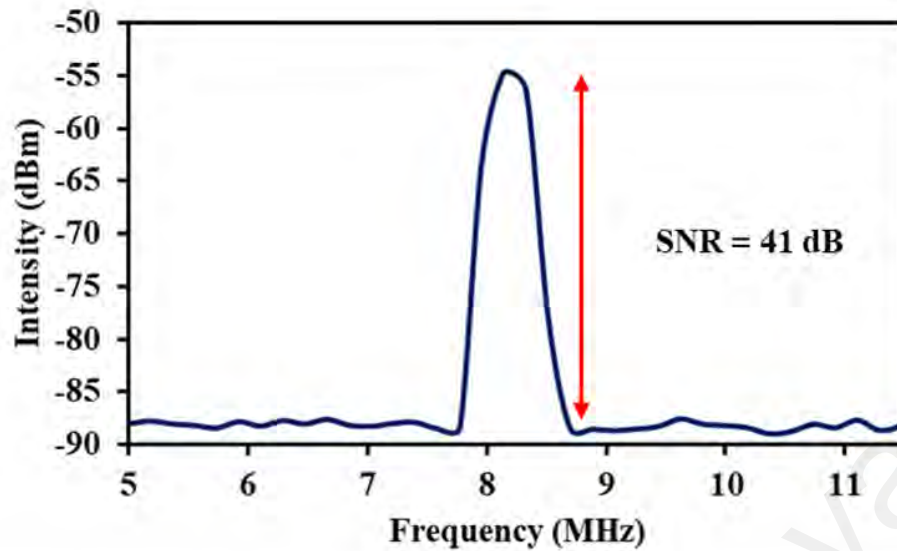
(b)

Figure 4.17 : (a) RF spectrum of the Bi$_2$Te$_3$ based mode-locked YDFL at the maximum pump power of 203.5 mW, and (b) the enlarged fundamental frequency with SNR of 44 dB.

The average output power and pulse energy of the mode-locked YDFL at various pump power are also investigated and the results are shown in Figure 4.18. Both output power and pulse energy are linearly related with the pump power. At the maximum pump power of 203.5 mW, the average output power is 20.3 mW. Therefore, the pulse energy and peak power are estimated at 2.13 nJ and 3.76 kW respectively. From the data, the calculated slope of efficiency for the average output power curve was 10.2 %. While the pump power is over 203.5 mW, the mode-locking pulses become unstable and spectrum fluctuates obviously. This unstable mode-locking maybe interpreted as the over-saturation of TI SA over 203.5 mW. However, the stable mode-locking operation was observed again when the pump power decreases, which indicates that TI SA was not destroyed by the thermal accumulation. The laser-induced damage threshold experiments for TI SA are made. The comparative results show that the topological insulator Bi$_2$Te$_3$ plays a key role in the mode-locking mechanism.
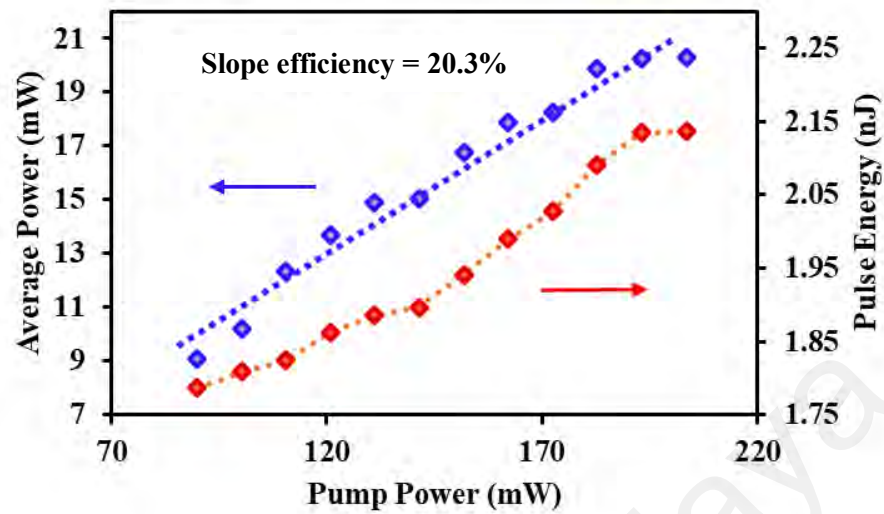
Figure 4.18 : Average output power and pulse energy as a function of 980 nm pump power for the mode- locked YDFL with TI Bi₂Te₃ SA.

4.6   Summary

Mode-locked YDFLs have been successfully demonstrated using the prepared four types of 2D nanomaterial based SAs; graphene based and TI based. The performance of these lasers are compared and summarized in Table 4.1. It is found that the YDFL configured with GO SA produced the most stable mode-locking pulses operating in soliton regime. With this kind of SA, the single pulse energy of 1.65 nJ and the pulse duration of 0.08 ps with central wavelength of 1053 nm are obtained. The fundamental repetition rate of the strong signal is 6.0 MHz and the signal-to-noise ratio is about 66 dB. The results also indicate that Bi₂Te₃ SA produced the highest pulse energy of 2.14 nJ. These results indicate that all the proposed 2D nanomaterials are a promising means for mode-locked fiber lasers.

Table 4.1 : Comparison of the YDFL performance with various SAs

Operation State	Type of SA	Pump Range (mW)	Average Output Power (mW)	Wavelength (nm)	Bandwidth (nm)	Repetition Rate (MHz)	SNR in RF spectrum (dB)	Pulse Width (ps)	Pulse Energy (nJ)
ML	Gr	120.9-203.5	2.91-6.81	1052.89	8.1	4.5	44	0.14	1.52
ML	GO	100.2-203.5	3.18-9.91	1053	14.26	6	66	0.08	1.65
ML	TI Bi_2Se_3	110.5-211.1	7.02-12.4	1051.8	1.05	8.3	41	1.107	1.5
ML	TI Bi_2Te_3	89.85-203.5	9.07-20.3	1050.28	2.3	9.5	44	0.5	2.14

CHAPTER 5: SOLITON PULSES GENERATION IN 1.5 µM REGION

5.1   Introduction

The solidarity of soliton in ultrafast laser ranging from femtosecond to microsecond is beneficial in increasing resolution in metrology (Udem et al., 2002), high accuracy spectroscopy (Mandon et al., 2009) and suppressed phase noise in high speed fiber optic communication (Hillerkuss et al., 2011). In the higher pump power regime, a soliton is most likely to operate in multi pulse operation. Depending on the parameters of the experimental settings, the multi pulse solitons can either rearrange themselves in a fixed position to form the harmonic mode-locking or the bound state pulses. This chapter presents various mode-locked soliton fiber lasers, which were obtained by using the previously developed graphene and topological insulator based SAs in an EDFL cavity.

5.2   Generation of soliton and bound state of solitons pulses with graphene film.

Soliton formation in mode-locked fiber lasers consist of ultra-short pulses with definite shape which was defined by the effect of gain and loss, dispersion, nonlinearity and the state of polarization with the period of a few round trips these short pulses (H. Haris et al., 2016). On the other hand, Bound states of solitons (BSs), also frequently referred to as soliton molecules, a kind of fundamental phenomenon of solitary waves in fiber laser, have also attracted consistent attention due to their potential applications in optical communication since the first prediction by Malomed in the late 20th century (Vazquez-Zuniga et al., 2012). Later, the BSs emerging from numerically and experimentally as an intrinsic feature of the laser. Up to date, bound state of solitons has been demonstrated based on various techniques such as nonlinear polarization rotation (NPR) with figure-of-eight configuration (Ling et al., 2012) and carbon nanotube (CNT) (X. Wu et al., 2011). Recently, graphene has arose as an enthralling material for

optoelectronic applications owing to its exceptional optical properties, such as broadband wavelength tunability, fast saturable absorption and short carrier relaxation time (Gui et al., 2013). Of late, reports have revealed that fiber lasers mode-locked by graphene may operate in various regimes, depending on the cavity dispersion: soliton-like (XL Li et al., 2012), stretched-pulse (J. Wang et al., 2009) or dissipative soliton (Bonaccorso et al., 2010).

In this section, an observation of soliton and bound state soliton in passive mode-locked EDFL was demonstrated by employing graphene embedded into polyethylene oxide (PEO) film as passive saturable absorber (SA). The SA was fabricated from the graphene flakes, which were obtained from electrochemical exfoliation process. The graphene flakes were mixed with PEO solution to form a polymer composite, which was then dried at room temperature to produce a film with a thickness of ~ 50 μm as described in Chapter 3. The film was then integrated in an EDFL cavity by attaching it to the end of a fiber ferrule with the aid of index matching gel and the output of the generated pulse laser was characterized. At first, the EDFL cavity was optimized to obtain conventional soliton pulses. It produced a mode-locking soliton pulses with 20.7 MHz repetition rate and 0.88 ps pulse width at the pump power region from 39.3 to 170.2 mW. When the cavity group delay dispersion was modified, bound soliton with two pulse separation of ~3.55 ps was recorded at the pump power region from 44.9 to 170.2 mW.

5.2.1 Laser configuration for the soliton pulses generation

A schematic of the soliton laser configuration was shown in Fig. 1 where a graphene SA (GSA) was used as a mode-locker. The SA was prepared by cutting a small part of the graphene film (2×2 mm^2) and then sticking it between two FC/PC fiber connectors with the help of index-matching gel. The insertion loss of the GSA was measured to be around 3 dB at 1550 nm. The laser resonator uses 3 m long Erbium-doped

fiber (EDF) as the gain medium. The EDF has an erbium concentration of 2000 ppm, a cut-off wavelength of 910 nm, a pump absorption rate of 24 dB/m at 980 nm and a group velocity dispersion (GVD) of 21.6 ps^2/km at λ = 1550 nm. A 1480 nm laser diode was used to pump the EDF through a 1480/1550 nm wavelength division multiplexer (WDM). An isolator was incorporated in the laser cavity to ensure unidirectional propagation. The output of the laser was taken out from the cavity via a 95/5 fiber coupler. On the other hand, the 5% port of the coupler was connected to the 1×2 3dB coupler so that the output laser can be split into two and each part was then connected to an optical spectrum analyzer (OSA) and an oscilloscope respectively. The OSA (Yokogawa, AQ6370B) with a spectral resolution of 0.02 nm was used for the spectral analysis whereas the oscilloscope (LeCroy,352A) was used to observe the output pulse train of the mode-locked operation in the form of electrical signal via a 6 GHz bandwidth photodetector (Hewlett Packard, 83440B). The pulse width was measured using Alnair intensity based autocorrelator (HAC 200). The total cavity length was approximately 9.7 m, which consists of 3 m long EDF, 0.6 m long WDM fiber and 6.1 m long standard single-mode fiber (SMF). The GVD of the WDM and SMF are -38.0 ps^2/km and -21.9 ps^2/km, respectively. Thus, the estimated net group delay dispersion was calculated to be -0.22 ps^2, which indicates that the proposed laser was operating in anomalous dispersion region.
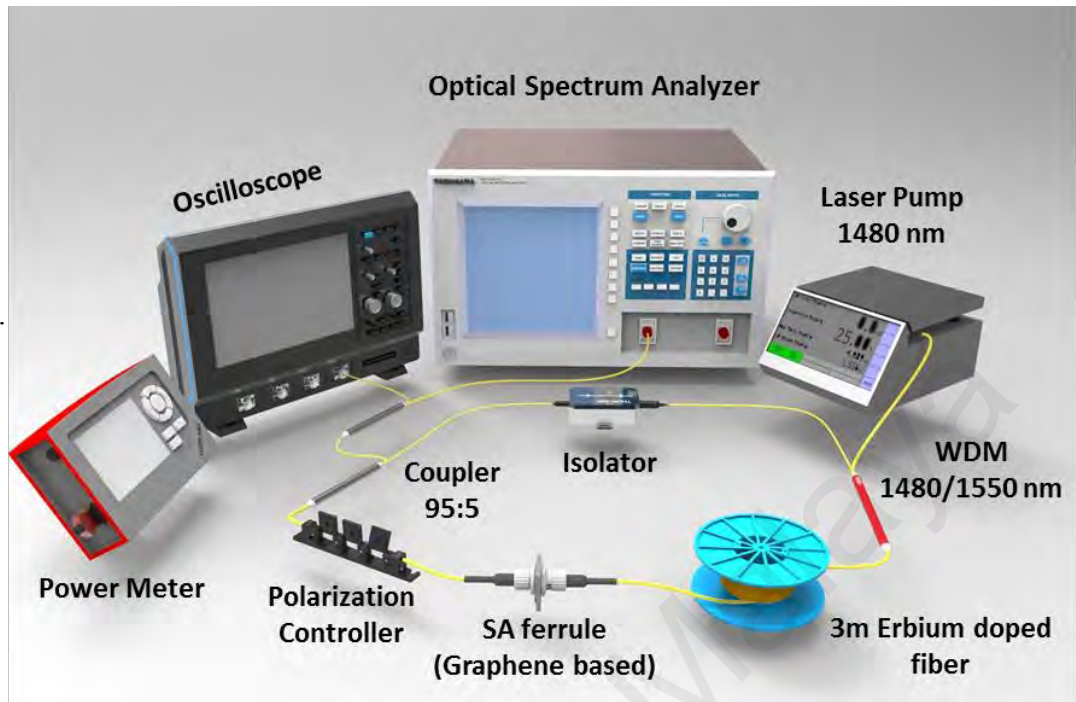
Figure 5.1 : Experimental setup of the proposed soliton mode-locked EDFL
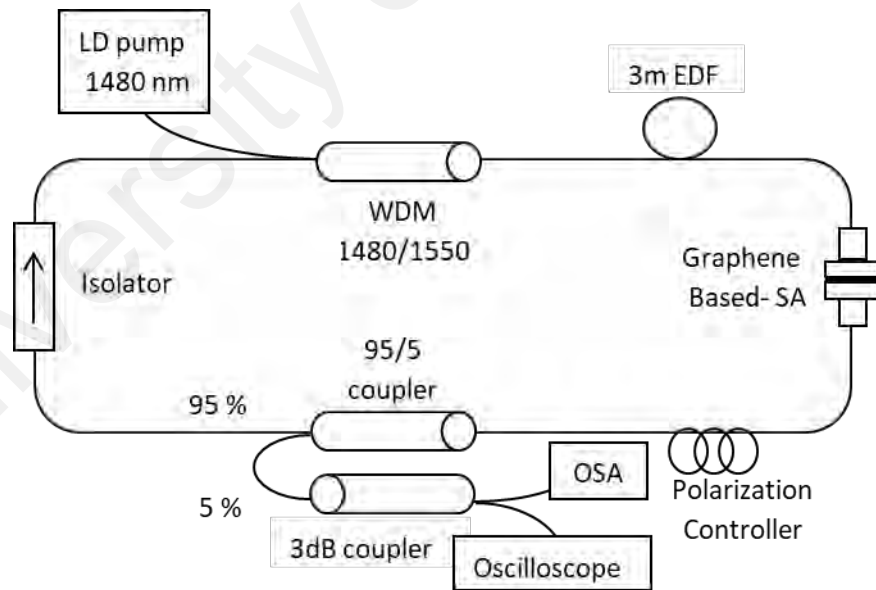
Figure 5.2 : Schematic diagram of the proposed soliton mode-locked EDFL

5.2.2 Performance of the soliton mode-locked EDFL

The proposed mode-locked EDFL started to produce CW lasing at the threshold pump power of 32 mW. A stable self-starting mode-locking soliton pulse was obtained as the pump power was further increased to around 39.3 mW. (Figure 5.3) shows soliton spectra of the mode-locked laser with Kelly's sideband at various pump power. As shown in the figure, it shown that the higher the pump power, the higher the intensity of the soliton spectrum and the more prominent the Kelly sideband. The generation of Kelly sidebands is due to the periodical perturbation of the intra-cavity, which confirms the realization of the soliton pulse in the anomalous dispersion region.
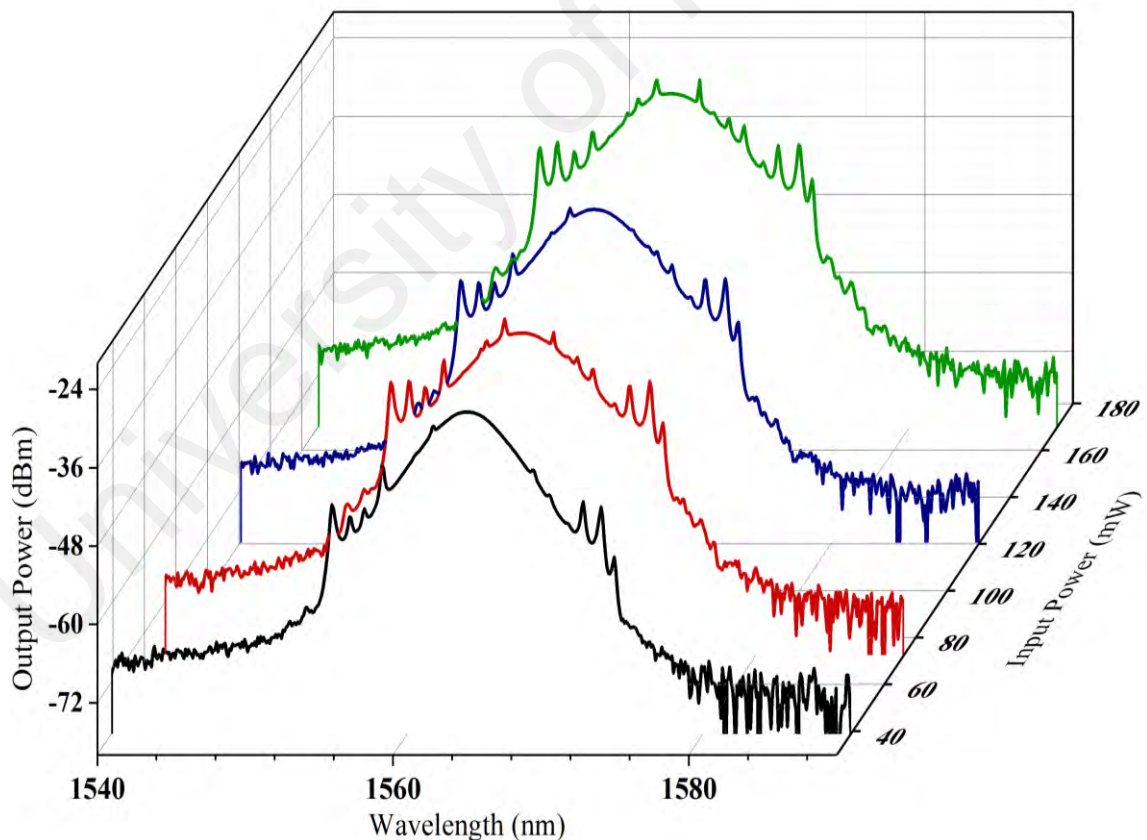
Figure 5.3 : Soliton spectrum with varying pump power (39.3mW, 75.51mW 120.1mW, and 170.2mW)

(Figure 5.4) shows the output spectrum, typical pulse train, auto-correlator trace and RF spectrum of the mode-locked soliton fiber laser at the pump power of 75.51 mW. As shown in (Figure 5.4(a)), the central emission wavelength is approximately 1565 nm with full-width half maximum (FWHM) spectral bandwidth of 5 nm. (Figure 5.4(b)) shows a typical output pulse train with a period of 44.3 ns, which corresponds to the repetition rate of 20.7 MHz as expected from the fiber cavity length. Typical soliton sidebands due to periodic intra-cavity perturbations are also observed. Assuming a sech^2 temporal profile, the pulse width inferred from the measured auto-correlator trace is 0.88 ps as shown in (Figure 5.4(c)). The calculated time-bandwidth product (TBP) is 0.539, slightly deviates from transform limited value of 0.315 for sech^2 pulse. This indicates that the soliton pulse was somehow chirped and the occurrence of chirping in the pulse obtained may cause by residual dispersion of the laser cavity (Kashiwagi et al., 2009). (Figure 5.4(d)) shows the optical-to-noise-ratio (OSNR) of the RF spectrum which is ~ 35 dB at the fundamental repetition rate of 20.7 MHz, signifying a good mode-locking stability. To verify that the mode locking operation is the result of using the graphene-PEO film, the SA from the cavity is purposely removed. No mode locking was observed subsequently, even under the maximum available pump power.
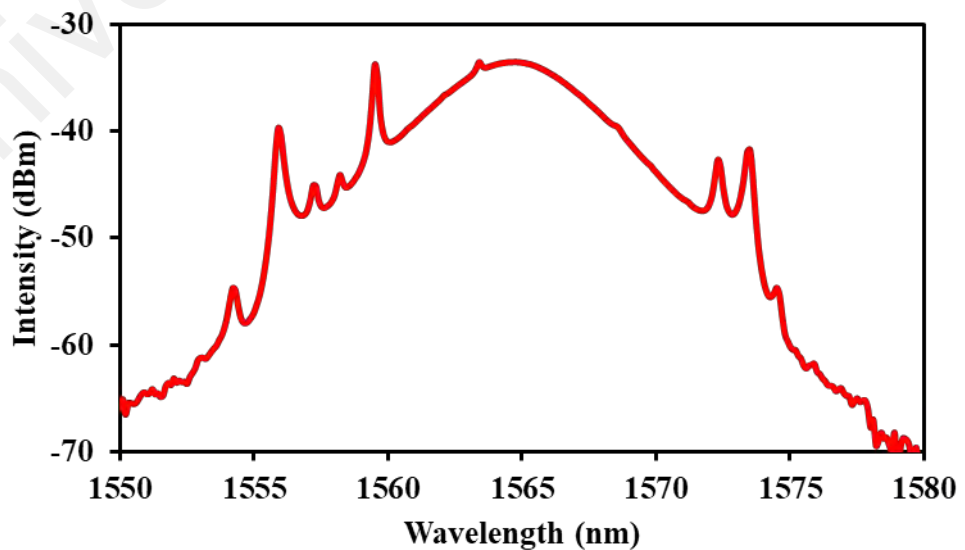
(a)
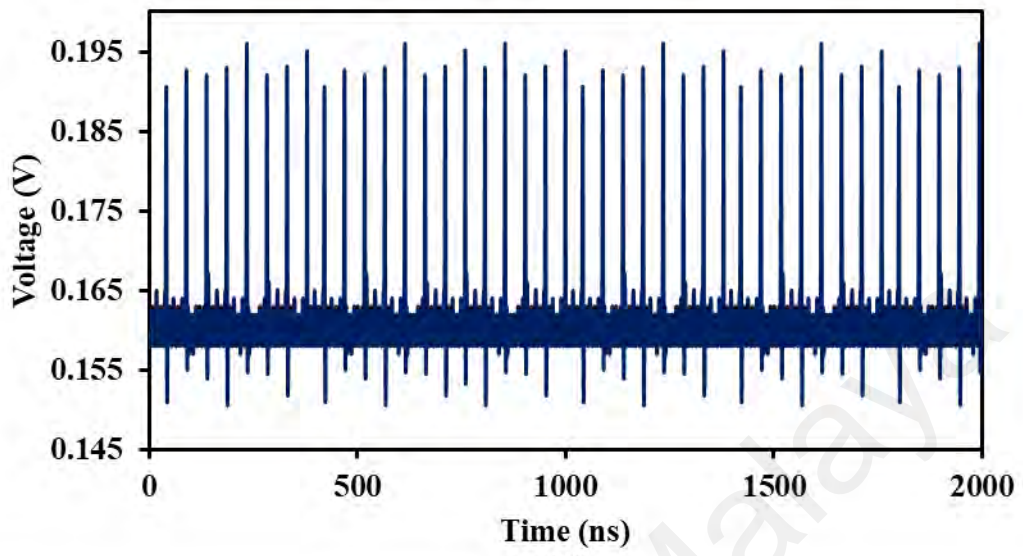
(b)
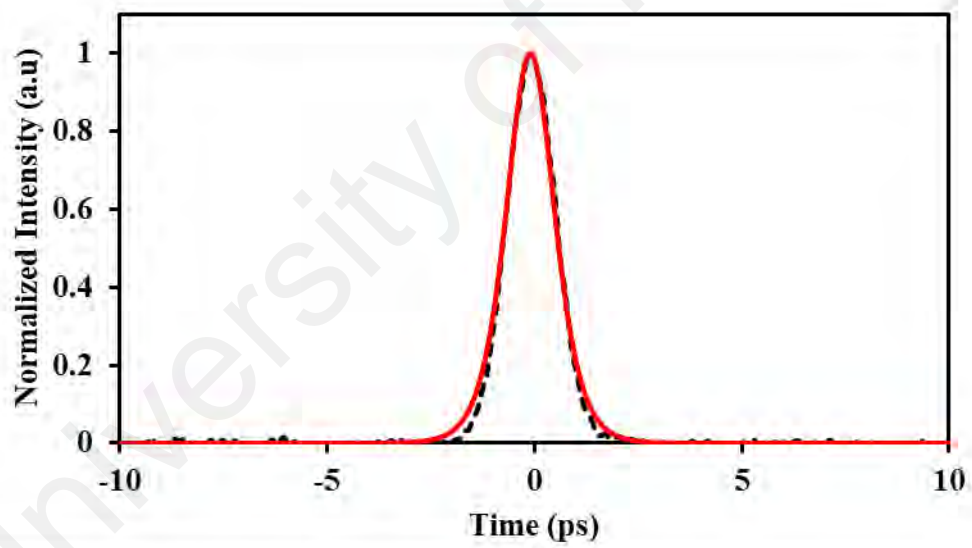
(c)
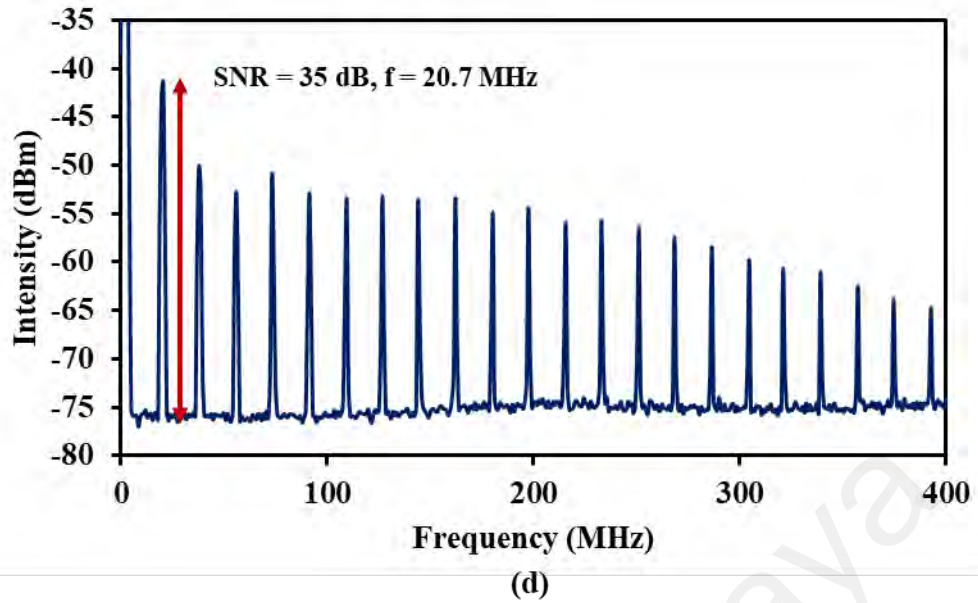
Figure 5.4 : The characteristic of the soliton EDFL obtained at pump power of 75.51 mW (a) OSA trace with FWHM bandwidth of 5 nm (b) Output pulse train with a repetition rate of 20.7 MHz (c) Autocorrelation trace with pulse width of 0.88 ps (d) RF spectrum with OSNR of 35 dB.

The relationship between the output average power and single pulse energy with respect to incident pump power was shown in (Figure 5.5). The output power increases monotonously with the pump power with a slope efficiency of 19.55 %. The pulse energy also increases with pump power. At the maximum pump power of 170.2 mW, the average output power and pulse energy were measured to be 31.5 mW and 1.5 nJ, respectively. It is worthy to note that, the mode-locking operation became unstable and could not be observed when the pump power was increased above 170.2 mW.
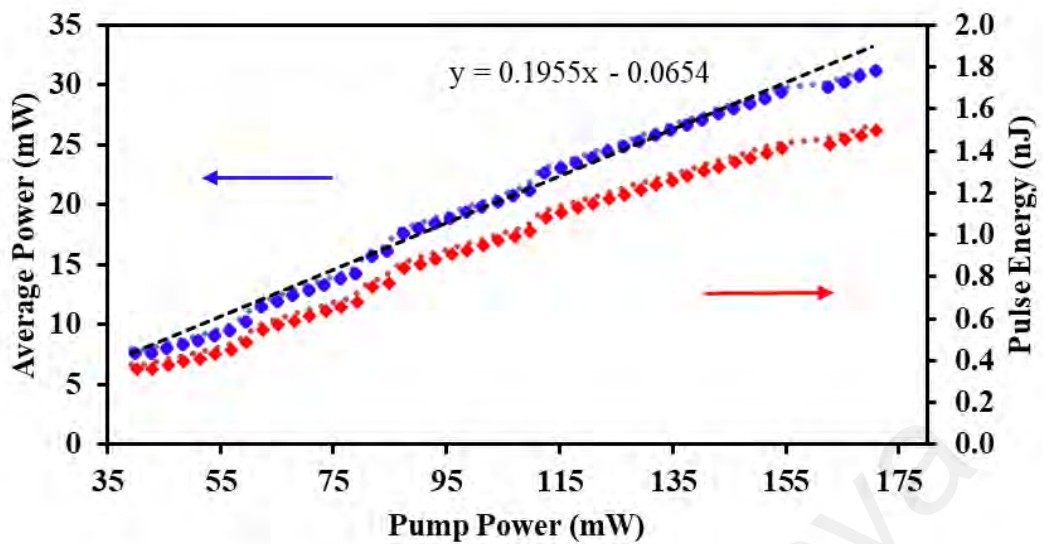
Figure 5.5 : Output power and pulse energy against the pump power

5.2.3 Bound soliton generation in the mode-locked EDFL

Solitons can bind together to form a bound state as the polarization stability was achieved in the cavity. Bound state of solitons could also be generated by the proposed mode-locked EDFL cavity with a slight adjustment on the laser cavity. In this work, a short SMF length (13.2 m) was added in the graphene based mode-locked EDFL cavity of (Figure 5.1) to generate a bound soliton pulses train. The modified cavity has a total length of 16.8 m with a total dispersion of 16.97 ps/nm and group delay dispersion of 0.37 ps^2 and the proposed laser was also operating in anomalous dispersion region. By carefully adjusting the PC orientation and raising the pump power to 44.9 mW, a single soliton splits into two pulses and then evolved into the bound state. The presence of the bound soliton was characterized by a dint in the central wavelength of the output spectrum which can be observed in (Figure 5.6(a)). The central wavelength is 1564.5 nm at the pump power of 110.8 mW. The formation of bound soliton is due to direct pulse to pulse interaction (D. Tang, Zhao, & Zhao, 2005). The optical spectrum also shows a regular and evident modulation with a period of 2.0 nm. The corresponding autocorrelation trace of the bound soliton was shown in (Figure 5.6(b)). Compared to the autocorrelation trace

of the conventional soliton, the autocorrelation for bound soliton has three peaks with two side peaks of the same height. This indicates that the two bound state pulses are identical. The measured pulse separation is ~ 3.55 ps while the pulse duration is ~ 1.04 ps. According to Fourier Transform theory (D. Tang, Zhao, Zhao, et al., 2005), the 3.55 ps separation between the two identical pulses in the temporal domain would lead to the 2.0 nm peak-to-peak spacing in the spectrum domain.
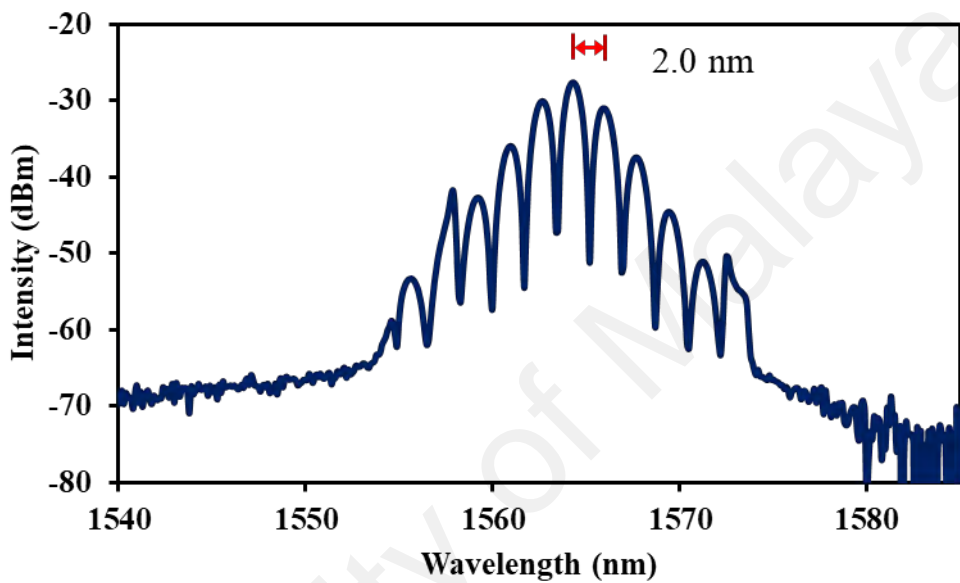
(a)
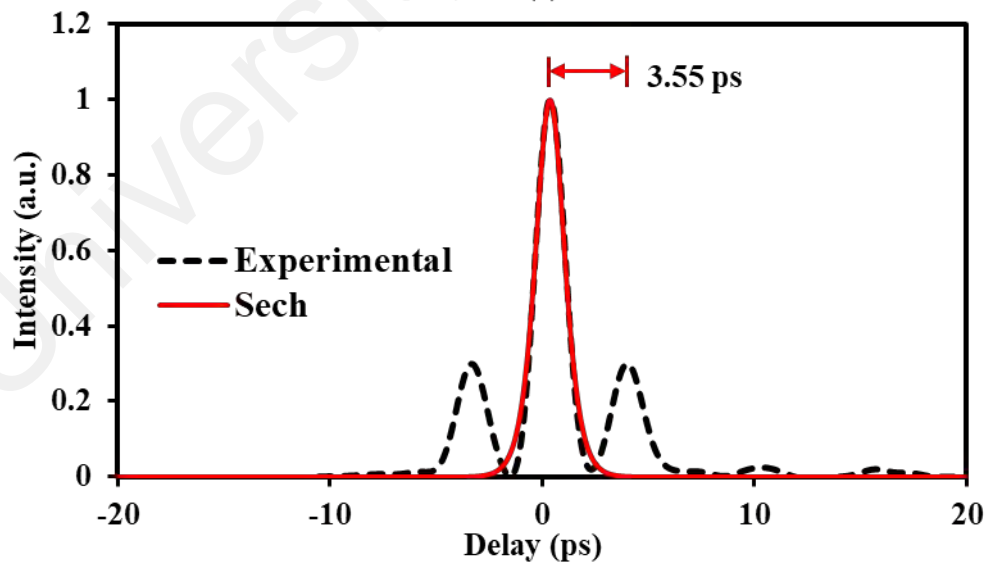
(b)

Figure 5.6 : The characteristic of the bound soliton EDFL, which was obtained by carefully adjusting the PC at pump power of 110.8 mW (a) OSA trace; and (b) Autocorrelation trace

(Figure 5.7) shows the pulse trains observed in the oscilloscope at two different span ranges of 1000 and 200 ns, respectively. It was clearly shown in (Figure 5.7(a)) that only one group of bound solitons pairs exists in the cavity, which was operating at repetition rate of 11.9 MHz. The repetition rate corresponds to the cavity length of 16.8 m. In one cavity round trip time of 84 ns, 7 solitons co-propagating in the fiber laser as shown in (Figure 5.7(b)). The separation of bound state of solitons was around 5.16 ns. (Figure 5.8) shows the RF spectrum of the bound-state solitons mode-locking. The fundamental repetition rate is given as 11.9 MHz, matching exactly with the cavity length. The signal to noise ratio is about 32 dB, indicating a good mode-locking stability. (Figure 5.9) shows the average output power and single pulse energy against the pump power. Both output power and pulse energy increase with the pump power. At the maximum pump power of 170.2 mW the average output power and pulse energy are obtained at 23.5 mW and 1.97 nJ, respectively. The bound state of solitons produces a higher pulse energy compared to the conventional soliton pulses. Improvement of performances of soliton and bound solitons formation are expected by further optimizing the graphene SA fabrication and reducing the loss in the laser cavity.

(a)
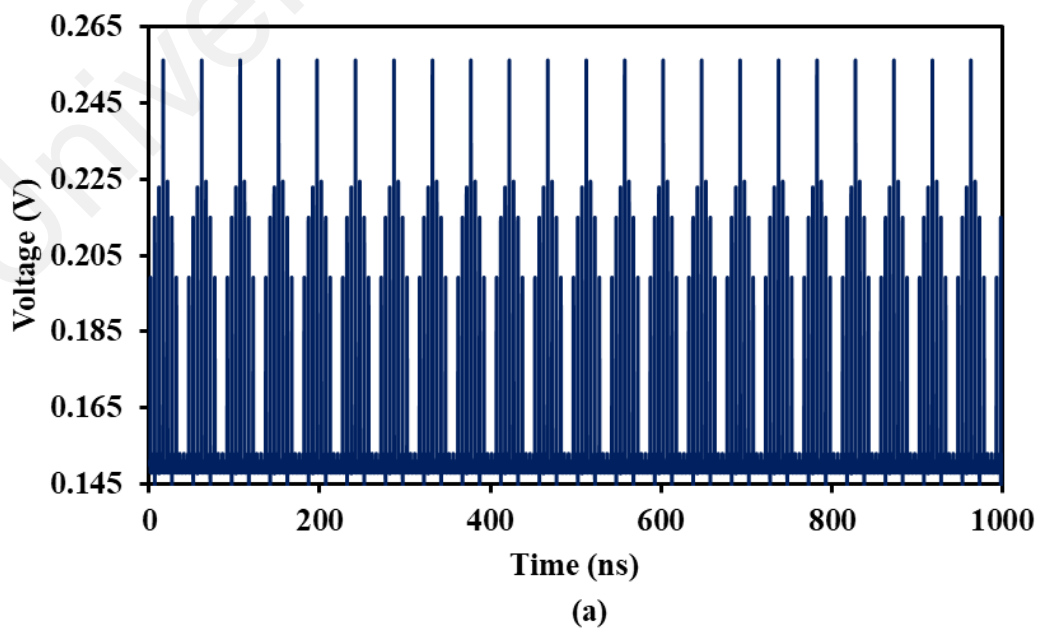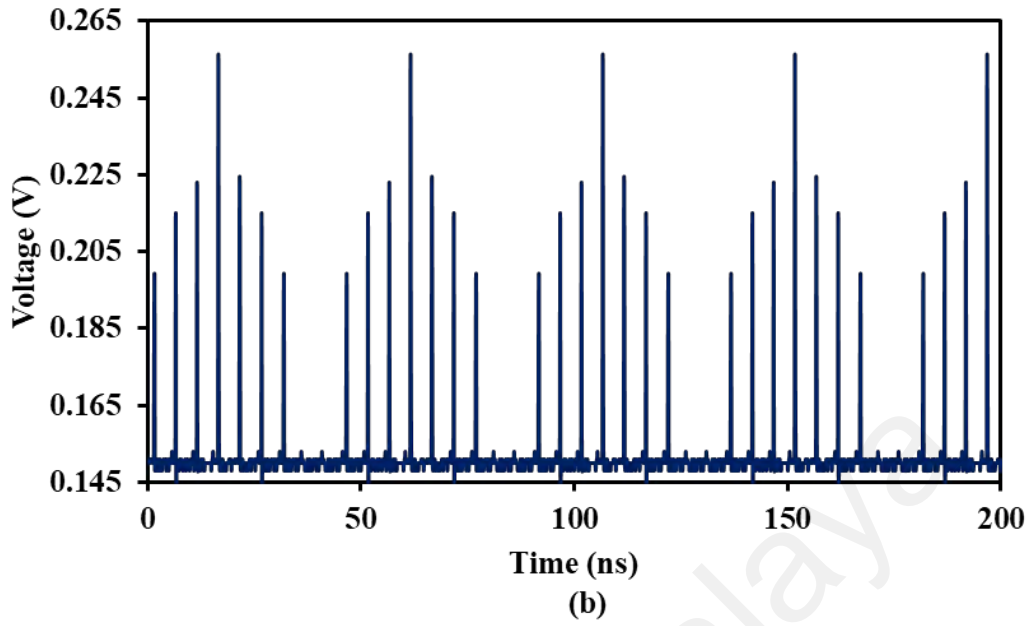
Figure 5.7 : Typical oscilloscope traces of bound-state solitons at two different span ranges (a) 1000 ns (b) 200 ns.
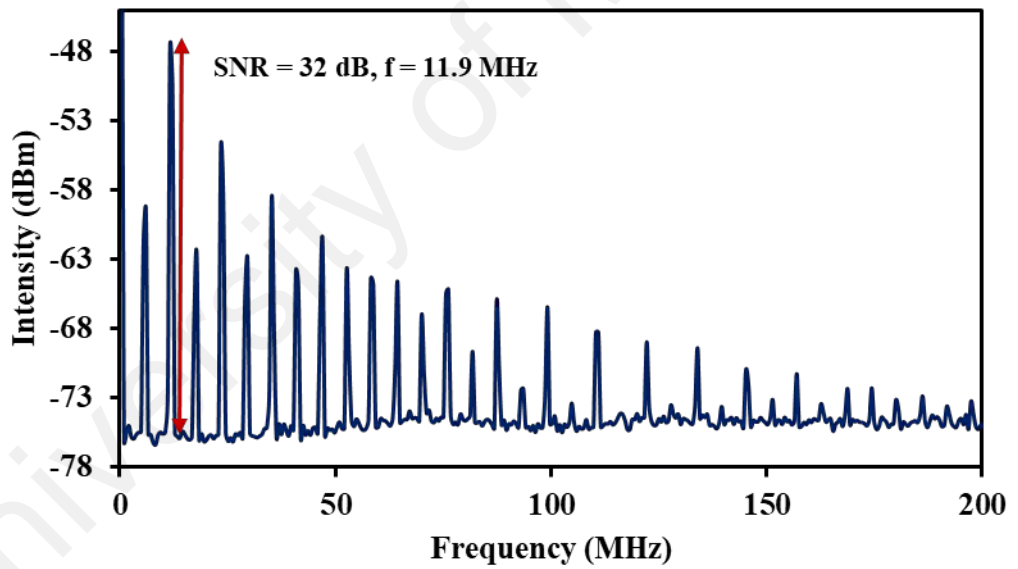
Figure 5.8 : RF spectrum of bound-state solitons
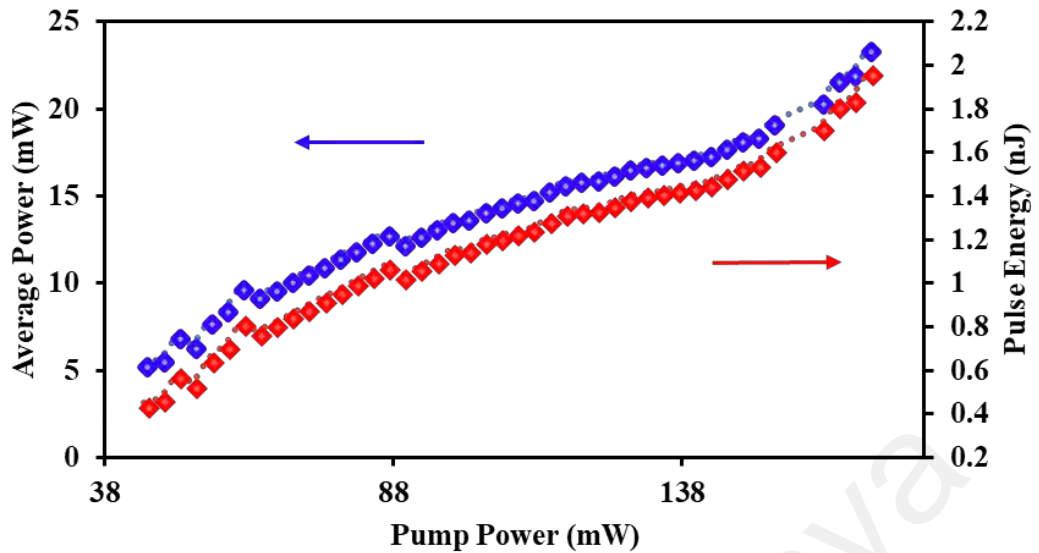
Figure 5.9 : Average output power and pulse energy against pump power for the EDFL with bound-state solitons output.

5.3 Generation of soliton and vector soliton pulses with graphene oxide film

Since the first demonstration on graphene mode-locked fiber lasers in 2009 (Q. L. Bao et al., 2009), graphene has been widely investigated as a novel saturable absorber, due to its strong saturable absorption and broad operational wavelength range. For instance, in the previous section, a mode-locked EDFL was demonstrated using a graphene film as a SA. More recently, the researchers have started to pay much attention to the graphene oxide material and its application on mode-locked fiber lasers (J. Xu et al., 2012). Graphene oxide is an atomically thin sheet of carbon bonded with oxygen functional groups. It can be produced by the oxidative treatment of graphite (Stankovich et al., 2007), which is the first step of graphene fabrication by chemical reduction method (Pei et al., 2012). Therefore, as a semi-product, the graphene oxide is easier and faster to obtain than graphene. Moreover, the covalent oxygen functional groups in graphene oxide not only render strongly hydrophilic property, but also give rise to remarkable mechanical strength (Khan et al., 2016), which offers superior flexibility and processability for production of graphene oxide based optoelectronics. Further investigation shows

graphene oxide has ultrafast recovery time and strong saturable absorption, which is comparable to that of graphene (Loh et al., 2010; X. Zhao et al., 2011).

In this section, an observation of soliton and vector soliton in passive mode-locked EDFL was demonstrated by employing multi-layer graphene oxide embedded into PEO film as passive SA. The GO was fabricated based on a modified Hummers method as described in Chapter 3. The fabricated GO film has nonlinear saturable absorption or modulation depth of 24.1% and it was integrated in an EDFL cavity to produce soliton pulses.

5.3.1   Soliton pulses generation with GO SA

The fabricated GO film was cut into a small piece to attach into an FC/PC fiber ferrule as shown in (Figure 5.10). The ferrule was then matched with another fresh ferrule via a connector after depositing index matching gel onto the fiber end to construct an all-fiber SA device. The insertion loss of the SA was measured to be around 1.5 dB at 1550 nm. SA device was integrated into an EDFL cavity, which was similar to (Figure 5.1). The mode-locked EDFL has total cavity length of 9 m which consists of 3 m long EDF, 0.6 m long WDM fiber and 5.4 m long SMF, with group velocity dispersion (GVD) of 21.6 ps^2/km, -38.0 ps^2/km, and -21.9 ps^2/km, respectively at 1550 nm. The cavity operates in anomalous fiber dispersion of -0.20 ps^2, and thus traditional soliton tends to be formed in the fiber laser.

Figure 5.10 : GO PEO film-based SA

In the experiment, a stable mode-locking pulses train was generated due to the balance between the GVD and nonlinearity effect inside the ring cavity. CW lasing was observed at around 32 mW pump power and the mode-locking laser operation was self-started when the pump power was increased to 39.3 mW. The mode-locking operation operated stably below the pump power of 170.2 mW. It was also confirmed that no mode-locking pulses were observed when GO film was removed during the experiment, indicating the mode-locked laser operation was indeed introduced by the fabricated GO SA instead of the nonlinear polarization rotation.

(Figure 5.11 (a)) illustrates the optical spectrum of the mode-locked EDFL at the pump power of 120.1 mW. The spectrum was centered at 1564.6 nm with a 3 dB bandwidth of 5.6 nm. Kelly sidebands are also clearly observed on both sides in the spectrum, indicating that the mode-locked operation was in anomalous dispersion soliton regime. Inter-correlation between dispersion and nonlinearity in the ring cavity produces

131

a good generation of soliton pulses. (Figure 5.11(b)) shows the typical oscilloscope trace at 120.1 mW pump power, which indicates a stable mode-locked pulse. The pulse train is uniform, but a slight distinct in amplitude was observed for each envelope spectrum due to Q-switching effect. The peak to peak period of the pulse train was measured to be 45.4 ns (Figure 5.11 (c)), which corresponds to the repetition rate of 22.0 MHz. The obtained repetition rate matches with the cavity length of about 9 m.

(Figure 5.11 (d)) shows the measured autocorrelation trace of the output pulse together with secant hyperbolic-fitting curve. The pulse duration was 0.8 ps and the time-bandwidth product (TBP) was 0.52, which was slightly higher to the 0.315 of transform-limited sech^2 pulses. This indicates that the optical pulse was slightly chirped. The RF spectrum of the laser was depicted in (Figure 5.11 (e)). The fundamental cavity frequency was 22.0 MHz (corresponding to the cavity round-trip time, 45.4 ns). The electrical signal to noise ratio (SNR) was 35.8 dB, demonstrating the mode-locking state was stable.
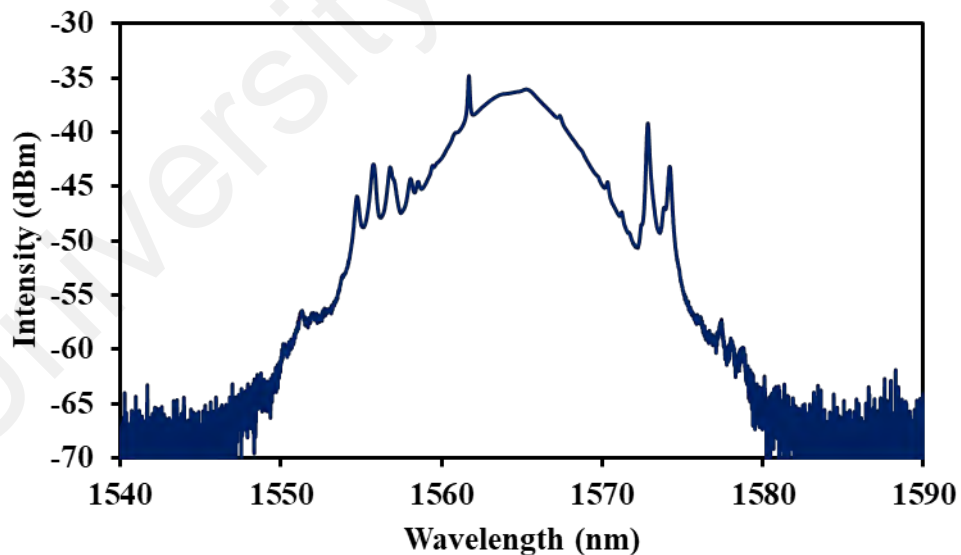
(a)
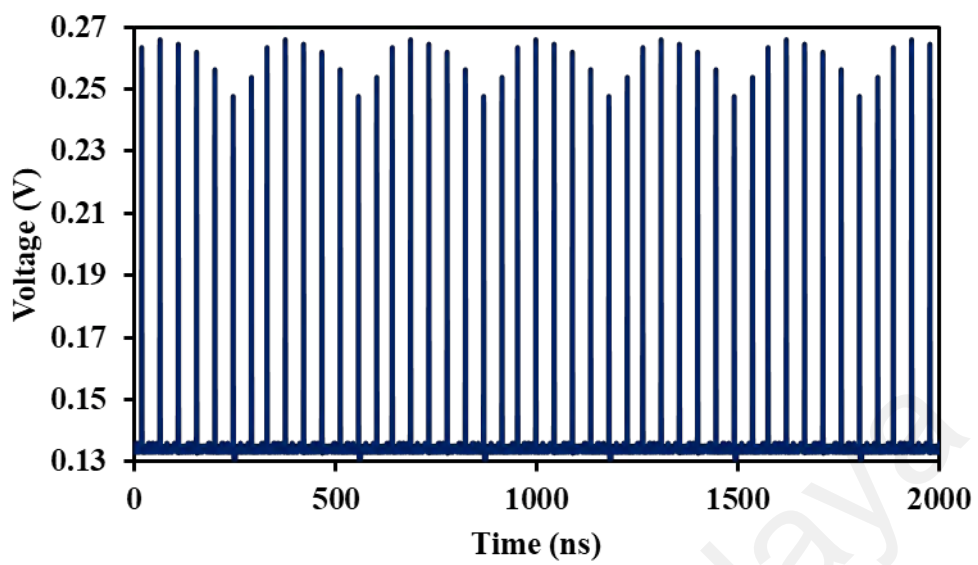
(b)
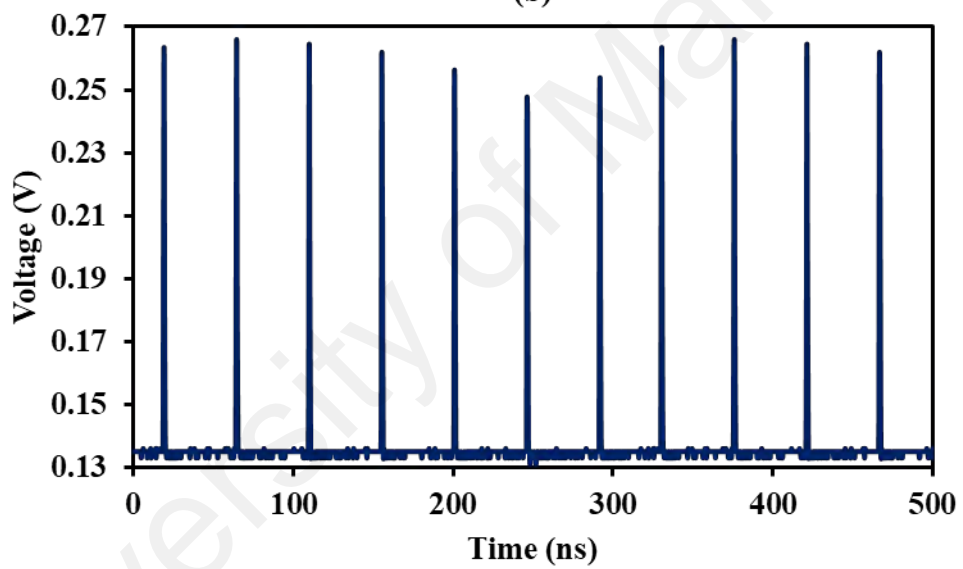
(c)
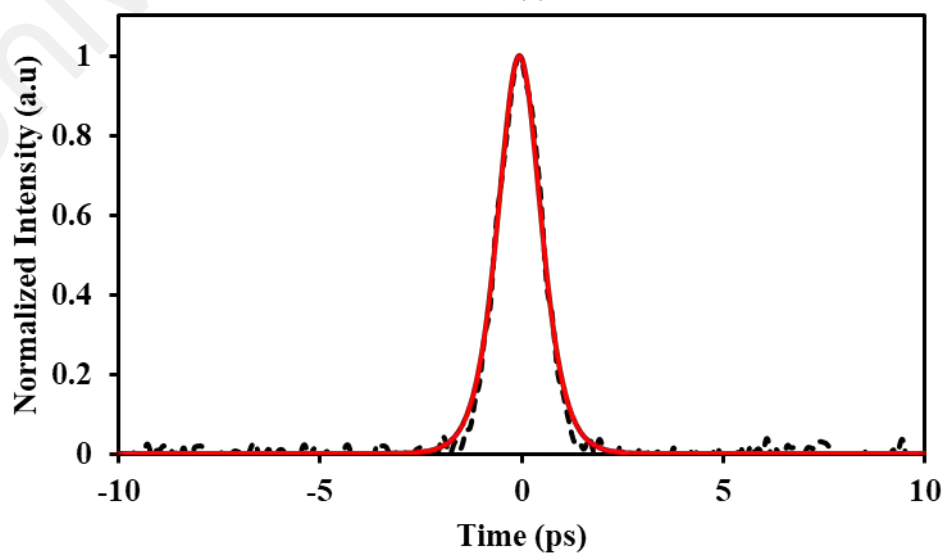
(d)
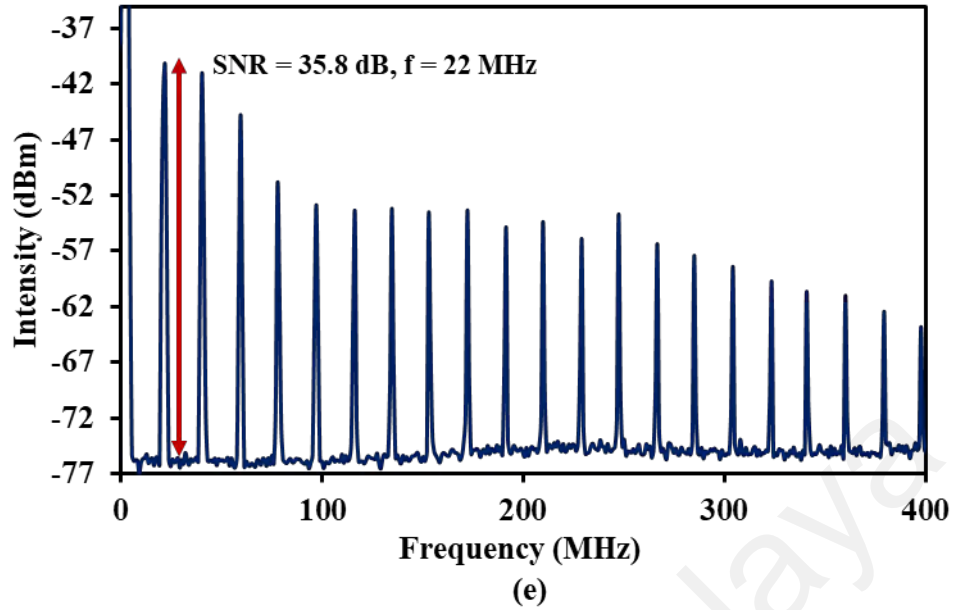
Figure 5.11 : Spectral and temporal characteristics of the soliton pulses train at pump power of 120.1 mW (a) Optical spectrum (b) typical pulse train (c) span 500 ns (d) auto-correlator trace (e) RF spectrum.

To check the stability, the pump power is change and found that the mode-locking state could start each time when the pump was retuned into the power range from 39.3 to 170.2 mW. It was observed that, the mode-locking operation became unstable and could not be observed when the pump power was increased above 170.2 mW. (Figure 5.12) shows the relationship between the output average power and single pulse energy with respect to incident pump power. We found that both output power and pulse energy increase monotonously with the pump power. The slope efficiency of the mode-locked laser was 23.65 %. At the maximum pump power of 170.2 mW, the average output power and pulse energy were measured to be 33.7 mW and 1.53 nJ, respectively. Compared to the previous graphene based mode-locked laser, the GO based laser produced a slightly higher output power and pulse energy.
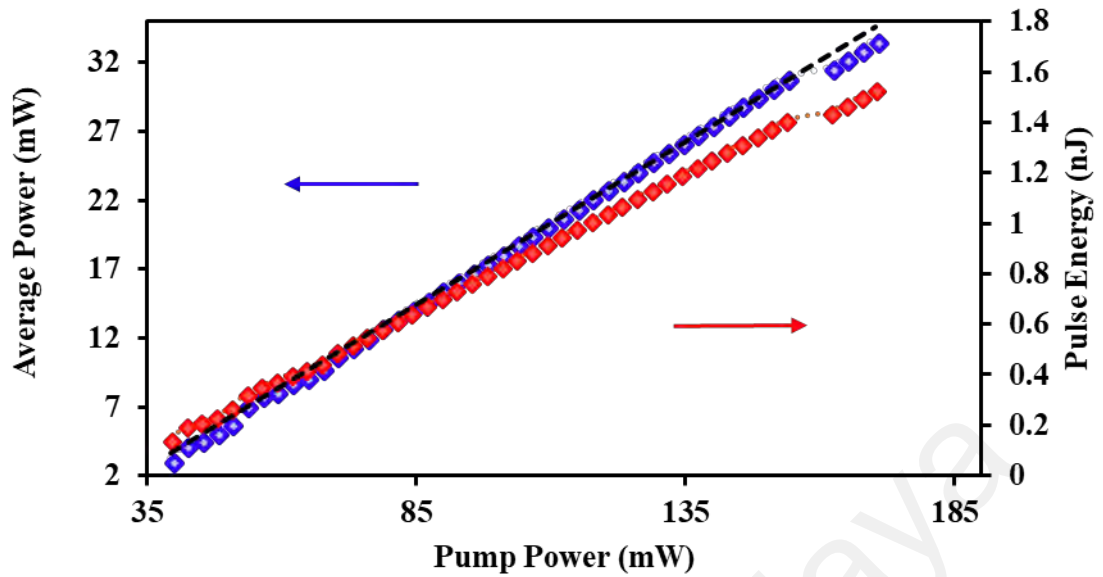
Figure 5.12 : Average output power and pulse energy against pump power for the GO based mode-locked soliton EDFL

5.3.2 Vector soliton pulses generation with GO SA

Solitons, as stable localized wave packets that can propagate long distance in dispersive media without changing their shapes, are ubiquitous in nonlinear physical systems. It was observed in the previous experimental studies that under strong pumping, mode locking could self-start in a fiber laser even without placing an intra-cavity SA device if a polarization sensitive component existed instead (J. Sotor et al., 2012). Interestingly, such kind of mode-locking operation will only allow for the generation of scalar solitons. These are soliton pulses with fixed polarization. In reality a SMF always supports two orthogonal polarization modes. Taking fiber birefringence into account, it was later reported that various types of vector solitons could be formed in SMFs. Therefore, it would be interesting to study the soliton polarization dynamics in fiber lasers mode locked by the GO-based SA, which shows weak linear polarization dependent absorption.

Polarization properties of ultrashort pulses are newly explored, which shows a distinctive regime for pulse generation. Therefore, a strong motivation to search for this new regime arises. On most occasions, due to the asymmetrical structure and bending, the birefringence of SMF gives rise to the differences of two orthogonal polarization modes in term of both phase and group velocities (Z. Wu, Liu, Li, et al., 2016) . On the other hand, when the soliton propagates periodically within a laser cavity, phase locking between two orthogonal polarization modes can be achieved, leading to the generation of vector soliton (Jin et al., 2016; Z. Wu, Liu, Fu, et al., 2016). Consequently, for a fiber laser without polarization sensitive components, it favors the generation of vector solitons. In order to generate vector solitons, polarization dependence of the laser cavity should be avoided as much as possible. Until now, SESAM and carbon nanotube (CNT) are the commonly-used mode-lockers to obtain vector soliton arising in the passively mode-locked fiber lasers. In this section, GO based SA was used inside an EDFL cavity to generate vector soliton. Due to the absence of the polarization constraints, two orthogonal polarization modes in the fiber laser can develop freely. Therefore, much enriched characteristics emerge from vector soliton fiber laser compared with the scalar one.

The mode-locked EDFL setup was schematically sketched in (Figure 5.1) and GO film was employed as SA. The laser cavity is a ring that consists of 3 m long EDF with GVD of 21.6 ps^2/km. Intra-cavity passive components are all made by SMF except for WDM fiber and connected by SMFs with GVD parameter of -21.9 ps^2/km, the total length of SMF is around 12 m. The WDM fiber is 0.6 m long with a GVD of -38.0 ps^2/km. The total cavity length is 15.6 m with group delay dispersion of -0.35 ps^2. The cavity is thus dispersion managed with net anomalous dispersion to support vector soliton generation through mutual balance between the gain, loss, dispersion and nonlinearity characteristics inside the cavity. It is worthy to note that no polarizer was utilized in the cavity, and all

fibers used had weak birefringence, vector soliton generation was therefore naturally obtained in the fiber laser.

The mode locking self-started as long as the pump power was increased to the mode-locked threshold of 44.9 mW. (Figure 5.13) depicts the mode-locking performance of the fiber laser. As shown in (Figure 5.13 (a)), the optical spectrum of the mode-locked pulses was centred at ~1558.9 nm. The 3-dB bandwidth of the spectrum is ~2.7 nm. Appearance of the Kelly sidebands on the spectrum, which is a typical feature of the soliton fiber lasers with net anomalous dispersion, indicates that the mode-locked pulses are solitons. To identify the pulse duration of the solitons, autocorrelation trace of the pulses was measured, as shown in (Figure 5.13 (b)). The pulse width is about 1.3 ps if the sech^2 intensity profile was assumed. Considering that the bandwidth of the spectrum is 2.7 nm, the time-bandwidth product is ~0.43, indicating that the mode-locked pulses are slightly chirped. (Figure 5.13 (c)) shows the RF spectrum of the mode locked pulses within a broad span frequency up to 2000 MHz. There is no obvious spectral modulation, confirming that the pulse train is stable. The fundamental repetition rate of the pulse train is ~12.8 MHz as shown in the inset figure. A signal to noise ratio of ~53.6 dB was also found. (Figure 5.13 (d)) shows the average output power and pulse energy against pump power. It was shown that both output power and pulse energy stably increase as the pump power increases, indicating that the passive mode locking in the laser is robust. The mode locking can be kept until the pump power is as high as 170.2 mW.

(a)

(b)

(c)
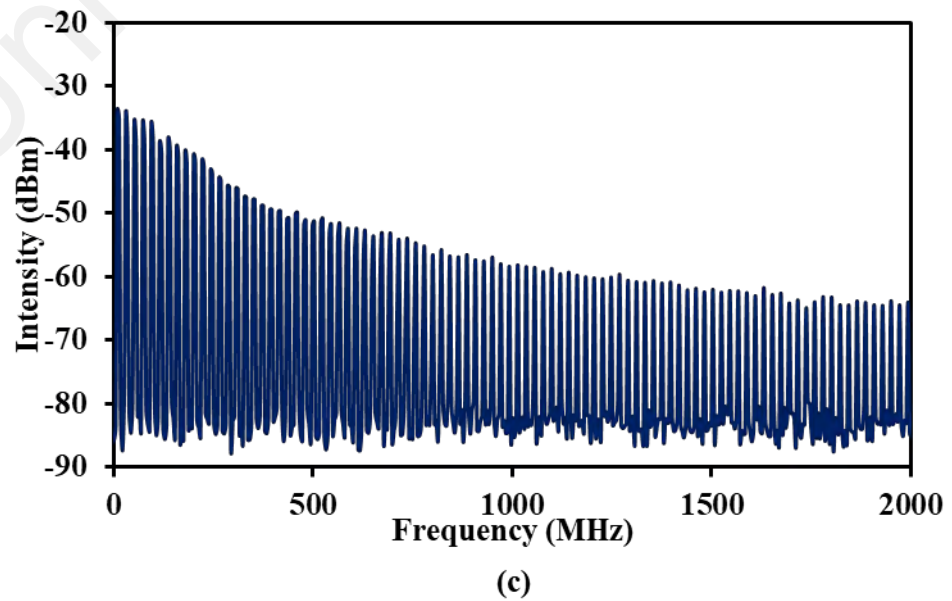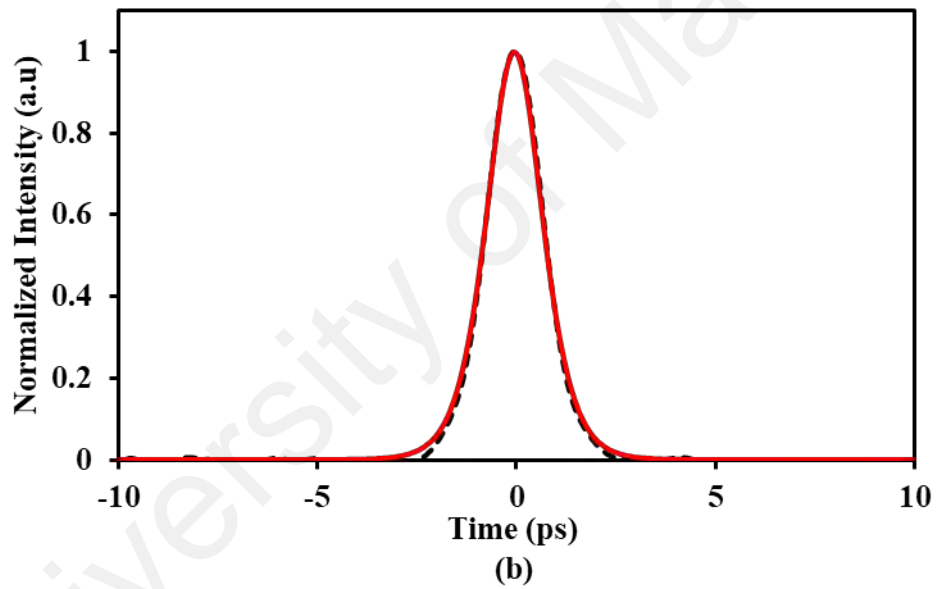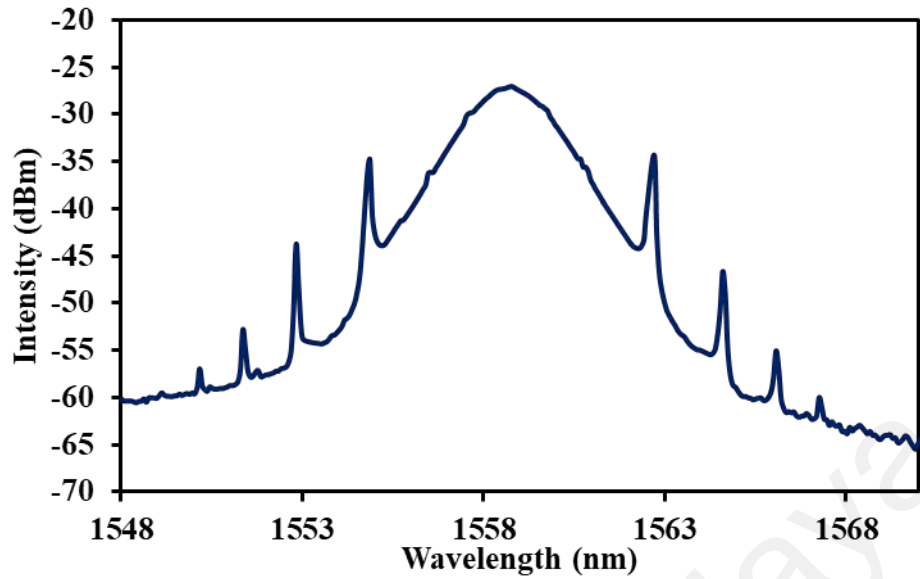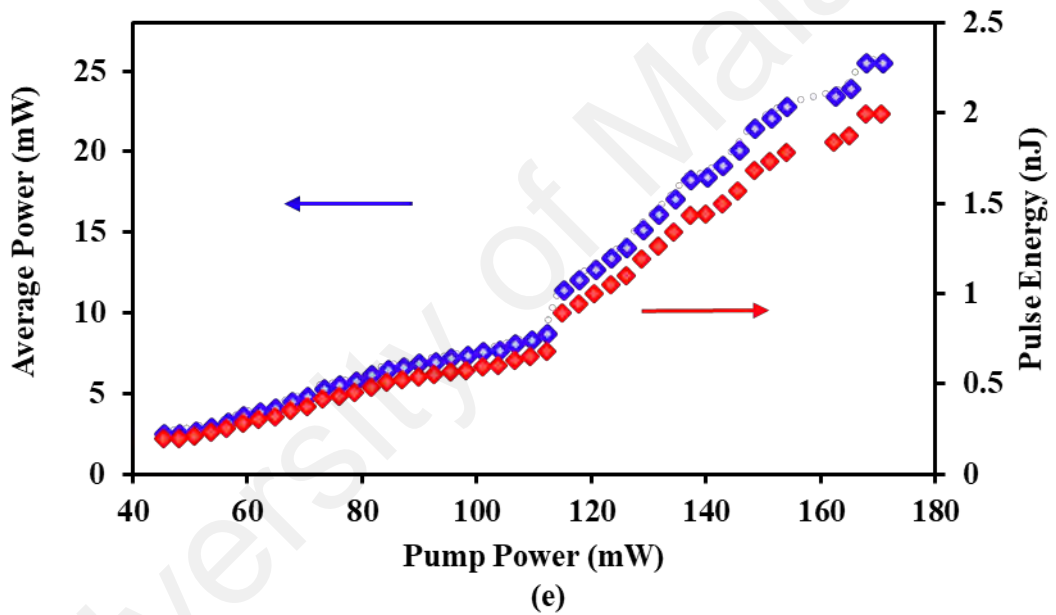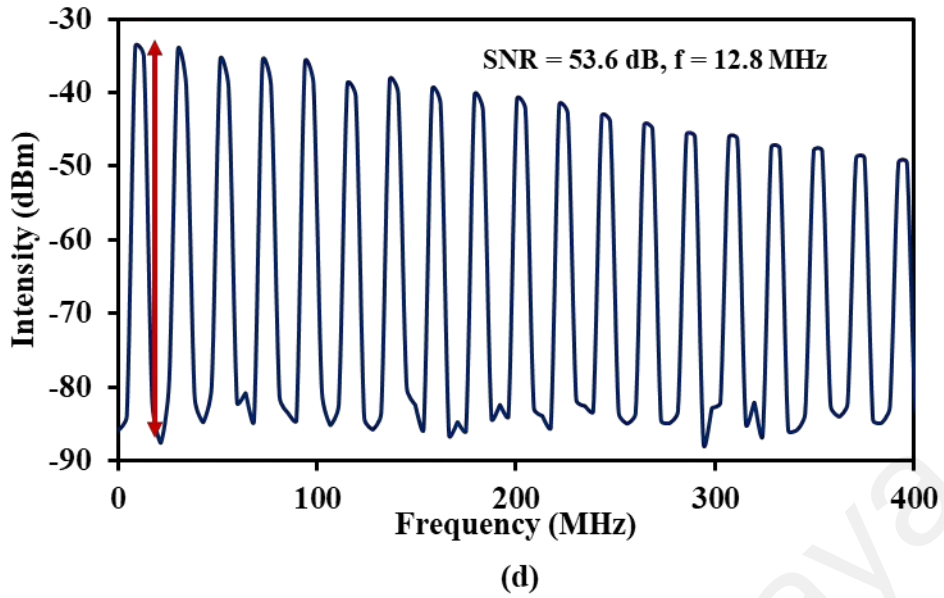
Figure 5.13 : Mode locking performance of GO as mode locker in the EDFL. (a) Optical spectrum; (b) Autocorrelation trace; (c) RF spectrum with (d) spectrum in 400 MHz span; (e) Output power and average power against pump power for the mode-locked fiber laser.

A typical oscilloscope trace of the mode-locked pulse-train was shown in (Figure 5.14) for three different time spans. There are six solitons in the cavity. Each soliton has different pulse energies as represented by the different pulse heights in the oscilloscope trace. These solitons also propagated with different group velocities in the cavity. The time between adjacent single pulses is ~78.1 ns, which coincides with the round trip time

of the ring cavity, which confirms the pulses are generated from mode locking mechanism. The polarization features of the pulses were further studied by using an external cavity polarizer. Through rotating the external cavity polarizer, it was identified that one soliton could be completely suppressed while the other still remained on the oscilloscope trace. (Figure 5.15) shows the polarization resolved optical spectra, which indicate the two orthogonal polarization components of the laser emission. It was noticed that the Kelly sidebands are similar in both polarizations.

(a)

(b)
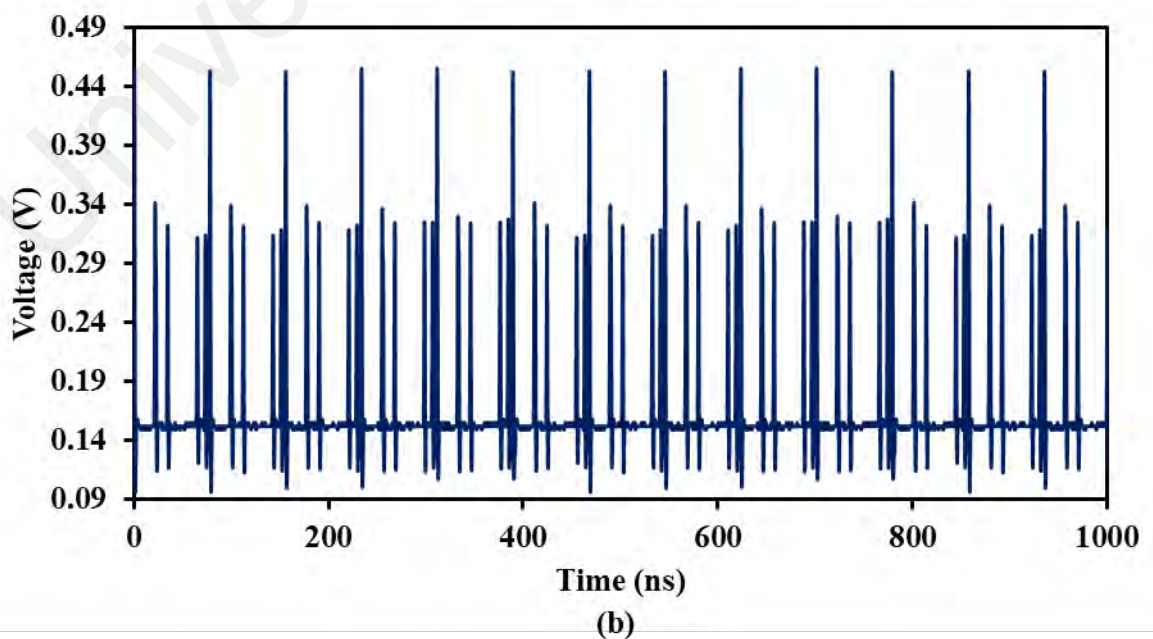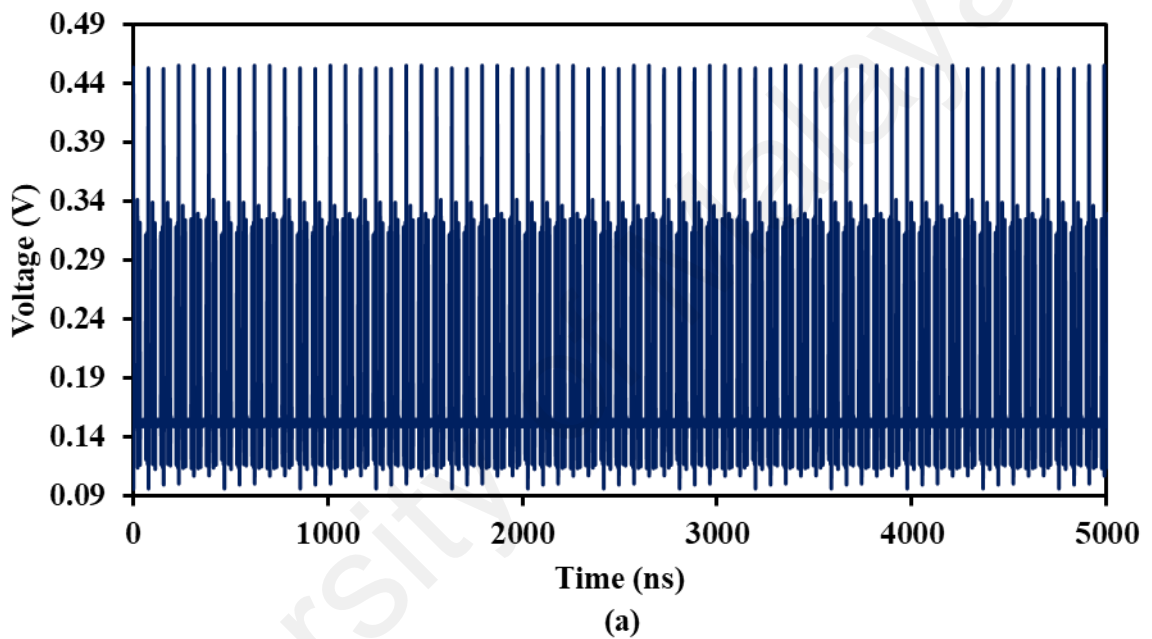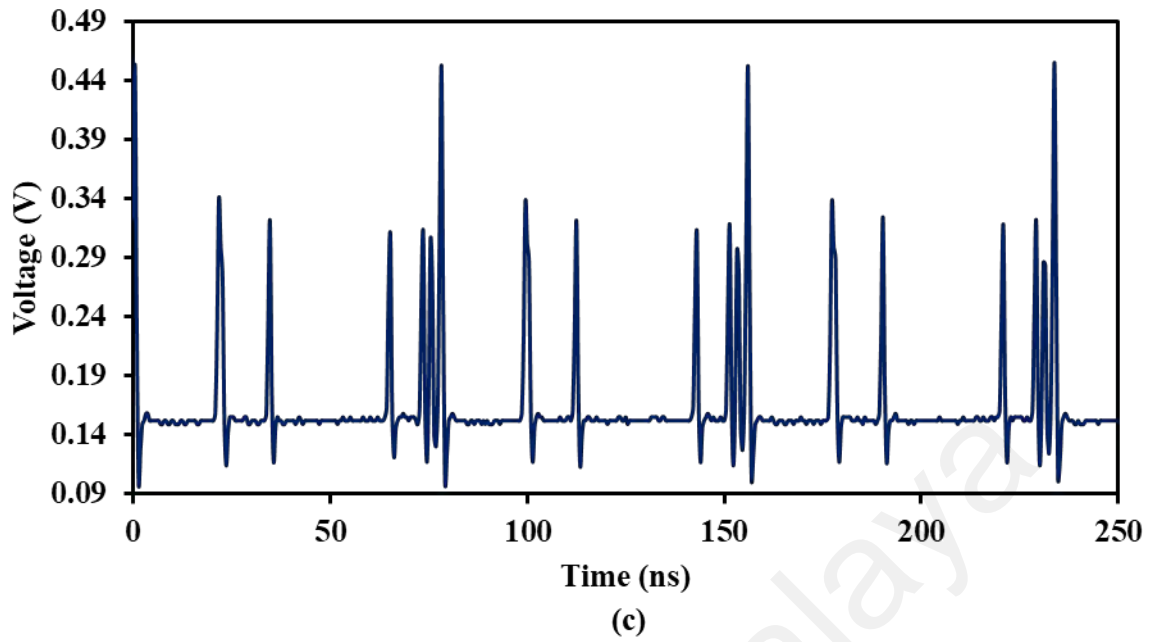
Figure 5.14 : Typical pulse train at three different time spans; (a) 5000 ns; (b) 1000 ns; (c) 250 ns
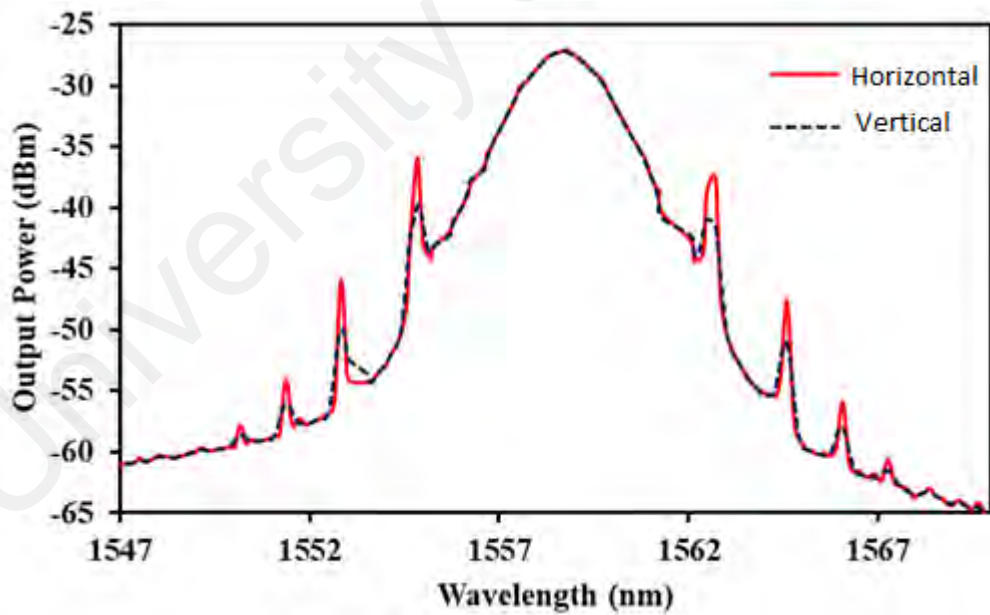
Figure 5.15 : Optical spectrum of vector soliton

5.4   Generation of soliton and multiple soliton pulses with BiSe SA

The mode-locked soliton pulse that was generated under anomalous cavity dispersion was widely investigated for optical communication purposes. Soliton pulse is desirable for long distance communication as its shape can be preserved and thus was envisioned to realize multiterabit/s, ultrahigh-speed optical transmission over several thousand kilometers. Compared to active method, passive method to generate pulse by using SA (which has characteristics where light absorbance decreases with the increase of light intensity) is more popular and viable method. In the previous sections, mode-locked pulse fiber lasers were demonstrated using graphene based SAs. However, graphene based SA offers relatively low modulation depth (Amos Martinez et al., 2013). In view of this, the search for novel and practical SA with excellent properties is still on going.

In the past few years, investigation of new class of nanomaterials, regarded as topological insulator (TI) had been carried out for mode-locked pulsed laser generation. TI possess graphene-like energy bandgap structure with Dirac cones characteristics and exhibits a very broad and relatively flat light absorption compared to graphene. Additionally, TI also demonstrates high third order nonlinear refractive index, at the level of 10^{-14} m^2/W (G. Sobon, 2015). Several TIs are identified such as Bi_2Te_3, Bi_2Se_3 and Sb_2Te_3 have found much attention and Bi_2Se_3 is the most outstanding among all as it has relatively larger bulk band gap at 0.3 eV (Sapkota et al., 2018). TI can be incorporated into cavity by using the same techniques as in (Y. Chen et al., 2013). Bi_2Se_3 as a Q-switcher was demonstrated in the 1 μm, 1.5 μm and 2μm (H Ahmad et al., 2015; H. Haris et al., 2017; Z. Luo et al., 2014) This proved that Bi_2Se_3 exhibits broadband saturable absorption characteristics. In the previous chapter, passively mode-locked Ytterbium-doped fiber laser (YDFL) operating at 1 micron region was demonstrated using a few-layers Bi_2Se_3 in a fully fiber-integrated laser cavity. In this section, mode-locked EDFLs

operating in 1.5 micron region are demonstrated using the newly developed Bi$_2$Se$_3$ SA, which was obtained by optical deposition method.

5.4.1 Single soliton mode-locked EDFL

(Figure 5.16) shows the configuration of the proposed TI based mode-locked EDFL. It consists of 3 m long EDF as the gain medium, a wavelength division multiplexer (WDM), a polarization controller (PC), an isolator and 95:5 coupler. TI Bi$_2$Se$_3$ SA (which was deposited on the fibre ferrule) was inserted between EDF and PC. The EDF was pumped by the 1480 nm laser diode (LD) via the 1480/1550 WDM. The EDF used has a core and cladding diameters of 4 μm and 125 μm, respectively, Erbium concentration of 2000 ppm and dispersion parameter of -21.64 ps/nm.km at wavelength 1550 nm. The remaining of the cavity consists of single mode fiber with dispersion coefficient of 17 ps/nm.km at wavelength 1545 nm. Incorporation of an isolator in the cavity is crucial in order to ensure unidirectional of the oscillating light. PC was integrated to adjust light polarization inside the laser configuration. 5 % of the output of this laser was tapped out from the configuration via the 95:5 coupler while keeping 95 % of the laser propagating inside the ring cavity. The OSA was used for the spectral analysis of the pulsed EDFL with a spectral resolution of 0.02 nm, while the oscilloscope (Tektronix TDS3052C) was used to observe the output pulse train of the mode-locked operation in the form of electrical signal via a 1.2 GHz bandwidth photodetector. The pulse width was measured using intensity based auto-correlator and the stability of pulse was characterized via a RF spectrum analyzer. The total cavity length is approximately 8.6 m. The estimated total Group Delay Dispersion (GDD), without SA, is -0.19 ps^2, suggesting that this cavity is operating in anomalous dispersion.
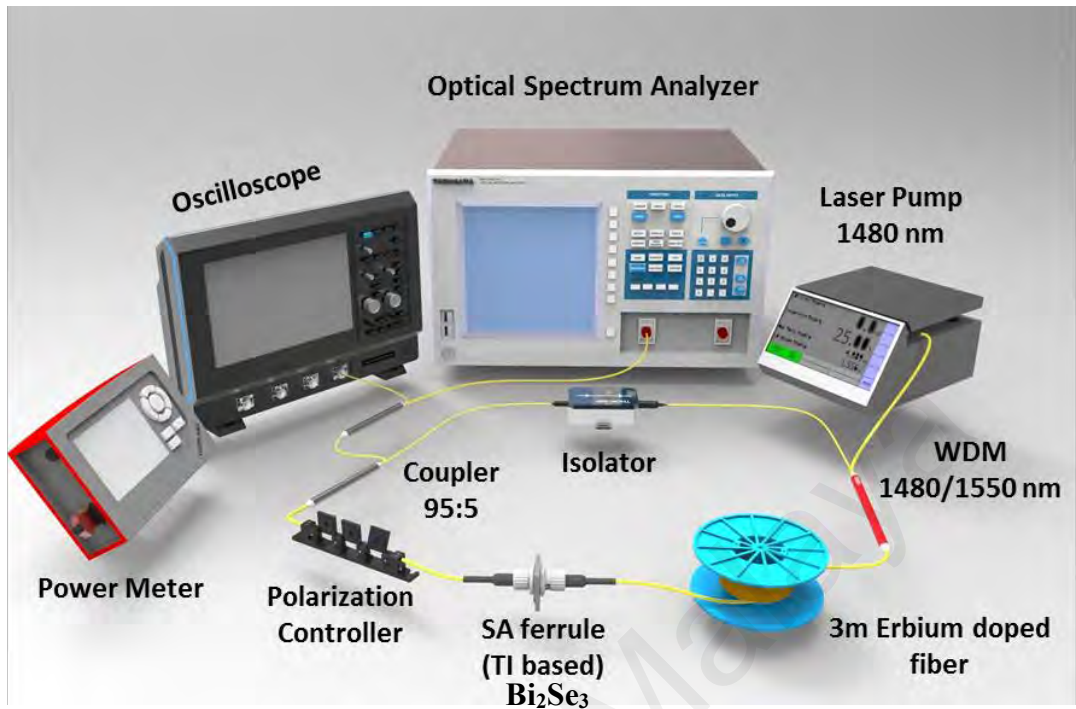
Figure 5.16 : Experimental setup of soliton mode-locked EDFL with Bi$_2$Se$_3$ SA
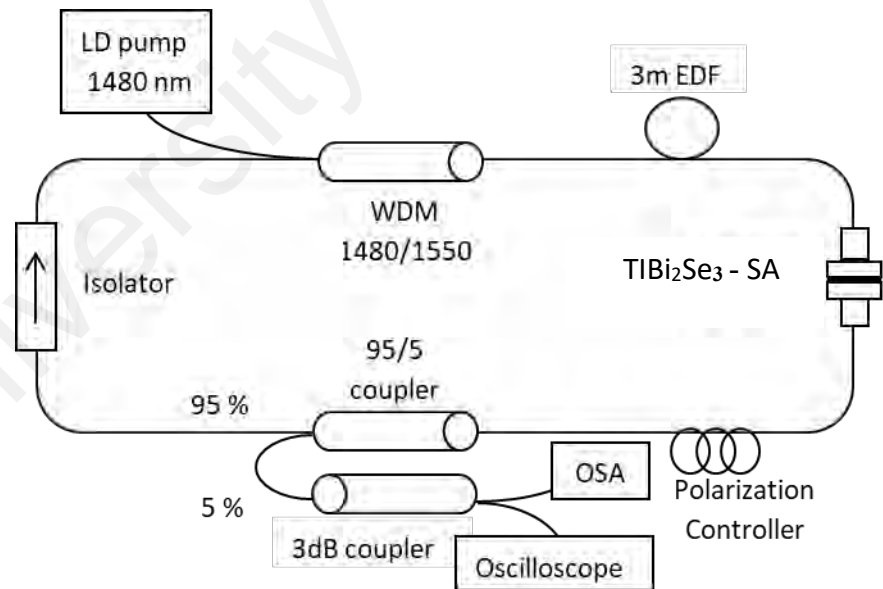
Figure 5.17 : Schematic diagram of soliton mode-locked EDFL with Bi$_2$Se$_3$ SA

Stable self-starting mode-locking regime was achieved at the pump power of approximately 39.3 mW. The longitudinal modes are locked in a fixed relationship producing pulses with narrower pulse width compared to Q-switched pulse. (Figure 5.18 (a)) shows the soliton mode-locked spectrum at the pump power of 39.3 mW. It has center wavelength of 1565 nm with approximately 7.9 nm of 3 dB bandwidth with the peak power of − 36.3 dBm. At this pump power, spectrum broadening was observed due to self-phase modulation (SPM) effect. Soliton pulse was produced due to the balance between anomalous dispersion and SPM. Kelly side-bands are observed too and this confirms the attainment of soliton pulse. The insertion of SA is crucial in our experiment and it should be noted that without the incorporation of the SA, no mode-locked soliton pulse was produced. This confirms that mode-locking operation was initiated from the SA.

(Figure 5.18 (b)) displays the pulse train of the mode-locked EDFL at the pump power 39.3 mW. The repetition rate achieved at this pump power is 23.3 MHz with peak-to-peak separation of 42.9 ns. The soliton mode-locked pulsed laser is operating at its fundamental repetition rate. The pulse width (τ) of the mode-locked operation was measured from the trace of auto-correlator as shown in (Figure 5.18 (c)). Our experimental autocorrelation trace follows the sech^2 fitting almost perfectly at the auto-correlator. The measured pulse width, τ is 0.63 ps and the calculated time-bandwidth product (TBP) is 1.3. This value is a significantly far from the theoretical value sech^2 profile of mode-locked pulses TBP of 0.315 signifying that the pulses produced was chirped. (Figure 5.18 (d)) shows the RF spectrum of the mode-locked laser at the same pump power of 39.3 mW. The optical signal-to-ratio (OSNR) value is more than 38 dB at the frequency of 23.3 MHz, implying excellent mode-locking stability and low noise fluctuation in the laser cavity.

(a)

(b)

(c)

SNR = 38.2 dB, f = 23.3 MHz

(d)
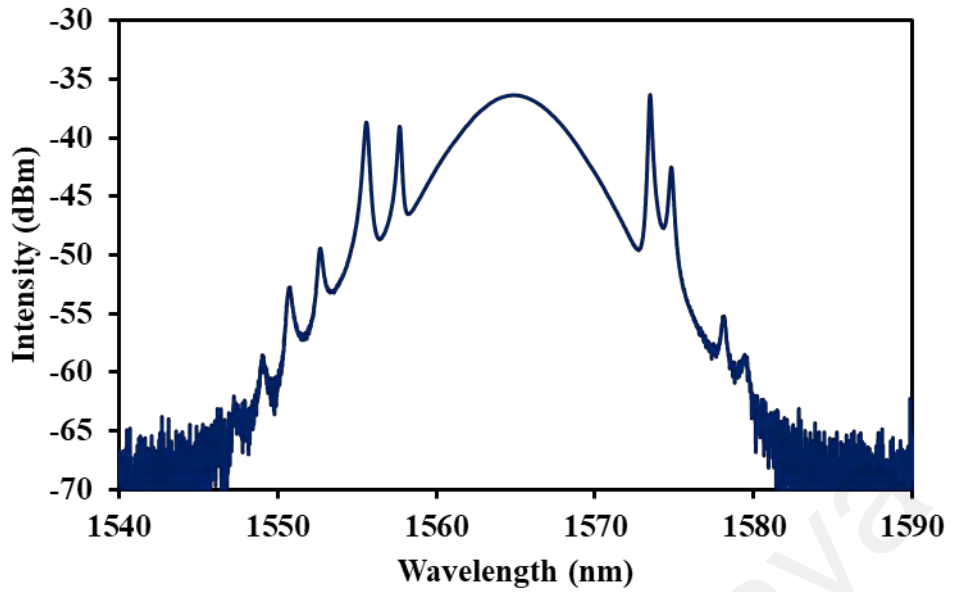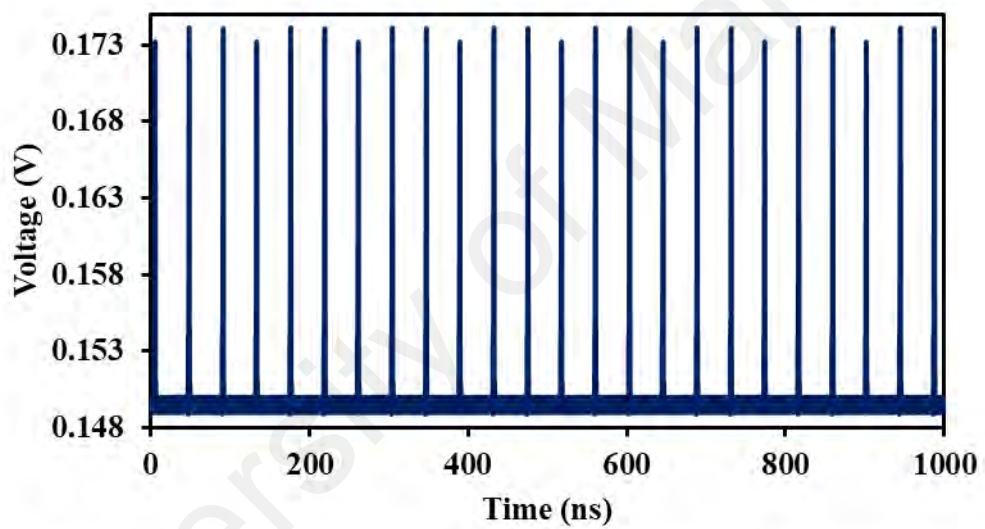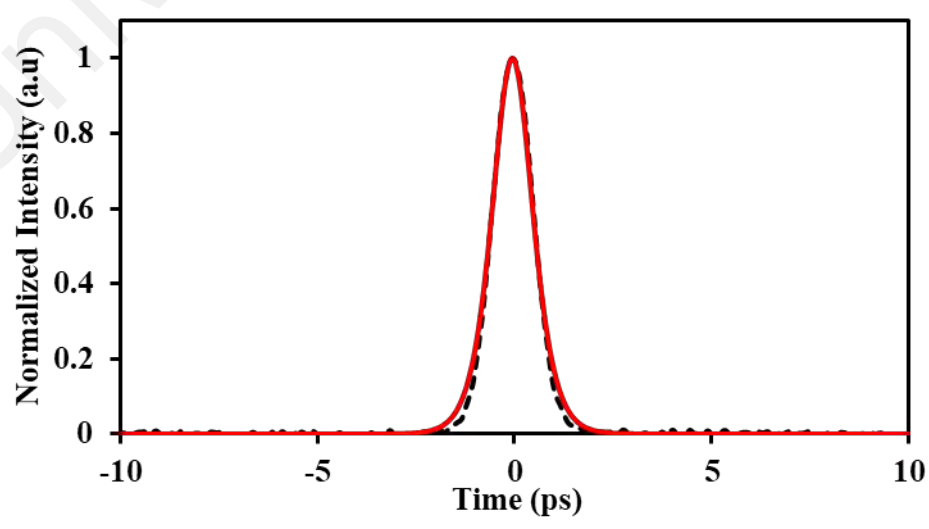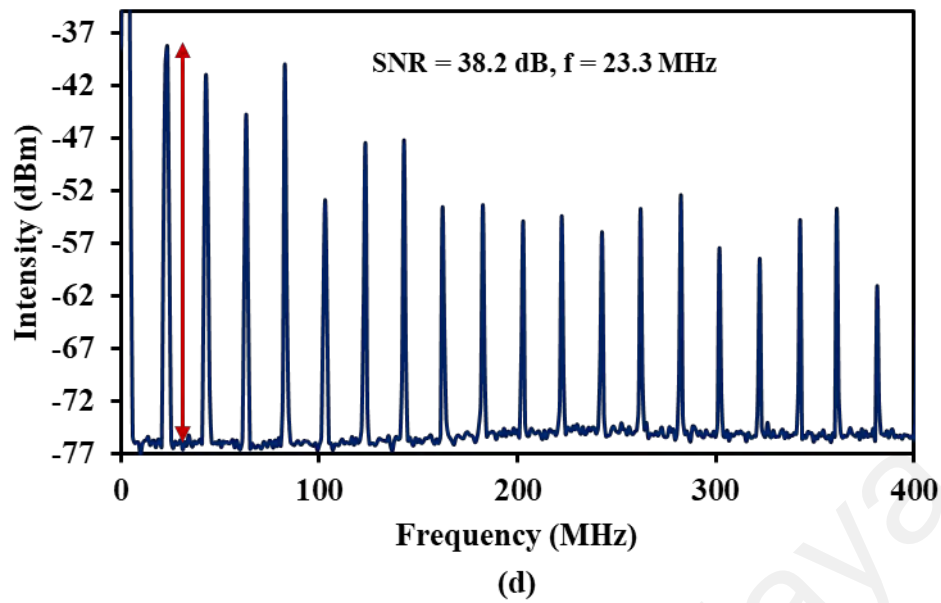
Figure 5.18 : Output traces of: (a) OSA, (b) oscilloscope, (c) autocorrelator, and (d) RF spectrum analyzer; at the fixed pump power of 39.3 mW.

(Figure 5.19) summarizes the evolution of the average output power and pulse energy as a function of the pump power. As the pump power was increased from 39.3 mW to 175.8 mW, the average power increases from 12.0 to 39.2 mW while the pulse energy increases from 0.52 nJ to 1.68 nJ. Actually, the maximum average power and pulse energy are limited by the available pump power and can be further enhanced by optimizing the SA, such as using fiber-taper based SAs.
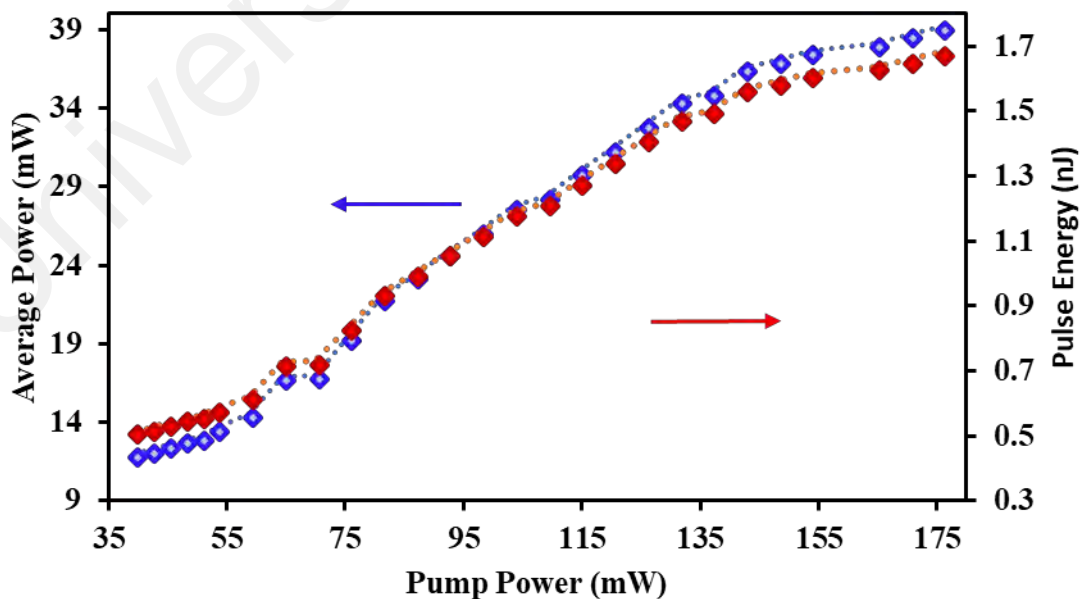
Figure 5.19: Average output power and pulse energy against pump power

5.4.2 Dissipative vector soliton generation

Dissipative solitons are localized formations of an electromagnetic field that are balanced through an energy exchange with the environment in presence of nonlinearity, dispersion and/or diffraction. The most common way to generate dissipative solitons in a fiber laser is using the mode locking method. There have been a lot of reports on the dissipative soliton formation in fiber lasers based on different mode locking techniques, such as the nonlinear-polarization rotation (NPR) technique (X. Yang et al., 2009) and the nonlinear saturable absorber method (R. Fork et al., 1981). The mode locking process generates an initial strong pulse circulating in the fiber laser cavity. In addition, the pulse is subject to the actions of the fiber nonlinearity and dispersion, laser gain and losses, as well as the effective laser gain bandwidth limitation and the mode-locker. When the actions come to a balance, then a dissipative soliton was formed. If the fiber lasers further have a quasi-isotropic cavity, it has been shown that the vector dissipative solitons could also be formed (Han Zhang, Tang, Zhao, Wu, et al., 2009).

Here, the vector dissipative soliton emission of a net anomalous dispersion cavity fiber laser caused by the combined effect of the nonlinearity induced wave mixing and gain bandwidth limitation was demonstrated using the Bi_2Se_3 based SA. (Figure 5.20) shows the configuration of the proposed mode-locked laser, which was modified from previous laser cavity by adding an additional 11.8 m long SMF. The proposed fiber laser has a dispersion-managed fiber ring cavity that consists of a piece of 3 m EDF with a dispersion parameter of -21.64 ps/nm.km and a total 15.4 m SMF with a dispersion parameter of 17 ps/nm.km. The total cavity length is ~15.4 m with a net anomalous total Group Delay Dispersion (GDD) of -0.39 ps^2. A polarization independent isolator was also inserted in the cavity to ensure unidirectional operation of the laser. The EDF was pumped by a 1480-nm laser diode with the highest power of 176 mW through the WDM. The output pulse train was monitored with a photodetector and visualized with an

oscilloscope. The spectral properties are analyzed with an optical spectrum analyzer (OSA, Anritsu MS9710C).
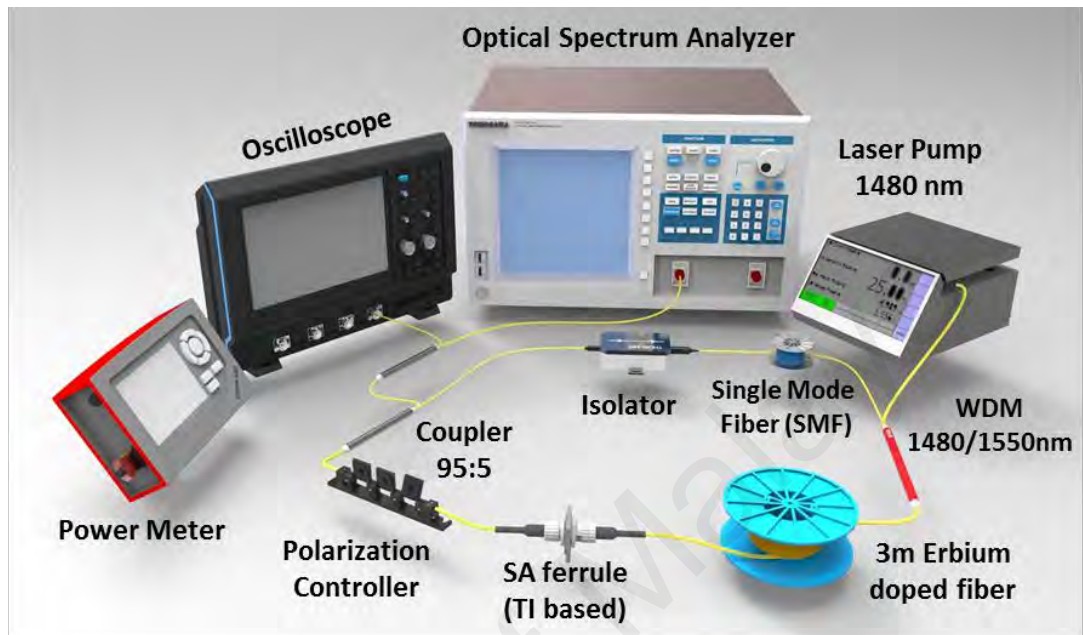
Figure 5.20 : Configuration of the mode-locked EDFL with dissipative multi-solitons emission
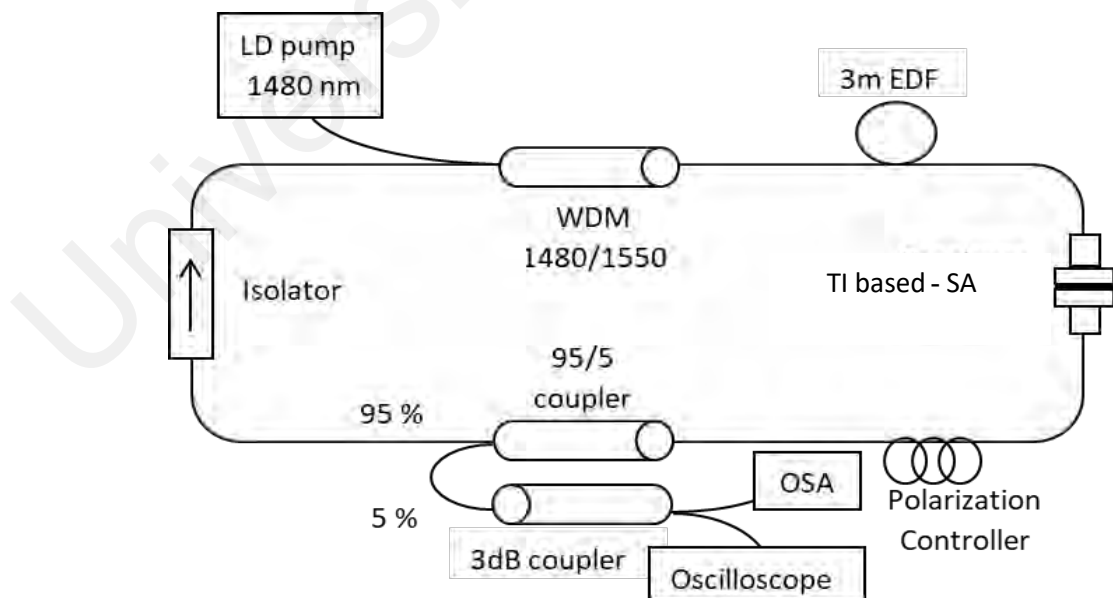
Figure 5.21 : Schematic diagram of the mode-locked EDFL with dissipative multi-solitons emission

When the pump power was increased to the mode-locked threshold of 44.9 mW, the mode-locking of the laser was obtained via carefully adjusting the intra-cavity PC. The multiple mode-locked pulses could be easily formed in the fiber laser while the number of the mode-locked pulses was able to be controlled by carefully tuning the pump power. The mode-locking operation was maintained up to the maximum pump power of 176 mW. (Figure 5.22) shows the typical pulses train at the maximum pump power at three different scanning spans. As can be seen here, multi-soliton patterns with uniform pulse trains were observed with the fundamental repetition rate of 13 MHz. The number of soliton pulses was counted to be 44. (Figure 5.23) presents the corresponding spectrum, in which the central wavelength is 1559.4 nm and the 3-dB bandwidth of the spectrum is about 2.7 nm. The spectra exhibit Kelly sidebands, confirming that the mode-locked pulse is solitary wave of a fiber laser with anomalous dispersion regime. The extra spectral sidebands induced by the four-wave-mixing effect were also observed. The autocorrelation trace of total pulse was shown in (Figure 5.24). If the sech^2 pulse profile was assumed, the duration of the autocorrelation trace is ~1.52 ps. Thus, the time-bandwidth product (TBP) is ~0.505. This indicates the mode-locking pulses are significantly chirped.
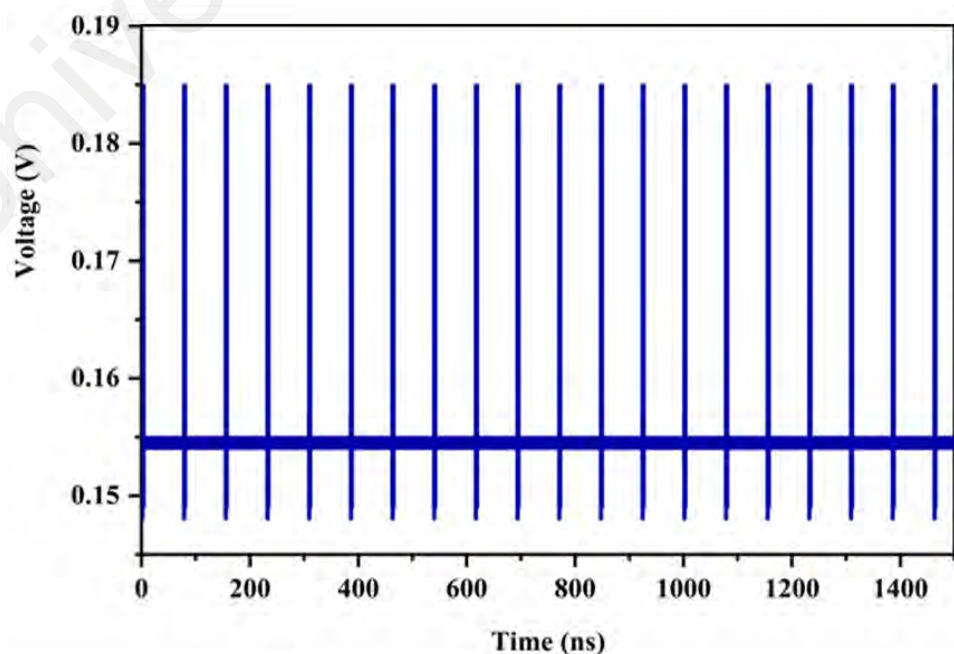
(a)
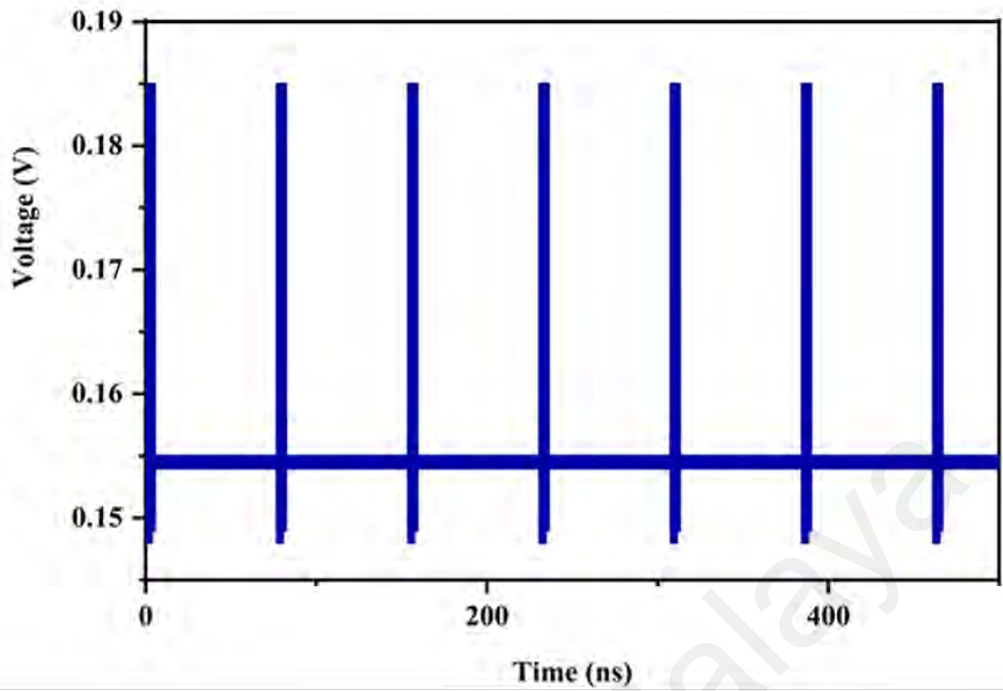
(b)
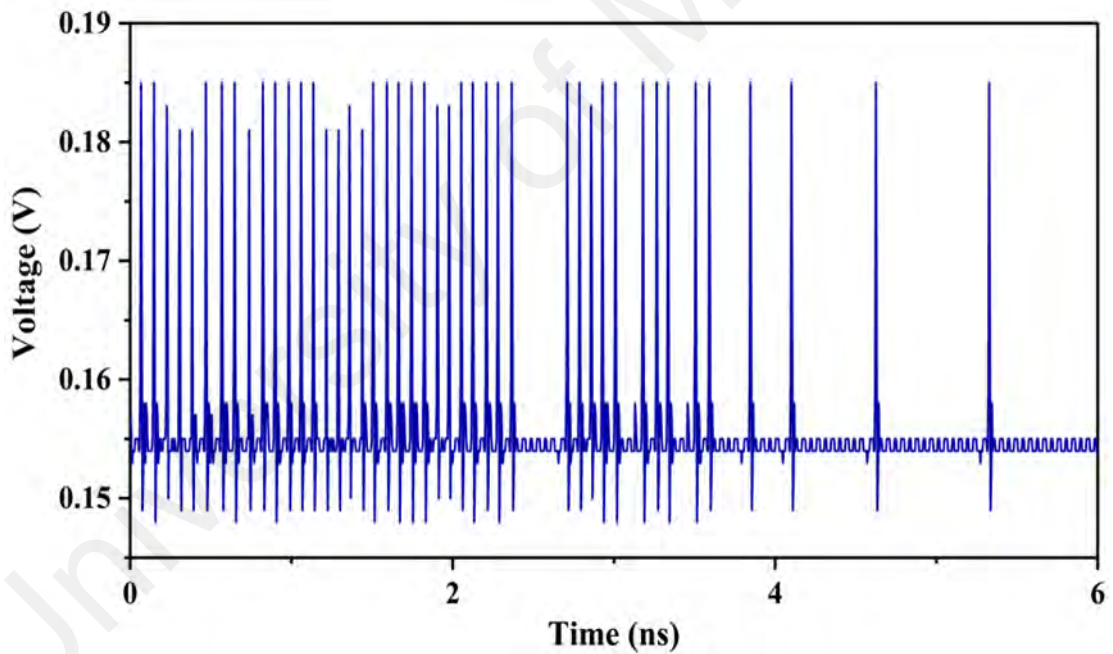
(c)

Figure 5.22 : Typical pulses train at pump power of 176 mW for three different scanning spans (a) 1500 ns, (b) 500 ns, and (c) 6 ns.
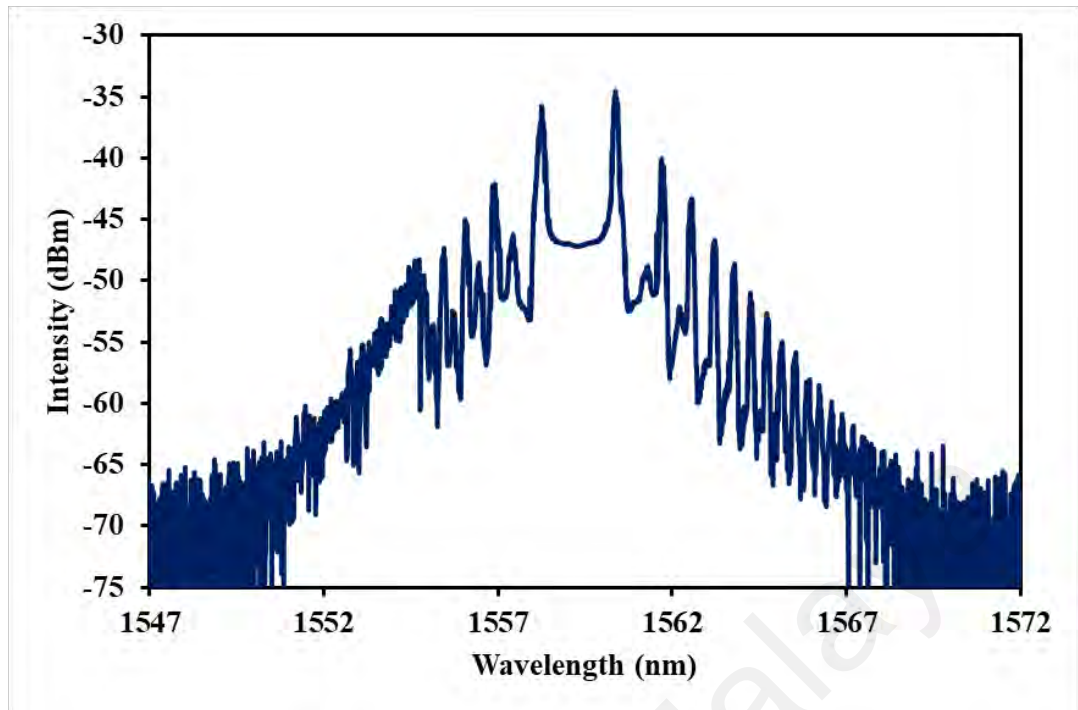
Figure 5.23 : Output spectrum at 176 mW pump power
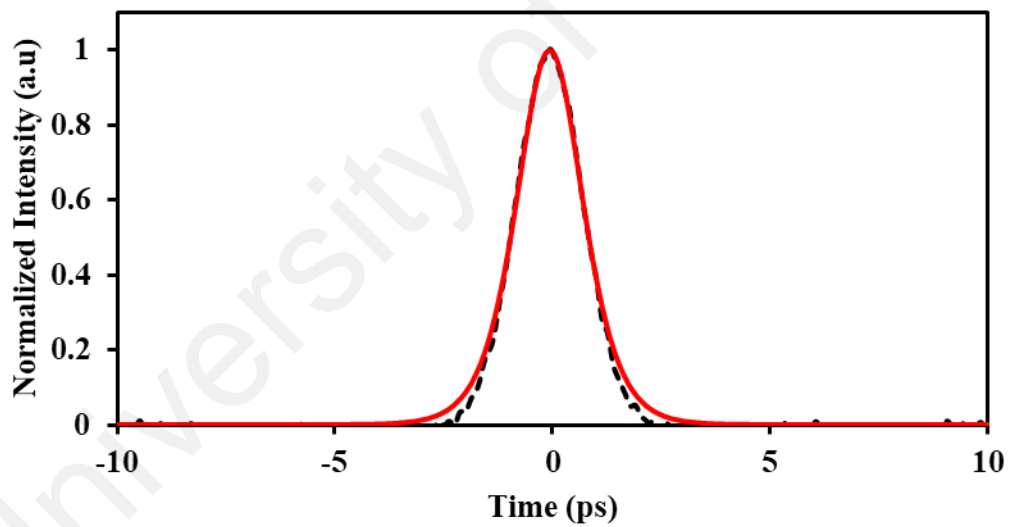
Figure 5.24 : Autocorrelator trace of the mode-locking pulses

(Figure 5.25) shows the RF spectrum for two different scanning spans. It shows a repetition rate of 13 MHz, which corresponds very well with the oscilloscope trace (Figure 5.22). The fundamental frequency has a signal to noise ratio of more than 78 dB, indicating the stability of the mode-locking pulses. (Figure 5.26) shows the average output power and pulse energy as a function of pump power. Both output power and pulse

energy increase with the pump power. At the maximum pump power of 176 mW, the maximum output power and pulse energy are obtained at 27.5 mW and 2.1 nJ, respectively. In this experiment, it was found that multiple solitons were sensitive to the pump power and the orientations of the intra-cavity PCs. It was easily understood that the multiple pulses could be observed constantly due to soliton energy quantization effect when the pump power or the accumulated nonlinear effect was increased to a high value in the fiber laser.
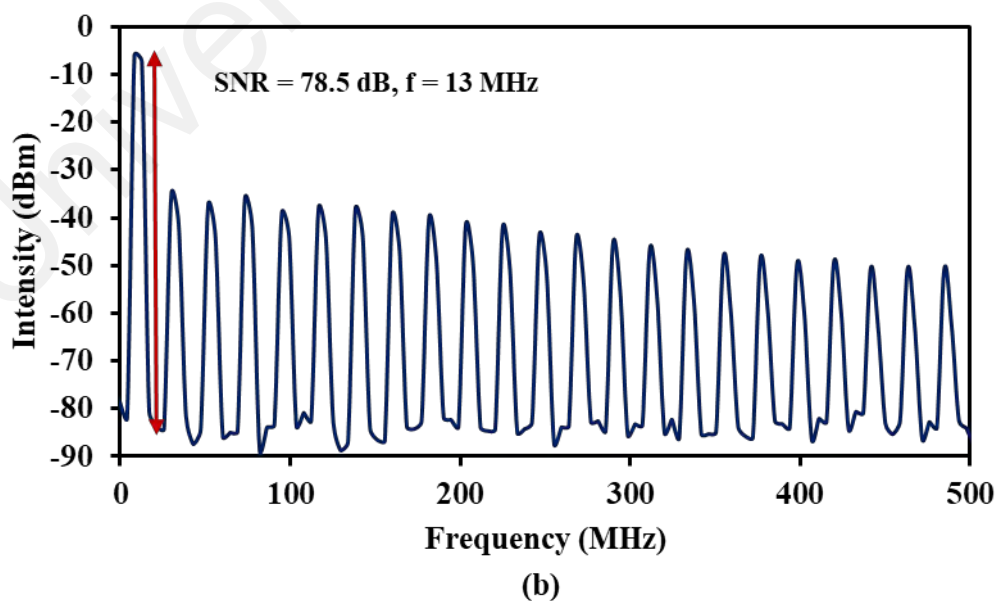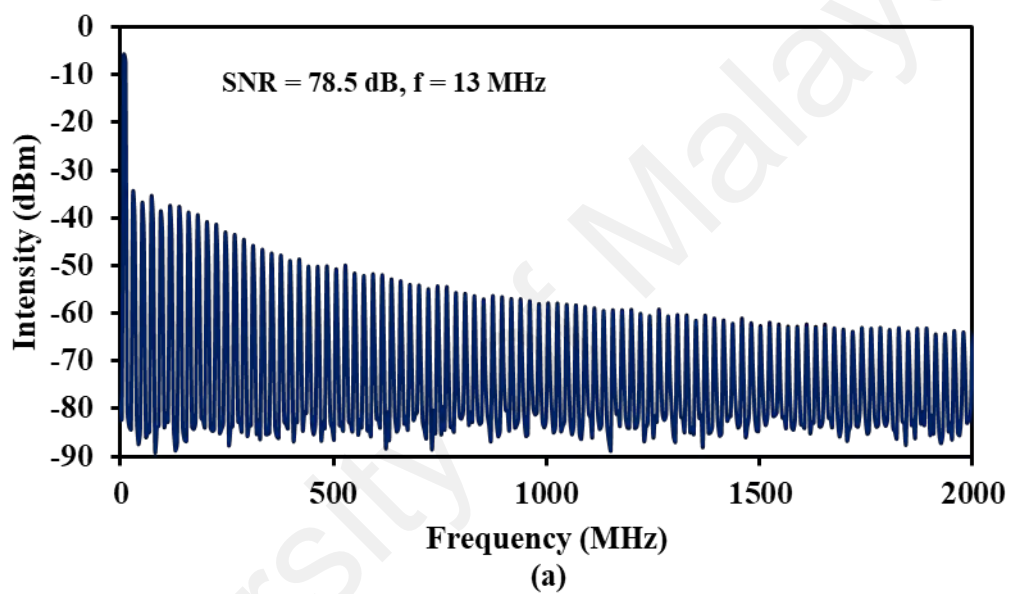
Figure 5.25 : RF spectra at two different scanning span (a) 2000 MHz and (b) 500 MHz.
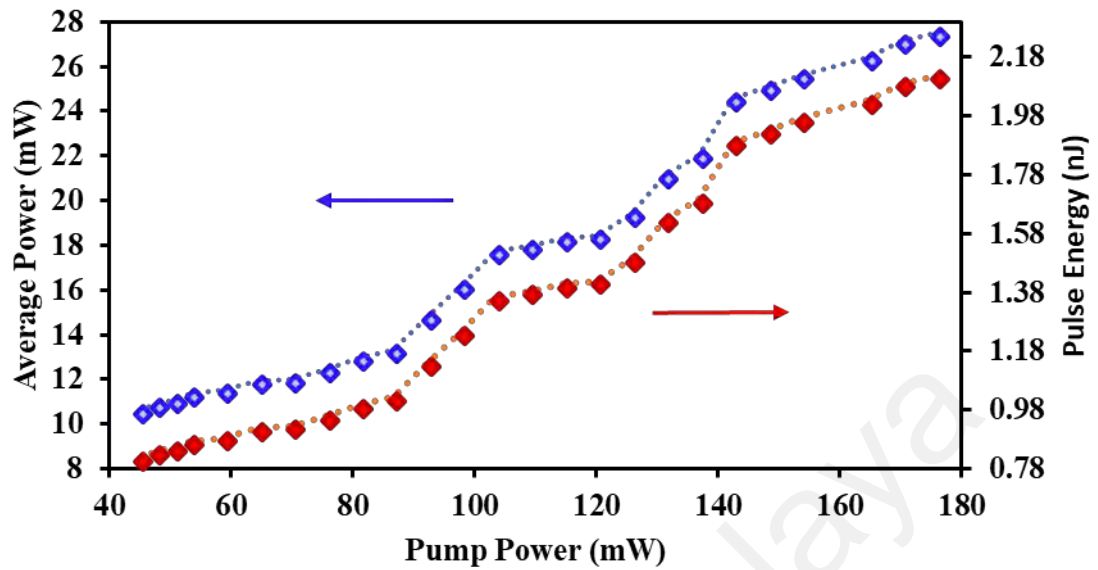
Figure 5.26 : Average output power and pulse energy against pump power

5.5 Generation of soliton and multiple soliton pulses with Bi_2Te_3 SA

Passively mode-locking techniques based on various SAs have been used in the previous section to obtain low cost and compact ultrafast lasers. In this section, soliton mode-locked fiber lasers at 1.5 μm are demonstrated by adopting TI Bi_2Te_3 SA. The Bi_2Te_3 SA was prepared by optical deposition method as described in Chapter 3. Self-started fundamentally mode-locked soliton pulses with a measured 3 dB spectral width of 6.8 nm, a pulse repetition rate of 24 MHz, and a pulse with of 2.4 ps were recorded. Moreover, by adjusting the cavity arrangement of the laser, stable soliton bunches with soliton number up to 144 in a single bunch were realized.

154

5.5.1 A single soliton generation

The Bi$_2$Te$_3$ based SA was incorporated into a ring cavity EDFL, which the experimental setup is almost similar to (Figure 5.15). The lasing gain at 1.5 μm was provided by a 3 m long EDF pumped by a 1480 nm laser diode via a 1480/1550 nm wavelength division multiplexer (WDM). The EDF had a core/cladding diameter of 4/125 μm with an Erbium concentration of 2000 ppm in the core. The input port of WDM was spliced to a polarization-independent isolator to ensure the unidirectional propagation of intra-cavity light. Between the Bi$_2$Te$_3$-based SA and a fused optical output coupler, a polarization controller (PC) was used to adjust the cavity polarization. The laser output was extracted from the 5% port of the coupler. The laser output was detected with a fast photodetector (bandwidth 1.2 GHz) monitored on a digital oscilloscope (bandwidth 350 MHz). And a second harmonic generation based autocorrelator was used to measure the pulse width. An OSA was used to measure the laser spectrum with a resolution of 0.02 nm. Other measuring equipment includes a power meter, and a radio frequency (RF) spectrum analyzer (bandwidth 7 GHz). The total cavity length is approximately 8.3 m. The estimated total Group Delay Dispersion (GDD), without SA, is -0.2 ps^2, suggesting that this cavity is operating in anomalous dispersion.

In the work, by increasing the pump power, amplified spontaneous emission (ASE) light and self-lasing were observed first. The intra-cavity polarization states was adjusted by rotating the PC and increasing a little pump power to ~39.3 mW, stable fundamentally mode-locked soliton pulses could be readily observed. The measured spectra of the output soliton are depicted in (Figure 5.27) for various pump powers ranging from 39.3 to 176 mW. They show pairs of Kelly sidebands which located almost symmetrically with respect to the central wavelength (1564 nm) of the spectrum. The full-width half-maximum (FWHM) value of the output spectrum was measured to be 6.8 nm.

(Figure 5.28) plots the output pulse train at pump power of 176 mW. It indicates a pulse repetition rate of 24 MHz which corresponds to the inverse of the cavity round time.
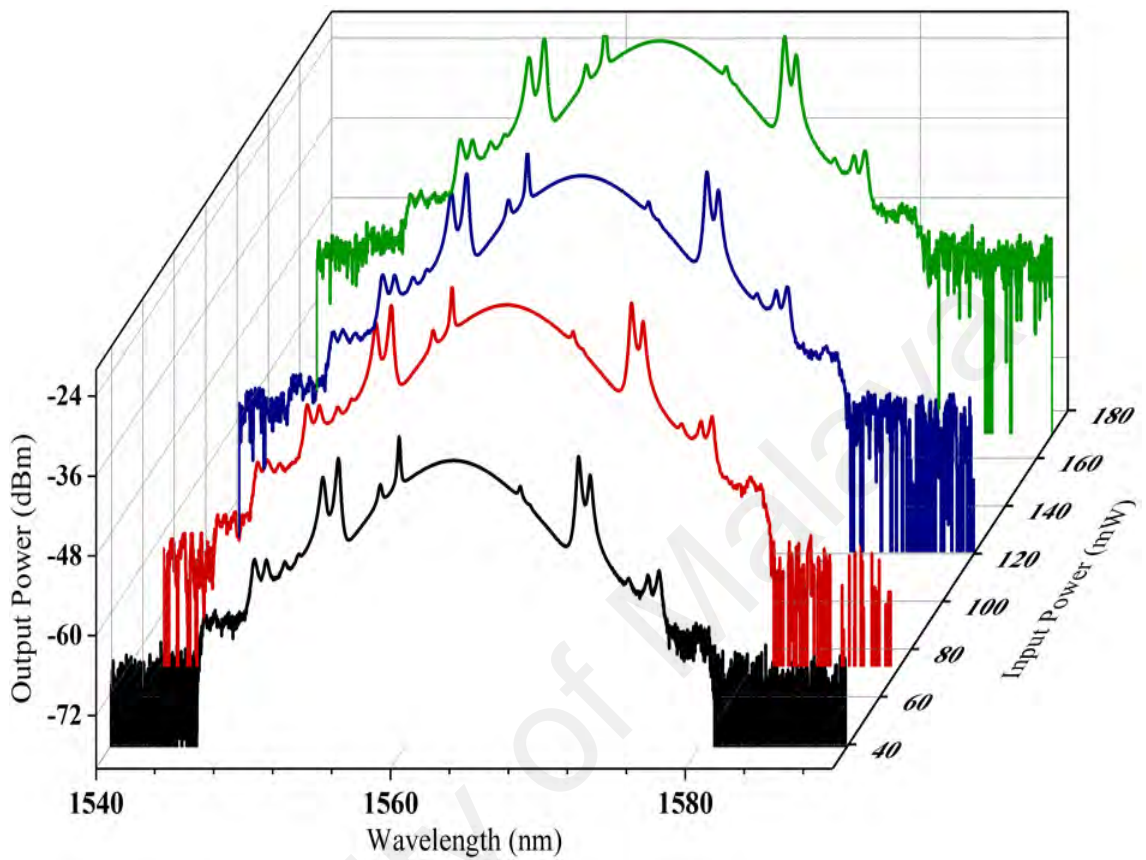
Figure 5.27 : Output spectra at various pump powers
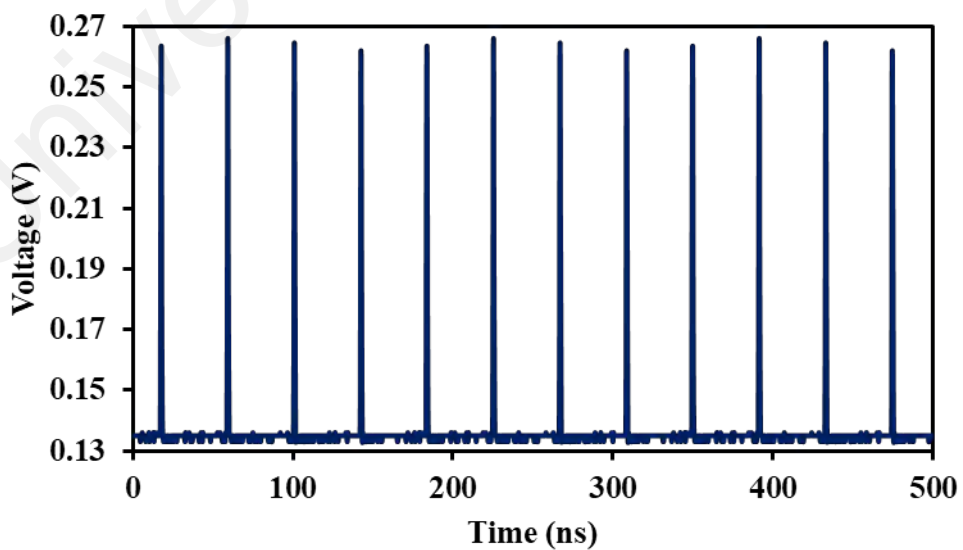
Figure 5.28 : Typical pulses train at pump power of 176 mW

The self-started mode-locking operation was observed at relatively low threshold pump power due to the high quality of the Bi_2Te_3 SA, which has a relatively small loss. The soliton mode-locked EDFL had a high temporal stability and could work steady for more than 48 hours. The measured RF spectrum as shown in (Figure 5.29) had a signal-to-noise ratio higher than 40 dB. (Figure 5.30) shows the measured autocorrelation trace with a pulse width of 2.4 ps by assuming a hyperbolic secant squared ($sech^2$) pulse profile. The time–bandwidth product (TBP) of the soliton pulses was calculated to be about 2, which is significantly larger than the transform-limited value of a soliton pulse of 0.315. (Figure 5.31) shows the average output power and pulse energy characteristics against pump power. It was shown that both output power and pulse energy linearly increase with pump power. The slope efficiency of the laser was calculated to be about 10.2%, which is larger than the previous mode-locked lasers. At the maximum pump power, the average output power and pulse energy were 59.3 mW and 2.5 nJ, which were higher compared to the previous graphene, graphene oxide and Bi_2Se_3 based mode-locked lasers.
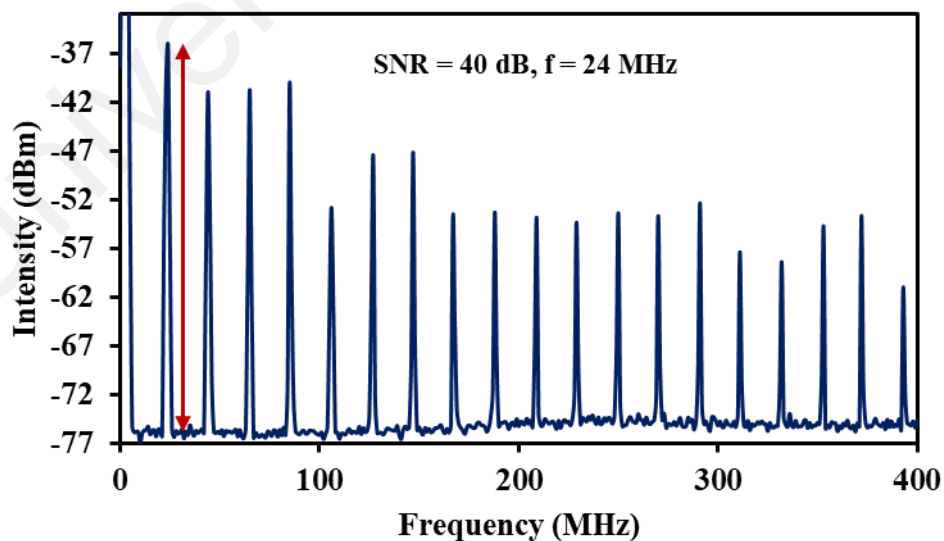
Figure 5.29 : RF spectrum of the Bi_2Te_3 based mode-locked EDFL
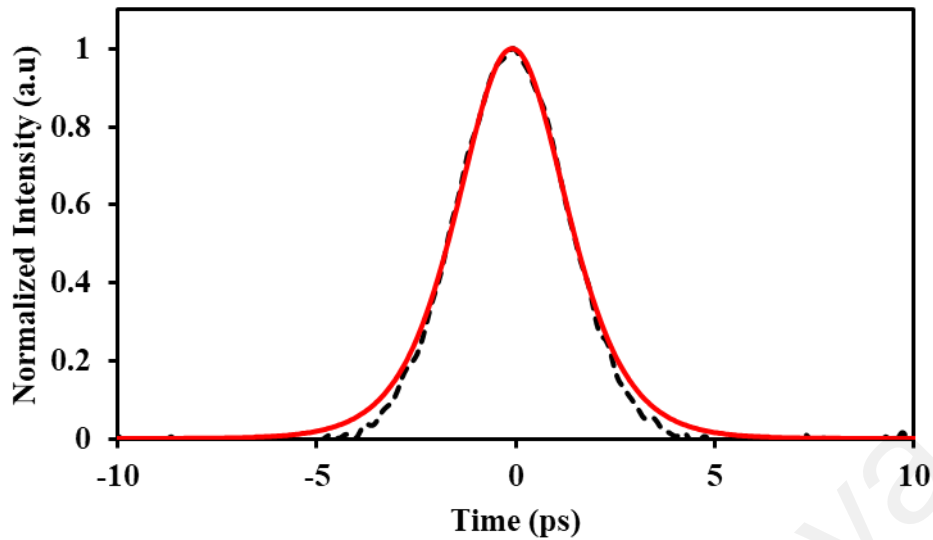
Figure 5.30 : Auto-correlator trace of the Bi$_2$Te$_3$ based mode-locked EDFL
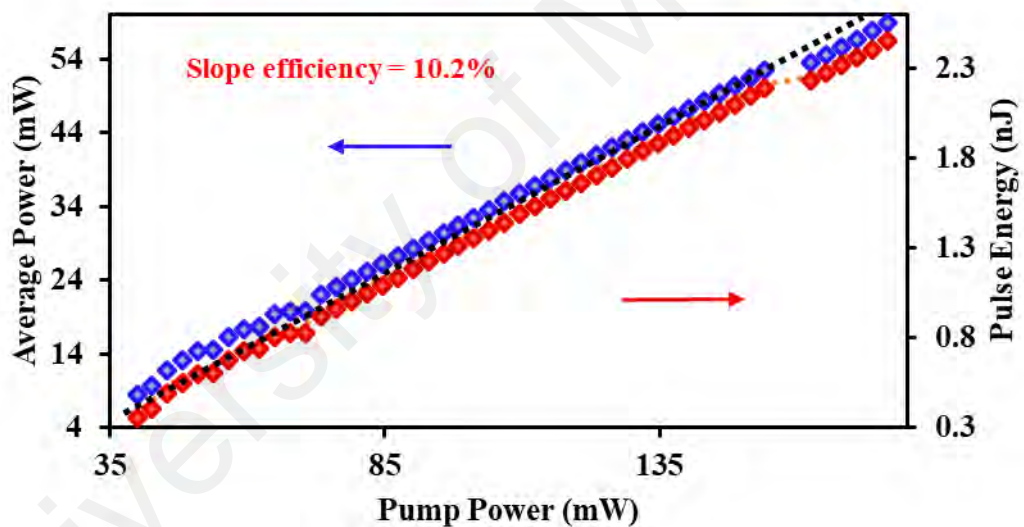
Figure 5.31 : Average output power and pulse energy as a function of pump power for the Bi$_2$Te$_3$ based mode-locked EDFL

5.5.2   Multi-soliton generation

When the cavity length was increased by incorporating additional 6.5 m long SMF inside the cavity, the output of the mode-locked EDFL behaved in accordance with the operation of soliton bunches. The laser configuration was similar to (Figure 5.20), which has a total cavity length of approximately 14.8 m. The estimated total Group Delay Dispersion (GDD), without SA, is -0.33 ps^2, suggesting that this cavity is also operating

in anomalous dispersion. This phenomenon mainly originates from the fact that soliton pulse energy sustained in an abnormal laser cavity has a limited value (Z.-C. Luo, Ning, et al., 2013; L. Zhao, Tang, Zhang, et al., 2009); when the intra-cavity loss and dispersion changed the soliton pulses would be split and result in the multi-soliton operation. In the work, it was found that the output split solitons were bunched together. The number of solitons in a single bunch could be continuously increased up to 144 by enhancing the pump power to the maximum of 176 mW.

In the experiment, by adjusting the intra-cavity polarization states by rotating the PC and increasing a pump power to 44.9 mW, stable mode-locked soliton pulses could be easily obtained. The mode-locking operation was maintained up to the maximum pump power of 176 mW. The measured spectrum of the output soliton was recorded at 176 mW pump power as depicted in (Figure 5.32). The spectrum shows many pairs of Kelly sidebands which located almost symmetrically with respect to the central wavelength (1556.7 nm) of the spectrum. The 3dB bandwidth of the output spectrum was measured to be 1.4 nm. (Figure 5.33) shows the output pulse train of the bunched soliton with a pulse repetition rate of 13.5 MHz which corresponds to the inverse of the cavity round time. It has the maximum numbers of 144 at the maximum pump power of 176 mW. The measured RF spectrum as shown in (Figure 5.34) had a signal-to-noise ratio of 77 dB. This indicates the stability of the solitons. (Figure 5.35) shows the measured autocorrelation trace with a pulse width of 1.63 ps. The TBP was calculated to be 0.282, which is very close to the transform-limited value of a soliton pulse of 0.315.
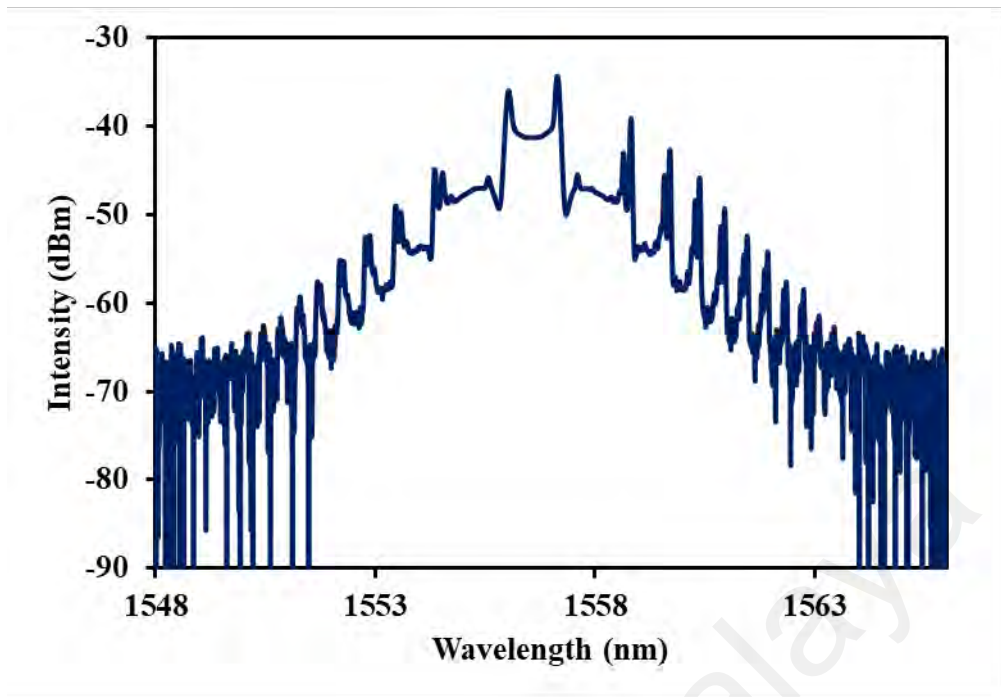
Figure 5.32 : Output spectrum of the multi-soliton laser

(a)
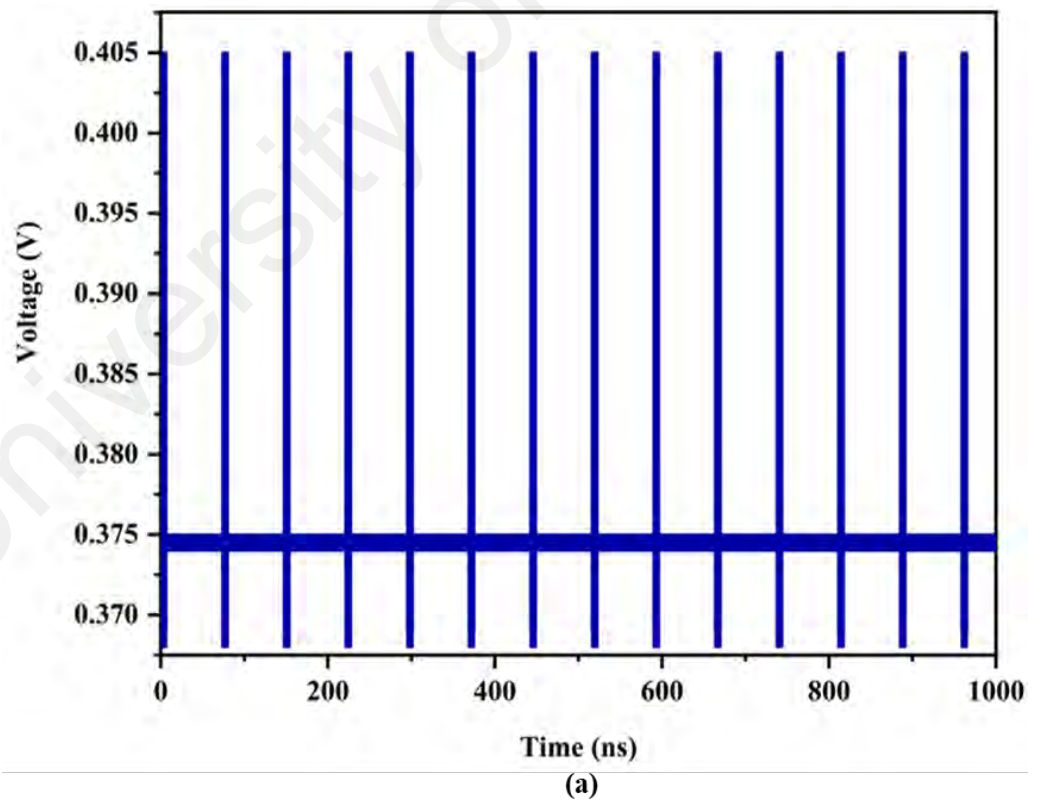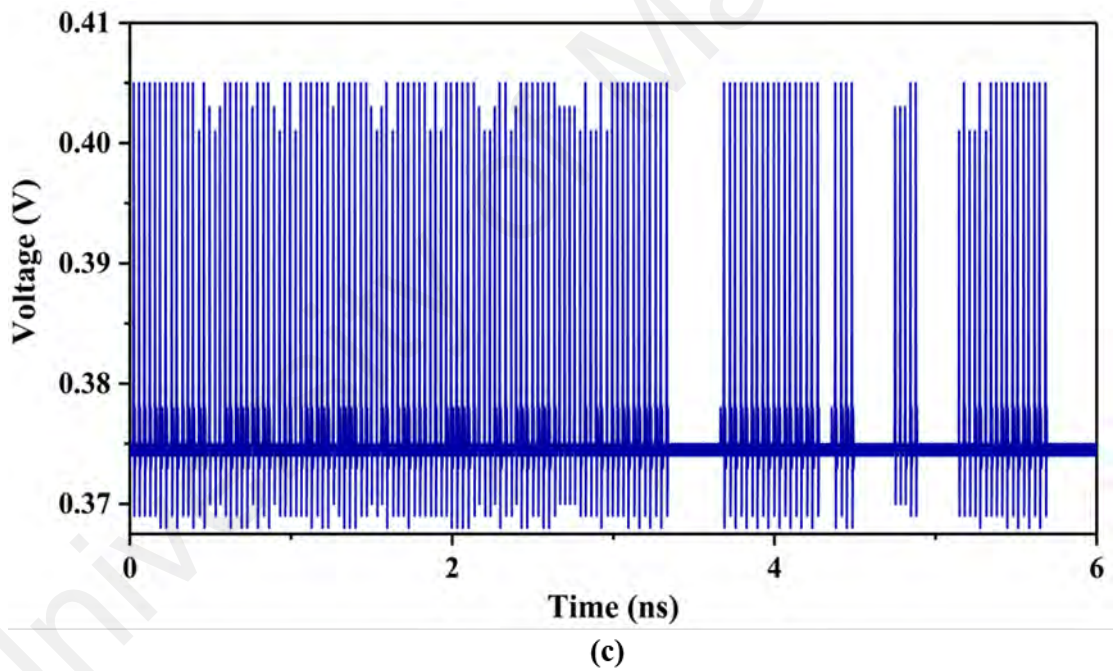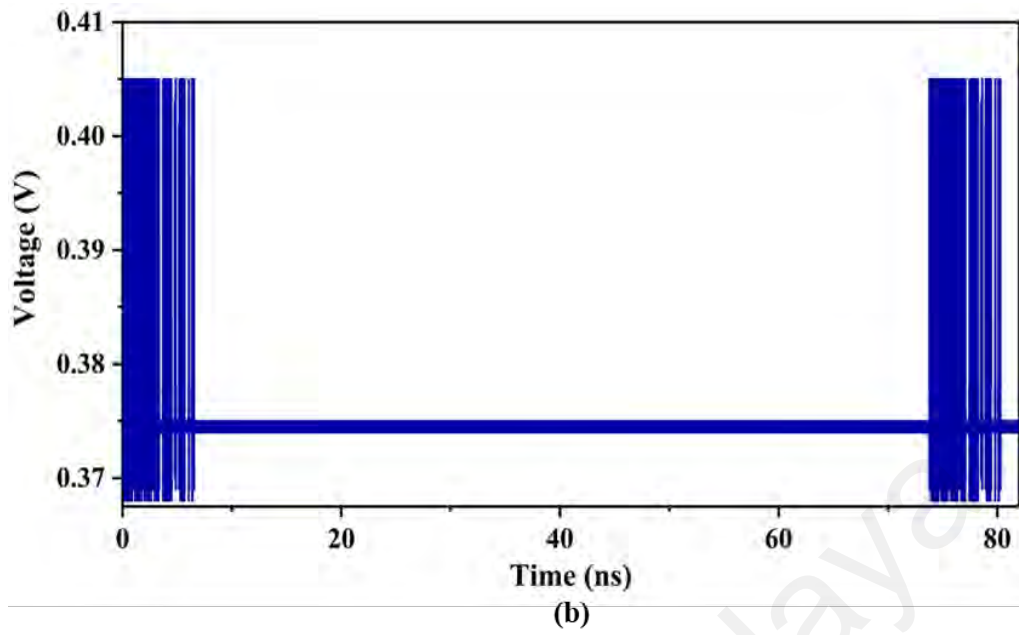
Figure 5.33 : Typical output pulses train of the bunched soliton at three different scanning span (a) 1000 ns, (b) 100 ns, and (c) 6 ns
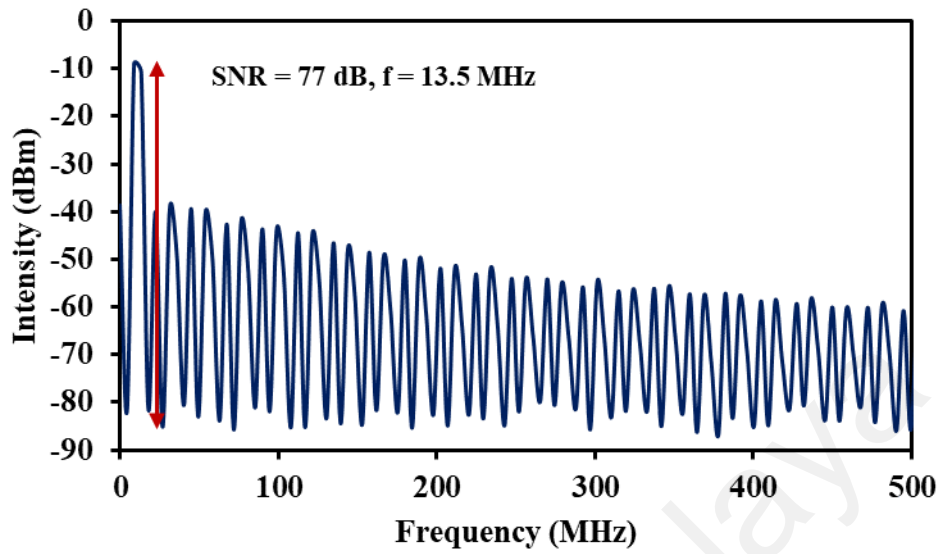
Figure 5.34 : RF spectrum of the bunched soliton
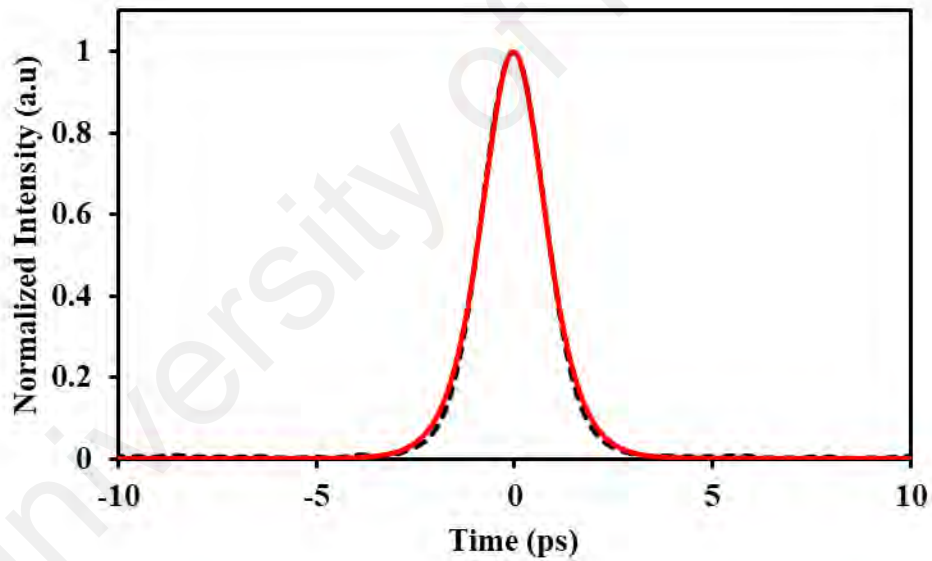
Figure 5.35 : Auto-correlator trace of the bunched soliton

The laser average output power and pulse energy trends versus the pump power was plotted in (Figure 5.36). Both output power and pulse energy increase with pump power. The maximum output power and pulse energy are 35.0 mW and 2.6 nJ, respectively at pump power of 176 mW. It has also verified whether the soliton mode-

locking operation of the EDFL was dependent on the Bi_2Te_3 material. For this purpose, the SA film was removed from the cavity. Although the PC was rotated and the pump power was adjusted on a very large scale, only continuous wave self-lasing output could be observed. This comparative result showed that the soliton operation of the previously mentioned EDFL was indeed generated by TI Bi_2Te_3 SA.
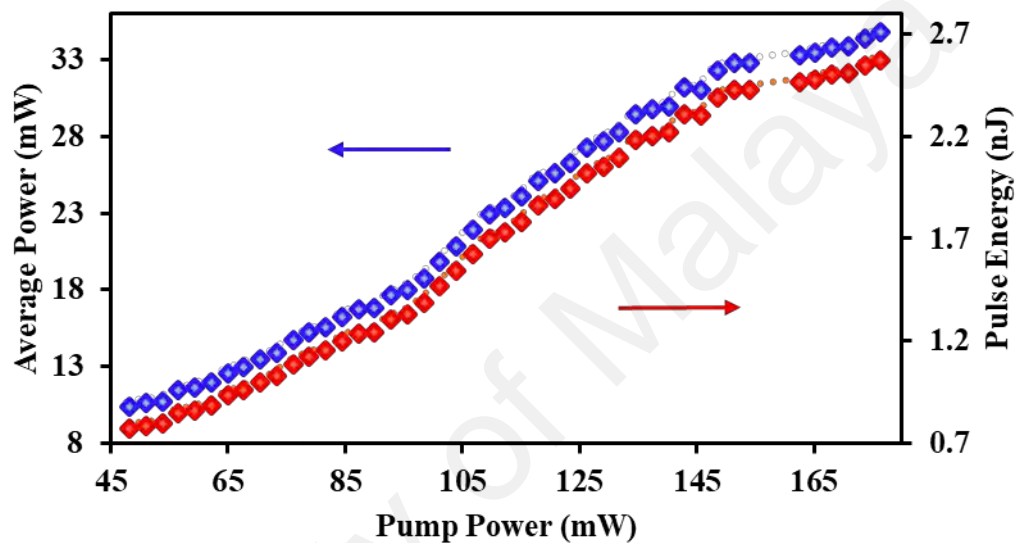
Figure 5.36 : Output power and pulse energy against pump power for the mode-locked EDFL

5.6 Summary

Various soliton mode-locking operations in an EDFL cavity were successfully demonstrated by incorporating the previously developed graphene and topological insulator based SAs in the laser cavity. By adjusting the cavity length and dispersion, fundamentally mode-locked soliton, bound soliton, vector soliton, dissipative soliton and soliton bunches trains at 1.5 μm region were realized. The experimental results show that TI Bi_2Te_3 nanosheets could produce the highest energy while the smallest pulse width of 0.63 ps was obtained with Bi_2Se_3 SA.

CHAPTER 6: CONCLUSION AND FUTURE WORK

6.1   Conclusion

Mode-locking is a commonly effective technique for the generation of short yet intense laser pulses operating at MHz range frequency and pulse duration in a range from fs to ps. Essentially, mode-locking involves loss modulation within the laser's cavity using a mode-locker. Their design's simplicity and cost effectiveness, coupled with the ability to generate laser pulses of high quality have made the mode-locked fiber lasers favorable in various fields, e.g. medical diagnostics, telecommunications and laser marking. There are two methods in achieving mode-locking regime in a laser system based on the way loss is modulated, namely active and passive techniques. Without the need of an external modulator as in actively mode-locked fiber lasers, passively mode-locked fiber lasers are comparably simpler, more flexible, cheaper and more compact in design. The underlying theme of this thesis is the development of mode-locked fiber lasers operating in both 1 and1.55- µm regions using new 2D nanomaterial based saturable absorbers.

In this thesis, four types of SA films based on graphene, graphene oxide, Bi_2Se_3 and Bi_2Te_3 nanomaterials were successfully fabricated and characterized. The fabrication of these SAs were simple and low cost. It was also found that these films have excellent characteristics and suitable to be integrated into lasers for generating high performance mode-locking pulses. By incorporating these films inside an Ytterbium-doped fiber laser (YDFL) cavity, ultra-short pulses trains operating at 1-micron region were successfully generated.   Mode-locked Erbium-doped fiber lasers (EDFLs) operating at 1.55- µm region were also realized by using the newly developed SAs. Toward this end, various soliton mode-locked fiber lasers were successfully demonstrated using these SAs by manipulating of cavity dispersion and length.

2D nanomaterials have gained much attention lately as low cost yet high-performance candidates, suitable to be integrated into lasers for better pulse generation. Hence, the thesis strives to fabricate several types of SAs based on graphene, graphene oxide, Bi_2Se_3 and Bi_2Te_3 nanomaterials for passively mode-locked YDFLs and EDFLs. The fabrication methods and subsequent characterization of the fabricated SAs were finely elaborated. In general, graphene and graphene oxide were homogenized with selected host polymer Polyethylene oxide (PEO) and subsequently evaporated by spreading at room temperature to form thin films (composites). Then preparation of TI (Bi_2Se_3 and Bi_2Te_3) as deposited TI nano-sheets on the fibre core, which the optical deposition process was carried out to place the Bi_2Se_3 and Bi_2Te_3 nanosheets onto the end surface of the ferrule. Characterization of the produced composites was done using Raman spectrometer and Field Emission Scanning Electron Microscopy (FESEM) prior to depositing the thin films and deposited TI nano-sheets on the fibre core in between FC/PC fiber connectors and incorporated into the cavity of YDFL and EDFL.

The presence of graphite within the fabricated composite (graphene and graphene oxide-based SA) was validated via Raman spectroscopy at the laser excitation wavelength of 532 nm. Distinct features of graphene spectrum such as the so-called D and G band were observed. The intensity ratio of the D to G band of the graphene sheets is about 1.2, as expected due to small size of the graphene sample. The existence of multi-layered graphene can be confirmed by considering the ratio of G to 2D peak which is higher than 0.5 and the modulation depth was measured to be around 16.2 % with non-saturable absorption of 22 % and saturation intensity of 87MW/cm^2. The Raman spectrum of the fabricated graphene oxide also clearly showed both D and G peaks. The intensity ratio between G and D band for GO was obtained at around 0.85. The ratio corresponds to the measure of disorder degree and is inversely proportional to the average size of the sp^2 clusters. The GO film has nonlinear saturable absorption or modulation depth of 24.1%,

saturable intensity of 72 MW/cm2 and non-saturable absorption of 35.1%. The Raman spectra from the Bi_2Se_3 and Bi_2Te_3 have three peaks assigned with different vibrational modes based on Raman selection rules. The modulation depth of the Bi_2Se_3 and Bi_2Te_3 film were about 39.8 % and 41.4%, respectively. Non-saturable absorption was measured to be about 10% for both materials.

A various mode-locked YDFLs have been successfully demonstrated using the prepared four types of 2D nanomaterial based SAs. By introducing the graphene SA into the YDFL cavity, a stable pulse laser was generated at 1052.89 nm wavelength with repetition rate of 4.5 MHz and pulse energy of 1.52 nJ. In another experiment, mode locked YDFL was generated at 1053 nm wavelength with repetition rate of 6 MHz and pulse energy of 1.65 nJ by employing GO SA. A mode-locking pulses train operating at approximately 1051 nm was generated when TI Bi_2Se_3 SA was used as a mode-locker. The laser operated with repetition rates of 8.3 MHz and the maximum pulse energy of 1.5 nJ was recorded. A stable mode-locking operation with the maximum pulse energy of 2.14 nJ was also successfully obtained with the use of TI Bi_2Te_3 SA. The pulse energy obtained was the highest compared to other SAs. This might be attributed to modulation depth of the SA, which was optimized for the YDFL cavity.

Soliton mode-locked EDFLs was demonstrated by using the previously developed graphene and topological insulator based SAs. By adjusting the cavity length and dispersion, fundamentally mode-locked soliton, bound soliton, vector soliton, dissipative soliton and soliton bunches trains at 1.5 μm region were realized. A stable passively mode-locked EDFL operating at 1565 nm was successfully demonstrated by integrating graphene SA in the laser cavity with estimated group delay dispersion of -0.22 ps^2. The laser generated soliton mode locking pulses with repetition rate of 20.7 MHz, pulse width of 0.88 ps and pulse energy of 1.5 nJ. A stable bound soliton operating at repetition rate

of 11.9 MHz was generated by manipulating the EDFL cavity with addition of 7.1 m extra single mode fiber (SMF) so that GDD becomes -0.37 ps^2. With GO SA, a mode-locked EDFL was also realized with pulse repetition rate of 22 MHz, pulse width of 0.8 ps and the pulse energy of 1.53 nJ. By changing the GDD from -0.197 ps^2 to $- 0.35$ ps^2, the GO based mode-locked EDFL produced a vector soliton bunch of 6 with a consistent repetition rate of 12.8 MHz and pulse energy of 2 nJ.

By incorporating a Bi_2Se_3 SA inside an EDFL cavity with $- 0.19$ ps^2 GDD, the laser generated mode-locking soliton pulses with 23.3 MHz repetition rate and 0.63 ps pulse width. The output pulses can be converted to multi-soliton pulses with pulse repetition rate of 13 MHz by adding SMF inside the cavity. The mode-locked laser operated at 1559.4 nm wavelength with 44 solitons in the bunch and the pulse energy of 2.1 nJ. A mode-locked EDFL based on TI Bi_2Te_3 SA was successfully demonstrated as well. The laser operated at 24 MHz repetition rate, 2.4 ps pulse width and 2.5 nJ pulse energy. The highest number of solitons in the bunch was exhibited with 144 solitons by inserted additional SMF into the cavity. The stable multi soliton was generated at 1556.7 nm with pulse energy of 2.6 nJ. The experimental results show that TI Bi_2Te_3 nanosheets could produce the highest energy while the smallest pulse width was obtained with Bi_2Se_3 SA.

The findings in this study validate the superiority of 2D nanomaterials such as graphene, graphene oxide, Bi_2Se_3 and Bi_2Te_3 as SAs in mode-locking operation over conventional SAs, provided they are integrated in suitable laser systems (YDFLs and EDFLs). The graphene and TI based fiber lasers designed in this study serve as potential alternative cost-effective laser sources for the applications in various fields, beneficiating human kinds from all aspects.

6.2   Future work

The key focus for future work is to investigate details on multiple soliton pulse fiber laser using another configuration such as figure-of-eight fiber laser based on the nonlinear amplifying loop mirror (NALM) on 1 micron, 1.5 micron and 2 micron regions.

Rare-earth doped fiber also recently gains attention in utilizing as SA device. So far not many works in fiber SA since the rare-earth materials used are only limits to single-mode thulium and holmium doped fiber. Relaxation time for thulium and holmium ions are in hundred microseconds and capability to produce a short pulse width is difficult.

In geometry perspective, fiber SA geometry has similar to standard fiber optic cable. It is easy to match to the fiber laser cavity. Less insertion loss and high. This enabled for wide possibility applications such as optoelectronics, sensors, communications and instrumentations.

REFERENCES

Adnan, N., Bidin, N., Taib, N., Haris, H., Fakaruddin, M., Hashim, A., Harun, S. (2016). Passively Q-switched flashlamp pumped Nd: YAG laser using liquid graphene oxide as saturable absorber. *Optics & Laser Technology, 80*, 28-32.

Aguergaray, C., Broderick, N. G., Erkintalo, M., Chen, J. S., & Kruglov, V. (2012). Mode-locked femtosecond all-normal all-PM Yb-doped fiber laser using a nonlinear amplifying loop mirror. *optics express, 20*(10), 10545-10551.

Ahmad, F., Harun, S., Nor, R., Zulkepely, N., Ahmad, H., & Shum, P. (2013). A passively mode-locked erbium-doped fiber laser based on a single-wall carbon nanotube polymer. *Chinese Physics Letters, 30*(5), 054210.

Ahmad, F., Harun, S., Nor, R., Zulkepely, N., Muhammad, F., Arof, H., & Ahmad, H. (2014). Mode-locked soliton erbium-doped fiber laser using a single-walled carbon nanotubes embedded in polyethylene oxide thin film saturable absorber. *Journal of Modern Optics, 61*(6), 541-545.

Ahmad, F., Harun, S. W., Nor, R. M., Ahmad, H., & Ibrahim, M. H. (2016). Soliton pulse generation using a swcntspolyvinyl alcohol thin film based passive saturable absorber. *ARPN Journal of Engineering and Applied Sciences, 11*(10), 6324-6327.

Ahmad, F., Harun, S. W., Nor, R. M., Zulkepely, N. R., Muhammad, F. D., Arof, H., & Ahmad, H. (2014). Mode-locked soliton erbium-doped fiber laser using a single-walled carbon nanotubes embedded in polyethylene oxide thin film saturable absorber. *Journal of Modern Optics, 61*(6), 541-545.

Ahmad, H., Salim, M., Azzuhri, S. R., Soltanian, M., & Harun, S. (2015). A passively Q-switched ytterbium-doped fiber laser based on a few-layer Bi2Se3 saturable absorber. *Laser Physics, 25*(6), 065102.

Ahmad, H., Tahrin, R. A. A., Azman, N., Kassim, S., Ismail, M. A., & Maah, M. J. (2017). 1.5-micron fiber laser passively mode-locked by gold nanoparticles saturable absorber. *Optics Communications, 403*, 115-120.

Ahmed, M., Ali, N., Salleh, Z., Rahman, A., Harun, S., Manaf, M., & Arof, H. (2014). All fiber mode-locked Erbium-doped fiber laser using single-walled carbon nanotubes embedded into polyvinyl alcohol film as saturable absorber. *Optics & Laser Technology, 62*, 40-43.

Akhmediev, N., & Ankiewicz, A. (2005). Dissipative solitons in the complex Ginzburg-Landau and Swift-Hohenberg equations *Dissipative solitons* (pp. 1-17): Springer.

Allen, M. J., Tung, V. C., & Kaner, R. B. (2009). Honeycomb carbon: a review of graphene. *Chemical Reviews, 110*(1), 132-145.

Ambrosio, C. Silas Alben.

Ando, Y. (2013). Topological insulator materials. *Journal of the Physical Society of Japan, 82*(10), 102001.

Anku, W. W., Oppong, S. O., & Govender, P. P. (2018). Bismuth-Based Nanoparticles as Photocatalytic Materials.

Antoncini, C. (2006). Ultrashort laser pulses. *University of Reading, Department of Physics*.

Antonelli, C., Chen, J., & Kartner, F. X. (2007). Intracavity pulse dynamics and stability for passively mode-locked lasers. *Opt Express, 15*(10), 5919-5924.

Anyi, C., Ali, N., Rahman, A., Harun, S., & Arof, H. (2013). Multi-wavelength Q-switched erbium-doped fibre laser using saturable absorber based on carbon nanotube film. *Ukrainian Journal of Physical Optics*(14,№ 4), 212-218.

Anyi, C., Haris, H., Harun, S. W., Ali, N. M., & Arof, H. (2013). Nanosecond pulse fibre laser based on nonlinear polarisation rotation effect. *Electronics Letters, 49*(19), 1240-1241.

Arumugam, M. (2001). Optical fiber communication—An overview. *Pramana, 57*(5-6), 849-869.

Bachmann, F. (2003). Industrial applications of high power diode lasers in materials processing. *Applied surface science, 208*, 125-136.

Bandrauk, A., & Shen, H. (1994). High-order split-step exponential methods for solving coupled nonlinear Schrodinger equations. *Journal of Physics A: Mathematical and General, 27*(21), 7147.

Bao, Q., Hoh, H., & Zhang, Y. (2017). *Graphene Photonics, Optoelectronics, and Plasmonics*: CRC Press.

Bao, Q., Zhang, H., Ni, Z., Wang, Y., Polavarapu, L., Shen, Z., Loh, K. P. (2011). Monolayer graphene as a saturable absorber in a mode-locked laser. *Nano Research, 4*(3), 297-307.

Bao, Q., Zhang, H., Wang, Y., Ni, Z., Yan, Y., Shen, Z. X., Tang, D. Y. (2009a). Atomic-Layer Graphene as a Saturable Absorber for Ultrafast Pulsed Lasers. *Advanced Functional Materials, 19*(19), 3077-3083.

Bao, Q., Zhang, H., Wang, Y., Ni, Z., Yan, Y., Shen, Z. X., Tang, D. Y. (2009b). Atomic-layer graphene as a saturable absorber for ultrafast pulsed lasers. *Advanced Functional Materials, 19*(19), 3077-3083.

Bao, Q. L., Zhang, H., Wang, Y., Ni, Z. H., Yan, Y. L., Shen, Z. X., Tang, D. Y. (2009). Atomic-Layer Graphene as a Saturable Absorber for Ultrafast Pulsed Lasers. *Advanced Functional Materials, 19*(19), 3077-3083.

Bednyakova, A., Babin, S., Kharenko, D., Podivilov, E., Fedoruk, M., Kalashnikov, V., & Apolonski, A. (2013). Evolution of dissipative solitons in a fiber laser oscillator in the presence of strong Raman scattering. *optics express, 21*(18), 20556-20564.

Bertolazzi, S., Brivio, J., & Kis, A. (2011). Stretching and breaking of ultrathin MoS2. *ACS Nano, 5*(12), 9703-9709.

Bhattarai, L. N. Graphene: A Peculiar Allotrope Of Carbon. *Himalayan Physics, 3*, 87-88.

Blow, K., Doran, N., & Wood, D. (1988). Generation and stabilization of short soliton pulses in the amplified nonlinear Schrödinger equation. *JOSA B, 5*(2), 381-391.

Boehm, H. P., Clauss, A., Fischer, G. O., & Hofmann, U. (1962). Das Adsorptionsverhalten sehr dünner Kohlenstoff-Folien. *Zeitschrift für anorganische und allgemeine Chemie, 316*(3-4), 119-127.

Bonaccorso, F., & Sun, Z. (2014). Solution processing of graphene, topological insulators and other 2d crystals for ultrafast photonics. *Optical Materials Express, 4*(1), 63-78.

Bonaccorso, F., Sun, Z., Hasan, T., & Ferrari, A. (2010). Graphene photonics and optoelectronics. *Nature Photonics, 4*(9), 611.

Bowers, J. E., Morton, P. A., Mar, A., & Corzine, S. W. (1989). Actively mode-locked semiconductor lasers. *IEEE Journal of Quantum Electronics, 25*(6), 1426-1439.

Brabec, T., Spielmann, C., Curley, P., & Krausz, F. (1992). Kerr lens mode locking. *Optics Letters, 17*(18), 1292-1294.

Breusing, M., Ropers, C., & Elsaesser, T. (2009). Ultrafast carrier dynamics in graphite. *Phys Rev Lett, 102*(8), 086809.

Brida, D., Krauss, G., Sell, A., & Leitenstorfer, A. (2014). Ultrabroadband Er: fiber lasers. *Laser & Photonics Reviews, 8*(3), 409-428.

Buckley, S. G. (2018). Lasers and Optics Interface Ultrafast Lasers in Spectroscopy-Moving into the Mainstream. *SPECTROSCOPY, 33*(4), 20-25.

Butler, S. Z., Hollen, S. M., Cao, L., Cui, Y., Gupta, J. A., Gutiérrez, H. R., Ismach, A. F. (2013). Progress, challenges, and opportunities in two-dimensional materials beyond graphene. *ACS nano, 7*(4), 2898-2926.

Carbone, F., Aubock, G., Cannizzo, A., Van Mourik, F., Nair, R., Geim, A., Chergui, M. (2011). Femtosecond carrier dynamics in bulk graphite and graphene paper. *Chemical Physics Letters, 504*(1-3), 37-40.

Castro Neto, A. H. (2007). Graphene: Phonons behaving badly. *Nat Mater, 6*(3), 176-177.

Castro Neto, A. H., & Novoselov, K. (2011). Two-Dimensional Crystals: Beyond Graphene. *Materials Express, 1*(1), 10-17.

Chang, Y. M., Lee, J., & Lee, J. H. (2012). Active Mode-Locking of an Erbium-Doped Fiber Laser Using an Ultrafast Silicon-Based Variable Optical Attenuator. *Japanese Journal of Applied Physics, 51*(7R), 072701.

Chen, Y.-S., Yan, P.-G., Chen, H., Liu, A.-J., & Ruan, S.-C. (2015). *Harmonic mode-locked fiber laser based on photonic crystal fiber filled with topological insulator solution.* Paper presented at the Photonics.

Chen, Y., Zhao, C., Huang, H., Chen, S., Tang, P., Wang, Z., Tang, D. (2013). Self-assembled topological insulator: Bi $ _ $ {2} $ $ Se $ _ $ {3} $ membrane as a passive Q-switcher in an Erbium-doped fiber laser. *Journal of Lightwave Technology, 31*(17), 2857-2863.

Chen, Y. C., Raravikar, N. R., Schadler, L. S., Ajayan, P. M., Zhao, Y. P., Lu, T. M., Zhang, X. C. (2002). Ultrafast optical switching properties of single-wall carbon nanotube polymer composites at 1.55 μm. *Applied Physics Letters, 81*(6), 975-977.

Chernikov, S. V., Dianov, E. M., Richardson, D., & Payne, D. N. (1993). Soliton pulse compression in dispersion-decreasing fiber. *Optics Letters, 18*(7), 476-478.

Chi, C., Lee, J., Koo, J., & Lee, J. H. (2014). All-normal-dispersion dissipative-soliton fiber laser at 1.06 μm using a bulk-structured Bi2Te3 topological insulator-deposited side-polished fiber. *Laser Physics, 24*(10), 105106.

Choi, S. Y., Rotermund, F., Jung, H., Oh, K., & Yeom, D.-I. (2009). Femtosecond mode-locked fiber laser employing a hollow optical fiber filled with carbon nanotube dispersion as saturable absorber. *Optics Express, 17*(24), 21788-21793.

Ciesielski, A., & Samorì, P. (2014). Graphene via sonication assisted liquid-phase exfoliation. *Chemical Society Reviews, 43*(1), 381-398.

Coleman, J. N., Lotya, M., O'Neill, A., Bergin, S. D., King, P. J., Khan, U., Smith, R. J. (2011). Two-dimensional nanosheets produced by liquid exfoliation of layered materials. *Science, 331*(6017), 568-571.

Collings, B. C., Cundiff, S. T., Akhmediev, N., Soto-Crespo, J. M., Bergman, K., & Knox, W. (2000). Polarization-locked temporal vector solitons in a fiber laser: experiment. *JOSA B, 17*(3), 354-365.

Conroy, R. S., Lake, T., Friel, G. J., Kemp, A. J., & Sinclair, B. D. (1998). Self-Q-switched Nd:YVO4 microchip lasers. *Opt Lett, 23*(6), 457-459.

Deissler, R. J. (1985). Noise-sustained structure, intermittency, and the Ginzburg-Landau equation. *Journal of statistical physics, 40*(3-4), 371-395.

Delgado-Pinar, M., Zalvidea, D., Diez, A., Pérez-Millán, P., & Andrés, M. (2006). Q-switching of an all-fiber laser by acousto-optic modulation of a fiber Bragg grating. *Optics Express, 14*(3), 1106-1112.

DeMaria, A., Stetser, D., & Heynau, H. (1966). Self mode-locking of lasers with saturable absorbers. *Applied Physics Letters, 8*(7), 174-176.

Doering, C. R., Gibbon, J. D., Holm, D. D., & Nicolaenko, B. (1988). Low-dimensional behaviour in the complex Ginzburg-Landau equation. *Nonlinearity, 1*(2), 279.

Driben, R., Malomed, B., Yulin, A., & Skryabin, D. (2013). Newton's cradles in optics: From N-soliton fission to soliton chains. *Physical Review A, 87*(6), 063808.

Druffel, E. R. M. (1997). Geochemistry of corals: Proxies of past ocean chemistry, ocean circulation, and climate. *Proceedings of the National Academy of Sciences, 94*(16), 8354-8361.

Etzel, H. W., Gandy, H. W., & Ginther, R. J. (1962). Stimulated Emission of Infrared Radiation from Ytterbium Activated Silicate Glass. *Applied Optics, 1*(4), 534.

Evangelides, S. G., Mollenauer, L. F., Gordon, J. P., & Bergano, N. S. (1992). Polarization multiplexing with solitons. *Journal of Lightwave Technology, 10*(1), 28-35.

Ezawa, M. (2008). Spin-dependent Coulomb interaction and quantum Hall effects in graphene. *Physica B: Condensed Matter, 403*(5-9), 1502-1504.

Fan, T., & Byer, R. (1987). Modeling and CW operation of a quasi-three-level 946 nm Nd: YAG laser. *IEEE Journal of Quantum Electronics, 23*(5), 605-612.

Faubert, D., & Chin, S. (1982). Short laser pulse generation: part one. *Optics & Laser Technology, 14*(4), 197-206.

Fermann, M., Andrejco, M., Silberberg, Y., & Stock, M. (1993). Passive mode locking by using nonlinear polarization evolution in a polarization-maintaining erbium-doped fiber. *Optics Letters, 18*(11), 894-896.

Fermann, M., Galvanauskas, A., Sucha, G., & Harter, D. (1997). Fiber-lasers for ultrafast optics. *Applied Physics B: Lasers and Optics, 65*(2), 259-275.

Fermann, M. E., & Harter, D. J. (1995). Technique for the generation of optical pulses in modelocked lasers by dispersive control of the oscillation pulse width: Google Patents.

Fermann, M. E., & Hartl, I. (2013). Ultrafast fibre lasers. *7*, 1006.

Fermann, M. E., Sucha, G. D., Galvanauskes, A., Hofer, M., & Harter, D. J. (1999). *Fiber lasers in ultrafast optics.* Paper presented at the Commercial and Biomedical Applications of Ultrafast Lasers.

Ferrari, A. C., & Basko, D. M. (2013). Raman spectroscopy as a versatile tool for studying the properties of graphene. *Nature nanotechnology, 8*(4), 235.

Ferrari, A. C., Meyer, J. C., Scardaci, V., Casiraghi, C., Lazzeri, M., Mauri, F., Geim, A. K. (2006). Raman spectrum of graphene and graphene layers. *Phys Rev Lett, 97*(18), 187401.

Fork, R., Greene, B., & Shank, C. V. (1981). Generation of optical pulses shorter than 0.1 psec by colliding pulse mode locking. *Applied Physics Letters, 38*(9), 671-672.

Fork, R. L., Cruz, C. B., Becker, P., & Shank, C. V. (1987). Compression of optical pulses to six femtoseconds by using cubic phase compensation. *Optics Letters, 12*(7), 483-485.

Foster, M. A., Turner, A. C., Sharping, J. E., Schmidt, B. S., Lipson, M., & Gaeta, A. L. (2006). Broad-band optical parametric gain on a silicon photonic chip. *Nature, 441*(7096), 960.

Frindt, R. (1965). Optical Absorption of a Few Unit-Cell Layers of Mo S 2. *Physical Review, 140*(2A), A536.

Frindt, R., & Yoffe, A. (1963). *Physical properties of layer structures: optical properties and photoconductivity of thin crystals of molybdenum disulphide.* Paper presented at the Proceedings of the Royal Society of London A: Mathematical, Physical and Engineering Sciences.

Ganatra, R., & Zhang, Q. (2014). Few-layer MoS2: a promising layered semiconductor. *ACS Nano, 8*(5), 4074-4099.

Gandy, H., Ginther, R., & Weller, J. (1965). Energy transfer in triply activated glasses. *Applied Physics Letters, 6*(3), 46-49.

Gao, W., Singh, N., Song, L., Liu, Z., Reddy, A. L. M., Ci, L., Ajayan, P. M. (2011). Direct laser writing of micro-supercapacitors on hydrated graphite oxide films. *Nature nanotechnology, 6*(8), 496.

Garanovich, I. L., Longhi, S., Sukhorukov, A. A., & Kivshar, Y. S. (2012). Light propagation and localization in modulated photonic lattices and waveguides. *Physics Reports, 518*(1-2), 1-79.

Geim, A. K., & Novoselov, K. S. (2007). The rise of graphene. *Nature Materials, 6*(3), 183-191.

Geim, A. K., & Novoselov, K. S. (2010). The rise of graphene *Nanoscience and Technology: A Collection of Reviews from Nature Journals* (pp. 11-19): World Scientific.

Georgakilas, V., Otyepka, M., Bourlinos, A. B., Chandra, V., Kim, N., Kemp, K. C., Kim, K. S. (2012). Functionalization of graphene: covalent and non-covalent approaches, derivatives and applications. *Chemical Reviews, 112*(11), 6156-6214.

Ghany, K. A., & Newishy, M. (2005). Cutting of 1.2 mm thick austenitic stainless steel sheet using pulsed and CW Nd: YAG laser. *Journal of Materials Processing Technology, 168*(3), 438-447.

Gomes, L. A., Orsila, L., Jouhti, T., & Okhotnikov, O. G. (2004). Picosecond SESAM-based ytterbium mode-locked fiber lasers. *IEEE Journal of Selected Topics in Quantum Electronics, 10*(1), 129-136.

Grelu, P., & Akhmediev, N. (2012). Dissipative solitons for mode-locked lasers. *Nature Photonics, 6*(2), 84.

Gu, M., Zhang, Q., & Lamon, S. (2016). Nanomaterials for optical data storage. *Nature Reviews Materials, 1*(12), 16070.

Gui, L., Xiao, X., & Yang, C. (2013). Observation of various bound solitons in a carbon-nanotube-based erbium fiber laser. *JOSA B, 30*(1), 158-164.

Guo, Y. Q., Sun, X. Y., Liu, Y., Wang, W., Qiu, H. X., & Gao, J. P. (2012). One pot preparation of reduced graphene oxide (RGO) or Au (Ag) nanoparticle-RGO hybrids using chitosan as a reducing and stabilizing agent and their use in methanol electrooxidation. *Carbon, 50*(7), 2513-2523.

Gupta, K. K., Onodera, N., Abedin, K. S., & Hyodo, M. (2002). Pulse repetition frequency multiplication via intracavity optical filtering in AM mode-locked fiber ring lasers. *IEEE Photonics Technology Letters, 14*(3), 284-286.

Gupta, M. C., & Ballato, J. (2006). *The handbook of photonics*: CRC press.

Hajlaoui, M., Papalazarou, E., Mauchain, J., Lantz, G., Moisan, N., Boschetto, D., Taleb-Ibrahimi, A. (2012). Ultrafast surface carrier dynamics in the topological insulator Bi2Te3. *Nano Letters, 12*(7), 3532-3536.

Hargrove, L., Fork, R. L., & Pollack, M. (1964). Locking of He–Ne laser modes induced by synchronous intracavity modulation. *Applied Physics Letters, 5*(1), 4-5.

Haris, H., Harun, S., Anyi, C., Muhammad, A., Ahmad, F., Tan, S., Arof, H. (2015). Generation of soliton and bound soliton pulses in mode-locked erbium-doped fiber laser using graphene film as saturable absorber. *Journal of Modern Optics*, 1-6.

Haris, H., Harun, S. W., Anyi, C. L., Muhammad, A. R., Ahmad, F., Tan, S. J., Arof, H. (2016). Generation of soliton and bound soliton pulses in mode-locked erbium-doped fiber laser using graphene film as saturable absorber. *Journal of Modern Optics, 63*(8), 777-782.

Haris, H., Harun, S. W., Muhammad, A. R., Anyi, C. L., Tan, S. J., Ahmad, F., Arof, H. (2017). Passively Q-switched Erbium-doped and Ytterbium-doped fibre lasers with topological insulator bismuth selenide (Bi2Se3) as saturable absorber. *Optics and Laser Technology, 88*, 121-127.

Hasan, B. A. (2014). Effect of Thickness on the Performance of Bi2S3 Thin Film for Photovoltaic Devices. *International journal of advanced scientific and technical research, 3*(4).

Hasan, T., Sun, Z., Tan, P., Popa, D., Flahaut, E., Kelleher, E. J., Torrisi, F. (2014). Double-wall carbon nanotubes for wide-band, ultrafast pulse generation. *ACS Nano, 8*(5), 4836-4847.

Hasan, T., Sun, Z. P., Wang, F. Q., Bonaccorso, F., Tan, P. H., Rozhin, A. G., & Ferrari, A. C. (2009). Nanotube-Polymer Composites for Ultrafast Photonics. *Advanced Materials, 21*(38-39), 3874-3899.

Haus, H. A. (2000). Mode-locking of lasers. *IEEE Journal of Selected Topics in Quantum Electronics, 6*(6), 1173-1185.

Hillerkuss, D., Schmogrow, R., Schellinger, T., Jordan, M., Winter, M., Huber, G., Frey, F. (2011). 26 Tbit s− 1 line-rate super-channel transmission utilizing all-optical fast Fourier transform processing. *Nature Photonics, 5*(6), 364.

Hossain, M. Z., Rumyantsev, S. L., Shahil, K. M., Teweldebrhan, D., Shur, M., & Balandin, A. A. (2011). Low-frequency current fluctuations in "graphene-like" exfoliated thin-films of bismuth selenide topological insulators. *ACS Nano, 5*(4), 2657-2663.

Hoy, C. L., Ferhanoglu, O., Yildirim, M., Kim, K. H., Karajanagi, S. S., Chan, K. M. C., Ben-Yakar, A. (2014). Clinical ultrafast laser surgery: recent advances and future directions. *IEEE Journal of Selected Topics in Quantum Electronics, 20*(2), 242-255.

Huang, J. Y., Huang, W. C., Zhuang, W. Z., Su, K. W., Chen, Y. F., & Huang, K. F. (2009). High-pulse-energy, passively Q-switched Yb-doped fiber laser with AlGaInAs quantum wells as a saturable absorber. *Optics Letters, 34*(15), 2360-2362.

Huang, X., Yin, Z., Wu, S., Qi, X., He, Q., Zhang, Q., Zhang, H. (2011). Graphene-based materials: synthesis, characterization, properties, and applications. *small, 7*(14), 1876-1902.

i Ponsoda, M., & Joan, J. (2013). Analysis of photodarkening effects in ytterbium-doped laser fibers.

Ismail, M. A., Ahmad, H., & Harun, S. W. (2014). Soliton mode-locked erbium-doped fiber laser using non-conductive graphene oxide paper. *IEEE Journal of Quantum Electronics, 50*(2), 85-87.

Ismail, M. A., Ahmad, H., & Harun, S. W. (2014). Soliton mode-locked erbium-doped fiber laser using non-conductive graphene oxide paper. *Quantum Electronics, IEEE Journal of, 50*(2), 85-87.

Ismail, M. A., Harun, S. W., Zulkepely, N. R., Nor, R. M., Ahmad, F., & Ahmad, H. (2012). Nanosecond soliton pulse generation by mode-locked erbium-doped fiber laser using single-walled carbon-nanotube-based saturable absorber. *Applied Optics, 51*(36), 8621-8624.

Itoh, T., Araki, T., Ashida, M., Iwata, T., Muro, K., & Yamada, N. (2011). Optical Properties *Springer Handbook of Metrology and Testing* (pp. 587-663): Springer.

Jaff, P. M. (2012). The Gain performance of Ytterbium Doped Fiber Amplifier. *Journal Of Wassit For Science & Medicine, 5*(1), 200-209.

Jhon, Y. I., Lee, J., Jhon, Y. M., & Lee, J. H. (2018). Topological Insulators for Mode-Locking of 2-μm Fiber Lasers. *IEEE Journal of Selected Topics in Quantum Electronics, 24*(5), 1-8.

Jiang, G., Yi, J., Miao, L., Tang, P., Huang, H., Zhao, C., & Wen, S. (2018). Bismuth Telluride nanocrystal: broadband nonlinear response and its application in ultrafast photonics. *Scientific reports, 8*(1), 2355.

Jiang, T., Xu, Y., Tian, Q., Liu, L., Kang, Z., Yang, R., Qin, W. (2012). Passively Q-switching induced by gold nanocrystals. *Applied Physics Letters, 101*(15), 151122.

Jin, X., Wu, Z., Li, L., Zhang, Q., Tang, D., Shen, D., Zhao, L. (2016). Manipulation of group-velocity-locked vector solitons from fiber lasers. *IEEE Photonics Journal, 8*(2), 1-6.

Jin, X., Wu, Z., Zhang, Q., Li, L., Tang, D., Shen, D., Zhao, L. (2015). Generation of high-order group-velocity-locked vector solitons. *IEEE Photonics Journal, 7*(5), 1-6.

Joensen, P., Frindt, R., & Morrison, S. R. (1986). Single-layer MoS 2. *Materials research bulletin, 21*(4), 457-461.

Jung, I., Kärtner, F., Matuschek, N., Sutter, D., Morier-Genoud, F., Shi, Z., Keller, U. (1997). Semiconductor saturable absorber mirrors supporting sub-10-fs pulses. *Applied Physics B: Lasers and Optics, 65*(2), 137-150.

Jung, I. D., Kartner, F. X., Matuschek, N., Sutter, D. H., MorierGenoud, F., Shi, Z., Keller, U. (1997). Semiconductor saturable absorber mirrors supporting sub-10-fs pulses. *Applied Physics B-Lasers and Optics, 65*(2), 137-150.

Kadi, F., Winzer, T., Knorr, A., & Malic, E. (2015). Impact of doping on the carrier dynamics in graphene. *Scientific Reports, 5*, 16841.

Kampfrath, T., Perfetti, L., Schapper, F., Frischkorn, C., & Wolf, M. (2005). Strongly coupled optical phonons in the ultrafast dynamics of the electronic energy and current relaxation in graphite. *Phys Rev Lett, 95*(18), 187403.

Kasap, S., & Capper, P. (2006). *Springer handbook of electronic and photonic materials*: Springer Science & Business Media.

Kashiwagi, K., & Yamashita, S. (2009). Deposition of carbon nanotubes around microfiber via evanescent light. *Optics express, 17*(20), 18364-18370.

Kataura, H., Kumazawa, Y., Maniwa, Y., Ohtsuka, Y., Sen, R., Suzuki, S., & Achiba, Y. (2000). Diameter control of single-walled carbon nanotubes. *Carbon, 38*(11-12), 1691-1697.

Keiser, G. (2008). *Optical fiber communications*: McGraw-Hill.

Kelleher, E., Travers, J., Sun, Z., Ferrari, A., Golant, K., Popov, S., & Taylor, J. (2010). Bismuth fiber integrated laser mode-locked by carbon nanotubes. *Laser Physics Letters, 7*(11), 790.

Keller, U. (2003). Recent developments in compact ultrafast lasers. *Nature, 424*(6950), 831-838.

Keller, U. (2010). Ultrafast solid-state laser oscillators: a success story for the last 20 years with no end in sight. *Applied Physics B, 100*(1), 15-28.

Keller, U., Miller, D., Boyd, G., Chiu, T., Ferguson, J., & Asom, M. (1992). Solid-state low-loss intracavity saturable absorber for Nd: YLF lasers: an antiresonant semiconductor Fabry–Perot saturable absorber. *Optics Letters, 17*(7), 505-507.

Keller, U., Miller, D. A. B., Boyd, G. D., Chiu, T. H., Ferguson, J. F., & Asom, M. T. (1992). Solid-state low-loss intracavity saturable absorber for Nd:YLF lasers: an antiresonant semiconductor Fabry–Perot saturable absorber. *Optics Letters, 17*(7), 505-507.

Keller, U., Weingarten, K. J., Kartner, F. X., Kopf, D., Braun, B., Jung, I. D., Au, J. A. d. (1996). Semiconductor saturable absorber mirrors (SESAM's) for femtosecond to nanosecond pulse generation in solid-state lasers. *IEEE Journal of Selected Topics in Quantum Electronics, 2*(3), 435-453.

Keller, U., Weingarten, K. J., Kartner, F. X., Kopf, D., Braun, B., Jung, I. D., derAu, J. A. (1996). Semiconductor saturable absorber mirrors (SESAM's) for femtosecond to nanosecond pulse generation in solid-state lasers. *IEEE Journal of Selected Topics in Quantum Electronics, 2*(3), 435-453.

Khan, Z. U., Kausar, A., Ullah, H., Badshah, A., & Khan, W. U. (2016). A review of graphene oxide, graphene buckypaper, and polymer/graphene composites: Properties and fabrication techniques. *Journal of plastic film & sheeting, 32*(4), 336-379.

Khazaeinezhad, R., Kassani, S. H., Jeong, H., Nazari, T., Yeom, D.-I., & Oh, K. (2015). Mode-Locked All-Fiber Lasers at Both Anomalous and Normal Dispersion Regimes Based on Spin-Coated $\hbox {MoS} _ {2} $ Nano-Sheets on a Side-Polished Fiber. *IEEE Photonics Journal, 7*(1), 1-9.

Kobtsev, S., Kukarin, S., & Fedotov, Y. (2008). Ultra-low repetition rate mode-locked fiber laser with high-energy pulses. *optics express, 16*(26), 21936-21941.

Koponen, J. J., Soderlund, M. J., Hoffman, H. J., & Tammela, S. K. (2006). Measuring photodarkening from single-mode ytterbium doped silica fibers. *Opt Express, 14*(24), 11539-11544.

Kornaszewski, L., Maker, G., Malcolm, G., Butkus, M., Rafailov, E. U., & Hamilton, C. J. (2012). SESAM-free mode-locked semiconductor disk laser. *Laser & Photonics Reviews, 6*(6), L20-L23.

Kuleshov, N., Lagatsky, A., Shcherbitsky, V., Mikhailov, V., Heumann, E., Jensen, T., Huber, G. (1997). CW laser performance of Yb and Er, Yb doped tungstates. *Applied Physics B, 64*(4), 409-413.

Kürti, J., Zólyomi, V., Grüneis, A., & Kuzmany, H. (2002). Double resonant Raman phenomena enhanced by van Hove singularities in single-wall carbon nanotubes. *Physical Review B, 65*(16).

Kuzmenko, A., Van Heumen, E., Carbone, F., & Van Der Marel, D. (2008). Universal optical conductance of graphite. *Physical review letters, 100*(11), 117401.

Lamb Jr, W. E. (1964). Theory of an optical maser. *Physical Review, 134*(6A), A1429.

Laroche, M., Chardon, A. M., Nilsson, J., Shepherd, D. P., Clarkson, W. A., Girard, S., & Moncorge, R. (2002). Compact diode-pumped passively Q-switched tunable Er-Yb double-clad fiber laser. *Opt Lett, 27*(22), 1980-1982.

Latiff, A. A., Kadir, N. A., Ismail, E. I., Shamsuddin, H., Ahmad, H., & Harun, S. W. (2017). All-fiber dual-wavelength Q-switched and mode-locked EDFL by SMF-THDF-SMF structure as a saturable absorber. *Optics Communications, 389*, 29-34.

Lee, E. J., Choi, S. Y., Jeong, H., Park, N. H., Yim, W., Kim, M. H., Kim, S. J. (2015). Active control of all-fibre graphene devices with electrical gating. *Nature communications, 6*, 6851.

Lee, J., Koo, J., Debnath, P., Song, Y., & Lee, J. (2013). A Q-switched, mode-locked fiber laser using a graphene oxide-based polarization sensitive saturable absorber. *Laser Physics Letters, 10*(3), 035103.

Lee, J., Koo, J., Jhon, Y. M., & Lee, J. H. (2014). A femtosecond pulse erbium fiber laser incorporating a saturable absorber based on bulk-structured Bi 2 Te 3 topological insulator. *optics express, 22*(5), 6165-6173.

Li, D., Li, L., Zhou, J., Zhao, L., Tang, D., & Shen, D. (2016). Characterization and compression of dissipative-soliton-resonance pulses in fiber lasers. *Scientific Reports, 6*, 23631.

Li, H., Xia, H., Lan, C., Li, C., Zhang, X., Li, J., & Liu, Y. (2015). Passively-Switched Erbium-Doped Fiber Laser Based on Few-Layer MoS 2 Saturable Absorber. *IEEE Photonics Technology Letters, 27*(1), 69-72.

Li, J., Luo, H., He, Y., Liu, Y., Zhang, L., Zhou, K., Turistyn, S. (2014). Semiconductor saturable absorber mirror passively Q-switched 2.97 μm fluoride fiber laser. *Laser Physics Letters, 11*(6), 065102.

Li, X., Cai, W., An, J., Kim, S., Nah, J., Yang, D., Tutuc, E. (2009). Large-area synthesis of high-quality and uniform graphene films on copper foils. *science, 324*(5932), 1312-1314.

Li, X., Magnuson, C. W., Venugopal, A., An, J., Suk, J. W., Han, B., Zhu, Y. (2010). Graphene films with large domain size by a two-step chemical vapor deposition process. *Nano Letters, 10*(11), 4328-4334.

Li, X., Yu, X., Sun, Z., Yan, Z., Sun, B., Cheng, Y., Wang, Q. J. (2015). High-power graphene mode-locked Tm/Ho co-doped fiber laser with evanescent field interaction. *Scientific Reports, 5*, 16624.

Li, X., Zhang, S., Meng, Y., Hao, Y., Li, H., Du, J., & Yang, Z. (2012). Observation of soliton bound states in a graphene mode locked erbium-doped fiber laser. *Laser physics, 22*(4), 774-777.

Lin, Q., Painter, O. J., & Agrawal, G. P. (2007). Nonlinear optical phenomena in silicon waveguides: modeling and applications. *optics express, 15*(25), 16604-16644.

Lin, Y.-T., & Lin, G.-R. (2006). Dual-stage soliton compression of a self-started additive pulse mode-locked erbium-doped fiber laser for 48 fs pulse generation. *Optics Letters, 31*(10), 1382-1384.

Ling, Y., & Xueming, L. (2012). Generation and Propagation of Bound-State Pulses in a Passively Mode-Locked Figure-Eight Laser. *Photonics Journal, IEEE, 4*(2), 512-519.

Linke, S. J., & Katz, T. (2016). *Complications in Corneal Laser Surgery*: Springer.

Liu, B., Li, L., & Mihalache, D. (2015). Vector soliton solutions in PT-symmetric coupled waveguides and their relevant properties. *ROMANIAN REPORTS IN PHYSICS, 67*(3), 802-818.

Liu, M., Liu, W., Pang, L., Teng, H., Fang, S., & Wei, Z. (2018). Ultrashort pulse generation in mode-locked erbium-doped fiber lasers with tungsten disulfide saturable absorber. *Optics Communications, 406*, 72-75.

Liu, S., Yan, J., He, G., Zhong, D., Chen, J., Shi, L., Jiang, H. (2012). Layer-by-layer assembled multilayer films of reduced graphene oxide/gold nanoparticles for the electrochemical detection of dopamine. *Journal of Electroanalytical Chemistry, 672*, 40-44.

Liu, X. (2011). Soliton formation and evolution in passively-mode-locked lasers with ultralong anomalous-dispersion fibers. *Physical Review A, 84*(2), 023835.

Liu, X., Han, D., Sun, Z., Zeng, C., Lu, H., Mao, D., Wang, F. (2013). Versatile multi-wavelength ultrafast fiber laser mode-locked by carbon nanotubes. *Sci Rep, 3*, 2718.

Liu, Y.-Y., Wang, Y., Walsh, T. R., Yi, L.-X., Zhang, R., Spencer, J., Huang, X. (2016). Emergence of plasmid-mediated colistin resistance mechanism MCR-1 in animals and human beings in China: a microbiological and molecular biological study. *The Lancet infectious diseases, 16*(2), 161-168.

Loh, K. P., Bao, Q., Eda, G., & Chhowalla, M. (2010). Graphene oxide as a chemically tunable platform for optical applications. *Nature chemistry, 2*(12), 1015.

Lu, J., Yang, J.-x., Wang, J., Lim, A., Wang, S., & Loh, K. P. (2009). One-pot synthesis of fluorescent carbon nanoribbons, nanoparticles, and graphene by the exfoliation of graphite in ionic liquids. *ACS Nano, 3*(8), 2367-2375.

Lu, S. B., Zhao, C. J., Zou, Y. H., Chen, S. Q., Chen, Y., Li, Y., Tang, D. Y. (2013). Third order nonlinear optical property of Bi2Se3. *optics express, 21*(2), 2072-2082.

Luo, A., Luo, Z., Xu, W., Dvoyrin, V., Mashinsky, V., & Dianov, E. (2011). Tunable and switchable dual-wavelength passively mode-locked Bi-doped all-fiber ring laser based on nonlinear polarization rotation. *Laser Physics Letters, 8*(8), 601.

Luo, Y., Cheng, J., Liu, B., Sun, Q., Li, L., Fu, S., Liu, D. (2017). Group-velocity-locked vector soliton molecules in fiber lasers. *Scientific Reports, 7*(1), 2369.

Luo, Z.-C., Liu, M., Liu, H., Zheng, X.-W., Luo, A.-P., Zhao, C.-J., Xu, W.-C. (2013). 2 GHz passively harmonic mode-locked fiber laser by a microfiber-based topological insulator saturable absorber. *Optics Letters, 38*(24), 5212-5215.

Luo, Z.-C., Luo, A.-P., & Xu, W.-C. (2011). Tunable and switchable multiwavelength passively mode-locked fiber laser based on SESAM and inline birefringence comb filter. *IEEE Photonics Journal, 3*(1), 64-70.

Luo, Z.-C., Ning, Q.-Y., Mo, H.-L., Cui, H., Liu, J., Wu, L.-J., Xu, W.-C. (2013). Vector dissipative soliton resonance in a fiber laser. *Optics Express, 21*(8), 10199-10204.

Luo, Z., Liu, C., Huang, Y., Wu, D., Wu, J., Xu, H., Weng, J. (2014). Topological-Insulator Passively Q-Switched Double-Clad Fiber Laser at 2μ m Wavelength. *IEEE Journal of Selected Topics in Quantum Electronics, 20*(5), 1-8.

Luo, Z., Zhou, M., Weng, J., Huang, G., Xu, H., Ye, C., & Cai, Z. (2010). Graphene-based passively Q-switched dual-wavelength erbium-doped fiber laser. *Optics Letters, 35*(21), 3709-3711.

Mak, K. F., He, K., Shan, J., & Heinz, T. F. (2012). Control of valley polarization in monolayer MoS2 by optical helicity. *Nat Nano, 7*(8), 494-498.

Mak, K. F., Lee, C., Hone, J., Shan, J., & Heinz, T. F. (2010). Atomically thin MoS 2: a new direct-gap semiconductor. *Physical review letters, 105*(13), 136805.

Malic, E., & Knorr, A. (2013). *Graphene and Carbon Nanotubes: Ultrafast Optics and Relaxation Dynamics*: John Wiley & Sons.

Malic, E., Winzer, T., Kadi, F., & Knorr, A. (2017). Microscopic view on the ultrafast carrier dynamics in graphene *Optical Properties of Graphene* (pp. 135-182): World Scientific.

Mandon, J., Guelachvili, G., & Picqué, N. (2009). Fourier transform spectroscopy with a laser frequency comb. *Nature Photonics, 3*(2), 99.

Markom, A., Tan, S., Haris, H., Paul, M., Dhar, A., Das, S., & Harun, S. (2018). Experimental Observation of Bright and Dark Solitons Mode-Locked with Zirconia-Based Erbium-Doped Fiber Laser. *Chinese Physics Letters, 35*(2), 024203.

Martinez, A., & Sun, Z. (2013). Nanotube and graphene saturable absorbers for fibre lasers. *Nature Photonics, 7*(11), 842-845.

Martinez, A., Zhou, K., Bennion, I., & Yamashita, S. (2008). In-fiber microchannel device filled with a carbon nanotube dispersion for passive mode-lock lasing. *Opt Express, 16*(20), 15425-15430.

Mary, R., Choudhury, D., & Kar, A. K. (2014). Applications of fiber lasers for the development of compact photonic devices. *IEEE Journal of Selected Topics in Quantum Electronics, 20*(5), 72-84.

Matniyaz, T. (2018). Free-space NPR mode locked erbium doped fiber laser based frequency comb for optical frequency measurement. *arXiv preprint arXiv:1802.10183*.

Matyba, P., Yamaguchi, H., Eda, G., Chhowalla, M., Edman, L., & Robinson, N. D. (2010). Graphene and mobile ions: the key to all-plastic, solution-processed light-emitting devices. *ACS Nano, 4*(2), 637-642.

Meijer, J., Du, K., Gillner, A., Hoffmann, D., Kovalenko, V., Masuzawa, T., Schulz, W. (2002). Laser machining by short and ultrashort pulses, state of the art and new opportunities in the age of the photons. *CIRP Annals-Manufacturing Technology, 51*(2), 531-550.

Merle, F., & Raphael, P. (2005). The blow-up dynamic and upper bound on the blow-up rate for critical nonlinear Schrödinger equation. *Annals of mathematics*, 157-222.

Minoshima, K., Kowalevicz, A. M., Hartl, I., Ippen, E. P., & Fujimoto, J. G. (2001). Photonic device fabrication in glass by use of nonlinear materials processing with a femtosecond laser oscillator. *Optics Letters, 26*(19), 1516-1518.

Mirov, S., Fedorov, V., Moskalev, I., Mirov, M., & Martyshkin, D. (2013). Frontiers of mid-infrared lasers based on transition metal doped II–VI semiconductors. *Journal of Luminescence, 133*, 268-275.

Mocker, H. W., & Collins, R. (1965). Mode competition and self-locking effects in aq-switched ruby laser. *Applied Physics Letters, 7*(10), 270-273.

Mollenauer, L., Gordon, J., & Islam, M. (1986). Soliton propagation in long fibers with periodically compensated loss. *IEEE Journal of Quantum Electronics, 22*(1), 157-173.

Nair, R. R., Blake, P., Grigorenko, A. N., Novoselov, K. S., Booth, T. J., Stauber, T., Geim, A. K. (2008). Fine structure constant defines visual transparency of graphene. *Science, 320*(5881), 1308-1308.

Nakazawa, M., Kubota, H., Suzuki, K., Yamada, E., & Sahara, A. (2000). Ultrahigh-speed long-distance TDM and WDM soliton transmission technologies. *IEEE Journal of Selected Topics in Quantum Electronics, 6*(2), 363-396.

Ning, Q.-Y., Liu, H., Zheng, X.-W., Yu, W., Luo, A.-P., Huang, X.-G., Yang, Z.-M. (2014). Vector nature of multi-soliton patterns in a passively mode-locked figure-eight fiber laser. *Optics Express, 22*(10), 11900-11911.

Novoselov, K. S., Fal, V., Colombo, L., Gellert, P., Schwab, M., & Kim, K. (2012). A roadmap for graphene. *Nature, 490*(7419), 192.

Novoselov, K. S., Geim, A. K., Morozov, S. V., Jiang, D., Zhang, Y., Dubonos, S. V., Firsov, A. A. (2004). Electric field effect in atomically thin carbon films. *Science, 306*(5696), 666-669.

Osellame, R., Cerullo, G., & Ramponi, R. (2012). *Femtosecond laser micromachining: photonic and microfluidic devices in transparent materials* (Vol. 123): Springer Science & Business Media.

Parvez, K., Li, R., Puniredd, S. R., Hernandez, Y., Hinkel, F., Wang, S., Müllen, K. (2013). Electrochemically exfoliated graphene as solution-processable, highly conductive electrodes for organic electronics. *ACS Nano, 7*(4), 3598-3606.

Parvizi, R., Arof, H., Ali, N., Ahmad, H., & Harun, S. (2011). 0.16 nm spaced multi-wavelength Brillouin fiber laser in a figure-of-eight configuration. *Optics & Laser Technology, 43*(4), 866-869.

Paschotta, R., & Keller, U. (2003). Ultrafast solid-state lasers. *Ultrafast Lasers: Technology and Applications*, 1-60.

Paschotta, R., Nilsson, J., Tropper, A. C., & Hanna, D. C. (1997). Ytterbium-doped fiber amplifiers. *IEEE Journal of Quantum Electronics, 33*(7), 1049-1056.

Payne, D. N., Laming, R. I., Morkel, P. R., & Tachibana, M. (1993). Erbium-doped fibre amplifier with shaped spectral gain: Google Patents.

Pei, S., & Cheng, H.-M. (2012). The reduction of graphene oxide. *Carbon, 50*(9), 3210-3228.

Peng, H., Dang, W., Cao, J., Chen, Y., Wu, D., Zheng, W., Liu, Z. (2012). Topological insulator nanostructures for near-infrared transparent flexible electrodes. *Nature chemistry, 4*(4), 281.

Peng, J., Sorokina, M., Sugavanam, S., Tarasov, N., Churkin, D. V., Turitsyn, S. K., & Zeng, H. (2018). Real-time observation of dissipative soliton formation in nonlinear polarization rotation mode-locked fibre lasers. *Communications Physics, 1*(1), 20.

Philippov, V. N., Kir'yanov, A. V., & Unger, S. (2004). Advanced Configuration of Erbium Fiber Passively using Crystal as Saturable Absorber. *IEEE Photonics Technology Letters, 16*(1), 57-59.

Popa, D., Sun, Z., Hasan, T., Torrisi, F., Wang, F., & Ferrari, A. C. (2011). Graphene Q-switched, tunable fiber laser. *Applied Physics Letters, 98*(7).

Popa, D., Sun, Z., Torrisi, F., Hasan, T., Wang, F., & Ferrari, A. C. (2010). Sub 200 fs pulse generation from a graphene mode-locked fiber laser. *Applied Physics Letters, 97*(20).

Radhakrishnan, R., & Lakshmanan, M. (1995). Bright and dark soliton solutions to coupled nonlinear Schrodinger equations. *Journal of Physics A: Mathematical and General, 28*(9), 2683.

Richardson, D., Nilsson, J., & Clarkson, W. (2010). High power fiber lasers: current status and future perspectives. *JOSA B, 27*(11), B63-B92.

Riesbeck, T., & Lux, O. (2009). AOM fourfold pass for efficient Q-switching and stable high peak power laser pulses. *Optics Communications, 282*(18), 3789-3792.

Rozhin, A. G., Sakakibara, Y., Tokumoto, M., Kataura, H., & Achiba, Y. (2004). Near-infrared nonlinear optical properties of single-wall carbon nanotubes embedded in polymer film. *Thin Solid Films, 464*, 368-372.

Saleh, Z., Anyi, C., Haris, H., Ahmad, F., Ali, N., Harun, S., & Arof, H. (2014). Q-switched Erbium-doped fiber laser using multi-layer graphene oxide based saturable absorber. *OPTOELECTRONICS AND ADVANCED MATERIALS-RAPID COMMUNICATIONS, 8*(7-8), 626-630.

Sapkota, Y. R., Alkabsh, A., Walber, A., Samassekou, H., & Mazumdar, D. (2017). Optical evidence for blue shift in topological insulator bismuth selenide in the few-layer limit. *Applied Physics Letters, 110*(18), 181901.

Sapkota, Y. R., & Mazumdar, D. (2018). Bulk transport properties of Bismuth selenide thin films approaching the two-dimensional limit. *arXiv preprint arXiv:1803.06593*.

Schmidt, A., Rivier, S., Cho, W. B., Yim, J. H., Choi, S. Y., Lee, S., Petrov, V. (2009). Sub-100 fs single-walled carbon nanotube saturable absorber mode-locked Yb-laser operation near 1 μm. *optics express, 17*(22), 20109-20116.

Sengupta, P. (2014). Theory of topological insulators and its applications.

Serkin, V. N., & Hasegawa, A. (2002). Exactly integrable nonlinear Schrodinger equation models with varying dispersion, nonlinearity and gain: application for soliton dispersion. *IEEE Journal of Selected Topics in Quantum Electronics, 8*(3), 418-431.

Set, S. Y., Yaguchi, H., Tanaka, Y., & Jablonski, M. (2004). Laser mode locking using a saturable absorber incorporating carbon nanotubes. *Journal of Lightwave Technology, 22*(1), 51.

Set, S. Y., Yaguchi, H., Tanaka, Y., & Jablonski, M. (2004). Ultrafast fiber pulsed lasers incorporating carbon nanotubes. *IEEE Journal of Selected Topics in Quantum Electronics, 10*(1), 137-146.

Set, S. Y., Yaguchi, H., Tanaka, Y., Jablonski, M., Sakakibara, Y., Rozhin, A., Kikuchi, K. (2003, 2003/03/23). *Mode-locked Fiber Lasers based on a Saturable Absorber Incorporating Carbon Nanotubes.* Paper presented at the Optical Fiber Communication Conference, Atlanta, Georgia.

Shahil, K., Hossain, M., Goyal, V., & Balandin, A. (2012). Micro-Raman spectroscopy of mechanically exfoliated few-quintuple layers of Bi2Te3, Bi2Se3, and Sb2Te3 materials. *Journal of Applied Physics, 111*(5), 054305.

Shank, C., & Ippen, E. (1974). Subpicosecond kilowatt pulses from a mode-locked cw dye laser. *Applied Physics Letters, 24*(8), 373-375.

Shi, W., Fang, Q., Zhu, X., Norwood, R., & Peyghambarian, N. (2014). Fiber lasers and their applications. *Applied Optics, 53*(28), 6554-6568.

Sibbett, W., Lagatsky, A., & Brown, C. (2012). The development and application of femtosecond laser systems. *optics express, 20*(7), 6989-7001.

Siegman, A., & Kuizenga, D. (1974). Active mode-coupling phenomena in pulsed and continuous lasers. *Opto-electronics, 6*(1), 43-66.

Snitzer, E. (1966). Glass lasers. *Appl Opt, 5*(10), 1487-1499.

Sobon, G. (2015). Mode-locking of fiber lasers using novel two-dimensional nanomaterials: graphene and topological insulators. *Photonics Research, 3*(2), A56-A63.

Sobon, G. (2015). Mode-locking of fiber lasers using novel two-dimensional nanomaterials: graphene and topological insulators [Invited]. *Photonics Research, 3*(2), A56-A63.

Sobon, G., & Sotor, J. (2016). Recent Advances in Ultrafast Fiber Lasers Mode-locked with Graphenebased Saturable Absorbers. *Current Nanoscience, 12*(3), 291-298.

Sobon, G., Sotor, J., Jagiello, J., Kozinski, R., Zdrojek, M., Holdynski, M., Abramski, K. M. (2012). Graphene oxide vs. reduced graphene oxide as saturable absorbers for Er-doped passively mode-locked fiber laser. *optics express, 20*(17), 19463-19473.

Solodyankin, M. A., Obraztsova, E. D., Lobach, A. S., Chernov, A. I., Tausenev, A. V., Konov, V. I., & Dianov, E. M. (2008). Mode-locked 1.93 μm thulium fiber laser with a carbon nanotube absorber. *Optics Letters, 33*(12), 1336-1338.

Sotor, J., Sobon, G., Krzempek, K., & Abramski, K. M. (2012). Fundamental and harmonic mode-locking in erbium-doped fiber laser based on graphene saturable absorber. *Optics Communications, 285*(13-14), 3174-3178.

Sotor, J., Sobon, G., Macherzynski, W., Paletko, P., & Abramski, K. M. (2015). Black phosphorus a new saturable absorber material for ultrashort pulse generation. *arXiv preprint arXiv:1504.04731*.

Sotor, J., Sobon, G., Macherzynski, W., Paletko, P., Grodecki, K., & Abramski, K. M. (2014). Mode-locking in Er-doped fiber laser based on mechanically exfoliated Sb 2 Te 3 saturable absorber. *Optical Materials Express, 4*(1), 1-6.

Spence, D. E., Kean, P. N., & Sibbett, W. (1991). 60-fsec pulse generation from a self-mode-locked Ti: sapphire laser. *Optics Letters, 16*(1), 42-44.

Splendiani, A., Sun, L., Zhang, Y., Li, T., Kim, J., Chim, C.-Y., Wang, F. (2010). Emerging photoluminescence in monolayer MoS2. *Nano Letters, 10*(4), 1271-1275.

Spuhler, G. J., Weingarten, K. J., Grange, R., Krainer, L., Haiml, M., Liverini, V., Keller, U. (2005). Semiconductor saturable absorber mirror structures with low saturation fluence. *Applied Physics B-Lasers and Optics, 81*(1), 27-32.

Sreeprasad, T., Maliyekkal, S. M., Lisha, K., & Pradeep, T. (2011). Reduced graphene oxide–metal/metal oxide composites: facile synthesis and application in water purification. *Journal of hazardous materials, 186*(1), 921-931.

Stankovich, S., Dikin, D. A., Piner, R. D., Kohlhaas, K. A., Kleinhammes, A., Jia, Y., Ruoff, R. S. (2007). Synthesis of graphene-based nanosheets via chemical reduction of exfoliated graphite oxide. *Carbon, 45*(7), 1558-1565.

Steen, W. M., & Mazumder, J. (2010). *Laser material processing*: springer science & business media.

Su, W.-P., Schrieffer, J., & Heeger, A. (1980). Soliton excitations in polyacetylene. *Physical Review B, 22*(4), 2099.

Suchkov, S. V., Sukhorukov, A. A., Huang, J., Dmitriev, S. V., Lee, C., & Kivshar, Y. S. (2016). Nonlinear switching and solitons in PT-symmetric photonic systems. *Laser & Photonics Reviews, 10*(2), 177-213.

Sun, D., Divin, C., Mihnev, M., Winzer, T., Malic, E., Knorr, A., First, P. N. (2012). Current relaxation due to hot carrier scattering in graphene. *New Journal of Physics, 14*(10), 105012.

Sun, Y., Tu, C., You, Z., Liao, J., Wang, Y., & Xu, J. (2018). One-dimensional Bi 2 Te 3 nanowire based broadband saturable absorber for passively Q-switched Yb-doped and Er-doped solid state lasers. *Optical Materials Express, 8*(1), 165-174.

Sun, Z., Hasan, T., & Ferrari, A. (2012). Ultrafast lasers mode-locked by nanotubes and graphene. *Physica E: Low-dimensional Systems and Nanostructures, 44*(6), 1082-1091.

Sun, Z., Hasan, T., & Ferrari, A. C. (2012). Ultrafast lasers mode-locked by nanotubes and graphene. *Physica E-Low-Dimensional Systems & Nanostructures, 44*(6), 1082-1091.

Sun, Z., Hasan, T., Torrisi, F., Popa, D., Privitera, G., Wang, F., Ferrari, A. C. (2010). Graphene mode-locked ultrafast laser. *ACS Nano, 4*(2), 803-810.

Sun, Z., Hasan, T., Torrisi, F., Popa, D., Privitera, G., Wang, F., Ferrari, A. C. (2010). Graphene Mode-Locked Ultrafast Laser. *ACS Nano, 4*(2), 803-810.

Sung, J. H., Heo, H., Hwang, I., Lim, M., Lee, D., Kang, K., Jo, M.-H. (2014). Atomic layer-by-layer thermoelectric conversion in topological insulator bismuth/antimony tellurides. *Nano Letters, 14*(7), 4030-4035.

Tan, S. J., Harun, S. W., & Ahmad, H. (2013). Controllable stretched pulse and dissipative soliton emission using non-linear polarisation rotation and cavity loss tuning mechanism. *IET Optoelectronics, 7*(2), 38-41.

Tang, D., Zhao, B., Shen, D., Lu, C., Man, W., & Tam, H. (2002). Bound-soliton fiber laser. *Physical Review A, 66*(3), 033806.

Tang, D., Zhao, B., Zhao, L., & Tam, H. (2005). Soliton interaction in a fiber ring laser. *Physical Review E, 72*(1), 016616.

Tang, D., Zhao, L., & Zhao, B. (2005). Multipulse bound solitons with fixed pulse separations formed by direct soliton interaction. *Applied Physics B, 80*(2), 239-242.

Tang, H., Liang, D., Qiu, R. L., & Gao, X. P. (2011). Two-dimensional transport-induced linear magneto-resistance in topological insulator Bi2Se3 nanoribbons. *ACS Nano, 5*(9), 7510-7516.

Telle, H. R., Steinmeyer, G., Dunlop, A., Stenger, J., Sutter, D., & Keller, U. (1999). Carrier-envelope offset phase control: A novel concept for absolute optical frequency measurement and ultrashort pulse generation. *Applied Physics B, 69*(4), 327-332.

Tiu, Z., Ahmad, F., Tan, S., Ahmad, H., & Harun, S. (2014). Passive Q-switched Erbium-doped fiber laser with graphene–polyethylene oxide saturable absorber in three different gain media. *Indian Journal of Physics, 88*(7), 727-731.

Tiu, Z. C., Tan, S. J., Zarei, A., Ahmad, H., & Harun, S. W. (2014). Nonlinear Polarization Rotation-Based Mode-Locked Erbium-Doped Fiber Laser with Three Switchable Operation States. *Chinese Physics Letters, 31*(9), 094206.

Udem, T., Holzwarth, R., & Hänsch, T. W. (2002). Optical frequency metrology. *Nature, 416*(6877), 233.

Usechak, N. G., Agrawal, G. P., & Zuegel, J. D. (2005). FM mode-locked fiber lasers operating in the autosoliton regime. *IEEE Journal of Quantum Electronics, 41*(6), 753-761.

Vazquez-Zuniga, L. A., & Jeong, Y. (2012). Super-broadband noise-like pulse erbium-doped fiber ring laser with a highly nonlinear fiber for Raman gain enhancement. *IEEE Photonics Technology Letters, 24*(17), 1549.

Vij, D., & Mahesh, K. (2013). *Medical applications of lasers*: Springer Science & Business Media. *Optics & Laser Technology, 44*(1), 167-170.

Villeneuve, C., Pacchini, S., Dilhan, M., Colin, D., Brouzes, A., Boulanger, P., & Plana, R. (2011). Make Carbon nanotube-polymer composite thin: application to water quality. *MRS Online Proceedings Library Archive, 1346*.

Wang, F., Rozhin, A., Scardaci, V., Sun, Z., Hennrich, F., White, I., Ferrari, A. C. (2008). Wideband-tuneable, nanotube mode-locked, fibre laser. *Nature nanotechnology, 3*(12), 738.

Wang, F., Rozhin, A., Sun, Z., Scardaci, V., Penty, R., White, I., & Ferrari, A. (2008). Fabrication, characterization and mode locking application of single-walled carbon nanotube/polymer composite saturable absorbers. *International Journal of Material Forming, 1*(2), 107.

Wang, J., Hernandez, Y., Lotya, M., Coleman, J. N., & Blau, W. J. (2009). Broadband nonlinear optical response of graphene dispersions. *Advanced Materials, 21*(23), 2430-2435.

Wang, J., Wang, C., Meng, X., Hu, X., Yu, Y., & Yu, S. (2012). Study on the periodic oscillation of plasma/vapour induced during high power fibre laser penetration welding. *Optics & Laser Technology, 44*(1), 67-70.

Wang, J. T.-W., Ball, J. M., Barea, E. M., Abate, A., Alexander-Webber, J. A., Huang, J., Snaith, H. J. (2013). Low-temperature processed electron collection layers of graphene/TiO2 nanocomposites in thin film perovskite solar cells. *Nano Letters, 14*(2), 724-730.

Wang, K., Wang, J., Fan, J., Lotya, M., O'Neill, A., Fox, D., Zhao, Q. (2013). Ultrafast saturable absorption of two-dimensional MoS2 nanosheets. *ACS Nano, 7*(10), 9260-9267.

Wang, Q. H., Kalantar-Zadeh, K., Kis, A., Coleman, J. N., & Strano, M. S. (2012). Electronics and optoelectronics of two-dimensional transition metal dichalcogenides. *Nature nanotechnology, 7*(11), 699-712.

Wang, S., Yu, H., Zhang, H., Wang, A., Zhao, M., Chen, Y., Wang, J. (2014). Broadband Few-Layer MoS2 Saturable Absorbers. *Advanced Materials, 26*(21), 3538-3544.

Wang, W., Meng, H., Wu, X., Xiong, R., Xue, H., Tan, C., & Huang, X. (2012). A nonlinear polarization rotation-based linear cavity waveband switchable multi-wavelength fiber laser. *Laser Physics Letters, 10*(1), 015104.

Wang, Z., Zhan, L., Majeed, A., & Zou, Z. (2015). Harmonic mode locking of bound solitons. *Optics Letters, 40*(6), 1065-1068.

Weber, H.-G., Ludwig, R., Ferber, S., Schmidt-Langhorst, C., Kroh, M., Marembert, V., Schubert, C. (2006). Ultrahigh-speed OTDM-transmission technology. *Journal of Lightwave Technology, 24*(12), 4616-4627.

Weber, H.-G., & Nakazawa, M. (2007). Introduction to ultra-high-speed optical transmission technology *Ultrahigh-Speed Optical Transmission Technology* (pp. 1-20): Springer. 1193-1335.

Weber, M., Lynch, J., Blackburn, D., & Cronin, D. (1983). Dependence of the stimulated emission cross section of Yb 3+ on host glass composition. *IEEE Journal of Quantum Electronics, 19*(10), 1600-1608.

Wei, D., Grande, L., Chundi, V., White, R., Bower, C., Andrew, P., & Ryhänen, T. (2012). Graphene from electrochemical exfoliation and its direct applications in enhanced energy storage devices. *Chem. Commun., 48*(9), 1239-1241.

Wilson, J., & Yoffe, A. (1969). The transition metal dichalcogenides discussion and interpretation of the observed optical, electrical and structural properties. *Advances in Physics, 18*(73), 193-335.

Wolfe, D. B., Ashcom, J. B., Hwang, J. C., Schaffer, C. B., Mazur, E., & Whitesides, G. M. (2003). Customization of Poly (dimethylsiloxane) Stamps by Micromachining Using a Femtosecond-Pulsed Laser. *Advanced Materials, 15*(1), 62-65.

Wong, J. H., Wu, K., Liu, H. H., Ouyang, C., Wang, H., Aditya, S., Chernov, A. (2011). Vector solitons in a laser passively mode-locked by single-wall carbon nanotubes. *Optics Communications, 284*(7), 2007-2011.

Woodward, R. (2015). Exploiting nonlinearity in optical fibres and nanomaterials for short-pulse laser technology. 293-435

Woodward, R. I., & Kelleher, E. J. (2015). 2D Saturable Absorbers for Fibre Lasers. *Applied Sciences, 5*(4), 1440-1456.

Wu, X., Tang, D., Zhang, H., & Zhao, L. (2009). Dissipative soliton resonance in an all-normal-dispersion erbium-doped fiber laser. *Optics Express, 17*(7), 5580-5584.

Wu, X., Tang, D. Y., Luan, X. N., & Zhang, Q. (2011). Bound states of solitons in a fiber laser mode locked with carbon nanotube saturable absorber. *Optics Communications, 284*(14), 3615-3618.

Wu, Z., Liu, D., Fu, S., Li, L., Tang, M., & Zhao, L. (2016). Scalar-vector soliton fiber laser mode-locked by nonlinear polarization rotation. *Optics Express, 24*(16), 18764-18771.

Wu, Z., Liu, D., Li, L., Luo, Y., Tang, D., Shen, D., Zhao, L. (2016). Scalar-vector soliton fiber lasers. 275-279

Xie, G., Ma, J., Lv, P., Gao, W., Yuan, P., Qian, L., Tang, D. (2012). Graphene saturable absorber for Q-switching and mode locking at 2 μm wavelength. *Optical Materials Express, 2*(6), 878-883.

Xu, J., Wu, S., Li, H., Liu, J., Sun, R., Tan, F., Wang, P. (2012). Dissipative soliton generation from a graphene oxide mode-locked Er-doped fiber laser. *Optics Express, 20*(21), 23653-23658.

Xu, Y., Liu, Z., Zhang, X., Wang, Y., Tian, J., Huang, Y., Chen, Y. (2009). A graphene hybrid material covalently functionalized with porphyrin: synthesis and optical limiting property. *Advanced Materials, 21*(12), 1275-1279.

Yamashita, S. (2012). A tutorial on nonlinear photonic applications of carbon nanotube and graphene. *Journal of Lightwave Technology, 30*(4), 427-447.

Yamashita, S., Inoue, Y., Maruyama, S., Murakami, Y., Yaguchi, H., Jablonski, M., & Set, S. (2004). Saturable absorbers incorporating carbon nanotubes directly synthesized onto substrates and fibers and their application to mode-locked fiber lasers. *Optics Letters, 29*(14), 1581-1583.

Yang, H., Withers, F., Gebremedhn, E., Lewis, E., Britnell, L., Felten, A., Casiraghi, C. (2014). Dielectric nanosheets made by liquid-phase exfoliation in water and their use in graphene-based electronics. *2D Materials, 1*(1), 011012.

Yang, J.-H., Song, S., Du, S., Gao, H.-J., & Yakobson, B. I. (2017). Design of Two-Dimensional Graphene-like Dirac Materials β12-XBeB5 (X= H, F, Cl) from Non-graphene-like β12-Borophene. *The Journal of Physical Chemistry Letters, 8*(18), 4594-4599.

Yang, X., & Yang, C. X. (2009). Q-switched mode-locking in an erbium-doped femtosecond fiber laser based on nonlinear polarization rotation. *Laser Physics, 19*(11), 2106-2109.

Yao, B., Rao, Y., Wang, Z., Wu, Y., Zhou, J., Wu, H., Chen, Y. (2015). Graphene based widely-tunable and singly-polarized pulse generation with random fiber lasers. *Scientific Reports, 5*, 18526.

Yim, J. H., Cho, W. B., Lee, S., Ahn, Y. H., Kim, K., Lim, H.,Rotermund, F. (2008). Fabrication and characterization of ultrafast carbon nanotube saturable absorbers for solid-state laser mode locking near 1 μ m. *Applied Physics Letters, 93*(16), 161106.

Yin, S., Zhang, Y., Kong, J., Zou, C., Li, C. M., Lu, X.,Chen, X. (2011). Assembly of graphene sheets into hierarchical structures for high-performance energy storage. *ACS Nano, 5*(5), 3831-3838.

Yin, X., Meng, J., Zu, J., & Chen, W. (2013). Semiconductor saturable-absorber mirror passively Q-switched Yb:YAG microchip laser. *Chinese Optics Letters, 11*(8), 081402.

Yin, Z., He, Q., Huang, X., Zhang, J., Wu, S., Chen, P., Zhang, H. (2012). Real-time DNA detection using Pt nanoparticle-decorated reduced graphene oxide field-effect transistors. *Nanoscale, 4*(1), 293-297.

Yu, G., Hu, L., Vosgueritchian, M., Wang, H., Xie, X., McDonough, J. R., Bao, Z. (2011). Solution-processed graphene/MnO2 nanostructured textiles for high-performance electrochemical capacitors. *Nano Letters, 11*(7), 2905-2911.

Zabusky, N. J., & Kruskal, M. D. (1965). Interaction of" solitons" in a collisionless plasma and the recurrence of initial states. *Physical review letters, 15*(6), 240.

Zakharov, V., & Schulman, E. (1982). To the integrability of the system of two coupled nonlinear Schrödinger equations. *Physica D: Nonlinear Phenomena, 4*(2), 270-274.

Zervas, M. N. (2014). High power ytterbium-doped fiber lasers—fundamentals and applications. *International Journal of Modern Physics B, 28*(12), 1442009.

Zervas, M. N., & Codemard, C. A. (2014). High power fiber lasers: a review. *IEEE Journal of Selected Topics in Quantum Electronics, 20*(5), 219-241.

Zhan, Y., Liu, Z., Najmaei, S., Ajayan, P. M., & Lou, J. (2012). Large-area vapor-phase growth and characterization of MoS2 atomic layers on a SiO2 substrate. *small, 8*(7), 966-971.

Zhang, H., Tang, D., Knize, R., Zhao, L., Bao, Q., & Loh, K. P. (2010). Graphene mode locked, wavelength-tunable, dissipative soliton fiber laser. *Applied Physics Letters, 96*(11), 111112.

Zhang, H., Tang, D., Zhao, L., Bao, Q., & Loh, K. (2009). Large energy mode locking of an erbium-doped fiber laser with atomic layer graphene. *optics express, 17*(20), 17630-17635.

Zhang, H., Tang, D., Zhao, L., Wu, X., & Tam, H. (2009). Dissipative vector solitons in a dispersion-managed cavity fiber laser with net positive cavity dispersion. *Optics Express, 17*(2), 455-460.

Zhang, H., Tang, D., Zhao, L., & Xiang, N. (2008). Coherent energy exchange between components of a vector soliton in fiber lasers. *optics express, 16*(17), 12618-12623.

Zhao, C., Zhang, H., Qi, X., Chen, Y., Wang, Z., Wen, S., J., D. A. (2012). Ultra-short pulse generation by a topological insulator based saturable absorber. *Applied Physics Letters, 101*(21), 211106.

Zhao, C., Zou, Y., Chen, Y., Wang, Z., Lu, S., Zhang, H., Tang, D. (2012). Wavelength-tunable picosecond soliton fiber laser with Topological Insulator: Bi2Se3 as a mode locker. *Opt Express, 20*(25), 27888-27895.

Zhao, L., Tang, D., Wu, X., Zhang, H., & Tam, H. (2009). Coexistence of polarization-locked and polarization-rotating vector solitons in a fiber laser with SESAM. *Optics Letters, 34*(20), 3059-3061.

Zhao, L., Tang, D., Zhang, H., & Wu, X. (2008). Polarization rotation locking of vector solitons in a fiber ring laser. *optics express, 16*(14), 10053-10058.

Zhao, L., Tang, D., Zhang, H., & Wu, X. (2009). Bunch of restless vector solitons in a fiber laser with SESAM. *Optics Express, 17*(10), 8103-8108.

Zhao, X., Liu, Z.-B., Yan, W.-B., Wu, Y., Zhang, X.-L., Chen, Y., & Tian, J.-G. (2011). Ultrafast carrier dynamics and saturable absorption of solution-processable few-layered graphene oxide. *Applied Physics Letters, 98*(12), 121905.

Zhao, Y., Chen, Z., Saxer, C., Xiang, S., de Boer, J. F., & Nelson, J. S. (2000). Phase-resolved optical coherence tomography and optical Doppler tomography for imaging blood flow in human skin with fast scanning speed and high velocity sensitivity. *Optics Letters, 25*(2), 114-116.

Zhong, Y., Zhang, Z., & Tao, X. (2010). Passively mode-locked fiber laser based on nonlinear optical loop mirror with semiconductor optical amplifier. *Laser Physics, 20*(8), 1756-1759.

Zhu, Y., Murali, S., Cai, W., Li, X., Suk, J. W., Potts, J. R., & Ruoff, R. S. (2010). Graphene and graphene oxide: synthesis, properties, and applications. *Advanced Materials, 22*(35), 3906-3924.

LIST OF PUBLICATIONS AND PAPERS PRESENTED

The following publications form the basis of the thesis:

ISI Journal Papers

1. **Haris, H**., Harun, S. W., Muhammad, A. R., Anyi, C. L., Tan, S. J., Ahmad, F., & Arof, H. (2017). *Passively Q-switched Erbium-doped and Ytterbium-doped fibre lasers with topological insulator bismuth selenide (Bi2Se3) as saturable absorber*. Optics & Laser Technology, 88, 121-127.

2. **Haris, H**., Harun, S. W., Anyi, C. L., Muhammad, A. R., Ahmad, F., Tan, S. J., & Arof, H. (2016). *Generation of soliton and bound soliton pulses in mode-locked erbium-doped fiber laser using graphene film as saturable absorber*. Journal of Modern Optics, 63(8), 777-782.

3. **Haris, H**., Anyi, C. L., Muhammad, A. R., Nor, R. M., Zulkepely, N. R., Ahmad, F., & Arof, H. (2015). *Q-Switched Ytterbium doped fiber laser with graphene oxide embedded in polyethylene oxide film based saturable absorber*. Journal of Optoelectronics and Advanced Materials, 17(5-6), 539-544.

Conference Paper

1. **Haris, H**., Harun, S. W., Muhammad, A. R., & Arof, H. (2016). *Graphene Oxide-Polyethylene Oxide (PEO) Film as Saturable Absorber on Mode-locked Erbium Doped Fiber Laser Generation*, Jurnal Teknologi, 78(3), 13-17.

Additional ISI Publications

In addition, the following papers were published during the period of PhD, but is beyond the scope of this thesis:

1. Markom, A. M., Tan, S. J., **Haris, H**., Paul, M. C., Dhar, A., Das, S., & Harun, S. W. (2018). Experimental Observation of Bright and Dark Solitons Mode-Locked with Zirconia-Based Erbium-Doped Fiber Laser. *Chinese Physics Letters*, *35*(2), 024203.

2. Tan, S. J., **Haris, H**., & Harun, S. W. (2017). Switchable Brillouin frequency multiwavelength and pulsed fiber laser. *Chinese Optics Letters*, *15*(10), 101401.

3. Saidin, N., Zen, D. I. M., Ahmad, F., **Haris, H**., Ahmad, H., Dimyati, K., & Bhadra, S. K. (2016). Q-switched 2 µm thulium bismuth co-doped fiber laser with multi-walled carbon nanotubes saturable absorber. *Optics & Laser Technology*, *83*, 89-93.

4. Adnan, N. N., Bidin, N., Taib, N. A. M., **Haris, H**., Fakaruddin, M., Hashim, A. M., & Harun, S. W. (2016). Passively Q-switched flashlamp pumped Nd: YAG laser using liquid graphene oxide as saturable absorber. *Optics & Laser Technology*, *80*, 28-32.

5. Taib, N. A. M., Bidin, N., **Haris, H**., Adnan, N. N., Ahmad, M. F. S., & Harun, S. W. (2016). Multi-walled carbon nanotubes saturable absorber in Q-switching flashlamp pumped Nd: YAG laser. *Optics & Laser Technology*, *79*, 193-197.

6. **Haris, H**., Anyi, C. L., Muhammad, A. R., Ahmad, F., Nor, R. M., Zulkepely, N. R., & Arof, H. (2015). Performance of passively Q-switched ring erbium-doped fiber laser using a multiwalled carbon nanotubes polyethylene oxide (PEO) polymer composite-based saturable absorber. *Microwave and Optical Technology Letters*, 57(8), 1897-1901.